Development of Targeted, Enzyme-Activated, Dendrimer-Drug Nano-Conjugates for Hepatic Cancer Therapy

by

Scott H. Medina

A dissertation submitted in partial fulfillment
of the requirements for the degree of Doctor
of Philosophy
(Biomedical Engineering)
in the University of Michigan
2012

Doctoral Committee:

Assistant Professor Mohamed E.H. El-Sayed, Chair
Professor Donna S. Shewach
Associate Professor Joseph L. Bull
Associate Professor Michael Mayer

DEDICATION

This thesis is dedicated to my loving wife Ashley L. Medina, who without her companionship, dedication and support I would not have been able to complete my doctoral work. Her persistent reassurance and warmth allowed me to persevere throughout the most trying of times. Also, to both my family and the Briggs family who consistently encouraged and provided invaluable support to my education endeavors.

Acknowledgements

Table of Contents

List of Figures

List of Tables

Tables

List of Schemes

Schemes

List of Abbreviations

10HCPT: 10-hydroxy-captothecin

5FU: 5-Fluorouracil

ASGPR: Asialoglycoprotein receptor

BCLC: Barcelona-Clinic Liver Cancer

D_h: Hydrodynamic diameter

DOTAP: dioleoyloxytrimethylammonium

DOX: Doxorubicin

Dtxl: Docetaxel

EPR: Enhanced Permeability and Retention

G5: Generation 5 PAMAM dendrimer

Gal: Galactosamine

GFLG: glycine-phenylalinine-lysine-glycine

HAI: Hepatic Arterial Infusion

HBV: Hepatitis B Virus

HCC: Hepatocellular Carcinoma

HCV: Hepatitis B Virus

HPMA: N-(2-hydroxypropyl) methacrylamide

hyd: Hydrazine

IL-12: Interleukin 12

IO: Iron Oxide

K$_d$: Dissociation Constant

MDR: Multi-drug Resistance

MLCRS: Modulatory Liposomal Controlled Release Systems

MMP: Matrix Metalloproteinase

MTX: Methotrexate

MW: Molecular Weight

NAcGal: *N*-acetylgalactosamine

NADPH: Nicotinamide Adenine Dinucleotide Phosphate

NCS: Neocarzinostatin

OLT: Orthotopic Liver Transplantation

PAMAM: poly(amido amine)

PBS: Phosphate Buffered Saline

PEG: poly(ethylene glycol)

PEI: Percutaneous Ethanol Injection

PEPE: polyether-copolyester

PGLSA: poly(glycerol succinic acid)

PIHCA: polyisohexylcyanoacrylate

PK2: Gal-targeted HPMA-DOX Conjugates

PLGA: poly(lactic-co-glycolic)

PPSD: PEGylated PAMAM pH-sensitive Dendrimers

Pt: Cisplatin

RES: Reticuloendothelial System

RFA: Radiofrequency Ablation

rhArg: Recombinant Human Arginase Deaminase

SMA: poly(styrene-co-maleic acid)

SMANCS: poly(styrene-co-maleic acid)-Neocarzinostatin Polymer-Protein Conjugate

SN: Silica Nanoparticles

SP94: Hepatic Cancer Cell-specific Peptide

TACE: Transarterial Chemoembolization

TAX: Taxol

Abstract

**Development of Targeted, Enzyme-Activated, Dendrimer-Drug Nano-Conjugates
for Hepatic Cancer Therapy**

by

Scott H. Medina

Chair: Mohamed E.H. El-Sayed

Primary liver cancer is the 4th most common malignancy worldwide, accounting for >600,000 deaths/year globally. Loco-regional chemotherapy fails to deliver anticancer drugs specifically to hepatic cancer cells resulting in low anticancer activity and severe toxicities. This dissertation describes development of targeted nanoparticles that can deliver and release chemotherapeutic agents selectively to the cytoplasm of hepatic cancer cells. Specifically, we conjugate doxorubicin (DOX) chemotherapeutic molecules to generation 5 (G5) poly(amidoamine) dendrimers via aromatic azo-linkers to prepare G5-DOX conjugates. We engineered these azo-linkers to be cleaved by liver-specific azoreductase enzymes, with tunable DOX release achieved by modulating the linker's enzyme affinity via increased azo-bond electronegativity, indicated by decreasing Hammett values (σ). We synthesized four G5-L(x)-DOX conjugates incorporating azo-linkers L1-L4 with decreasing σ values and evaluated their cleavage by human liver microsomal (HLM) enzymes, HepG2 hepatic cancer cell and rat cardiomyocyte S9

xvi

enzyme fractions, or control proteins. This resulted in selective cleavage of G5-L(x)-DOX by azoreductase enzymes with increased DOX release rates observed as azo-linker σ value decreased, achieving 100% DOX release from G5-L4-DOX conjugates by HLM enzymes. We evaluated the anticancer activity of G5-L(x)-DOX towards hepatic cancer cells using a clonogenic cell survival assay. Results showed increased cytotoxicity of G5-L(x)-DOX which matched their DOX release rank order, reaching a similar IC_{50} for G5-L4-DOX and free DOX in HepG2 cells at equivalent drug concentrations. Hepatic cancer cell-specific delivery of G5 dendrimers was achieved by surface functionalization with N-acetylgalactosamine (NAcGal) sugars, resulting in binding and receptor-mediated endocytosis of G5-NAcGal by the liver-specific asialoglycoprotein receptor. Biodistribution of G5-NAcGal in liver-tumor bearing mice showed a 2-fold increase in tumor-specific carrier accumulation versus non-targeted dendrimers, while attachment of poly(ethylene glycol) (PEG) to the G5 surface limited carrier distribution to healthy liver tissue. This prompted synthesis of G5-PEG carriers displaying the targeting ligand at the PEG terminus, leading to selective carrier internalization into HepG2 cells while avoiding opsonization and subsequent uptake into liver macrophages and rat hepatocytes. By combining this targeting approach with tunable G5-DOX conjugates we expect to achieve specific delivery of free DOX to hepatic cancer cells for effective liver cancer therapy with minimal side effects.

Chapter 1

Introduction

1.1   Primary Liver Cancer: Incidence, Epidemiology and Risk Factors

Primary liver cancer is the 4th most common malignancy worldwide accounting

for >600,000 annual deaths globally.[1,2] In the United States the American Cancer Society

has estimated 28,720 new cases of primary liver for 2012, resulting in 20,550 related

patient deaths.[2] Hepatocellular Carcinoma (HCC) is the most common form of liver

cancer developing from malignant transformation of hepatocytes, and accounts for

approximately 75% of patient diagnoses.[1,2] While overall incidence of cancer in the last

decade has decreased by 0.8% each year the frequency of primary liver cancer diagnoses

has approximately doubled since 1988.[3] Worldwide rates of liver cancer diagnosis are on

average 2 to 4 times more likely in men than in women, with incidence in men increasing

sharply after 50 years of age.[1,2] This results in a cumulative life-time risk for developing

liver cancer of 0.88% for men and 0.42% in women.[1] However, the incidence rate of

primary liver cancer differs greatly based on geographic region with diagnoses of liver

cancer in men per 100,000 of 4.1 in Northern America, while in Middle Africa and

Eastern Asia it is estimated to be as high as 24-35.[1] This difference is a result of limited

vaccination of Eastern and African populations against hepatitis B (HBV) and C (HCV)

viral infection.[1,2,4] Worldwide, 75%-80% of primary liver cancer cases are attributed to long-term hepatitis infection,[1] which causes frequent cycles of hepatocyte damage and repair leading to cirrhosis and eventual malignant development. Specifically, HBV is the more predominant viral risk factor attributed to 50%-55% of HCC cases in Chinese, Southeast Asia and African patients.[4] Other major risk factors include alcohol abuse, alcoholic cirrhosis, and tobacco use,[1,2,4] which accounts for 45% of primary liver cancer cases in the United States and Europe.[1] In these same regions HCV is the more common viral factor attributed to 25%-30% of cases due in large part to contact with contaminated blood during infusions and injectable drug use from 1960-1970.[1] There have also been links of HCC incidence to diabetes, obesity, anabolic steroid use and liver damage due to exposure to aflatoxin, a fungus that contaminates peanuts and grains, as these conditions increase the probability of fatty liver disease and cirrhosis.[1]

1.2   Staging and Treatment of HCC

For patients diagnosed with HCC staging and selection of treatment regimen is implemented using a number of prognostic scoring systems which incorporate categorizations of liver damage severity, number and size of tumor nodules, as well as tumor pathology and infiltration. Standard staging systems include the Barcelona-Clinic Liver Cancer (BCLC) system, the Chinese University Prognostic Index and the Japanese Integrated Staging.[5] BCLC is the most widely utilized staging index in North America and groups patients into 5 stages with associated treatment recommendations (**Figure 1.1**).

Figure 1.1: Diagram of the BCLC staging and treatment algorithm for HCC patients based on size, number and spread of tumor nodule, as well as patient performance status (PS = measure of physical impairment; OLT = orthotopic liver transplantation; PEI = percutaneous ethanol injection; RFA = radiofrequency ablation; HAI = hepatic arterial infusion; TACE = transarterial chemoembolization).

The standard of care for non-cirrhotic HCC patients is surgical resection in which the tumor mass and surrounding tissue is excised leaving enough healthy liver to preserve normal function.[5] For patients who present a small tumor nodule of ≤5cm in its longest diameter 5-year survival rates range between 50%-60% after resection, while resection of large tumor masses (>5cm) has shown 5-year patient survival of approximately 30%.[4,5] As a result patient eligibility criterion for surgical resection has been established as presentation of a single solitary lesion ≤5cm, or multiple nodules <3cm, with well-defined boundaries and no indication of vascular invasion or extrahepatic spread.[5] Furthermore, resection is contraindicated in cirrhotic patients where extensive lobectomy will compromise liver function.[5] The recurrence rate and long term survival of liver

cancer patients after surgical resection has been shown to be a function of tumor size and number of nodules,[5] with a 32% recurrence rate when tumor is ≤5cm in diameter and 43% when the nodule is >5cm. In addition, 5-year survival rates for single tumor patients were 57%, whereas a 26% survival rate was observed for patients with 3 or more nodules.[4,5]

While surgical resection treats the HCC tumor, orthotopic liver transplantation (OLT) represents a potential cure for both the HCC lesion(s) as well as underlying cirrhosis. Patients with a single nodule ≤5cm in the longest diameter, or up to 3 lesions <3cm in diameter, who receive OLT have shown 5-year survival rates >70%, with a 15% recurrence rate.[5,6] However, due to the low availability of organs OLT is applied selectively for patients with early stage HCC (≤5cm tumor diameter) who show recurrence or progressive hepatic failure after resection.[5] As a result of these selection criteria it is estimated that 80%-95% of HCC patients are ineligible for surgical intervention due to extensive tumor burden and poor underlying liver function due to cirrhosis.[5,7] These unresectable HCC patients therefore rely on loco-regional ablative therapy via percutaneous ethanol injection (PEI) or radio-frequency ablation (RFA).[5,7-9] PEI induces tumor necrosis through cellular dehydration, protein denaturation and small vein thrombosis, while RFA generates high temperatures to induce necrosis of hepatic cancer cells.[9] Both procedures are typically well tolerated with a 0.1% rate of treatment-related death and 1.7% of patients experiencing severe complications.[9] For patients with a small tumor mass ≤3 cm in diameter, and low-grade cirrhosis, 1 and 2 year recurrence-free survival rates ranged between 77%-86% and 43%-64%, respectively.[5,9] In general, these procedures are safe, easy to perform, and relatively inexpensive making them the

therapy of choice for patients with a single solitary lesion <5cm in diameter or up to three lesions each <3cm.[10]

However, the underutilization of screening procedures, which are applied only in high risk populations with chronic viral hepatitis infection or liver cirrhosis, results in >80% of liver cancer patients diagnosed at intermediate and advanced stage HCC when tumor size is large (>5cm) and symptomatic.[4,5] This results in the majority of unresectable HCC patients relying on loco-regional chemotherapy via hepatic arterial infusion (HAI) or transarterial chemoembolization (TACE).[5,7,8] These procedures are performed by localizing a catheter to the hepatic artery and administering a large, local dose of a chemotherapeutic agent (e.g. Doxorubicin; DOX) directly to the tumor tissue where it can passively diffuse to the cytoplasm of hepatic cancer cells. In the case of TACE the chemotherapeutic agent is typically loaded into a polymeric bead to control the release rate, followed by injection of a polymer-lipid embolic agent to limit blood supply from the hepatic artery to the lesion.[8] HAI therapy is associated with higher response rates versus systemic therapy in the treatment of a single tumor lesion,[11] while TACE has been shown to be more effective in the larger population of intermediate and advanced stage HCC patients who commonly present multi-focal hepatomas with numerous feeder vessels.[12] Multiple clinical trials have shown objective response and slowed tumor progression in 35% of HCC patients receiving TACE therapy,[7] with >50% 5-year patient survival rates.[5] However, HAI and TACE are limited by a number of procedural complications, which include hemorrhage, hepatic arterial occlusion, hepatic failure and sepsis.[7,9,13] Furthermore, these procedures fail to achieve therapeutic concentrations of the administered anticancer drugs in the cytoplasm of hepatic cancer cells leading to poor

therapeutic response.[8,13] In addition, leakage of the chemotherapeutic agent back into the systemic circulation leads to non-specific distribution of the drug to cardiac, neural and bone marrow tissue resulting in severe toxicities.[8,13] In particular, acute and chronic cardiomyopathy is observed in patients receiving high doses of DOX, which is the standard chemotherapeutic utilized for loco-regional chemotherapy,[8,13] resulting in impaired myocardial function in 18%-48% of patients receiving a cumulative dose of 700 mg/m^2.[14]

Sorafenib, an oral tyrosine kinase inhibitor, was recently approved in the United States as a palliative treatment for Child-Pugh class A patients with advanced HCC and compromised liver function.[15] Phase III clinical trials showed a 3-month improvement in median survival and time to progression of 10.7 months for HCC patients receiving Sorafenib versus 7.9 for the placebo group.[15] However, Sorafenib failed approval in the United Kingdom when the National Institute of Clinical Excellence stated "its effectiveness did not justify the high patient cost".[16] Despite approval of Sorafenib in the United States, standard therapeutic regimens for intermediate and advanced staged HCC patients are largely ineffectual resulting in a mean survival time of <12 months after diagnosis.[5] These results highlight the urgent clinical need for alternative targeted therapies which can selective delivery a high concentration of the chemotherapeutic agents in the cytoplasm of hepatic cancer cells while minimizing their distribution to healthy tissues to limit toxic side effects.

1.3   Nano-Therapeutics for HCC Therapy

The use of novel nanoparticles to develop HCC targeted therapies have shown promise as therapeutic platforms capable of selective delivery of loaded therapeutic molecules to liver tumor tissue while minimizing side effects. Specifically, the field of nanotechnology has allowed for engineering of bioactive nano-scale systems capable of being loaded with a high density of anticancer imaging and drug agents, while achieving preferential delivery of the therapeutic cargo to the cytoplasm of cancer cells.[17] The development of nano-therapeutics for HCC therapy have utilized a range of carrier compositions including liposomes,[18-20] micelles,[21] inorganic nanoparticles,[22,23] hydrogels,[24] and polymers[25-30] for the delivery of chemotherapeutic molecules,[22,24,31] gene agents,[32] and therapeutic proteins[33,3433] selectively to liver cancer cells *in vitro* and *in vivo*. Díez and co-workers recently published on lipopolymeric cationic micelles composed of a polymer and dioleoyloxytrimethylammonium propane (DOTAP) lipids which were loaded with 1 μg of a therapeutic interleukin 12 (IL-12) gene by either encapsulation in the micelle core or complexing it to the cationic surface.[32] Intratumoral administration of these nano-complexes to tumor-bearing mouse models prepared from subcutaneous BNL (undifferentiated murine hepatocarcinoma) xenografts resulted in 75% of treated animals showing complete tumor regression and extension of survival of up to 60 days compared to administration of free IL-12. This therapeutic effect correlated to the maximum levels of IL-12 in animal serum 14-days after administration of the gene loaded nanoparticles, while administration of the naked gene did not modulate IL-12 cytokine expression. These results highlight the ability of nanoparticle systems to increase the concentration and residence time of anticancer drugs in the systemic

circulation compared to administration of the free drug resulting in enhanced liver cancer therapeutic activity.

In addition to polymer-based micelles, inorganic silica and metallic nanoparticles have been broadly used as vehicles for selective targeting and drug delivery to hepatic cancer cells *in vitro* and *in vivo*.[22] Li et al. developed multi-layered PEGylated silica nanoparticles (SN) loaded with 32 mole% Docetaxel (Dtxl), and showed 50% release of the loaded Dtxl after 40 hours in 37°C PBS buffer.[22] *In vitro* cytotoxicity of SN-Dtxl complexes towards HepG2 cells showed a 10-fold reduction in IC_{50} values compared to an equivalent dose of the free drug. This resulted in a 2-fold reduction in tumor weight after four i.v. treatments of a 20 mg/kg equivalent dose of Dtxl to H22 subcutaneous liver tumor-bearing mice as compared to animals receiving an equivalent dose of the free drug. In 2010, the development of peptide-targeted gold nanoshells for photothermal therapy of liver cancer cells was reported in which a SN template was coated with a gold nanoshell followed by conjugation of A54 targeting peptides to the particle surface.[23] Incubation of BEL-7404 hepatic cancer cells with these therapeutic gold nanoparticles resulted in significant cancer cell apoptosis as determined by a fluorescent microscopy viability assay after exposure to near infrared light, which is absorbed by the gold nanoshells and released as heat causing thermal ablation of neighboring hepatic cancer cells. Maeng and co-workers designed theranostic iron oxide (IO) nano-particle systems encapsulating DOX molecules after intercalation of folate-targeted poly(ethylene oxide) polymer chains to produce aggregate particles for liver cancer therapy and imaging.[31] These IO complexes containing 45.6 wt% DOX had a release half-life of 24 hours at pH 5.1 in water, which translated to cytotoxicity profiles in Hep3B human hepatic cancer cells

similar to that of cells treated with free DOX after a 24 and 48 hour incubation period. Intravenous administration of these nanoparticles to liver-tumor bearing rats at a 2 mg/kg equivalent DOX dose three times at 5-day intervals led to a significant reduction in relative tumor volume compared to animals receiving an equivalent dose of free DOX. In addition, the IO-DOX formulations were better tolerated compared to administration of the free drug as determined by change in animal body weight and histological analysis of cardiac tissue.

These results show the potential of drug-loaded nanoparticles to enhance the stability, drug loading efficiency and tumor targeting of the delivered anticancer agents *in vitro* and *in vivo* leading to enhanced anticancer activity. However, these systems failed to be translated to the clinic due to issues of large scale synthesis, water solubility, lack of selective drug release and non-specific toxicity of the carrier system. To address these issues polymeric carriers have been utilized to develop targeted liver cancer therapeutics which take advantage of versatile polymer synthetic chemistries to develop monodisperse carrier compositions with high water solubility and biocompatability.[34] Consequently, polymer-based nano-therapeutics have been the only systems translated to the clinic and market for HCC therapy. One of the first to be clinically approved for treatment of HCC were poly(styrene-co-maleic acid) (SMA) polymers conjugated to the antitumor protein neocarzinostatin (NCS), known as SMANCS, developed by Maeda and co-workers in the 1980's[35,36] and brought to market in the 1990's.[37] When utilized in TACE therapy the tumor concentration of SMANCS was found to be 100-times the minimal inhibitory concentration of the free protein 2-3 months post-administration.[38] The long tumor residence time of the SMANCS nano-therapeutic system resulted in unprecedented

antitumor effect in HCC patients,[38,39] with 95% of patients showing tumor shrinkage and 86% showing decreased α-fetoprotein levels, a liver cancer diagnostic marker.[37] However, this system is administered loco-regionally to tumor tissue via TACE and therefore suffers from the invasiveness and procedural complications associated with chemoembolization. In another example, PEGylated recombinant human arginase deaminase (rhArg), which is an antimetabolite targeted at arginine, resulted in similar IC_{50} values towards HepG2 and Hep3B cells after a 72 hour incubation at $0 - 100$ U/mL concentrations, indicating the PEGylated protein retained similar toxicity to the native enzyme.[33] Barraud et al. reported the synthesis of DOX-loaded polyisohexylcyanoacrylate (PIHCA) polymeric nanoparticles intended to overcome multi-drug resistance (MDR) in hepatoma cell lines.[40] *In vitro* cytotoxicity results from this study found an approximate 1.5-fold reduction in IC_{50} values in a panel of hepatic cancer cell lines after treatment with PIHCA-DOX nanoparticles compared to equivalent concentrations of free DOX. In addition, administration of PIHCA-DOX at a single 9 mg/kg equivalent DOX dose to X/*myc* transgenic liver tumor-bearing MDR mouse models resulted in a nearly 2-fold increase in the percent of apoptotic tumor cells compared to an equivalent dose of DOX as determined by histologic TUNEL analysis. These studies highlight the ability of polymer-based therapeutics to achieve selective delivery of therapeutic agents to the cytoplasm of hepatic cancer cells, while overcoming multi-drug resistance mechanisms, leading to effective anticancer activity. In addition, these reports establish the potential of polymeric carriers to be translated to the clinic for HCC therapy. However, these systemic therapeutic systems have failed to make it to market due to poor delivery of the loaded therapeutic molecules to tumor tissue *in vivo*

due to a lack of targeting, resulting in non-specific distribution and drug release to healthy organs after i.v. administration to resulting in dose-limiting toxicities.

To address this issue attachment of sugar molecules to the polymeric carrier has been employed to target nanoparticles to the liver-specific asialoglycoprotein cell-surface receptor (ASGPR)[41] highly expressed on the surface of hepatic cancer cell,[42] which selectively binds and internalizes galactose, galactosamine (Gal) and N-acetylgalactosamine (NAcGal) sugar residues via receptor-mediated endocytosis.[41] This targeting strategy was employed in the development of Gal-targeted N-(2-hydroxypropyl) methacrylamide (HPMA)-DOX conjugates prepared by Kopecek and co-workers.[28] Gal-loaded HPMA conjugates were synthesized possessing 14-29 mole% of loaded sugar residues, and investigated for their selective targeting to hepatic cancer cells *in vitro*.[27] Results showed HPMA-Gal conjugates achieved a 20-fold greater extent of internalization into HepG2 human hepatic cancer cells compared to non-targeted controls.[27] Administration of Gal-targeted HPMA carriers to Wister rats resulted in 80%-90% of the injected dose accumulating in liver tissue 1 hour after intravenous injection.[28,43] Coupling of DOX chemotherapeutic molecules to the polymer backbone of Gal-targeted HPMA carriers was achieved via covalent attachment through glycine-phenylalinine-lysine-glycine (GFLG) oligopeptides designed to be specifically reduced by lysosomal cathepsin enzymes.[44] Results showed Gal-targeted HPMA-DOX conjugates containing 2 mole% DOX released the loaded drug molecules specifically to the cytoplasm of cancer cells after endocytosis and trafficking of the nanoparticle to the lysosome, with a release half-life of approximately 45 hours.[44] *In vitro* anticancer activity of Gal-containing HPMA-DOX conjugates showed an IC_{50} value of 3.1 µM in HepG2

cells after a 72 hour incubation, which was found to be over 300-fold less toxic compared to an equivalent concentration of free DOX under the same conditions.[26] *In vivo* biodistribution studies of Gal-targeted HPMA-DOX conjugates showed 40% of the injected dose per gram tissue weight accumulating in liver tissue of colon-carcinoma bearing rats (established as a subcutaneous metastatic liver tumor model) 24 hours after administration, while distribution to tumor tissue was 2.69% and 9.67% of the injected dose per gram of tissue at 1 and 24 hours, respectively.[45] Preclinical efficacy studies for HPMA-DOX conjugates with 2 mole% DOX loading (dosed at 2.5 – 100 mg/kg of equivalent DOX) against a panel of hematologic cancers, sarcomas and carcinoma subcutaneous tumor-bearing Sprague-Dawley rat models found an average of >50% improvement in survival time and 3-fold reduction in the percentage animals showing metastatic invasion after i.p. or i.v. administration of the conjugate versus an equivalent dose of free DOX.[46] Furthermore, *in vivo* toxicity of Gal-targeted HPMA-DOX conjugates showed a 9-fold increase in the maximum tolerated dose (MTD) and a 5-fold reduction in cardiotoxicity, as indicated by cardiac output, in a non-tumor bearing Sprague-Dawley rat model when compared to an equal dose of free DOX.[29] These results prompted phase I/II clinical evaluation of Gal-targeted HPMA-DOX conjugates (titled PK2) bearing 2.4 and 1.5 mole% of DOX and Gal, respectively, for HCC therapy.[47,48] During these studies patients received 20 – 160 mg/m^2 equivalent DOX dose of PK2 via intravenous infusion once weekly for three weeks, with dose-limiting side effects of severe fatigue, grade 4 neutropenia and grade 3 mucositits observed at the maximum tolerated dose.[48] Monitoring of left ventricular ejection fraction, a technique which screens for potential cardiomyopathy, showed no change for all patients between

initiation of the treatment and after six treatment cycles. In the same study biodistribution of PK2 after intravenous administration was assessed using gamma-camera imaging and single-photon emission computed tomography resulting in 16.9% ± 3.9% of the injected DOX dose delivered to the normal liver tissue, while only 3.3% ± 5.6% of the injected conjugate accumulated in the tumor tissue. Of the 31 enrolled patients there were three partial responses with a single patient displaying partial remissions up to 47 months after therapy.

While the ability of targeted polymer-drug conjugates to progress into clinical trials highlights the potential of these anticancer systems to deliver a high therapeutic dose of drugs to the cytoplasm of cancer cells *in vitro* and *in vivo*, the failure to translate these therapeutics to market is due to three limitations:

1. Low loading efficiencies of the targeting and drug molecules to the polymer carrier. Specifically, the HPMA-DOX (PK2) conjugates prepared for phase I/II clinical studies contained 2.4 and 1.5 mole% of DOX and Gal, respectively.[29] This Gal loading ratio is much lower than the 14-29 mole% ratios described during *in vitro* uptake studies of Gal-targeted HPMA required to achieve selective internalization of the carrier into hepatic cancer cells.[43] Furthermore, only approximately 2 DOX molecules were attached per polymer backbone likely due to steric limitations inhibiting high co-loading efficiencies of the DOX and Gal moieties to a single HPMA carrier. As a result high concentrations of the polymer were required to deliver a therapeutic dose of the loaded DOX molecules likely contributing to the systemic toxicities observed during clinical trials.

2. Poor specificity and long intracellular residence times required for drug release results in low therapeutic activity and dose limiting systemic toxicity. Kopecek's HPMA-DOX conjugates utilized lysosomal-cleavable oligopeptide linkers to attach the DOX molecules to the HPMA polymer backbone resulting in a 45 hour DOX release half-life upon incubation with cathepsin enzymes.[26] This slow drug release rate translated to a significant reduction in the anticancer activity of HPMA-DOX conjugates towards hepatic cancer cells *in vitro* versus a similar dose of the free drug, and is likely the reason for the limited therapeutic response of patients receiving the conjugate during clinical trials. Moreover, this lysosomal enzyme-mediated drug release is not selective for hepatic cancer cells and has the potential to release the loaded DOX molecules after internalization and lysosomal trafficking of the conjugates in neighboring healthy cells. As a result this is expected to be the primary cause of the dose-limiting toxicities observed during phase I/II clinical trials of HPMA-DOX conjugates.

3. Recognition and clearance of nanoparticles by liver, spleen and lungs. Specifically, administration of Gal-targeted HPMA-DOX conjugates showed a 5-fold greater accumulation of the administered dose in normal liver over the tumor tissue during clinical biodistribution studies.[48] This is likely due opsonization of the non-stealth particles after systemic administration leading to clearance by macrophages in the liver and other reticuloendothelial organs.[49] In addition, it has also been established that Kupffer cells possess a functional galactose receptor that specifically recognizes

and internalizes Gal residues spaced <20Å from the point of branching.[50] Gal-targeted HPMA polymers had an approximate 12Å spacing of the sugar moiety from the polymer backbone and therefore it is likely that Kupffer cell phagocytosis of Gal-targeted HPMA-DOX conjugates significantly contributed to non-specific distribution of the conjugate to the healthy liver tissue, thereby limiting its clinical therapeutic potential and increasing the likelihood of hepatotoxicity.

To address these limitations of PK2 and other published polymer-based anticancer agents this dissertation describes our efforts to develop targeted, enzyme-activated nano-conjugates that can deliver and release a large dose of chemotherapeutic agents selectively to the cytoplasm of hepatic cancer cells leading to high anticancer activity while avoiding non-specific toxicity to neighboring cells. Chapter 2 of this thesis describes the selection of the liver-specific azoreductase enzymes as the target for design of enzyme-sensitive chemical linkages to achieve selective drug release to the cytoplasm hepatic cancer cells. In addition, the advantages of hyperbranched dendrimer polymers as carriers of chemotherapeutic agents is discussed, with targeting strategies to achieve preferential delivery of the dendrimer carrier to liver tumor tissue and selective internalization into hepatic cancer cells presented. In chapter 3 we report the covalent attachment of DOX chemotherapeutic molecules to generation 5 (G5) of poly(amidoamine) dendrimers via aromatic azo-linkers to prepare G5-DOX nano-conjugates. We engineered these azo-linkers to be specifically recognized and cleaved by azoreductase enzymes, which provides a unique strategy to achieve cancer cell-specific release of the loaded DOX. Previous studies showed that increasing the relative

electronegativity of the azo-bond, indicated by a decrease in their Hammett constant (σ), increase their affinity to azoreductase enzymes. Therefore, we hypothesized that changing the substituents in the para and ortho positions to the azo-bond will allow us to modulate the electronegativity of the azo-linkers, control its reduction by the azoreductase enzymes, and consequently tune the kinetics of DOX release. We tested this hypothesis by synthesizing a series of four different azo-linkers (L1-L4) and incorporated them into G5-L(x)-DOX conjugates with similar DOX loading but exhibit a controlled increase in their electronegativity (i.e. lower linker σ value). We evaluated the cleavage of G5-L(x)-DOX conjugates by human liver microsomal (HLM) enzymes, S9 fractions isolated from HepG2 hepatic cancer cells and primary rat cardiomyocytes, as well as control non-enzymatic proteins. Results show G5-L1-DOX with σ of -0.44 released only 5% of the loaded DOX upon incubation with HLM enzymes. In comparison, G5-L4-DOX with σ of -1.27 released 100% of the loaded DOX molecules under the same experimental conditions. G5-L2-DOX and G5-L3-DOX conjugates with σ of -0.71 and -1.00 released 17% and 60% of the loaded DOX in the presence of HLM enzymes, respectively. These results confirm the rank order of DOX release from G5-L(x)-DOX conjugates is a function of the azo-linker electronegativity as indicated by their decreasing σ values. We evaluated the anticancer activity of G5-L(x)-DOX conjugates compared to free DOX by quantifying the fraction of surviving HepG2 human hepatic cancer cells as a function of conjugate's concentration. Results show that IC_{50} of free DOX in HepG2 was 10nM, while G5-L1-DOX, G5-L2-DOX, G5-L3-DOX and G5-L4-DOX conjugates achieved an IC_{50} of 12,303nM, 2,042nM, 158nM and 13nM, respectively. These results confirm that increasing the DOX release rate from G5-L(x)-

DOX conjugates by decreasing the azo-linker σ values results in a matching rank order of conjugate cytotoxicity towards hepatic cancer cells. Selective DOX release from G5-L(x)-DOX conjugates due to azoreductase activation was confirmed with limited DOX release in the presence of control proteins and cardiomyocytes S9 enzymes, and as a result G5-L4-DOX conjugates were non-toxic towards cardiac cells. Chapter 4 of this dissertation describes coupling of the liver-specific N-acetylgalactosamine (NAcGal) sugar to the surface of G5 dendrimers to achieve cell-specific delivery to hepatic cancer cells. These G5-NAcGal conjugates were prepared through a short peptide-bond or longer thiourea linkage, and evaluated for their internalization into HepG2 human hepatic cancer cells as a function of spacer length, particle concentration and incubation time. Results show G5-NAcGal conjugates bound to the ASGPR expressed specifically on the surface of liver cells resulting in rapid receptor-mediated endocytosis of the conjugates selectively into hepatic cancer cells, with enhanced receptor recognition achieved for G5-NAcGal carriers incorporating the longer thiourea-linker. In chapter 5 we evaluate the *in vivo* biodistribution of G5-NAcGal carriers prepared via thiourea-linkers in a liver-tumor bearing mouse model. Results showed a 2-fold increase in tumor-specific distribution of G5-NAcGal carriers versus the parent G5 dendrimers after 48 hours, while >50% of the injected dose accumulated in normal healthy liver tissue under the same conditions. Functionalization of G5 dendrimers with poly(ethylene glycol) (PEG) polymers substantially reduced accumulation of the carrier in the liver, but was also accompanied by poor retention of G5-PEG in tumor tissue due to lack of targeting. Based on these results a second generation targeted G5-PEG carrier was synthesized by coupling the targeting ligand to the free end of 2kDa PEG chains immobilized on the surface of the G5

carrier through an acid-sensitive cis-aconityl (*c*) linkage to achieve hepatic cancer cell specific delivery of targeted G5-(*c*PEG) carriers while avoiding particle internalization into normal liver macrophage Kupffer cells and hepatocytes. G5-(*c*PEG[NAcGal]) carriers were prepared with NAcGal ligands in the α- and β-sugar conformation and incubated with HepG2 hepatic cancer cells to determine the effect of sugar conformation on cancer cell internalization as a function of ligand concentration and incubation time. Results confirmed G5-(*c*PEG[NAcGal$_\beta$]) conjugates were rapidly internalized into HepG2 cells while NAcGal$_\alpha$-targeted carriers were not, confirming G5-(*c*PEG[NAcGal$_\beta$]) conjugates are endocytosed into hepatic cancer cells via the ASGPR which shows selective affinity towards β-sugars. This internalization profile was compared to the uptake of G5-(*c*PEG[SP94]) into HepG2 cells, incorporating the hepatic cancer-specific SP94 peptide, which showed a much slower internalization rate of SP94-targeted carriers versus G5-(*c*PEG[NAcGal$_\beta$]) conjugates. We then confirmed that PEGylation of G5 dendrimers resulted in reduced particle phagocytosis by isolated mouse liver macrophage Kupffer cells, which is due to limited carrier opsonization as determined by a bovine serum albumin binding assay. Finally, minimal uptake of G5-(*c*PEG[NAcGal$_\beta$]) conjugates into normal rat hepatocytes confirmed that these carriers achieve cell-specific delivery to hepatic cancer cells while avoiding internalization into neighboring healthy liver cells. Chapter 6 discusses the conclusion of this research work and proposes future work to advance the developed targeted, enzyme-activated nano-conjugates to preclinical and clinical studies.

References

1   Bosch, F. X., Ribes, J., Díaz, M. & Cléries, R. Primary liver cancer: worldwide incidence and trends. *Gastroenterology* **127**, S5-S16 (2004).

2   ACS. Vol. . (American Cancer Society, Atlanta, 2011).

3   NCI. (ed USDHHS) (National Cancer Institute, 2011).

4   Tang, Z.-Y. Hepatocellular carcinoma-cause, treatment and metastasis. *World J. Gastroentero.* **7**, 445-454 (2001).

5   El-Serag, H. B., Marrero, J. A., Rudolph, L. & Reddy, K. R. Diagnosis and treatment of hepatocellular carcinoma. *Gastroenterology* **134**, 1752-1763 (2008).

6   Bruix, J. & Sherman, M. Management of hepatocellular carcinoma. *Hepatology* **42**, 1208-1236 (2005).

7   Llovet, J. M. & Bruix, J. Systematic review of randomized trials for unresectable hepatocellular carcinoma: chemoembolization improves survival. *Hepatology* **37**, 429-442 (2003).

8   Kettenbach, J. *et al.* Drug-loaded microspheres for the treatment of liver cancer: review of current results. *Cardiovasc. Inter. Rad.* **31**, 468-476 (2008).

9   Livraghi, T. Radiofrequency ablation, PEIT, and TACE for hepatocellular carcinoma. *J. Hepato.-Biliary-Pan.* **10**, 67-76 (2003).

10   Blum, H. E. Treatment of hepatocellular carcinoma. *Best Pract. Res. Cl. Ga.* **19**, 129-145 (2005).

11   Skitzki, J. J. & Chang, A. E. Hepatic artery chemotherapy for colorectal liver metastases: technical considerations and review of clinical trials. *Surg. Oncol.* **11**, 123-135 (2002).

12   Vogl, T. J. *et al.* Review on transarterial chemoembolization in hepatocellular carcinoma: Palliative, combined, neoadjuvant, bridging, and symptomatic indications. *Eur. J. Radiol.* **72**, 505-516 (2009).

13   Barnett, K. & Malafa, M. Complications of hepatic artery infusion. *Int. J. Gastro. Cancer* **30**, 147-160 (2001).

14   Curigliano, G., Mayer, E. L., Burstein, H. J., Winer, E. P. & Goldhirsch, A. Cardiac toxicity from systemic cancer therapy: a comprehensive review. *Prog. Cardiovasc. Dis.* **53**, 94-104 (2010).

15   Keating, G. M. & Santoro, A. Sorafenib: a review of its use in advanced hepatocellular carcinoma. *Drugs* **69** (2009).

16   NICE rules against liver cancer drug sorafenib. *Cancer News* (2009).

17   Wang, X., Yang, L., Chen, Z. & Shin, D. M. Application of nanotechnology in cancer therapy and imaging. *CA-Cancer J. Clin.* **58**, 97-110 (2008).

18   Lian, T. & Ho, R. J. Y. Trends and developments in liposome drug delivery systems. *J. Pharm. Sci.* **90**, 667-680 (2001).

19   Papagiannaros, A., Dimas, K., Papaioannou, G. T. & Demetzos, C. Doxorubicin-PAMAM dendrimer complex attached to liposomes: cytotoxic studies against human cancer cell lines. *Int. J. Pharm.* **302**, 29 (2005).

20   Wang, S. L. *et al.* Design and synthesis of novel galactosylated polymers for liposomes as gene drug carriers targeting the hepatic asialoglycoprotein receptor. *J. Drug Target.* **16**, 233-242 (2008).

21 Kataoka, K., Harada, A. & Nagasaki, Y. Block copolymer micelles for drug delivery: design, characterization and biological significance. *Adv. Drug Deliver. Rev.* **47**, 113-131 (2001).

22 Li, L. *et al.* In vivo delivery of silica nanorattle encapsulated docetaxel for liver cancer therapy with low toxicity and high efficacy. *ACS Nano* **4**, 6874-6882 (2010).

23 Liu, S.-Y., Liang, Z.-S., Gao, F., Luo, S.-F. & Lu, G.-Q. In vitro photothermal study of gold nanoshells functionalized with small targeting peptides to liver cancer cells. *J. Mater. Sci.* **21**, 665-674 (2010).

24 Na, K., Park, K.-H., Kim, S. W. & Bae, Y. H. Self-assembled hydrogel nanoparticles from curdlan derivatives: characterization, anti-cancer drug release and interaction with a hepatoma cell line (HepG2). *J. Control. Release* **69**, 225-236 (2000).

25 Choi, J. S., Lee, E. J., Choi, Y. H., Jeong, Y. J. & Park, J. S. Poly(ethylene glycol)-*block*-(poly(L-lysine) dendrimer: novel linear polymer/dendrimer block copolymer forming a spherical water-soluble polyionic complex with DNA. *Bioconjugate Chem.* **10**, 62 (1999).

26 David, A., Kopečková, P., Minko, T., Rubinstein, A. & Kopeček, J. Design of a multivalent galactoside ligand for selective targeting of HPMA copolymer–doxorubicin conjugates to human colon cancer cells. *Eur. J. Cancer* **40**, 148-157 (2004).

27 David, A., Kopečková, P., Rubinstein, A. & Kopeček, J. Enhanced biorecognition and internalization of HPMA copolymers containing multiple or multivalent carbohydrate side-chains by human hepatocarcinoma cells. *Bioconjugate Chem.* **12**, 890-899 (2001).

28 Duncan, R., Kopeček, J., Rejmanová, P. & Lloyd, J. B. Targeting of N-(2-hydroxypropyl)methacrylamide copolymers to liver by incorporation of galactose residues. *BBA-Gen. Subjects* **755**, 518-521 (1983).

29 Hopewell, J. W., Duncan, R., Wilding, D. & Chakrabarti, K. Preclinical evaluation of the cardiotoxicity of PK2: a novel HPMA copolymer–doxorubicin–galactosamine conjugate antitumour agent. *Hum. Exp. Toxicol.* **20**, 461-470 (2001).

30 Veronese, F. M. *et al.* PEG−doxorubicin conjugates: influence of polymer structure on drug release, in vitro cytotoxicity, biodistribution, and antitumor activity. *Bioconjugate Chem.* **16**, 775-784 (2005).

31 Maeng, J. H. *et al.* Multifunctional doxorubicin loaded superparamagnetic iron oxide nanoparticles for chemotherapy and magnetic resonance imaging in liver cancer. *Biomaterials* **31**, 4995-5006 (2010).

32 Díez, S., Navarro, G. & de Ilarduya, C. T. In vivo targeted gene delivery by cationic nanoparticles for treatment of hepatocellular carcinoma. *J. Gene. Med.* **11**, 38-45 (2009).

33 Tsui, S.-M. *et al.* Pegylated derivatives of recombinant human arginase (rhArg1) for sustained in vivo activity in cancer therapy: preparation, characterization and analysis of their pharmacodynamics in vivo and in vitro and action upon hepatocellular carcinoma cell (HCC). *Cancer Cell Int.* **9**, 9 (2009).

34 Duncan, R. The dawning era of polymer therapeutics. *Nat. Rev. Drug. Discov.* **2**, 347-360 (2003).

35   Maeda, H., Ueda, M., Morinaga, T. & Matsumoto, T. Conjugation of poly(styrene-co-maleic acid) derivatives to the antitumor protein neocarzinostatin: pronounced improvements in pharmacological properties. *J. Med. Chem.* **28**, 455-461 (1985).

36   Maeda, H. SMANCS and polymer-conjugated macromolecular drugs: advantages in cancer chemotherapy. *Adv. Drug Deliver. Rev.* **46**, 169-185 (2001).

37   Vicent, M. J. & Duncan, R. Polymer conjugates: nanosized medicines for treating cancer. *Trends Biotechnol.* **24**, 39-47 (2006).

38   Greish, K., Fang, J., Inutsuka, T., Nagamitsu, A. & Maeda, H. Macromolecular therapeutics: advantages and prospects with special emphasis on solid tumour Targeting. *Clin. Pharmacokinet.* **42**, 1089-1105 (2003).

39   Blanco, E., Kessinger, C. W., Sumer, B. D. & Gao, J. Multifunctional micellar nanomedicine for cancer therapy. *Exp. Biol. M.* **234**, 123-131 (2009).

40   Barraud, L. *et al.* Increase of doxorubicin sensitivity by doxorubicin-loading into nanoparticles for hepatocellular carcinoma cells in vitro and in vivo. *J. Hepatol.* **42**, 736-743 (2005).

41   Stockert, R. J. The asialoglycoprotein receptor: relationships between structure, function, and expression. *Physiol. Rev.* **75**, 591-609 (1995).

42   Schwartz, A. L., Fridovich, S. E., Knowles, B. B. & Lodish, H. F. Characterization of the asialoglycoprotein receptor in a continuous hepatoma line. *J. Biol. Chem.* **256**, 8878-8881 (1981).

43   Duncan, R. *et al.* Fate of N-(2-hydroxypropyl)methacrylamide copolymers with pendent galactosamine residues after intravenous administration to rats. *BBA-Gen. Subjects* **880**, 62-71 (1986).

44   Tang, A., Kopečková, P. & Kopeček, J. Binding and cytotoxicity of HPMA copolymer conjugates to lymphocytes mediated by receptor-binding epitopes. *Pharm. Res.* **20**, 360-367 (2003).

45   Pimm, M. V., Perkins, A. C., Strohalm, J., Ulbrich, K. & Duncan, R. Gamma scintigraphy of a 123I-labelled N-(2-hydroxypropyl)methacrylamide copolymer-doxorubicin conjugate containing galactosamine following intravenous administration to nude mice bearing hepatic human colon carcinoma. *J. Drug Target.* **3**, 385-390 (1996).

46   Duncan, R. *et al.* Preclinical evaluation of polymer-bound doxorubicin. *J. Control. Release* **19**, 331-346 (1992).

47   Li, C. & Wallace, S. Polymer-drug conjugates: recent development in clinical oncology. *Adv. Drug Deliver. Rev.* **60**, 886-898 (2008).

48   Seymour, L. W. *et al.* Hepatic drug targeting: phase I evaluation of polymer-bound doxorubicin. *J. Clin. Oncol.* **20**, 1668-1676 (2002).

49   Owens III, D. E. & Peppas, N. A. Opsonization, biodistribution, and pharmacokinetics of polymeric nanoparticles. *Int. J. Pharm.* **307**, 93-102 (2006).

50   Popielarski, S. R., Hu-Lieskovan, S., French, S. W., Triche, T. J. & Davis, M. E. A nanoparticle-based model delivery system to guide the rational design of gene delivery to the liver. 2. In vitro and in vivo uptake results. *Bioconjugate Chem.* **16**, 1071-1080 (2005).

Chapter 2

Background

2.1 Rationale and Design of Azoreductase-Cleavable Azo-Linkers for Hepatic Cancer Cell Specific DOX Release from G5-DOX Conjugates

2.1.1 Liver-specific Azoreductase Enzyme and Azo-substrate Structure-Activity

Since the 1970's azo-compounds, which are organic molecules characterized by a nitrogen-nitrogen double bond, have been used extensively as colorants in pharmaceuticals, textiles and printing.[1] Metabolic reduction of azobenzene dyes has been found to be catalyzed selectively by the liver-specific azoreductase enzymes through a Nicotinamide adenine dinucleotide phosphate (NADPH)-mediated two-electron reduction.[1,2] The biotransformation of azo-compounds in liver microsomes has been extensively studied by Zbaida et al. resulting in the publication of structure-activity relationships for azobenzenes (**Figure 2.1**) as they relate to affinity of the liver-specific azoreductase enzyme and reduction kinetics.[1] These studies showed reduction of azo dyes requires polar electron-donating substituents (e.g. hydroxyl or amine) *ortho* and/or *para* to the azo-bond (**Figure 2.1, X** & **Y** on ring **A**) for azoreductase binding and reduction.[2,3] Furthermore, it was found that electron-withdrawing groups on the opposite ring (**Figure**

2.1, Z on ring **B**) alters the redox potential of the azo-bond and subsequently changes the rate and mechanism of reduction.[4] This resulted in categorization of azobenzene molecules found to be substrates for the azoreductase enzymes as either insensitive (I-substrates) or sensitive

Figure 2.1: General chemical structure for an azobenzene substrate of the liver-specific azoreductase enzyme with chemical substituents **X,Y** and **Z**.
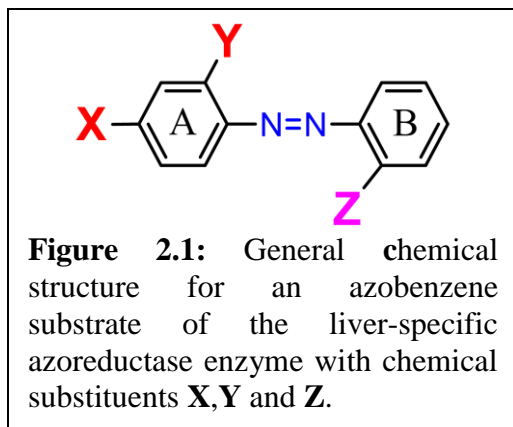
(S-substrates) to oxygen and carbon monoxide.[1] I-substrates contain only polar electron donating substituents on the azobenzenes structure (**Figure 2.1, X** & **Y** on ring **A**), while S-substrates have both electron-donating and electron-withdrawing substituents on opposite benzene rings.

A series of mechanistic studies by Zbaida and co-workers elucidated the mechanism of binding and reduction of substrate azobenzenes by the azoreductase enzymes (**Figure 2.2**).[2,4,5] Results from this work showed that azoreductase enzyme binding to the azo-substrate (**Figure 2.2**, **A**) initiates addition of an electron pair from NADPH to the complex (**Figure 2.2**, **B**). This is followed by addition of a second electron pair from the non-bonding electrons of the electron-withdrawing substituents (**Figure 2.2**, **C**). Dissociable protons from water form the unstable hydrazo intermediate (**Figure 2.2**, **D**) leading to cleavage of the bond to produce the corresponding amines (**Figure 2.2**, **E**). Zbaida also showed that S-substrates stabilize the 1e$^-$ intermediate, formed after electron donation from NADPH, long enough to allow interaction with molecular oxygen converting the azobenzene back to the parent azo-dye (**Figure 2.2**, **F**).

Figure 2.2: Mechanism of binding and reduction of azobenzenes (X-N=N-X) by the liver-specific azoreductase enzymes. After binding of the azoreductase enzyme to the azo-substrate (**A**) it catalyzes the addition of an electron pair from NADPH to the complex (**B**), followed by the addition of a second electron from the non-bonding electrons on the polar substituents (**C**). Dissociable protons from water form the unstable hydrazo intermediate (**D**) leading to cleavage of the bond to produce the corresponding amines (**E**). S-substrates stabilize the 1e⁻ intermediate (**B**) long enough to allow interaction with molecular oxygen to convert back to the parent azo-dye (**F**).

2.1.2 Dependence of Hammett Substituent Constant (σ) on Azobenzene Reduction Kinetics

Zbaida's mechanistic work on azobenzene reduction by azoreductase enzymes also showed kinetics of their reduction correlated to the electron donating properties of the chemical substituents present in the *para* (**X**) or *ortho* (**Y**) positions to the substrate azo-bond (**Figure 2.1**).[6] Calculating the relative electron donating potential for each substituent on different azo-dyes is based on the published values of the Hammett constant (σ).[6,7] This value is obtained from the Hammett equation published by Louis Plack Hammett in 1937,[6] which describes the free-energy relation between reaction rates and equilibrium constants for benzoic acid derivatives.[6] Specifically, this relationship describes the linear correlation of ionization rates for an un-substituted benzoic acid to *para-* and *meta*-substituted compounds at 25°C in water. The effect of each chemical substituent is then related to the reaction rate by a Hammett σ value. Utilizing published libraries of substituent σ values Zbaida calculated the total σ value of each azobenzene substrate by summing the contribution of each substituent on the azo-dye, and found that that azobenzenes with a cumulative σ ≤ -0.37 are substrates for the azoreductase enzymes and their reduction rate increases with the decrease in σ value below this threshold.[1,3]

2.1.3 Design of Enzyme-Activated Azo-Linkers to Develop G5-DOX Nano-Conjugates with Tunable Drug Release

Utilizing the azobenzene structure as a nucleus we designed a library of azo-linkers with varied oxygen or nitrogen substitutions in the electron-donating substituent positions (**Figure 2.1, X** & **Y** on ring **A**) to control linker σ value. Furthermore, we designed I-substrate azo-linkers with only electron-donating groups, while avoiding electron-withdrawing groups of S-substrates which lead to their sensitivity to the molecular oxygen abundant in aerobic physiologic environments. We replaced the benzyl moiety of ring B (**Figure 2.1**) with toluene to incorporate a 1'6 self-eliminating spacer in the linker composition (**Figure 2.3**), which will undergo a spontaneous electron cascade

Figure 2.3: General **c**hemical structure for G5-DOX conjugates incorporating azoreductase-cleavable azo-linkers. After reduction of the azo-bond (blue) to amines by azoreductase a rapid electronic cascade eliminates ring B, and the carbon-dioxide by-product, resulting in release of free DOX.
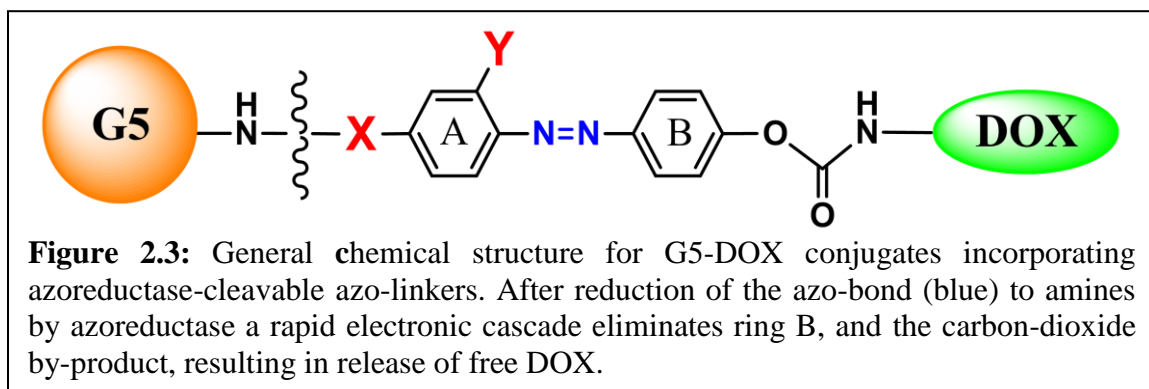
to allow for release of the free drug after reduction of the azo-bond by the azoreductase enzyme. Self immolative 1'6-elimination of benzyl compounds bearing *ortho* or *para* electron-donating groups were first described in 1981 by Carl et al.,[8] and since then they have been utilized broadly in pro-drug and polymeric drug delivery systems for rapid, triggerable drug release.[9-11] As a result this 1'6 self-eliminating spacer will release "clean" DOX molecules without any hanging "linker debris" that may diminish its anticancer activity after reduction of the azo-linker. To deliver these DOX molecules to liver tumor tissue azo-DOX was coupled to generation 5 (G5) of PAMAM dendrimers to

prepare G5-DOX nano-conjugates. This strategy allowed for the coupling of a large number of DOX molecules to a single polymer carrier due to the high density of amine groups present on the surface of PAMAM dendrimers. The high drug loading capacity of dendrimers has been exploited previously for the delivery of chemotherapeutic agents to cancer cells.

2.2   Dendrimers as Effective Drug Delivery Carriers

Dendrimers are a family of nano-sized, three-dimensional polymers characterized by a unique tree-like branching architecture and compact spherical geometry in solution. Their name is derived from the Greek word "dendron" which means "tree" and refers to the distinctive organization of polymer units. Research into the development of dendrimers started in the 1970's by Vogtle and co-workers who studied the controlled synthesis of dendritic arms by repetitive reactions of mono- and di-amines with a central core to produce polymeric branching units with large molecular cavities.[12] It wasn't until 1984 that the first family of hyperbranched polymers was developed by Tomalia and his team, who described the iterative coupling of ethylene diamine to a central ammonia

Figure 2.4: Cross section of a G2 dendrimer showing their characteristic tree-like branching architecture where each monomer unit is added to a branching point to yield a spherical polymer with a large number of surface groups. Each successive layer of branching units constitutes a new generation (G) with a specific number in the dendrimer series.

27
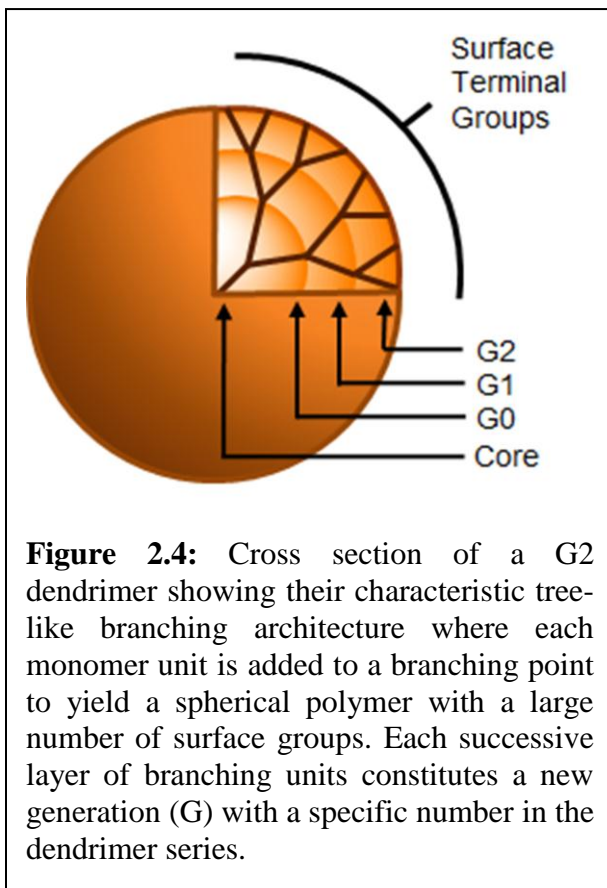
core to produce series of branched macromolecules named "starburst dendrimers".[13] Dendrimers are composed of individual "wedges" or dendrons that radiate from a central core where each layer of concentric branching units constitutes one complete generation (G) in the dendrimer series and identified with a specific generation number (**Figure 2.4**).[14] This branching architecture leads to a controlled incremental increase in dendrimer's molecular weight, size and number of surface functional groups. As a result dendritic polymers have emerged as promising scaffolds for drug delivery due to their multivalency allowing for the attachment of a large number of drug molecules and solubilizing groups.[15] Over the past three decades, several synthetic strategies were developed to generate multiple dendrimers' families with versatile chemical compositions and spherical architectures allowing for successful use of dendritic systems for the development of vaccine, antiviral and anticancer therapeutics.[15-17]

2.2.1 Potential of Dendrimers in Cancer Therapy

Dendrimers are particularly well suited for the delivery of anticancer drugs and imaging agents[15,18,19] due to their high water solubility,[20-22] monodisperse size, and uniform composition,[23] which leads to consistent batch-to-batch anticancer activity of dendrimers-based drug delivery systems.[24] In addition, dendrimer's unique branching architecture and high number of functional groups present on the surface can be utilized to either encapsulate[25] or directly conjugate[18,26] large payloads of therapeutic molecules that will be shuttled to the cytoplasm of cancer cells.[27,28] Cellular uptake of dendrimers-based drug delivery systems proved to be significantly higher than linear polymeric carriers such as N-(2-hydroxypropyl)methacrylamide (HPMA)[29-31] and PEG,[32,33] which

can be attributed to dendrimers' nano size and compact spherical geometry in solution. For example, Jelinkova *et al.* compared the toxic effect of antibody-targeted, linear and branched HPMA-DOX conjugates on T-cell lymphoma and human colorectal carcinoma cell lines.[29] Branched HPMA polymers incorporated an equal weight % of DOX at approximately half the molecular weight of the linear HPMA carrier while simultaneously displaying 1.5-2 folds the weight % of the targeting antibody. These branched HPMA-DOX conjugates were 3-11 fold more toxic towards both cancer cell lines compared to linear HPMA-DOX conjugates.[29] Furthermore, branched HPMA-DOX conjugates produced a significant increase in the plasma residence time of the incorporated DOX compared to linear HPMA-DOX conjugates at late time points (12-48 hours) after a single intravenous injection of each conjugate into male Balb/c mice.[29] Another study by Minko and co-workers compared the anticancer activity of G4-Paclitaxel (TAX) conjugates to linear PEG-TAX carrying an equal amount of TAX against ovarian carcinoma cells showed that G4-TAX conjugates were 10-fold more toxic compared to free TAX whereas PEG-TAX conjugates were 25-fold less toxic than the free drug.[32] Minko and co-workers also compared the anticancer activity of peptide-targeted stealth liposomes that encapsulate an equal amount of TAX to that incorporated in targeted G4-TAX and targeted linear PEG-TAX conjugates against human lung cancer cells.[34] These three formulations showed similar *in vitro* cytotoxic effect and reduction in tumor size *in vivo*. However, G4-TAX conjugates displayed the highest tumor to liver accumulation ratio, which indicate their preferential distribution to tumor tissue and the ability to escape recognition by the RES system. In addition, the covalent bonding of dendrimers' branching structure yields more stable carriers that withstand physiological

conditions compared to liposomes and amphiphilic particles, which undergo rapid dissociation that results in non-specific drug release.[17,35] In addition, dendritic carriers have been shown to improve the therapeutic activity of the incorporated anticancer drugs against normal and resistant cancer cells.[36,37] For example, one study compared the anticancer activity of the drug Methotrexate (MTX) when conjugated to a dendrimer carrier on sensitive and resistant human acute lymphoblastoid leukemia cell lines, which showed that dendrimer-MTX conjugates are 8-fold more cytotoxic toward resistant cells than free MTX drug at similar concentrations.[37] These studies collectively indicate that dendrimers-based drug delivery systems are more potent in delivering anticancer drugs compared to their linear counterparts due to favorable internalization kinetics and efficient escape into the cytoplasm of the targeted cells.

2.2.2   Mechanisms of Drug Loading onto Dendrimer Carriers

2.2.2.1 Physical Encapsulation of Drug Molecules

The work of Vogtle and co-workers, who looked at entrapment of guest molecules into branched polymers,[12] represents an earlier form of physical encapsulation of poorly soluble drug molecules in dendrimer's voids to improve their aqueous solubility and control their release profile (**Figure 2.5**).[38-43] Inclusion of hydrophobic molecules into dendrimers is typically accomplished by simple mixing of the polymer and drug solutions where the hydrophobic drug associates with the non-polar core through hydrophobic interactions.[38-41] As a result of this physical interface between the guest molecules and the dendrimer carrier, release of the encapsulated molecules in an aqueous

environment is passively controlled by a range of non-covalent interactions including hydrophobic forces, hydrogen bonding, steric hindrance, and electrostatic interactions. To maximize the loading capacity of drug molecules within the dendrimer one has to carefully consider polymer architecture, specifically the characteristics of the internal voids. Initial computational and

Figure 2.5: Drawing of a dendrimer carrier encapsulating hydrophobic drug molecules in the dendrimers voids to increase their aqueous solubility and control their release rate.

experimental studies by Goddard and Tomalia showed that G1-G3 β-alanine dendrimers exhibit an oblong open structure while G4 and higher generations possess a densely packed surface that is necessary to produce enclosed internal voids that can effectively encapsulate and retain guest molecules.[25,41] Spin-lattice relaxation profiles of acetyl salicyclic acid and 2,4-dichlorophenoxy acetic acid encapsulated within a dendritic carrier displayed a decline in carbon-13 relaxation time with increasing dendrimer's generation number from G0.5 – G5.5 thus indicating the shielding of the guest molecules in the polymer network. These findings set the stage for development of different inclusion complexes where dendrimers can encapsulate hydrophobic anticancer drugs to improve their aqueous solubility, control their release rates, and achieve cancer therapy.

Kojima *et al.* reported the encapsulation of DOX and MTX anticancer drugs in PEGylated G3-NH$_2$ and G4-NH$_2$ dendrimers with a maximum DOX and MTX encapsulation efficiency of 6.5 and 25 mole/mole dendrimer, respectively.[40] The

encapsulation efficiency of both drugs appeared to increase with the increase in dendrimer's generation number and the increase in the molecular weight of the surface bound PEG chains from 550 Da to 2 kDa. These results were further supported by another study that compared the *in vitro* and *in vivo* release of 5-Fluorouracil (5FU) encapsulated in non-PEGylated G4-NH$_2$ dendrimers and PEGylated ones displaying 25% capping of the surface groups using 5 kDa PEG chains.[42] The *in vitro* data indicates that the PEGylated dendrimers show 12-fold higher loading capacity and 6-fold slower release of 5FU drug molecules compared to non-PEGylated dendrimers with complete drug release from the PEGylated carriers in 6 days.[42] Furthermore, intravenous administration of PAMAM-5FU complexes (1000 µg 5FU equivalent) to albino rats showed that the residence time of 5FU in the systemic circulation achieved by the PEGylated complexes was 3 times longer than the non-PEGylated derivatives.[42] These results indicate that the attachment of PEG chains to the dendrimer's surface not only slows down the release of the encapsulated drug but also modulates the conformation of the internal voids thereby improving drug loading efficiency.

Similarly, another study showed that MTX encapsulation into G2 polyether-copolyester (PEPE) dendrimers improved when PEG chains (200 – 400 Da) were present in the internal cavities and increased with the increase in PEG molecular weight.[44] However, attachment of four glucosamine molecules to the dendrimer's surface decreased the encapsulation of MTX molecules.[44] As expected, PEGylation improved MTX loading (20.3-24.5 mg MTX/mg dendrimer) and slowed its release through PEG steric effects, whereas attachment of glucosamine ligands to the dendrimers led to a 10%-15% decline in MTX encapsulation, which is possibly due to folding of the conjugated

glucosamine molecules into the dendritic structure causing congestion of the dendrimer's surface and limiting the penetration of the MTX molecules.

Despite these improvements in the encapsulation and retention of molecules into PEGylated dendrimers, sustained and controlled release of the encapsulated molecules in physiological solutions remains hard to achieve. For example, MTX molecules loaded into PEGylated dendrimers are released 10 times faster in isotonic Tris buffer containing 150 mM NaCl solution compared to non-isotonic Tris buffer.[40] Similarly, Baker and co-workers reported 70% release of the MTX loaded into G5-MTX inclusion complexes upon incubation for 2.5 hours in phosphate buffered saline (PBS) compared to insignificant MTX release in water under the same experimental conditions.[39] Grinstaff and co-workers also reported the release of 90% of the anticancer drug 10-hydroxy-captothecin (10HCPT) loaded into G4.5 PGLSA dendrimers upon incubation for 2.5 hours in PBS.[38] It is important to note that PEPE-MTX[44] and poly(glycerol succinic acid) (PGLSA)-10HPCT[45] inclusion complexes exhibited 10 and 4-fold higher cytotoxicity against cancer cells compared to equal concentrations of the free drug, respectively. However, this enhanced anticancer activity is simply a result of rapid bolus release of the encapsulated drug due to the interaction of the buffer salts with the dendrimers thus weakening of the ionic forces "holding" the loaded drug, which will happen *in vivo* upon administration of these inclusion complexes resulting in premature drug release into the systemic circulation causing non-specific toxicity.

One approach to control the rate of drug release from the inclusion complexes is to encapsulate them in a liposomal envelope forming Modulatory Liposomal Controlled Release Systems (MLCRS).[46] DOX was the drug used in this hybrid system where 3.7

33

moles of DOX were loaded per 1 mole of G4-NH$_2$ dendrimers. In this study, TES buffer (pH 7.5) resulted in 96.6% loading of the added DOX compared to 68.9% DOX loading in acetate buffer (pH 4.5), which is possibly due to the limited electrostatic repulsion between the cationic dendrimers and ionized DOX molecules at pH 4.5. Incubation of MLCRS in RPMI cell culture medium at 37ºC for 48 hours resulted in release of 12% of the loaded DOX, which is a significant improvement compared to the observed rapid drug release with the conventional inclusion complexes. These studies collectively show that loading of therapeutic molecules into different dendrimers depend on dendrimer generation number, internal composition, net surface charge, and type and degree of functionalization of surface groups. These parameters affect the volume of the internal voids and the physical interactions between guest molecules and the dendrimers core, thus controlling the degree of drug loading and the associated release kinetics. Nevertheless, the issue of rapid drug release from dendrimer-based inclusion complexes remains a significant challenge. While liposomal encapsulated complexes seem promising in terms of controlling the release rates of the encapsulated drugs, their activity against different tumors need to be further evaluated both *in vitro* and *in vivo*.

2.2.2.2 Chemical Conjugation of Drug Molecules

Covalent conjugation of anticancer drugs to dendrimer's surface groups has been used to achieve controlled spatial and temporal release of the attached drugs (**Figure 2.6**). The large number of dendrimers' surface groups and the versatility in their chemical structures allow the conjugation of different anticancer drugs, imaging agents, and/or targeting ligands while maintaining the dendrimer's compact spherical geometry in

34

solution. These dendrimer-drug conjugates have been prepared through a variety of non-cleavable and cleavable chemical linkages.

Direct Coupling

In early 1990's Barth and co-workers conjugated boronated monoclonal antibodies to a dendrimer carrier via stable urea linkages and utilized this conjugate for neutron capture therapy where localized neutron

Figure 2.6: A schematic drawing showing a dendrimer-drug conjugate where the drug molecules (red ovals) are either directly coupled (solid lines) or via a pH-sensitive linkage (blue rectangle) to dendrimers' surface groups.
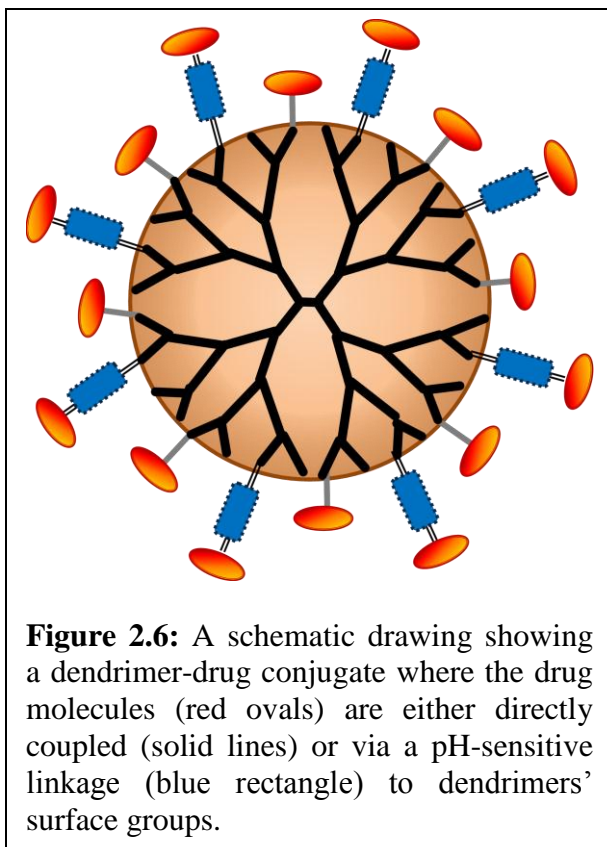
ionization would cause necrosis of neighboring cancer cells.[47,48] This conjugate achieved high loading capacities of 250-1000 boron atoms per G4 dendrimer while retaining 82% of the antibodies activity *in vitro*. A few years later, Duncan and co-workers reported the coupling of cisplatin (Pt), a hydrophobic DNA intercalating agent, to G3.5 PAMAM dendrimers via an ester linkage.[49] PAMAM-Pt conjugates carried 20-25 weight % platinum exhibiting 10-fold higher aqueous solubility compared to free Pt and displayed great stability (<1% Pt release) upon incubation in PBS (pH 7.4) and citrate buffers (pH 5.5) at 37 ℃ for 72 hours.[49] Despite the high aqueous solubility and stability of these conjugates, they failed to produce the desired anticancer activity due to limited drug release. Specifically, PAMAM-Pt conjugates displayed insignificant toxicity towards three cancer cells lines when treated with $0.1 \times 10^{-5} - 0.01$ mg/mL Pt equivalent for 72

hours.[49] Similarly, PAMAM-DOX conjugates exhibited 5-fold lower toxicity towards HeLa cells upon incubation with 0.001 – 1000 μM DOX equivalent for 24 hours compared to free DOX, which is a result of insignificant drug release (< 5% of DOX is released upon incubation in PBS solution for 24 hours).[50] These observations were further supported by a separate evaluation of the *in vitro* and *in vivo* activity of amide-linked PAMAM-MTX conjugates where results showed that PAMAM-MTX has 2.7 log units higher IC_{50} values on glioma cells compared to free MTX *in vitro* and there was no increase in the survival rate of glioma-bearing rats receiving the PAMAM-MTX conjugates compared to those receiving an equal dose of free MTX.[45] Other classes of therapeutic molecules including Che6 and DOX anticancer drugs,[51-53] natural curcumin derivatives,[54] BH3 pro-apoptotic peptide[55] and photosensitizing agents[56,57] were coupled to a dendritic carrier, which significantly increased the solubility of the loaded drug, however the associated *in vitro* and *in vivo* anticancer activity markedly decreased due to limited release of the loaded drug.

Studies also showed that the conformation of the anticancer drug molecules displayed on the dendrimer's surface is a critical design parameter for retention of their cytotoxic activity. Gurdag *et al.* compared the anticancer activity of MTX when coupled through its amine group to the carboxylic acid surface groups of G2.5-COOH dendrimers forming stable amide linkages versus MTX coupling through its carboxylic group to the primary amine groups of G3-NH_2 dendrimers.[37] Results showed that G2.5-MTX conjugates were 3-fold more cytotoxic compared to free MTX towards lymphoblastic leukemia cells, whereas G3-MTX conjugates were 10-fold less toxic than the free MTX. Similarly, Baker and co-workers compared the *in vitro* anticancer activity of G5-OH and

G5-NH$_2$ conjugates with MTX attached via ester and amide linkages, respectively.[58] Incubation of ester-linked G5-MTX conjugates with KB cells at a concentration of 1 – 100 nM MTX equivalent resulted in a 10-fold lower IC$_{50}$ value compared to amide-linked G5-MTX conjugates, which is a result of faster hydrolysis of the ester linkages and release of the incorporated MTX drug molecules.[58] This data was further supported by Minko's report showing that ester-linked PAMAM-TAX conjugates release 25% of the loaded TAX upon incubation for 24 hours in PBS solution and produce a 10-fold decrease in the IC$_{50}$ value observed upon incubation with human ovarian carcinoma cells for 24 hours compared to the free drug.[32]

pH-Sensitive Linkages

The desire to achieve cancer cell-specific delivery and release of anticancer drugs motivated the development of dendrimer-drug conjugates with hydrolysable linkages. Specifically, the sought linkages had to remain intact in the systemic circulation but quickly degrade once internalized into the cancer cell and release the attached drug to produce the desired therapeutic activity. The incorporation of pH-sensitive linkages into dendrimer-drug conjugates seemed to fit the desired criteria as they remain stable in the systemic circulation (pH 7.4) but quickly hydrolyze in acidic environment (pH 5-6) like the endosomes/lysosomes thus releasing the incorporated drug inside the target cell.[59]

In 2006 Szoka and co-workers reported the synthesis of asymmetric "bow-tie" polyester G3-G4 dendrimers.[59] DOX was conjugated to the G4 side via either a pH-sensitive hydrazone (hyd) or a carbamate linkage to yield dendrimer-hyd-DOX and dendrimer-DOX conjugates, respectively. Dendrimer-hyd-DOX conjugates were stable at

pH 7.4 as indicated by the release of <10% of the incorporated DOX compared to the release of 100% of the attached DOX upon incubation at pH 5.0 for 48 hours. Dendrimer-hyd-DOX conjugates were more cytotoxic towards colon carcinoma cells with an IC_{50} of 1.4 μg DOX/ml compared to carbamate-linked dendrimer-DOX conjugates with an IC_{50} of 2.0 μg DOX/ml upon incubation for 72 hours.[51,52] In addition, dendrimer-hyd-DOX conjugates displayed a remarkable anticancer activity *in vivo* where a single injection at 20 mg/kg DOX equivalent administered 8 days after tumor implantation resulted in complete tumor regression and 100% survival of the treated animals for 60 days.[52] Subsequent reports confirmed the higher *in vitro* and *in vivo* anticancer activity of dendrimer-hyd-DOX conjugates compared to amide-linked conjugates and the free drug.[50,57] For example, G4-hyd-DOX conjugates (IC_{50} = 8.7 μM) were nearly 7 times more cytotoxic towards HeLa cells compared to G4-amide-DOX conjugates (IC_{50} = 60.2 μM).[50] In addition, G4-hyd-DOX conjugates proved to be equally effective against DOX-sensitive and -resistant cells, whereas free DOX was 58 times less effective in inducing apoptosis in resistant cancer cells.[50]

Fluorescence microscopy studies of Ca9-22 cells separately treated with G4.5-hyd-DOX and G4.5-amide-DOX conjugates revealed that the hydrolysis of the hydrazone linkage allows the liberated DOX molecules to enter the nucleus whereas G4.5-amide-DOX conjugates fail to release the incorporated drug thus limiting its access to the nucleus and diminish its therapeutic activity.[57] It is interesting to note that another study showed that similar G0-DOX conjugates were able to enter the nucleus regardless of the linkage chemistry.[50]

Acid-sensitive *cis*-aconityl linkages have also been utilized to conjugate DOX to PAMAM dendrimers with increasing functionalization ratios of PEG groups from 4 to 20 PEG per dendrimer to prepare pH-sensitive PEGylated PAMAM sensitive dendrimers (PPSD)[60]. DOX released from these dendrimers increased as a function of PEGylation degree in pH 4.5 citrate buffer achieving a maximum of 60% DOX release after 100 hours, while limited DOX release was observed upon incubation with all PPSD in pH 7.4 buffer. These results were explained by enhanced solubilization of PPSD due to increasing PEGylation degree which could enhance the bulk solubility of DOX and therefore increase the release of the cleaved drug. Administration of these conjugates i.v. to B16 melanoma-bearing mice resulted in a 23% enhancement in the calculated inhibitory rate of tumor volume increase (determined by comparing tumor volume of treated and saline groups) and an increase in median survival time of 7 days compared to mice receiving an equivalent dose of free DOX. While pH-sensitive linkages represent a significant improvement over non-cleavable conjugates for intracellular drug delivery of anticancer drugs, they only sense the acidity of the endosomal compartment but fail to differentiate between cancer cells and normal healthy ones.

Activated Linkages

Further selectivity of drug release from dendrimer conjugates can be achieved by development of novel chemical linkages that are cleaved by controlled inducible release mechanisms at the tumor site (e.g. photo and thermal reduction) or are sensitive to cancer-specific markers (e.g. intracellular enzymes). Recent work by Baker et al. developed G5-MTX conjugates incorporating *ortho*-benzyl linkers which are

photochemically cleaved by UV irradiation, and found that MTX was fully released from these conjugates after a 10 minute UV exposure time.[61] However, *in vitro* cytotoxicity showed no difference in cytotoxicity when these photo-cleavable G5-MTX conjugates were incubated with KB cells with or without UV exposure, indicating that MTX is likely able to cause its therapeutic activity even when attached to the nano-carrier.

Initial studies on enzyme-activated dendrimers showed that incubation of 1,3,5-tris(3-aminopropyl)benzene dendrimers displaying specific amino acids on their surface, which include phenylalanine, methionine, aspartic acid or diaminopropionic acid, with proteolytic enzymes would selectively cleave these amino acids with cleavage rate dependent on the dendrimer's generation number.[62] Recently, Thiagarajan et al. synthesized PAMAM-CPT conjugates through esterase-cleavable succinic acid-glycine amino-acid spacers, however <10% of the drug was released after 48 hours in physiologic conditions resulting in nearly a 50-fold reduction in cytotoxicity of the conjugate compared to free CPT in HCT-116 human colorectal carcinoma cells.[63] Likewise, enzyme-cleavable peptide linkages have been utilized to attach DOX or MTX molecules to dendrimer carriers which are cleaved in the presence of proteases overexpressed in tumors. Kaminskas et al. described the conjugation of MTX to G4 PEGylated polylysine dendrimers through matrix metalloproteinase (MMP) cleavable hexapeptide substrates, which showed 80% drug release after a 24 hour incubation with MMP enzymes.[64] Calderon and co-workers reported on the conjugation of DOX or MTX to polyglycerol dendrimer carriers via dipeptide Phe-Lys and tripeptide D-Ala-Phe-Lys substrates, respectively, cleaved by the cathepsin B enzyme.[65] Release of free DOX from these enzyme-cleavable conjugates was observed after a 2.5 hour incubation with cathepsin B

enzymes, and while DOX-loaded conjugates showed a 10-fold reduction in cytotoxicity against MDA-MB 231 (mammarian carcinoma) and AsPC1 (pancreatic carcinoma) cells as compared to the free drug, the MTX-loaded compositions were significantly more toxic than MTX alone. These results show the potential of enzyme-cleavable linkages to preferentially release the loaded chemotherapeutic molecules to tumor tissue in the presence of the target enzyme. While these conjugates rely on enzymes overexpressed in the tumor tissue the presence of these enzymes is not specific to the diseased tissue, increasing the potential for non-specific toxicity from these systems *in vivo*. For the case of the MMP-cleavable conjugates liberation of the drug occurs primarily in the tumor microenvironment requiring passive diffusion of the drug into tumor cells, therefore decreasing the drug's efficacy due to degradation and drug resistance mechanisms. Finally, these systems rely on static drug release rates limited by the degradation kinetics of the enzymes with no control over the release rate of the drug from the conjugate to optimize its activity *in vitro* and *in vivo*. Based on these limitations we sought to develop enzyme-cleavable linkages which are cleaved solely in the diseased tissue by intracellular enzymes, while 'tuning' the extent and rate of drug release through small modifications to the linkage.

2.3   Targeting Strategies of Dendrimer-Based Therapeutics for Cancer Cell Specific Drug Delivery

The ability of macromolecular carriers to effectively deliver loaded drug molecules to the target cancer cells while avoiding non-specific toxicity depends on their ability to selectively accumulate in tumor tissue and be shuttled into cancer cells through

passive and active targeting strategies. Passive targeting describes the modulation of the MW, size and architecture of polymeric nano-carriers to enhance plasma circulation time and inhibit elimination, thereby increasing its exposure to tumor vasculature and enhancing tumor-specific accumulation. Active targeting strategies utilize chemical (e.g. sugars and vitamins) or biologic (e.g. antibodies and peptides) motifs displayed on the surface of the polymer carrier which selectively interact with specific proteins or receptors present on the target cancer cell. This allows for selective recognition, binding and internalization of the targeted carriers into cancer cells to increase intracellular concentrations of the loaded therapeutic while minimizing non-specific uptake into healthy tissues.

2.3.1   Passive Targeting of Dendrimer Carriers

Therapeutic macromolecules, including dendrimer drug delivery systems, exploit the pathophysiological patterns of solid tumors, particularly their leaky vasculature, to preferentially extravasate and accumulate in tumor tissue in a process known as the Enhanced Permeability and Retention (EPR) effect (**Figure 2.7**).[66] The rapid angiogenesis and hypervascularization of tumor tissue results in a dense network of vessels with defective vascular architecture and lack of a smooth muscle layer resulting in large fenestrations through which macromolecules preferentially extravasate from the systemic circulation and are then retained due to impaired lymphatic drainage.[67] The amount of nanoparticles which accumulates in tumor tissue after intravenous administration is influenced primarily by their size and molecular weight.[68] These features play the most significant role in modulation of a carriers residence time in the

Figure 2.7: Cartoon showing the diffusion of drug delivery systems (yellow) across the leaky vasculature into the tumor mass, and their retention due to impaired lymphatic drainage, which is a phenomenon known as the enhanced permeability and retention (EPR) effect.
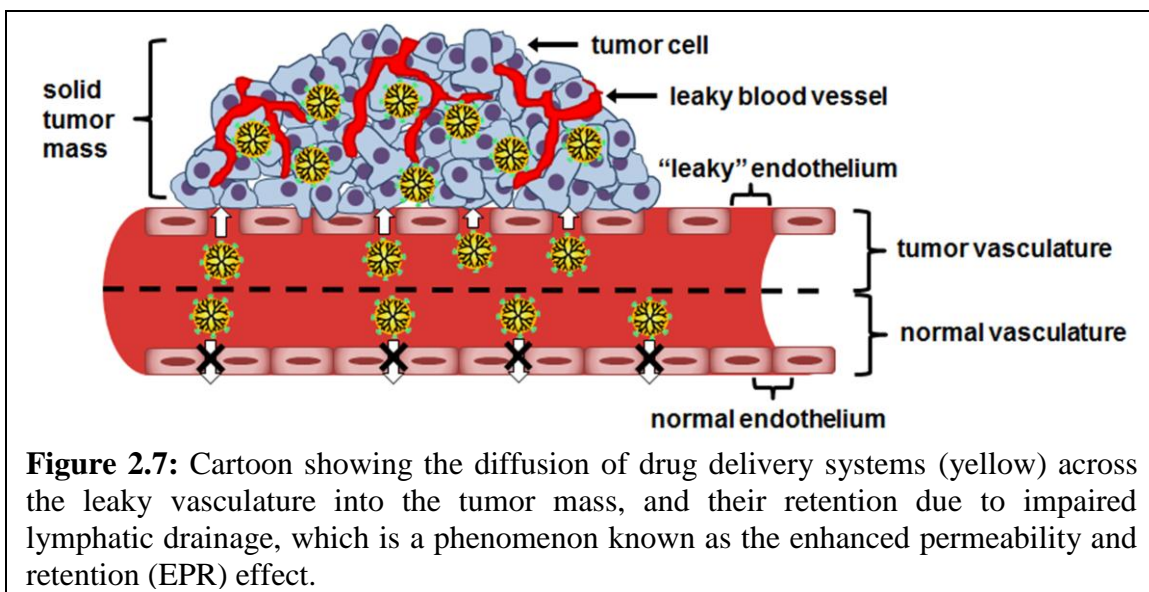
systemic circulation, excretion profiles, non-specific recognition and uptake by the reticuloendothelial system (RES), distribution to tumor tissue and ability to transport across the cellular membrane.[68] In particular, as the hydrodynamic diameter (D_h) of macromolecular carriers surpasses the renal threshold limit of ~10 nm the urinary filtration rate of these macromolecules decreases as a function of increasing D_h.[69] Polymeric nanoparticles with $D_h < 100$ nm, minimize activation and sequestering of these particles by the RES.[70] Furthermore, intracellular uptake studies of nanoparticles in different cancer cells have shown polymeric carriers with $D_h < 100$ nm exhibited significantly greater uptake compared to particles with $D_h > 100$ nm.[71,72] As a result carriers between 10 – 100 nm in diameter are considered ideal vehicles for drug delivery systems due to their capability to minimize elimination kinetics and achieve prolonged plasma residence half-lives ($t_{1/2}$). This results in increased exposure to tumor vasculature resulting in enhanced tumor tissue distribution, as well as their ability to be efficiently internalized into cancer cells via endocytosis.

In addition, the plasma residence time of nanoparticles is dependent on polymer MW, with increased half-lives observed for particles above the renal excretion limit of ~50kDa.[70,73] Murakami et al. studied the effect of increasing PEG MW on their tumor accumulation 3 hours after intravenous administration to Meth-A fibrosarcoma tumor-bearing mice and found tumor accumulation increased from 2.5% of the injected dose per gram of tissue for 31kDa PEG to 6.5% for 215 kDa PEG.[74] However, increasing PEG MW beyond 215kDa resulted in decreased tumor accumulation, with 5% of the injected dose per gram observed after administration of 275kDa PEG.[74] This is due to restricted transport of large MW polymers ($\geq$215kDa) through the tumor vasculature openings and impaired diffusion through the collagen and glycoprotein tumor interstitial matrix.[73] Additionally, the conformation and flexibility of the polymer macromolecule significantly impacts the carrier's tumor distribution and elimination profile.[73] In particular linear or random-coiled structured polymers, such as PEG, HPMA, chitosan and poly(amino acid) chains can readily deform to pass through pores in liver and kidney endothelium leading to facile systemic clearance. Branched polymers on the other hand significantly improve plasma residence time compared to their linear counterparts due to decreased glomerular permeability.[75,76] Studies by Szoka and Frechet et al. found that $t_{1/2}$ of PEGylated polyester branched polymers administered i.v. to mice increased from 1.4 hours for a linear conformation to 26 and 31 hours for four- and eight-arm branched polymers, respectively, at an equivalent MW of 40kDa.[75] This resulted in tumor distribution of the eight-arm branched PEG polymers of 15% of the injected dose per gram of tissue 48 hours after i.v. administration to B16F10 melanoma tumor bearing mice.[75] Linear HPMA and PEG polymer carriers, however, achieved a maximum of 10%

44

and 4.5% of the injected dose per gram of tumor tissue 24 hours after i.v. administration to B16F10 melanoma[77] and Meth-A fibrosarcoma[74] tumor-bearing mice. These results highlight the ability of hyperbranched polymeric carriers, like dendrimers, to control the MW of subsequent molecular therapeutics and tune their *in vivo* distribution profiles.

In addition to the influence of size and molecular weight on polymer pharmacokinetics *in vivo*, the surface charge of dendrimers has also been found to play a significant role in their behavior in *in vitro* and *in vivo* systems. El-Sayed *et al.* studied the effect of size, molecular weight, and surface charge on the permeability of fluorescently-labeled PAMAM-NH$_2$ (G0-G4) dendrimers across epithelial and endothelial barriers.[78-81] Data showed the increase in dendrimers' size/molecular weight results in a corresponding exponential increase in their extravasation time constant (τ) across the microvascular endothelium of the cremaster muscle of Syrian hamsters.[81] It is important to note that this study was done using a normal endothelial barrier, which is quite different in terms of barrier properties compared to the endothelial lining of the tumor vasculature. A subsequent investigation by Kobayashi and co-workers studied the biodistribution of Gadolinium-functionalized G2-NH$_2$ to G10-NH$_2$ conjugates administered intravenously into normal mice, which showed that Gadolinium-functionalized G2-G4 dendrimers were quickly excreted in urine after 3 minutes of their intravenous injection whereas G5 and higher generations displayed limited renal secretion due to their larger hydrodynamic volume.[19] These results clearly indicate the influence of dendrimers' physicochemical properties, particularly their size, on their transport behavior *in vivo*.

Cationic dendrimers show high non-specific uptake by the RES particularly in the liver and lungs, which reduces their accumulation in tumor tissue.[47,51,82-85] Upon comparing the biodistribution of cationic G5-NH$_2$ dendrimers and their neutral counterparts prepared by partial or full acetylation of the surface amine groups in nude mice bearing melanoma and prostate tumors, results showed that both dendrimers displayed a similar distribution profile to all major organs within 1 hour after dendrimers injection with particularly high accumulation in the lungs, kidneys and liver (27.9-28.6 % injected dose per gram).[83] While the cationic and neutral dendrimers displayed similar biodistribution profiles, cationic dendrimers showed higher net accumulation in each organ due to their favorable electrostatic interaction with the negatively charged epithelial and endothelial cell surface. It is interesting to note that all polylysines,[82,84] anionic PAMAM-COOH dendrimers,[85] and polyester dendrimers[51] exhibit high distribution to the liver and quick elimination into the urine. This biodistribution profile can be attributed to the dendrimer's small hydrodynamic volumes, which results in less than 5% of the initial dose remaining in the systemic circulation 24 hours after administration.[51,84]

Attachment of PEG arms to the dendrimer surface increases their size and molecular weight thus reducing their systemic clearance and improve their biocompatability.[15,82,86,87] Specifically, attachment of PEG chains with molecular weight up to 20 kDa to the dendrimer's surface groups increases their plasma half-life to 50 hours for G3 polyester dendrimers,[15,82] 75.4 hours for polylysine dendrimers,[82] and to 100 hours for triazine dendrimers.[86] Bhadra *et al.* showed that the attachment of PEG (5 kDa) chains to 25% of the surface groups of G4-NH$_2$ dendrimers results in 3-fold reduction in

their hemolytic activity compared to the parent dendrimers.[42] Another *in vivo* study showed that intra-peritoneal administration of melamine dendrimers into Swiss-Webster mice induce significant hepatic toxicity at doses $\geq$ 10 mg/kg,[88] whereas PEGylation of 50% of the surface NH_2 groups would enhance its biocompatibility and increase the tolerated dose to 1 gm/kg.[89] These studies clearly indicate the positive effect of surface PEGylation of PAMAM dendrimers by enhancing their plasma residence time and reducing non-specific toxicity. Furthermore, the well-established ability of PEGylated nanoparticles to avoid opsonization,[90] and as a result limit recognition and clearance by the RES system, has made this an attractive passive targeting strategy to selective deliver dendrimer-based therapeutics to tumor tissue.[60,84,87]

2.3.2 Active Targeting Strategies to Hepatic Cancer Cells

The development of glycosides, or sugars bound to an organic molecule, has been extensively utilized to target macromolecular therapeutics selectively to hepatic cancer cells. The sugar residues displayed on the surface of these glycoconjugates are selectively recognized by the liver-specific asialoglycoprotein receptor (ASGPR) after systemic administration leading to receptor-mediated endocytosis. Recently, an HCC specific peptide (SP94) was reported to have a significantly greater binding affinity to hepatic cancer cells versus normal hepatocytes.[91] We have employed both of these targeting strategies to develop selectively delivery dendrimer carriers to the cytoplasm of hepatic cancer cells.

2.3.2.1 Glycoside Targeted Systems

The ASGPR is a Ca^{2+} dependent human C-type lectin transmembrane receptor specifically expressed on the sinusoidal and basolateral membrane of hepatocytes and hepatic cancer cells, and mediates the endocytosis and intracellular degradation of desialylated glycoproteins.[92] In HepG2 human hepatic cancer cells there as many as 150,000 surface binding sites/cell,[93] with 34% of the total cellular receptors present on the plasma membrane in the absence of ligand with the remainder occupying intracellular compartments.[94] In clinically obtained liver tumor biopsies 80% of well differentiated HCC tumors are positive for ASGPR as determined by immunostaining techniques, while poorly differentiated tumors are 20% ASGPR positive.[95]

The ASGPR is composed of a helical membrane-spanning region which acts as the internal signal and transmembrane anchor,[96] while the cytoplasmic domain determines the position of the receptor in the membrane.[97] The extracellular binding domain is characterized by a 48 kDa (H1) and 40 kDa (H2) subunit,[98] which is presented as a tripartite triangular lattice with 2 H1 subunits spaced 15Å apart, and 1 H2 subunit spaced 22 and 25Å from the H1 domains, respectively.[99] Ligand binding to the ASGPR was found to be specific for lactose, galactose and galactosamine (Gal) residues,[92] with N-acetylgalactosamine (NAcGal) sugars showing 50-80 fold greater binding affinity to the receptor versus galactose and lactose.[100] In addition, binding affinity of glycosides for the ASGPR is dependent on the valency and three-dimensional arraignment of sugar residues. Biessen et al. reported the synthesis of triantennary NAcGal ligands with inter-sugar spacing increasing from 4-20Å, and showed that binding affinity to rat parenchymal liver cells for the 20Å ligand was 4,000-fold higher than the single sugar molecule and 2,000-fold greater than the 4Å trivalent ligand.[101] These results are due to

the "glycoside cluster effect", termed by Lee and Lee, describing the exponential increase in binding affinity of multivalent sugar ligands which is greater than the effect of increased sugar concentration alone.[102] This enhancement of binding affinity for multivalent ligands results from a decrease in the entropic energy penalty of ligand-receptor binding and is maximally attained for flexible trivalent structures which occupy all three binding subunits of the extracellular ASGPR domain. Once bound, the receptor-ligand complex migrates into a clathrin-coated endosome where the acidification of the endosomal environment results in dissociation of the receptor-ligand complex allowing the receptor to recycle back to the cell surface.[103] In the presence of ligand, internalization of the bound ASGPR occurs within 4 – 4.4 minutes.[104] Receptor recycling from the lysosome back to the membrane surface occurs roughly 5 – 6 minutes after ligand internalization, with the cycle repeating constitutively.

The high density of ASGPR expressed on the surface of hepatic cancer cells, and the systemic accessibility of the receptor due to its presence of the sinusoidal hepatic endothelium, have made ASGPR-targeted polymeric systems the most extensively explored for selective targeting to liver tumor tissue. Early studies by Duncan et al. reported the synthesis of HPMA polymers functionalized with 1.0 – 11.6 mole% Gal residues and explored the effect of targeting ligand density on liver-specific distribution *in vivo*.[105] Results showed 11% to >80% of the injected Gal-containing HPMA polymer dose distributed to normal liver tissue as a function of increased Gal incorporation 30 minutes after intravenous administration to Wistar rats. In a later report Gal-targeted HPMA polymers incubated for 24 hours with HepG2 human hepatic cancer cells showed a roughly 16-fold greater affinity for HPMA conjugates containing 30 mole% trivalent

galactose residues versus non-targeted polymers.[106] In the same study internalization of targeted HPMA polymers showed a 5.6- and 2-fold increase in HepG2 cellular uptake for 10 and 30 mole% trivalent galactose-targeted HPMA conjugates compared to a similar loading of monovalent Gal-targeted polymers, respectively. These results show the increase in binding affinity of trivalent galactosides due to the glycoside cluster effect can be mimicked by sugar-functionalized synthetic macromolecules. However, it's important to note that this study did not directly compare trivalent galactosides incorporating the same sugar residue. Fluorescent microscopy studies confirmed Gal-targeted HPMA conjugates were trafficked to lysosomes after internalization into HepG2 cells, and that incorporation of DOX into Gal-targeted HPMA polymers resulted in nuclei specific drug accumulation after a 24 hour incubation period.[107] Phase I clinical studies of radio-labeled HPMA-DOX conjugates containing 1.5 mole% pendant Gal (PK2) showed 3.3% and 16.9% of the injected dose distributed to tumor and liver tissue, respectively, 24 hours after intravenous infusion to a single HCC patient as determined via single photon emission computed tomography whole body imaging.[108] This distribution profile reflects the strong affinity of galactosalyted glycoproteins reported for normal human liver tissue,[109] leading to 15%-20% of the total administered PK2 to be delivered to the liver and tumor tissue while non-targeted HPMA conjugates showed general body distribution with no significant distribution to the liver.[108] Nevertheless, concentrations of DOX delivered to liver tumor tissue from PK2 were 12-50 folds higher than are achieved through free DOX.[108]

Since these early works a growing number of glycoconjugated polymer-drug therapeutic systems have been reported with enhanced targeting and efficacy *in vitro* and

in vivo. Galactose-targeted poly(γ-benzyl L-glutamate) and PEG diblock copolymer micelles loaded with 17.0 wt% paclitaxel showed a 10%-15% enhancement in cytotoxicity towards ASGPR-expressing HepG2 cells compared to non-ASGPR expressing Sk-Hep1 human hepatic cancer cells at low concentrations (<0.01μg/mL).[110] Fluorescently-labeled G5 PAMAM dendrimers functionalized with 7.7 lactobionic acid (La) sugar molecules per dendrimer showed a 4-fold increase in intracellular HepG2 fluorescence compared to non-targeted controls after a 2 hour incubation at the highest concentration.[111] In addition, La-targeted liposomes (10 mole% La) loaded with DOX showed nearly 75% of the injected dose accumulating in liver tissue 1 hour after intravenous injection to mice, while approximately 12% of non-targeted liposomes accumulated in the liver 4 hours after administration.[112] Pullulan, a water-soluble polysaccharide, has also been utilized as an ASGPR targeting moiety to prepare poly(lactic-co-glycolic) (PLGA)-DOX nanoparticles, which showed limited delivery of DOX (<5%) to HepG2 cells due to the large carrier particle size (>125 nm) limiting endocytic uptake of these nano systems.[113] Targeting to the liver-specific ASGPR has also been exploited for gene delivery systems using lactose-functionalized polymer-liposomal hybrid nano carriers,[114] galactose terminated chitosan derivatives,[115,116] and asialofetuin-targeted PLGA cationic polymers.[117] In addition, galactose[118] and arabinogalactan[119] coated superparamagnetic iron oxide particles have been prepared for liver-specific MRI imaging.

These systems clearly show the enhancement of glycoconjugated nano-therapeutics for selective internalization into hepatic cancer cells, while highlighting the need for glycosides which can differentiate between malignant and normal hepatocytes to

limit distribution to healthy liver tissue and avoid dose-limiting hepatotoxicity. To address this need NAcGal sugar residues have been utilized to develop novel glycoconjugate systems[120-122] and targeted therapeutic macromolecules[123-125] with high affinity to ASGPR. This strategy relies on the enhanced avidity of NAcGal sugar residues to the ASGPR compared to other lectins.[122,126] Based on these reports the targeted carrier systems described in this dissertation utilized NAcGal-ligands to selectively deliver the therapeutic nano-conjugates to hepatic cancer cells *in vitro* and *in vivo*.

2.3.2.2 Peptide Targeted Systems

To develop targeted therapeutics against HCC which can discriminate between tumor cells and nonmalignant liver parenchymal cells phage display technology has been utilized to identify novel surface epitopes which are overexpressed or uniquely present on hepatic cancer cells. In 2008 Lo and co-workers identified an HCC targeting peptide, named SP94, with potential as a ligand for selective drug delivery to liver cancer cells.[91] This 12 amino-acid sequence (SFSIIHTPILPL) was found to bind strongly to six out of nine HCC cancer cell lines (47%-81% cell labeling) and moderately bind to two cell lines (25%-31% cell labeling) after a 1 hour incubation period. Immunohistochemistry of human HCC tumor samples reported in the same article showed SP94 positive staining for 61.3% of tumor tissue specimens and no staining in non-tumor surgical specimens. In this same work, i*n vivo* administration of SP94 by tail vein injection to Mahlavu-derived tumor-bearing mouse models showed a 32- and 23-fold increase in bound SP94 particles from recovered tumor tissue compared to heart and lung tissue, respectively. Finally, the same group prepared SP94-targeted PEGylated liposomal-DOX formulations and

administered them intravenously to the *in vivo* tumor model resulting in a 15% increase in tumor volume reduction versus non-targeted liposomal-DOX particles prepared with a scrambled peptide sequence. Later Ashley et al. reported SP94-targeted nano-therapeutics called 'protocells' composed of a silica core coated with a fluid lipid bilayer chemically conjugated to the targeting peptides.[127] Dissociation constant (K_d; represents the inverse of ligand-receptor affinity) results for Hep3B hepatic cancer cells incubated with SP94-targeted protocells showed a very high affinity of $K_d = 0.94 - 0.08$ nM. Furthermore, they reported this affinity largely depended on the fluidity of the lipid bilayer due to the potential of the fluid surface to allow recruitment of multiple peptide ligands for multivalent interactions. This binding of SP94-targeted protocells to Hep3B was 2.25 x 10^4-fold higher in affinity compared to normal hepatocytes, and 10^4-fold higher compared to human endothelial, mononuclear and lymphocyte control cell lines. Furthermore, K_d of SP94-targeted protocells towards Hep3B cells was nearly 200-fold lower than free SP94 due to multivalent peptide recruitment, and roughly 50,000 times lower than non-targeted protocells. Fluorescent microscopy revealed the SP94-targeted protocols were rapidly endocytosed into Hep3B cells ($t_{1/2} = 15$ min) and were trafficked to lysosomes. In the same study, multi-drug resistant Hep3B hepatic cancer cells and hepatocytes treated for 24 hours with SP94-targeted protocells loaded with DOX (9.6 μM equivalent DOX concentration) resulted in 90% hepatocyte viability while only 3% of Hep3B hepatic cancer cells were viable. These results highlight the potential of SP94 peptides as an efficient targeting strategy of therapeutic nano-conjugates which leads to selective delivery of chemotherapeutic agents to hepatic cancer cells.

2.4   Development and Hypothesis for Targeted, Enzyme-Activated Dendrimer-DOX Nano-Conjugates for Hepatic Cancer Therapy

Enzyme-activated dendrimer-DOX nano-conjugates were developed utilizing Generation 5 (G5) PAMAM-NH$_2$ dendrimers based on their commercial availability, monodisperse composition, high density of chemical surface groups and their optimal *in vivo* pharmacokinetic and toxicity profiles. Specifically, due to their well-defined and controlled synthetic techniques PAMAM dendrimers are characterized by low polydispersity values (1.000002 – 1.005),[128] allowing for low batch-to-batch variability when preparing G5 dendrimer-based therapeutics.[24,129] Characterization of G5 dendrimers by analytical chemistry techniques show these polymers to possess a D$_h$ of 5.4 nm and 128 surface NH$_2$ groups available for conjugation of targeting and chemotherapeutic molecules. This has allowed for G5 PAMAM dendrimer-based nano-conjugates to be loaded with a high density of chemotherapeutic groups while maintaining the particle size and solubility requirements necessary to exploit the EPR effect and allow for efficient internalization into hepatic cancer cells. In addition, the selected PAMAM dendrimers contain a diaminobutane-core which are reported to have high affinity towards liver-specific distribution resulting from their characteristic oblong geometry and hydrophobic core.[19] Biocompatability studies of PAMAM dendrimers have shown hemolytic toxicity associated with the cationic nature of the dendrimer surface NH$_2$ groups which increases as a function of generation.[130] As a result G5 dendrimers have been found to be well-tolerated *in vitro* and *in vivo*, while poor biocompatibility profiles were observed for the large G6 dendrimers.[131] Therefore we covalently linked the DOX chemotherapeutic molecules to a G5 dendrimer carrier via the described enzyme-

activated azo-linkages to prepare enzyme-activated G5-DOX conjugates. DOX was selected as the model chemotherapeutic agent due to its well established clinical use in systemic and loco-regional HCC chemotherapy.[132,133] In addition, the dose-limiting cardiotoxicity and bone marrow suppression common for administration of DOX limits its effectiveness in the clinic, and as a result it is an attractive candidate for drug delivery systems which can increase its therapeutic activity while minimizing toxic side effects.

The hypothesis for the described targeted, enzyme-activated G5-DOX nano-conjugates is summarized in **Figure 2.8**. Specifically, after intravenous administration to HCC patients targeted G5-DOX conjugates will preferentially extravasate from the systemic circulation and accumulate in liver tumor tissue due to the EPR effect. Once localized to the tumor tissue the displayed targeting ligand will bind to receptors expressed on the surface of hepatic cancer cells resulting in their receptor-mediated endocytosis selectively into the cytoplasm of hepatic cancer cells. After internalization targeted G5-DOX nano-conjugates will escape the endosome via the proton sponge mechanism characteristic of cationic polymers like dendrimers,[134] and release free DOX to the cytoplasm after reduction of the azo-linkers by azoreductase enzymes. These targeted, enzyme-activated G5-DOX nano-conjugates show potential as a novel therapeutic alternative to loco-regional chemotherapy techniques in the treatment of unresectable HCC, which will preferentially accumulate in tumor tissue and selectively release the loaded DOX molecules to hepatic cancer cells to achieve high anticancer activity with reduced DOX-mediated cardiotoxicity in the clinic. Furthermore, the flexibility in the design of the descibed azo-linkers offers the opportunity to incorporate a variety of linker compositions into a single nanoparticle to achieve differential activation

and DOX release rates in the presence of azoreductase enzymes to design personalized medicines for HCC therapy.

Figure 2.8: A diagram describing the hypothesis for targeted, enzyme-activated G5-DOX nano-conjugates for HCC therapy. After intravenous administration (**A**) G5-DOX will preferentially distribute to liver tumor tissue via the EPR effect. Once localized to the tumor tissue (**B**) the displayed targeting ligand will selectively bind to the hepatic cell-specific surface receptor leading to receptor-mediated endocytosis of the conjugate into hepatic cancer cells. This is followed by escape of the nano-conjugates from the endosome via the proton sponge mechanism and (**C**) release of the loaded DOX molecules selectively to the cancer cell cytoplasm after reduction by the liver-specific azoreductase enzymes. This system will lead to selective apoptosis of hepatic cancer cells while avoiding non-specific toxicity to healthy tissues.

References

1   Zbaida, S. in *Enzyme Systems that Metabolise Drugs and Other Xenobiotics*   555-566 (John Wiley & Sons, Ltd, 2002).

2   Zbaida, S. The mechanism of microsomal azoreduction: predictions based on electronic aspects of structure-activity relationships. *Drug Metab. Rev.* **27**, 497-516 (1995).

3   Zbaida, S., Brewer, C. F. & Levine, W. G. Substrates for microsomal azoreductase. Hammett substituent effects, NMR studies, and response to inhibitors. *Drug Metab. Dispos.* **20**, 902-908 (1992).

4   Zbaida, S. & Levine, W. G. Characteristics of two classes of azo dye reductase activity associated with rat liver microsomal cytochrome P450. *Biochem. Pharmacol.* **40**, 2415-2423 (1990).

5   Zbaida, S., Stoddart, A. M. & Levine, W. G. Studies on the mechanism of reduction of azo dye carcinogens by rat liver microsomal cytochrome P-450. *Chem.-Biol. Interact.* **69**, 61-71 (1989).

6   Hammett, L. P. The effect of structure upon the reactions of organic compounds. Benzene derivatives. *J. Am. Chem. Soc.* **59**, 96-103 (1937).

7   McDaniel, D. H. & Brown, H. C. An extended table of hammett substitutent constants based on the ionization of substituted benzoic acids. *J. Org. Chem.* **23**, 420-427 (1958).

8   Carl, P. L., Chakravarty, P. K. & Katzenellenbogen, J. A. A novel connector linkage applicable in prodrug design. *J. Med. Chem.* **24**, 479-480 (1981).

9   Gao, S.-Q., Lu, Z.-R., Petri, B., Kopečková, P. & Kopeček, J. Colon-specific 9-aminocamptothecin-HPMA copolymer conjugates containing a 1,6-elimination spacer. *J. Control. Release* **110**, 323-331 (2006).

10   Lee, S., Greenwald, R. B., McGuire, J., Yang, K. & Shi, C. Drug delivery systems employing 1,6-elimination: releasable poly(ethylene glycol) conjugates of proteins. *Bioconjugate Chem.* **12**, 163-169 (2001).

11   de Groot, F. M. H. *et al.* Elongated multiple electronic cascade and cyclization spacer systems in activatible anticancer prodrugs for enhanced drug release. *J. Org. Chem.* **66**, 8815-8830 (2001).

12   Buhleier, E., Wehner, W. & Vogtle, F. "Cascade"- and "nonskid-chain-like" syntheses of molecular cavity topologies. *Synthesis*, 155 (1978).

13   Tomalia, D. A. *et al.* A New Class of Polymers: Starburst-Dendritic Macromolcules. *Polymer J.* **17**, 117 (1985).

14   Tomalia, D. A., Naylor, A. M. & Goddard, W. A. Starburst Dendrimers: Molecular-Level Control of Size, Shape, Surface Chemistry, Topology, and Flexibility from Atoms to Macroscopic Matter. *Angew. Chem. Int. Ed.* **29**, 138 (1990).

15   Gillies, E. R. & Frechet, J. M. J. Dendrimer and dendritic polymers in drug delivery. *Drug Discov. Today* **10**, 35 (2005).

16   Boas, U. & Heegaard, P. M. H. Dendrimers in drug research. *Chem. Soc. Rev.* **33**, 43 (2004).

17   Svenson, S. Dendrimers as versatile platform in drug delivery applications. *Eur. J. Pharm. Biopharm.* **71**, 445 (2009).

18   D'Emanuele, A. & Attwood, D. Dendrimer-drug interactions. *Adv. Drug Deliver. Rev.* **57**, 2147 (2005).

19   Kobayashi, H. & Brechbiel, M. W. Nano-sized MRI contrast agents with dendrimer cores. *Adv. Drug Deliver. Rev.* **57**, 2271 (2005).

20   Sezaki, H., Takakura, Y. & Hashida, M. Soluble macromolecular carriers for the delivery of antitumour drugs. *Adv. Drug Deliver. Rev.* **3**, 247 (1989).

21   Singer, J. W. *et al.* Water-soluble poly-(L-glutamic acid)-Gly-camptothecin conjugates enhance camptothecin stability and efficacy in vivo. *J. Control. Release* **74**, 243 (2001).

22   Winne, K. D., Seymour, L. W. & Schacht, E. H. Synthesis and in vitro evaluation of macromolecular antitumour derivatives based on phenylenediamine mustard. *Eur. J. Pharm. Sci.* **24**, 159 (2005).

23   Shi, X. *et al.* Molecular heterogeneity analysis of poly(amidoamine) dendrimer-based mono- and multifunctional nanodevices by capillary electrophoresis. *Analyst* **131**, 374 (2006).

24   Myc, A. *et al.* Preclinical antitumor efficacy evaluation of dendrimer-based methotrexate conjugates. *Anticancer Drugs* **19**, 143 (2008).

25   Naylor, A. M., Goddard, W. A., Keifer, G. E. & Tomalia, D. A. Starburst dendrimers. 5. Molecular shape control. *J. Am. Chem. Soc.* **111**, 2339 (1989).

26   Lee, C. C., MacKay, J. A., Frechet, J. M. J. & Szoka, F. C. Designing dendrimers for biological applications. *Nat. Biotechnol.* **23**, 1517 (2005).

27   Choi, J. S., Lee, E. J., Choi, Y. H., Jeong, Y. J. & Park, J. S. Poly(ethylene glycol)-*block*-(poly(L-lysine) dendrimer: novel linear polymer/dendrimer block copolymer forming a spherical water-soluble polyionic complex with DNA. *Bioconjugate Chem.* **10**, 62 (1999).

28   Ooya, T., Lee, J. & Park, K. Hydrotropic dendrimers of generations 4 and 5: synthesis, characterization and hydrotropic solubilization of paclitaxel. *Bioconjugate Chem.* **15**, 1221 (2004).

29   Jelinkova, M., Strohalm, J., Etrych, T., Ulbrich, K. & Rihova, B. Starlike vs. classic macromolecular prodrugs: two different antibody-targeted HPMA copolymers of doxorubicin studied in vitro and in vivo as potential anticancer drugs. *Pharm. Res.* **20**, 1558 (2003).

30   Kopecek, J., Kopecková, P., Minko, T. & Lu, Z.-R. HPMA copolymer-anticancer drug conjugates: design, activity, and mechanism of action. *Eur. J. Pharm. Biopharm.* **50**, 61-81 (2000).

31   Minko, T., Kopeckova, P. & Kopecek, J. Comparison of the anticancer effect of free and HPMA copolymer-bound adriamycin in human ovarian carcinoma cells. *Pharm. Res.* **16**, 986-996 (1999).

32   Khandare, J. J. *et al.* Dendrimer versus linear conjugate: influence of polymeric architecture on the delivery and anticancer effect of paclitaxel. *Bioconjugate Chem.* **17**, 1464 (2006).

33   Greenwald, R. B. PEG drugs: an overview. *J. Control. Release* **74**, 159 (2001).

34   Saad, M. *et al.* Receptor targeted polymers, dendrimers, liposomes: Which nanocarrier is the most efficient for tumor-specific treatment and imaging? *J. Contr. Release* **130**, 107 (2008).

35   Svenson, S. & Tomalia, D. A. Dendrimers in biomedical applications--reflections on the field. *Adv. Drug Deliv. Rev.* **57**, 2106 (2005).

36   Nori, A. & Kopecek, J. Intracellular targeting of polymer-bound drugs for cancer chemotherapy. *Adv. Drug Deliver. Rev.* **57**, 609 (2005).

37 Gurdag, S., Khandare, J., Stapels, S., Matherly, L. H. & Kannan, R. M. Activity of dendrimer-methotrexate conjugates on methotrexate-sensitive and -resistant cell lines. *Bioconjugate Chem.* **17**, 275 (2006).

38 Morgan, M. T. *et al.* Dendrimer-encapsulated camptothecins: increased solubility,cellular uptake, and cellular retention affords enhanced anticancer activity in vitro. *Cancer Res.* **66**, 11913 (2006).

39 Patri, A. K., Kukowska-Latallo, J. F. & Baker, J. R. Targeted drug delivery with dendrimer: comparison of the release kinetics of covalently conjugate drug and non-covalent drug inclusion complex. *Adv. Drug Deliver. Rev.* **57**, 2203 (2005).

40 Kojima, C., Kono, K., Maruyama, K. & Takagishi, T. Synthesis of polyamidoamine dendrimers having poly(ethylene glycol) grafts and their ability to encapsulate anticancer drugs. *Bioconjugate Chem.* **11**, 910 (2000).

41 Morgan, M. T. *et al.* Dendritic molecular capsules for hydrophobic compounds. *J. Am. Chem. Soc.* **125**, 15485 (2003).

42 Bhadra, D., Bhadra, S., Jain, S. & Jain, N. K. A PEGylated dendritic nanoparticlate carrier of fluorouracil. *Int. J. Pharm.* **257**, 111 (2003).

43 Chauhan, A. S., Svenson, S., Reyna, L. & Tomalia, D. Solubility enhancement of poorly water soluble molecules using dendrimers. *Material Matters* **2**, 24 (2007).

44 Dhanikula, R. S., Argaw, A., Bouchard, J.-F. & Hildgen, P. Methotrexate loaded polyether-copolyester dendrimers for the treatment of gliomas: enhanced efficacy and intratumoral transport capability. *Mol. Pharm.* **5**, 105 (2007).

45 Wu, G. *et al.* Targeted delivery of methotrexate to epidermal growth factor receptor-positive brain tumors by means of cetuximab (IMC-C225) dendrimer bioconjugates. *Mol. Cancer Ther.* **5**, 52 (2006).

46 Papagiannaros, A., Dimas, K., Papaioannou, G. T. & Demetzos, C. Doxorubicin-PAMAM dendrimer complex attached to liposomes: cytotoxic studies against human cancer cell lines. *Int. J. Pharm.* **302**, 29 (2005).

47 Barth, R. F., Adams, D. M., Soloway, A. H., Alam, F. & Darby, M. V. Boronated starburst dendrimer-monoclonal antibody immunoconjugates: evaluation as a potential delivery system for neutron capture therapy. *Bioconjugate Chem.* **5**, 58 (1994).

48 Alam, F. *et al.* Boron neutron capture therapy: linkage of a boronated macromolecule to monoclonal antibodies directed against tumor-associated antigens. *J. Med. Chem.* **32**, 2326 (1989).

49 Malik, N., Evagorou, E. G. & Duncan, R. Dendrimer-platinate: a novel approach to cancer chemotherapy. *Anticancer Drugs* **10**, 767 (1999).

50 Kono, K. *et al.* Preparation and cytotoxic activity of poly(ethylene glycol)-modified poly(amidoamine) dendrimers bearing adriamycin. *Polymer* **29**, 1664 (2008).

51 Padilla De Jess, O. L., Ihre, H. R., Gagne, L., Frechet, J. M. J. & Szoka, F. C. Polyester dendritic systems for drug delivery applications: in vitro and in vivo evaluation. *Bioconjugate Chem.* **13**, 453 (2002).

52 Lee, C. C. *et al.* A single dose of doxorubicin-functionalized bow-tie dendrimer cures mice bearing C-26 colon carcinomas. *Proc. Natl. Acad. Sci. U.S.A.* **103**, 16649 (2006).

53 Falciani, C. *et al.* Synthesis and biological activity of stable branched neuotensin peptides for tumor targeting. *Mol. Cancer Ther.* **6**, 2441 (2007).

54   Shi, W. *et al.* Synthesis of monofunctional curcumin derivatives, clicked curcumin dimer, and a PAMAM dendrimer curcumin. *Org. Lett.* **9**, 5461 (2007).

55   Myc, A., Patri, A. K. & Baker, J. R. Dendrimer-based BH3 conjugate that targets human carcinoma cells. *Biomacromolecules* **8**, 2986 (2007).

56   Battah, S. *et al.* Macromolecular delivery of 5-aminolaevulinic acid for photodynamic therapy using dendrimer conjugates. *Mol. Pharm.* **6**, 876 (2007).

57   Lai, P.-S. *et al.* Doxorubicin delivery by polyamidoamine dendrimer conjugation and photochemical internalization for cancer therapy. *J. Control. Release* **122**, 39 (2007).

58   Quintana, A. *et al.* Design and function of a dendrimer-based therapeutic nanodevice targeted to tumor cells through the folate receptor. *Pharm. Res.* **19**, 1310 (2002).

59   Rihova, B. *et al.* Doxorubicin bound to a HPMA copolymer carrier through hydrazone bond is effective also in a cancer cell line with a limited content of lysosomes. *J. Control. Release* **74**, 225 (2001).

60   Zhu, S. *et al.* Partly PEGylated polyamidoamine dendrimer for tumor-selective targeting of doxorubicin: the effects of PEGylation degree and drug conjugation style. *Biomaterials* **31**, 1360-1371 (2010).

61   Choi, S. K. *et al.* Photochemical release of methotrexate from folate receptor-targeting PAMAM dendrimer nanoconjugate. *Photoch. Photobio. Sci.* (2012).

62   Kapp, T., Francke, P. & Gust, R. Investigations on surface modified dendrimers: enzymatic hydrolysis and uptake into MCF-7 breast canccells. *ChemMedChem* **3**, 635 (2008).

63   Thiagarajan, G., Ray, A., Malugin, A. & Ghandehari, H. PAMAM-camptothecin conjugate inhibits proliferation and induces nuclear fragmentation in colorectal carcinoma cells. *Pharm. Res.* **27**, 2307-2316 (2010).

64   Kaminskas, L. M. *et al.* Capping methotrexate α-carboxyl groups enhances systemic exposure and retains the cytotoxicity of drug conjugated PEGylated polylysine dendrimers. *Mol. Pharm.* **8**, 338-349 (2010).

65   Calderón, M., Graeser, R., Kratz, F. & Haag, R. Development of enzymatically cleavable prodrugs derived from dendritic polyglycerol. *Bioorg. Med. Chem. Lett.* **19**, 3725-3728 (2009).

66   Maeda, H., Wu, J., Sawa, T., Matsumura, Y. & Hori, K. Tumor vascular permeability and the EPR effect in macromolecular therapeutics: a review *J. Contr. Release* **65**, 271 (2000).

67   Maeda, H., Wu, J., Sawa, T., Matsumura, Y. & Hori, K. Tumor vascular permeability and the EPR effect in macromolecular therapeutics: a review. *J. Control. Release* **65**, 271-284 (2000).

68   Haag, R. & Kratz, F. Polymer therapeutics: concepts and applications. *Angew. Chem. Int. Ed.* **45**, 1198 (2006).

69   Venkatachalam, M. & Rennke, H. The structural and molecular basis of glomerular filtration. *Circ. Res.* **43**, 337-347 (1978).

70   Acharya, S. & Sahoo, S. K. PLGA nanoparticles containing various anticancer agents and tumour delivery by EPR effect. *Adv. Drug Deliver. Rev.* **63**, 170-183 (2011).

71   Desai, M., Labhasetwar, V., Walter, E., Levy, R. & Amidon, G. The mechanism of uptake of biodegradable microparticles in Caco-2 cells is size dependent. *Pharm. Res.* **14**, 1568-1573 (1997).

72   Prabha, S., Zhou, W.-Z., Panyam, J. & Labhasetwar, V. Size-dependency of nanoparticle-mediated gene transfection: studies with fractionated nanoparticles. *Int. J. Pharm.* **244**, 105-115 (2002).

73   Fox, M. E., Szoka, F. C. & Fréchet, J. M. J. Soluble polymer carriers for the treatment of cancer: the importance of molecular architecture. *Accounts Chem. Res.* **42**, 1141-1151 (2009).

74   Murakami, Y., Tabata, Y. & Ikada, Y. Tumor accumulation of poly(ethylene glycol) with different molecular weights after intravenous injection. *Drug Delivery* **4**, 23-31 (1997).

75   Gillies, E. R., Dy, E., Fréchet, J. M. J. & Szoka, F. C. Biological evaluation of polyester dendrimer: poly(ethylene oxide) "bow-tie" hybrids with tunable molecular weight and architecture. *Mol. Pharm.* **2**, 129-138 (2005).

76   Yamaoka, T., Tabata, Y. & Ikada, Y. Distribution and tissue uptake of poly(ethylene glycol) with different molecular weights after intravenous administration to mice. *J. Pharm. Sci.* **83**, 601-606 (1994).

77   Seymour, L. W. *et al.* Influence of molecular weight on passive tumour accumulation of a soluble macromolecular drug carrier. *Eur. J. Cancer* **31**, 766-770 (1995).

78   El-Sayed, M., Ginski, M., Rhodes, C. & Ghandehari, H. Transepithelial transport of poly(amidoamine) dendrimers across Caco-2 cell monolayers. *J. Control. Release* **81**, 355 (2002).

79   El-Sayed, M., Ginski, M., Rhodes, C. A. & Ghandehari, H. Influence of surface chemistry of poly(amidoamine) dendrimers on Caco-2 cell monolayers. *J. Bioact. Compat. Pol.* **18**, 7 (2003).

80   El-Sayed, M., Rhodes, C. A., Ginski, M. & Ghandehari, H. Transport mechanism(s) of poly (amidoamine) dendrimers across Caco-2 cell monolayers. *Int. J. Pharm.* **265**, 151 (2003).

81   El-Sayed, M., Kiani, M. F., Naimark, M. D., Hikal, A. H. & Ghandehari, H. Extravasation of poly(amidoamine) (PAMAM) dendrimers across microvascular network endothelium. *Pharm. Res.* **18**, 23 (2001).

82   Kaminskas, L. M. *et al.* The impact of molecular weight and PEG chain length on the systemic pharmacokinetics of PEGylated poly l-lysine dendrimers. *Mol. Pharm.* **5**, 449 (2008).

83   Nigavekar, S. S. *et al.* [3]H dendrimer nanoparticle organ/tumor distribution. *Pharm. Res.* **21**, 476 (2004).

84   Okuda, T. *et al.* PEGylated lysine dendrimers for tumor-selective targeting after intravenous injection in tumor-bearing mice. *J. Control. Release* **116**, 330 (2006).

85   Malik, N. *et al.* Dendrimers: relationship between structure and biocompatibility in vitro, and preliminary studies on the biodistribution of ^{125}I-labelled polyamidoamine dendrimers in vivo. *J. Control. Release* **65**, 133 (2000).

86   Lim, J. *et al.* The Role of the size and number of polyethylene glycol chains in the biodistribution and tumor localization of triazine dendrimers. *Mol. Pharm.* **5**, 540 (2008).

87   Gajbhiye, V., Kumar, P. V., Tekade, R. K. & Jain, N. K. Pharmaceutical and biomedical potential of PEGylated dendrimers. *Curr. Pharm. Design* **13**, 415 (2007).

88   Roberts, J. C., Bhalgat, M. K. & Zera, R. T. Preliminary biological evaluation of polyamidoamine (PAMAM) StarburstTM dendrimers. *J. Biomed. Mater. Res.* **30**, 53 (1996).

89   Chen, H.-T., Neerman, M. F., Parrish, A. R. & Simanek, E. E. Cytotoxicity, hemolysis, and acute in vivo toxicity of dendrimers based on melamine, candidate vehicles for drug delivery. *J. Am. Chem. Soc.* **162**, 10044 (2004).

90   Owens III, D. E. & Peppas, N. A. Opsonization, biodistribution, and pharmacokinetics of polymeric nanoparticles. *Int. J. Pharm.* **307**, 93-102 (2006).

91   Lo, A., Lin, C.-T. & Wu, H.-C. Hepatocellular carcinoma cell-specific peptide ligand for targeted drug delivery. *Mol. Cancer Ther.* **7**, 579-589 (2008).

92   Stockert, R. J. The asialoglycoprotein receptor: relationships between structure, function, and expression. *Physiol. Rev.* **75**, 591-609 (1995).

93   Schwartz, A. L., Fridovich, S. E., Knowles, B. B. & Lodish, H. F. Characterization of the asialoglycoprotein receptor in a continuous hepatoma line. *J. Biol. Chem.* **256**, 8878-8881 (1981).

94   Zijderhand-Bleekemolen, J. E., Schwartz, A. L., Slot, J. W., Strous, G. J. & Geuze, H. J. Ligand- and weak base-induced redistribution of asialoglycoprotein receptors in hepatoma cells. *J. Cell. Biol.* **104**, 1647-1654 (1987).

95   Trere, D. *et al.* The asialoglycoprotein receptor in human hepatocellular carcinomas: its expression on proliferating cells. *Br. J. Cancer* **81**, 404-408 (1999).

96   Spiess, M. & Lodish, H. F. An internal signal sequence: the asialoglycoprotein receptor membrane anchor. *Cell* **44**, 177-185 (1986).

97   Schmid, S. R. & Spiess, M. Deletion of the amino-terminal domain of asialoglycoprotein receptor H1 allows cleavage of the internal signal sequence. *J. Biol. Chem.* **263**, 16886-16891 (1988).

98   Schwartz, A. L. & Rup, D. Biosynthesis of the human asialoglycoprotein receptor. *J. Biol. Chem.* **258**, 11249-11255 (1983).

99   Hardy, M. R., Townsend, R. R., Parkhurst, S. M. & Lee, Y. C. Different modes of ligand binding to the hepatic galactose/N-acetylgalactosamine lectin on the surface of rabbit hepatocytes. *Biochemistry* **24**, 22-28 (1985).

100   Stockert, R. J., Morell, A. G. & Scheinberg, I. H. Mammalian hepatic lectin. *Science* **186**, 365-366 (1974).

101   Biessen, E. A. L. *et al.* Synthesis of cluster galactosides with high affinity for the hepatic asialoglycoprotein receptor. *J. Med. Chem.* **38**, 1538-1546 (1995).

102   Lee, R. T. & Lee, Y. C. Affinity enhancement by multivalent lectin–carbohydrate interaction. *Glycoconjugate J.* **17**, 543-551 (2000).

103   Wall, D. A., Wilson, G. & Hubbard, A. L. The galactose-specific recognition system of mammalian liver: the route of ligand internalization in rat hepatocytes. *Cell* **21**, 79-93 (1980).

104   Strous, G. J., Du Maine, A., Zijderhand-Bleekemolen, J. E., Slot, J. W. & Schwartz, A. L. Effect of lysosomotropic amines on the secretory pathway and on the recycling of the asialoglycoprotein receptor in human hepatoma cells. *J. Cell. Biol.* **101**, 531-539 (1985).

105 Duncan, R. *et al.* Fate of N-(2-hydroxypropyl)methacrylamide copolymers with pendent galactosamine residues after intravenous administration to rats. *BBA-Gen. Subjects* **880**, 62-71 (1986).

106 David, A., Kopečková, P., Rubinstein, A. & Kopeček, J. Enhanced biorecognition and internalization of HPMA copolymers containing multiple or multivalent carbohydrate side-chains by human hepatocarcinoma cells. *Bioconjugate Chem.* **12**, 890-899 (2001).

107 Omelyanenko, V., Kopečková, P., Gentry, C. & Kopeček, J. Targetable HPMA copolymer-adriamycin conjugates. Recognition, internalization, and subcellular fate. *J. Control. Release* **53**, 25-37 (1998).

108 Seymour, L. W. *et al.* Hepatic drug targeting: phase I evaluation of polymer-bound doxorubicin. *J. Clin. Oncol.* **20**, 1668-1676 (2002).

109 Virgolini, I. *et al.* Decreased hepatic function in patients with hepatoma or liver metastasis monitored by a hepatocyte specific galactosylated radioligand. *Br. J. Cancer* **61**, 937-941 (1990).

110 Jeong, Y.-I. *et al.* Cellular recognition of paclitaxel-loaded polymeric nanoparticles composed of poly(γ-benzyl l-glutamate) and poly(ethylene glycol) diblock copolymer endcapped with galactose moiety. *Int. J. Pharm.* **296**, 151-161 (2005).

111 Guo, R. *et al.* Synthesis of glycoconjugated poly(amindoamine) dendrimers for targeting human liver cancer cells. *RSC Advances* **2** (2012).

112 Wang, S.-n. *et al.* Synthesis of a novel galactosylated lipid and its application to the hepatocyte-selective targeting of liposomal doxorubicin. *Eur. J. Pharm. Biopharm.* **62**, 32-38 (2006).

113 Guhagarkar, S., Majee, S., Samad, A. & Devarajan, P. Evaluation of pullulan-functionalized doxorubicin nanoparticles for asialoglycoprotein receptor-mediated uptake in Hep G2 cell line. *Cancer Nanotech.* **2**, 49-55 (2011).

114 Wang, S. L. *et al.* Design and synthesis of novel galactosylated polymers for liposomes as gene drug carriers targeting the hepatic asialoglycoprotein receptor. *J. Drug Target.* **16**, 233-242 (2008).

115 Jiang, H. L. *et al.* Galactosylated chitosan-graft-polyethylenimine as a gene carrier for hepatocyte targeting. *Gene. Ther.* **14**, 1389-1398 (2007).

116 Mi, F.-L. *et al.* Synthesis and characterization of a novel glycoconjugated macromolecule. *Polymer* **47**, 4348-4358 (2006).

117 Díez, S., Navarro, G. & de Ilarduya, C. T. In vivo targeted gene delivery by cationic nanoparticles for treatment of hepatocellular carcinoma. *J. Gene. Med.* **11**, 38-45 (2009).

118 Weissleder, R., Reimer, P., Lee, A. S., Wittenberg, J. & Brady, T. J. MR receptor imaging: ultrasmall iron oxide particles targeted to asialoglycoprotein receptors. *Am. J. Roentgenol.* **155**, 1161-1167 (1990).

119 Reimer, P., Weissleder, R., Lee, A. S., Wittenberg, J. & Brady, T. J. Receptor imaging: application to MR imaging of liver cancer. *Radiology* **177**, 729-734 (1990).

120 Mamidyala, S. K. *et al.* Glycomimetic ligands for the human asialoglycoprotein receptor. *J. Am. Chem. Soc.* (2012).

121 van Rossenberg, S. M. W. *et al.* Improvement of hepatocyte-specific gene expression by a targeted colchicine prodrug. *ChemBioChem* **4**, 633-639 (2003).

122 Lee, R. T. & Lee, Y. C. Facile synthesis of a high-affinity ligand for mammalian hepatic lectin containing three terminal N-acetylgalactosamine residues. *Bioconjugate Chem.* **8**, 762-765 (1997).

123 Akinc, A. *et al.* Targeted delivery of RNAi therapeutics with endogenous and exogenous ligand-based mechanisms. *Mol. Ther.* **18**, 1357-1364 (2010).

124 Liang, H.-F., Yang, T.-F., Huang, C.-T., Chen, M.-C. & Sung, H.-W. Preparation of nanoparticles composed of poly(γ-glutamic acid)-poly(lactide) block copolymers and evaluation of their uptake by HepG2 cells. *J. Control. Release* **105**, 213-225 (2005).

125 Medina, S. H. *et al.* N-acetylgalactosamine-functionalized dendrimers as hepatic cancer cell-targeted carriers. *Biomaterials* **32**, 4118-4129 (2011).

126 Rensen, P. C. N., van Leeuwen, S. H., Sliedregt, L. A. J. M., van Berkel, T. J. C. & Biessen, E. A. L. Design and synthesis of novel N-acetylgalactosamine-terminated glycolipids for targeting of lipoproteins to the hepatic asialoglycoprotein receptor. *J. Med. Chem.* **47**, 5798-5808 (2004).

127 Ashley, C. E. *et al.* The targeted delivery of multicomponent cargos to cancer cells by nanoporous particle-supported lipid bilayers. *Nat. Mater.* **10**, 389-397 (2011).

128 Esfand, R. & Tomalia, D. A. Poly(amidoamine) (PAMAM) dendrimers: from biomimicry to drug delivery and biomedical applications. *Drug Discov. Today* **6**, 427 (2001).

129 Majoros, I. J., Williams, C. R., Becker, A. & Baker Jr., J. R. Methotrexate delivery via folate targeted dendrimer-based nanotherapeutic platform. *Wiley Interdiscip. Rev. Nanomed. Nanobiotechnol.* **1**, 502-510 (2009).

130 Jevprasesphant, R., Penny, J., Jalal, R. & Attwood, D. The influence of surface modification on the cytotoxicity of PAMAM dendrimers. *Int. J. Pharm.* **252**, 263 (2003).

131 Jain, K., Kesharwani, P., Gupta, U. & Jain, N. K. Dendrimer toxicity: Let's meet the challenge. *Int. J. Pharm.* **394**, 122-142 (2010).

132 Kettenbach, J. *et al.* Drug-loaded microspheres for the treatment of liver cancer: review of current results. *Cardiovasc. Inter. Rad.* **31**, 468-476 (2008).

133 Nowak, A. K., Chow, P. K. H. & Findlay, M. Systemic therapy for advanced hepatocellular carcinoma: a review. *Eur. J. Cancer* **40**, 1474-1484 (2004).

134 Behr, J.-P. The proton sponge: a trick to enter cells the viruses did not exploit. *CHIMIA* **51**, 34-36 (1997).

<center>**Chapter 3**</center>

<center>**Development of Enzyme-Activated Nano-Conjugates for Tunable Release of**</center>

<center>**Chemotherapeutic Agents to Hepatic Cancer Cells**</center>

3.1   Introduction

Primary liver cancer is the 4th most common malignancy worldwide accounting

for > 600,000 annual deaths globally.[1] Hepatocellular Carcinoma (HCC) is a single or

multi-focal hepatoma developed from malignant transformation of normal hepatocytes

and accounts for approximately 75% of patients diagnosed with liver-cancer.[2,3] Currently,

surgical resection of tumor tissue offers the best prognosis for patient's long-term

survival.[4] However, > 80% of HCC patients are ineligible for surgical intervention due to

large and widespread tumor burden, vascular invasion by cancer cells and poor liver

function.[4] Therefore, treatment of patients diagnosed with unresectable HCC relies on

percutaneous administration of chemotherapeutic agents via hepatic arterial infusion

(HAI) or transarterial chemoembolization (TACE) to achieve a high, local concentration

of anticancer agents (e.g. Doxorubicin; DOX) in the tumor tissue.[4,5] However, HAI and

TACE are highly invasive procedures with potential for inducing hemorrhaging and

hepatic failure during therapy.[4] HAI and TACE have also failed to achieve therapeutic

<center>65</center>

concentrations of the chemotherapeutic agents in the cytoplasm of hepatic cancer cells resulting in low tumor response rates (24% − 53%), an average life span < 12 months, and an average 5-year survival <50% for HCC patients.[4,5] Furthermore, administration of chemotherapeutic agents via HAI or TACE is associated with significant drug leakage into the systemic circulation and non-specific distribution to healthy tissues, which results in severe cardiac, neural, and bone marrow toxicity that further deteriorates patient's quality of life.[6,7]

Silica,[8,9] metallic,[9,10] hydrogel,[11] and polymeric[12-14] nanoparticles (NPs) have been used to deliver anticancer drugs such as DOX, docetaxel, retinoic acid, and neocarzinostatin into hepatic cancer cells. These NPs showed longer circulation residence time, increased accumulation in tumor tissue, higher anticancer activity, and lower systemic toxicity compared to free anticancer drugs in preclinical animal models.[6] For example, DOX was conjugated to water-soluble *N*-(2-hydroxypropyl)methacrylamide (HPMA) polymers through a peptide (GFLG) spacer to prepare HPMA-DOX conjugates for treatment of hepatic cancer.[14] *In vitro* studies showed that HPMA-DOX conjugates enter hepatic cancer cells by endocytosis and follow the endosomal/lysosomal trafficking pathway.[15] In the lysosome, the GFLG peptide linker between DOX molecules and the HPMA backbone is cleaved by cathepsin enzymes releasing the anticancer drug, which diffuses into the cytoplasm to produce the desired anticancer activity.[8,14] Galactosamine molecules were attached to the HPMA backbone to function as targeting ligands to trigger selective recognition and internalization of HPMA-DOX conjugates by the asialoglycoprotein receptor highly expressed on the surface of hepatic cancer cells via receptor-mediated endocytosis.[16] Preclinical studies showed that HPMA-DOX conjugates

66

permeate across tumor's leaky vasculature and preferentially accumulate in cancer tissue when administered intravenously into nude tumor-bearing murine models, which results in enhanced anticancer activity compared to the free drug.[8,17] However, phase I/II clinical trials of galactosamine-targeted HPMA-DOX conjugates in HCC patients showed limited therapeutic benefit,[10] which is attributed to low DOX content (approximately 2 mole%) and slow DOX release kinetics (half-life of GFLG hydrolysis by cathepsin enzymes is 45 hours).[15] In addition, clinical studies showed that the administration of HPMA-DOX conjugates to HCC patients was associated with significant dose-limiting toxicity likely due to non-specific release of the loaded DOX molecules by the metabolizing effect of cathepsin enzymes present in the lysosomes of normal healthy cells.[18] These studies clearly show that it is critical to achieve high concentrations of anticancer drugs selectively in the cytoplasm of hepatic cancer cells while sparing neighboring healthy cells to trigger efficient cancer cell death without inducing non-specific toxicity.

We report the synthesis of four aromatic azo-linkers (L1-L4) used to covalently attach DOX as a model anticancer drug to generation 5 (G5) of poly(amido amine) dendrimers forming G5-L(x)-DOX nano-conjugates (where L(x) denotes linkers L1-L4). These aromatic azo-linkers are engineered to be recognized and cleaved by azoreductase enzymes present exclusively in hepatic cells,[19] which will allow for the release of the loaded DOX molecules selectively in the cytoplasm of hepatic cancer cells. Specifically, we designed four aromatic azo-linkers based on aryl-azo organic dyes that proved to be selectively reduced by microsomal azoreductase enzymes present in hepatic cancer cells via an NADPH-dependent mechanism.[19] Binding of the azoreductase enzymes to azo-dyes and the kinetics of their reduction has been shown to correlate to the electron

donating properties of the chemical substituents present in the *para* (**X**) or *ortho* (**Y**) positions to the substrate azo-bond (**Figure 3.1**).[20,21] Calculating the relative electron donating potential for each substituent on different azo-dyes, based on the published values of the Hammett constant (σ),[22,23] showed that azobenzenes with a cumulative $\sigma \leq -0.37$ are substrates for the azoreductase enzymes and their reduction rate increases with the decrease in σ value below this threshold.[20,21] Mechanistic studies showed that azoreductase enzymes initiate the reduction of azobenzenes with NADPH donating an electron pair to the azo-bond, followed by the addition of a second electron pair from the non-bonding electrons of the *para* (**X**) or *ortho* (**Y**) substituents.[21] This leads to protonation of the azo-bond by dissociable water protons to form an unstable hydrazo intermediate, which is quickly reduced cleaving the azo-bond into its respective

Figure 3.1: Azo-dyes with electron-donating groups in the *para* (**X**) or *ortho* (**Y**) positions relative to the azo-bond, and have Hammett constant $\sigma \leq -0.37$, are substrates for the azoreductase enzymes present exclusively in the cytoplasm of hepatic cells. (**1**) Azoreductase enzymes catalyze the addition of an electron pair from NADPH to the azo-bond, followed by the addition of a second pair of electrons from the non-bonding polar substituents (**X** & **Y**). Dissociable protons from water add to the azo-bond forming an unstable hydrazo intermediate, (**2**) that is quickly reduced to the respective amines.

68

amines.

We utilized azobenzenes as a nucleus to develop a series of azo-linkers (denoted as L1-L4) with different electron-donating substituents on ring **A** (**Figure 3.2**). We replaced the benzyl moiety of ring **B** with toluene to incorporate a 1'6 self-eliminating spacer in the linker composition, which will undergo a spontaneous electron cascade[24] after reduction of the azo-bond by the azoreductase enzymes (**Figure 3.2**).
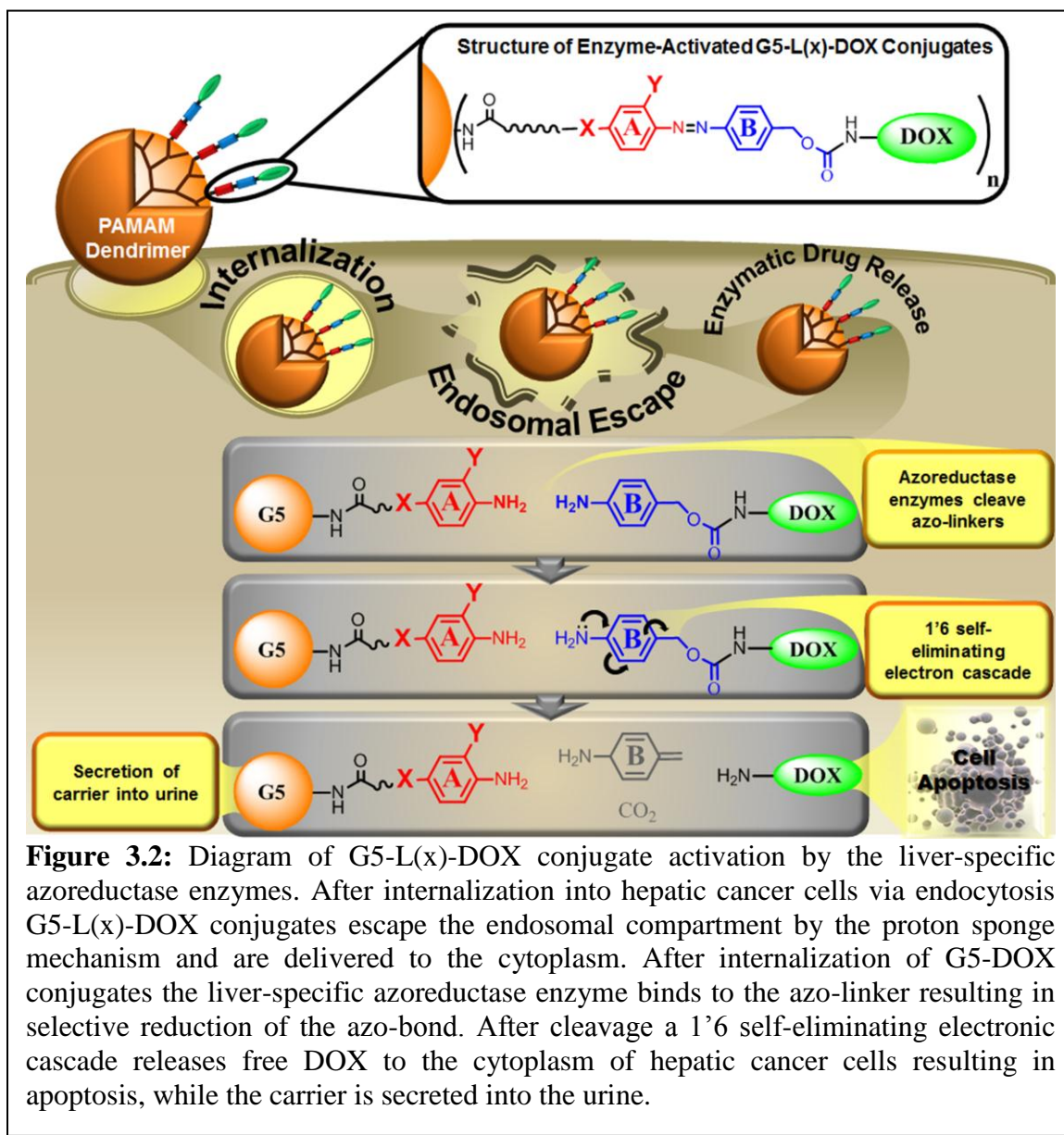
Figure 3.2: Diagram of G5-L(x)-DOX conjugate activation by the liver-specific azoreductase enzymes. After internalization into hepatic cancer cells via endocytosis G5-L(x)-DOX conjugates escape the endosomal compartment by the proton sponge mechanism and are delivered to the cytoplasm. After internalization of G5-DOX conjugates the liver-specific azoreductase enzyme binds to the azo-linker resulting in selective reduction of the azo-bond. After cleavage a 1'6 self-eliminating electronic cascade releases free DOX to the cytoplasm of hepatic cancer cells resulting in apoptosis, while the carrier is secreted into the urine.

This 1'6 self-eliminating spacer will release "clean" DOX molecules without any hanging "linker debris" that may diminish its anticancer activity. G5-L(x)-DOX conjugates were synthesized by varying oxygen (O) or nitrogen (N) chemical substitutions in the *para* (**X**) and *ortho* (**Y**) positions of the azo-linkages to modulate its total σ value, which is calculated by summing each substituents σ value on ring **A** of the aromatic azo-substrate, along with the electron donating effect of the R-CH$_2$-R' group in the *para* position of ring **B** (σ = -0.17). Specifically, G5-L1-DOX was synthesized based on the 4-hydroxyazobenzene (4-HAB) azo-dye with O (σ = -0.27) in the **X** position, while G5-L2-DOX incorporated O in both the **X** and **Y** positions combining their electronegative contribution and further decreasing the azo-linker σ value. To synthesize G5-L3-DOX conjugates the more electronegative N (σ = -0.83) group was substituted in the **X** position, while G5-L4-DOX incorporated N and O atoms in the **X** and **Y** substituents, respectively, to achieve the lowest σ value of the four synthesized azo-linkers. The deceasing σ values for azo-linkers L1-L4 will enhance the electron-density of the azo-bond and as a result increase its affinity to azoreductase-mediated reduction. We hypothesize that increasing the electron density from L1 to L4, shown by their decreasing Hammett constant (σ), will result in a corresponding increase in the reduction rate of different G5-L(x)-DOX conjugates and matching "tunable" release of the conjugated DOX molecules in response to the azoreductase enzymes.

To test this hypothesis we synthesized G5-L1-DOX, G5-L2-DOX, G5-L3-DOX and G5-L4-DOX conjugates with similar number of conjugated DOX molecules and measured their size, molecular weight, surface charge, and electrochemical properties using dynamic light scattering, MALDI-TOF analysis, zeta potential measurements, and

cyclic voltammetry (CV), respectively. Reduction of L1-L4 azo-linkers incorporated in different G5-L(x)-DOX conjugates upon incubation with human liver microsomal enzymes (HLM) and S9 cytoplasmic fractions (containing cytosolic and microsomal enzymes) isolated from hepatic cancer cells were compared to that observed upon incubation with control insect proteins by quantifying the loss of UV absorbance (λ_{max} = 346 − 485 nm) characteristic for the azo-bonds. We quantified DOX release associated with the reduction of different G5-L(x)-DOX conjugates by measuring the amount of free DOX present in the chloroform extracts of different solutions using high pressure liquid chromatography (HPLC). Uptake and intracellular release of DOX molecules from G5-L(x)-DOX conjugates in HepG2 and Hep3B human hepatic cancer cells was quantified by flow cytometry and HPLC analysis, respectively. Cytotoxicity of G5-L(x)-DOX conjugates towards hepatic cancer cells was investigated using the established clonogenic survival assay.[25] We evaluated the specificity of intracellular reduction of azo-linkers and the associated DOX release in rat cardiomyocytes to examine the biocompatibility of G5-L(x)-DOX conjugates given the established acute and chronic cardiac toxicity clinically observed with the administration of free DOX.[26]

3.2   Materials and Methods

3.2.1   Materials

G5-$(NH_2)_{128}$ PAMAM dendrimers with a dimethylaminobutane core were purchased from Dendritic Nanotechnologies Inc. (Midland, MI) and purified by dialysis against deionized water using Slide-A-Lyzer dialysis cassettes (MWCO 10kDa, Thermo Fisher

71

Scientific, Rockford, IL) to remove imperfect dendrimers and polymer debris. Doxorubicin-HCl was purchased from AvaChem Scientific (San Antonio, TX). All solvents, chemicals and reagents were purchased from Sigma-Aldrich Inc. (St. Louis, MO) as American Chemical Society purity grade unless otherwise specified. BD Gentest™ human liver microsomes (HLM) (50 donor pool, protein concentration of 20mg/mL), insect control protein and NADPH generating system were purchased from Becton-Dickinson (Franklin Lakes, NJ). BCA total protein assay kit and cytotoxicity detection kit (Lactate Dehydrogenase leakage detection assay) were purchased from Thermo Fisher Scientific (Rockford, IL) and Roche Diagnostics (Indianapolis, IN), respectively. Dulbecco's modified eagle medium (DMEM), Minimum essential medium (MEM), OPTI-MEM reduced serum medium, Hanks balanced salt solution (HBSS), fetal bovine serum (FBS), 0.25% trypsin / 0.20% EDTA solution, phosphate buffered saline (PBS), penicillin/streptomycin/amphotericin solution, sodium pyruvate and non-essential amino acid solutions were purchased from Invitrogen Corporation (Carlsbad, CA). HepG2 and Hep3B human hepatic cancer cell lines were a generous gift from Dr. Donna Shewach (University of Michigan, Department of Pharmacology, Ann Arbor, MI 48109) and adult rat cardiomyocytes were isolated and provided as a suspension or seeded in 24-well plates as a generous gift from Dr. Margaret V. Westfall and Dr. Daniel E. Michele (University of Michigan, Department of Molecular and Integrative Physiology, Ann Arbor, MI 48109), respectively.

3.2.2 Synthesis of G5-L1-DOX and G5-L2-DOX Conjugates

Scheme 3.1: Synthetic strategy for G5-L1-DOX and G5-L2-DOX conjugates prepared by coupling azo-bond containing enzyme-activated linkages to G5 dendrimers through a stable peptide bond.
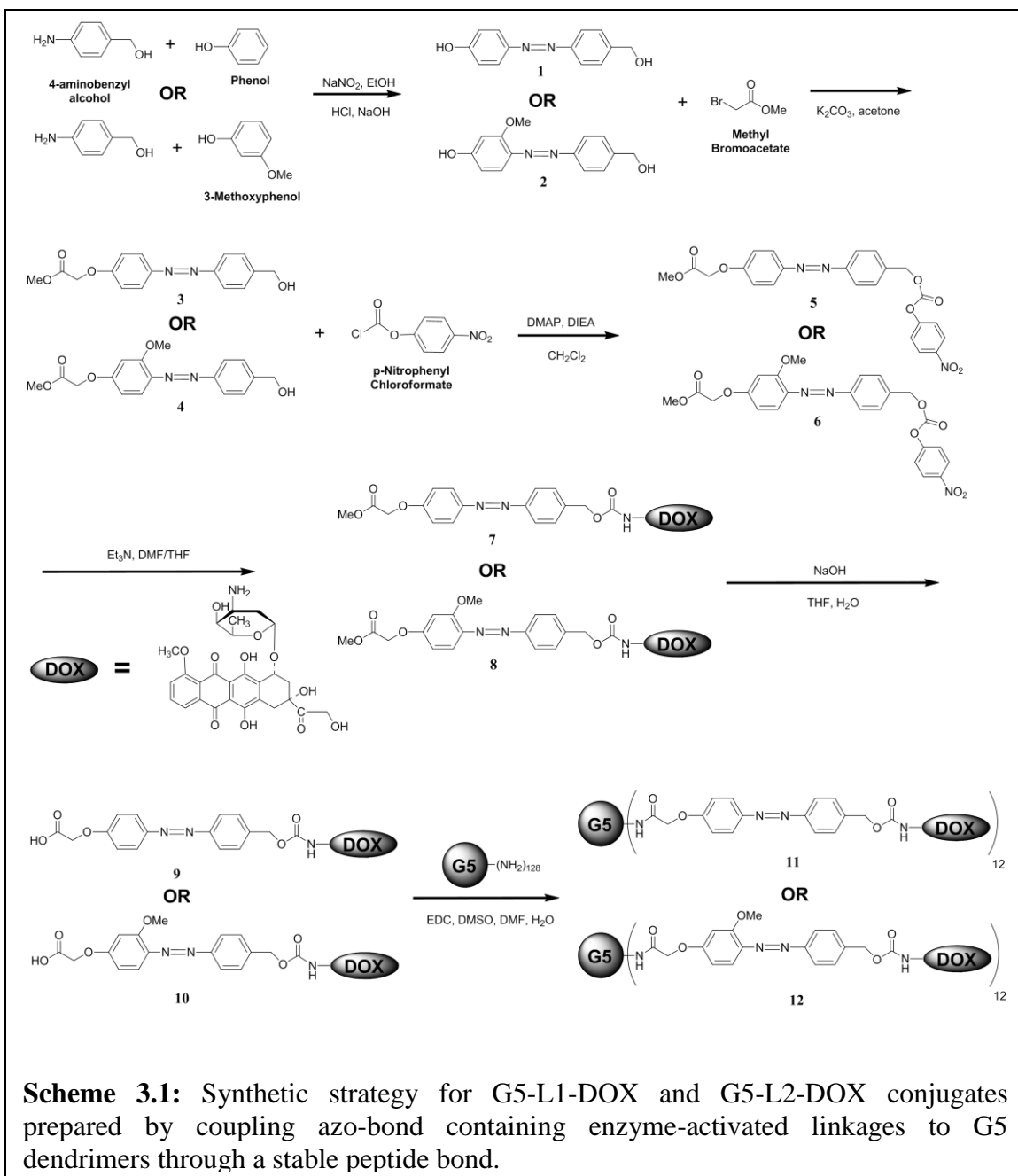
3.2.2.1 *Synthesis of 4-((4-(hydroxymethyl)phenyl)diazenyl)phenol* (**1**)

4-Aminobenzyl alcohol (0.36 g, 2.92 mmol) and $NaNO_2$ (0.22 g, 3.21 mmol) were dissolved in 7.5 mL EtOH:water (1.5:1), added to 2 N HCl solution (4.5 mL) and stirred at 0 °C for 1 hour. Phenol (0.275 g, 2.92 mmol) in EtOH was added followed by NaOAc

(0.15 g) at 0 °C and stirred for 6 hours at room temperature. Reaction mixture was quenched with saturated sodium bicarbonate solution (150 mL) and extracted with DCM. The organic layer was washed with water (200 mL), brine (950 mL), and dried over Na_2SO_4. Solvents were evaporated under reduced pressure and the residue was purified by silica gel column chromatography (EtOAc:*n*-hexane 4:6) to obtain compound **1.** Yield: 0.473 g (71%). ^{1}H NMR and mass-spectrum data are in good agreement with previously published results.[27]

3.2.2.2 *Synthesis of 4-((4-(hydroxymethyl)phenyl)diazenyl)-3-methoxyphenol* (**2**)

4-Aminobenzyl alcohol (0.275 g, 2.24 mmol) and $NaNO_2$ (0.16 g, 2.35 mmol) were dissolved in 7.5 mL EtOH:water (1.5:1) and added to 2 N HCl solution (4.5 mL) and reaction mixture stirred at 0 °C for 1 hour. 3-methoxyphenol (0.25 g, 2.01 mmol) in EtOH was added, followed by addition of NaOAc (0.15 g) at 0 °C and remaining procedure followed as described for compound **1** to obtain compound **2.** Yield: 0.435 g (84%). ^{1}H NMR (500 MHz, CD_3SOCD_3) δ 3.34 (bs, 4H, OMe, -OH), 4.55 (bs, 2H, H_f), 5.31 (s, 1H, phenol-OH), 6.43-6.46 (m, 1H, H_b), 6.57-6.60 (m, 1H, H_c), 7.44-7.48 (m, 2H, H_e), 7.53-7.57 (m, 1H, H_a), 7.69-7.74 (m, 2H, H_d). ^{13}C NMR (125 MHz, CD_3SOCD_3) δ 55.7 (OMe), 62.5 (C_f), 99.9 (C_c), 107.9 (C_b), 117.4 (C_i), 121.9 (C_d), 127.0 (C_e), 134.8 (C_a), 144.7 (C_k), 151.5 (C_j), 158.9 (C_h), 162.6 (C_g). ESI-MS: [M+H][+] $C_{14}H_{15}N_2O_3$ calcd 259.1083, obsd 259.10.

3.2.2.3 *Synthesis of 4-(4-(Carbomethoxy)methoxyphenylazo)benzyl alcohol* (**3**)

Compound **1** (0.4 g, 1.75 mmol) and methyl bromoacetate (0.28 g, 1.83 mmol) were dissolved in 40 mL of acetone, and K_2CO_3 (0.726 mg, 5.26 mmol) was added at room temperature followed by stirring overnight. The reaction mixture was diluted with 100 mL of EtOAc and washed with water (2×50 ml), brine (50 ml), and dried over Mg_2SO_4. After evaporation of solvents under reduced pressure the residue was purified by silica gel column chromatography (EtOAc:*n*-hexane 4:6) affording compound **3**. Yield: 0.395 g (75%). ^1H NMR (400 MHz, DMSO-d_6) δ 3.71 (s, 3H, H_g), 4.58 (s, 2H, H_e), 4.92 (s, 2H, H_f), 5.33 (s, 1H, -OH), 7.10-7.14 (m, 2H, H_a), 7.47-7.49 (m, 2H, H_d), 7.80−7.86 (m, 4H, H_b, H_c). ^{13}C NMR (100 MH, DMSO-d_6) δ 52.4 (C_g), 62.9 (C_f), 65.3(C_e), 115.7, 122.6, 124.8, 127.6, 146.3, 147.1, 151.4, 160.6169.4. HRMS (ESI$^+$) *m/z*: [M+H]$^+$ calcd for $C_{16}H_{17}N_2O_4$ 301.1188, found 301.1176.

3.2.2.4 *Synthesis of methyl 2-(4-((4-(hydroxymethyl)phenyl)diazenyl)-3-methoxyphenoxy) acetate* (**4**)

Compound **2** (0.375 g, 1.45 mmol) was dissolved in 20mL anhydrous acetone to which K_2CO_3 (0.6 g, 4.35 mmol) was added, followed by methyl-bromoacetate (0.15 mL, 1.59 mmol) at room temperature and reaction mixture stirred for 12 hours. The remaining procedure was followed as described for compound **3** to obtain compound **4**. Yield: 0.41 g (86%). ^1H NMR (500 MHz, CD_3SOCD_3) δ 3.71 (s, 3H, H_n (OMe)), 3.94 (s, 3H, aromatic-OCH_3), 4.56 (d, 2H, *J* = 6.0 Hz, H_f), 4.93 (s, 2H, H_l), 5.34 (t, 1H, *J* = 6.0 Hz, -OH), 6.54-6.64 (m, 1H, H_b), 6.78-6.82 (m, 1H, H_c), 7.45-7.49 (m, 2H, H_e), 7.57-7.61 (m, 1H, H_a), 7.73-7.78 (m, 2H, H_d). ^{13}C NMR (125 MHz, CD_3SOCD_3) δ 51.96 (C_m), 52.2 (aromatic-OMe), 62.5 (C_f), 64.8 (C_l), 100.0 (C_c), 106.4 (C_b), 117.2 (C_i), 122.1 (C_d), 127.0

(C$_e$), 136.2 (C$_a$), 145.3 (C$_k$), 151.4 (C$_j$), 158.4 (C$_h$), 161.7 (C$_g$), 168.8 (CO). ESI-MS: [M+H]$^+$ C$_{17}$H$_{19}$N$_2$O$_5$ calcd 331.1294, obsd 331.11.

3.2.2.5 *Synthesis of 4-(4-(carbomethoxy)methoxyphenylazo)benzyl-4'-nitrophenyl carbonate* (**5**)

Compound **3** (0.2 g, 0.67 mmol) was dissolved in DCM (15 mL) to which freshly activated 4 °A M.S (0.1 g) was added and reaction mixture stirred for 10 minutes. DIPEA (0.35 mL, 2.01 mmol) and DMAP (0.01 g) were then added at 0°C. *p*-Nitrophenyl chloroformate (0.471 g, 2.35 mmol) in DCM (3 mL) was added slowly and mixture stirred at 0°C for 1 hour, followed by an additional 4 hours at room temperature. The solvents were evaporated under reduced pressure and the residue was purified by silica gel column chromatography (EtOAc:*n*-hexane 3.5:6.5) affording compound **5**. Yield: 0.28 g (86%). ^{1}H NMR (400 MHz, CDCl$_3$) δ 3.82 (s, 3H, H$_g$), 4.72 (s, 2H, H$_f$), 5.35 (s, 2H, H$_e$), 6.96-7.02 (m, 2H, H$_a$), 7.34-7.38 (m, 2H, H$_d$), 7.53-7.57 (m, 2H, H$_h$), 7.86-7.90 (m, 4H, H$_b$, H$_c$), 8.24–8.28 (m, 2H, H$_i$); ^{13}C NMR (100 MHz Varian, CDCl$_3$) δ 52.5 (C$_g$), 65.3(C$_f$), 70.4(C$_e$), 114.9, 115.6, 121.8, 123.0, 124.9, 125.3, 126.2, 129.3, 136.3, 145.4, 147.5, 152.4, 152.9, 155.5, 160.2, 161.7, 169.1. HRMS (ESI$^+$) *m/z*: [M+H]$^+$ calcd for C$_{23}$H$_{20}$N$_3$O$_8$ 466.1250, found 466.1246.

3.2.2.6 *Synthesis of methyl 2-(3-methoxy-4-((4-(((((4-nitrophenoxy) carbonyl) oxy) methyl) phenyl) diazenyl) phenoxy) acetate* (**6**)

Compound **4** (0.1 g, 0.0302 mmol) was dissolved in DCM (15 mL) and freshly activated 4°A M.S (0.15 g) was added and reaction mixture stirred for 10 minutes. DIPEA (0.215

mL, 1.2 mmol) and DMAP (0.05 g) were added and reaction mixture cooled to 0 °C. *p*-Nitrophenyl chloroformate (0.15 g, 0.0757 mmol) in DCM was added slowly and reaction mixture stirred at 0 °C for 1 hour, followed by an additional 4 hours at room temperature. The remaining procedure was followed as described for compound **5** to obtain compound **6** (E:Z isomers). Yield: 0.11 g (76%). ^{1}H NMR (500 MHz, CDCl$_3$) δ 3.79 (s, 3H, H$_n$ (OMe), for Z), 3.82 (s, 3H, H$_n$ (OMe), for E), 3.99 (s, 3H, aromatic-OMe for Z), 4.00 (s, 3H, aromatic-OMe for E), 4.58 (s, 2H, H$_f$ for Z), 4.71 (s, 2H, H$_f$ for E), 5.21 (s, 2H, H$_l$ for Z), 5.34 (s, 2H, H$_l$ for E), 6.22-6.28 (m, 1H, H$_b$ for Z), 6.44-6.50 (m, 2H, H$_b$ for E), 6.52-6.60 (m, 1H, H$_c$ for Z), 6.64-6.70 (m, 1H, H$_c$ for E), 6.84-6.95 (m, 2H, H$_e$ for Z), 7.30-7.40 (m, 2H, H$_e$ for E), 7.42-7.50 (m, 1H, H$_a$ for Z), 7.50-7.54 (m, 1H, H$_a$ for E), 7.54-7.58 (m, 2H, H$_n$ for Z), 7.68-7.75 (m, 2H, H$_n$ for E), 7.80-7.90 (m, 4H, H$_d$ for Z and E), 8.08-8.14 (m, 2H, H$_o$ for Z), 8.22-8.30 (m, 2H, H$_o$ for E). ^{13}C NMR (125 MHz, CD$_3$SOCD$_3$) δ 52.3, 52.44 (C$_n$), 55.4, 56.34 (aromatic-OMe), 65.2, 65.2 (C$_f$), 67.3, 67.4 (C$_l$), 70.1, 70.4, 100.2 (C$_c$), 104.2, 105.3 (C$_b$), 115.62, 116.9 (C$_i$), 118.0, 120.04, 121.5, 121.7, 121.75, 122.8, 122.9, 125.3, 126.0, 128.7, 128.9, 129.2, 135.9, 137.3, 145.3, 152.3, 154.4, 155.4, 158.7, 161.7, 168.7 (CO). ESI-MS: [M+H]$^+$ C$_{24}$H$_{22}$N$_3$O$_9$ calcd 496.1356, obsd 496.12.

3.2.2.7 *Synthesis of N-(4-(4-(carbomethoxy) methoxyphenylazo) benzyloxycarbonyl) doxorubicin* (**7**)

Compound **5** (0.02 g, 0.043 mmol) was dissolved in anhydrous DMF (1.5 mL) and freshly activated 4°A M.S (0.15 g) was added, followed by stirring of the reaction mixture for 10 minutes. Neutralized Doxorubicin-HCl (0.035 g, 0.060 mmol, 1.4 eq.) was

added in 3 mL of DMF via syringe at room temperature, followed by the addition of Et₃N

(0.015 mL, 0.11 mmol, 2.8 eq.) and reaction mixture stirred at 32°C for 24 hours. After

completion of the reaction (monitored by TLC) water (25 mL) and EtOAc (50 mL) was

added and product extracted twice. The organic layer was washed with water (2×50 ml),

brine (50 ml), and dried over Na_2SO_4. After evaporation of solvents under reduced

pressure the product was purified by silica gel column chromatography (DCM:MeOH

9.5:0.5) affording compound **7**. Yield: 0.03 g (80%). ^{1}H NMR (400 MHz, CDCl₃) δ 1.27

(d, J = 6.7 Hz, 3H, H_g), 1.76-1.79 (m, 1H, H_i), 1.86-1.90 (m, 1H, H_j), 2.03 (bd, J = 6.7

Hz, 1H, H_p), 2.14 (dd, J = 14.4 and 4.0 Hz, 1H, H_p), 2.32 (d, J =14.4 Hz, 1H, H_p), 3.04-

2.92 (m, 2H, H_q, H_h), 3.23 (d, J = 18.8 Hz, 1H, H_q), 3.67 (bd, 1H, H_k), 3.81 (s, 3H, H_g),

3.86 (m, 1H, H_l), 4.04 (s, 3H, H_w), 4.13 (m, 1H, H_o), 4.51 (bs, 1H, -OH), 4.69 (s, 2H, H_f),

4.74 (d, J = 4.0 Hz, 2H, H_r), 5.07 (s, 2H, H_e), 5.24 (m, 2H, H_i), 5.48 (d, J = 3.8 Hz, 1H, -

OH), 6.94-6.98 (m, 2H, H_a), 7.32-7.38 (m, 3H, H_d, H_v), 7.88-7.69 (m, 5H, H_b, H_c, H_t),

7.99 (d, J = 7.4 Hz, 1H, NH), 13.19 (s, 1H, H_s), 13.97 (s, 1H, H_s). ESI/MS *m/z* 892.3

(M+Na)⁺; HRMS (ESI⁺) *m/z*: [M+Na]⁺ calcd for $C_{44}H_{43}N_3O_{16}Na$ 892.2541, found

892.2555.

3.2.2.8 *Synthesis of methyl 2-(3-methoxy-4-((4-(((carbonyl) oxy) methyl) phenyl)*
diazenyl) phenoxy) acetate doxorubicin (**8**)

Compound **6** (0.052 g, 0.0105 mmol) was dissolved in anhydrous DMF (2 mL) and

freshly activated 4°A M.S (0.15 g) was added and reaction mixture stirred for 10 minutes.

Neutralized Doxorubicin-HCl (0.091 g, 0.01575 mmol) in DIPEA (0.075 mL) in DMF (2

mL) was added and reaction mixture stirred at 30 °C for 24 hours. The remaining

procedure was followed as described for compound **7** to obtain compound **8** (E:Z isomers). Yield: 0.07 g (76%). ^{1}H NMR (500 MHz, CDCl$_3$): δ 1.28 (d, 3H, J = 7.5 Hz, H$_m$), 1.78 (dt, 2H, J = 3.0, 7.5 Hz, H$_h$, H$_i$), 1.87 (dt, 2H, J = 3.0, 7.5 Hz, H$_h$, H$_i$), 2.02-2.08 (m, 1H, H$_l$), 2.13-2.20 (m, 2H, H$_p$), 2.28-2.36 (m, 1H, H$_n$), 2.94-3.08 (m, 2H, H$_q$), 3.23 (bs, 1H, -OH), 3.27 (bs, 1H, -OH), 3.60-3.70 (m, 2H, H$_{j,k}$), 3.80-3.92 (m, 4H, OMe & OH), 3.97 (s, 3H, OMe), 4.06 (s, 3H, OMe), 4.10-4.18 (m, 1H, H$_o$), 4.54 (d, 1H, J = 2.5 Hz, -OH), 4.69 (s, 2H, H$_r$), 4.75 (s, 2H, H$_g$), 5.07 (s, 2H, H$_f$), 5.22 (d, 1H, J = 4.0 Hz, -OH), 5.26 (bs, 1H, phenolic-OH), 5.50 (d, 1H, J = 4.0 Hz, -OH), 6.42-6.52 (m, 1H, H$_b$), 6.64-6.68 (m, 1H, H$_c$), 7.34-7.44 (m, 3H, H$_e$, H$_v$), 7.62-7.84 (m, 5H, H$_a$, H$_d$, H$_u$, H$_w$), 8.00 (d, 1H, J = 7.5 Hz, -NH), 13.21 (bs, 1H, OH, H$_s$), 13.96 (bs, 1H, OH, H$_t$). ESI-MS: [M+H]$^+$ C$_{46}$H$_{48}$N$_3$O$_{16}$ calcd 898.3035, obsd 898.32.

3.2.2.9 *Synthesis of N-(4-(4-carboxymethoxyphenylazo)benzyloxycarbonyl)doxorubicin* (**9**)

Compound **7** (0.1 g, 0.011 mmol) was dissolved in THF:water mixture (1.5:1 = 3 mL) and added to a 1 N NaOH solution (0.1 mL) at -4 °C, followed by stirring of the reaction mixture for 20 minutes. After completion of the reaction (monitored by TLC) the mixture was neutralized by addition of 1 N HCl solution at 0 °C to until it reached pH 2-3. After neutralization, water (20 mL) was added and product extracted with EtOAc (2 x 30 mL). The organic layer was washed with water (2×50 ml), brine (50 ml), and dried over Na$_2$SO$_4$. Solvents were evaporated under reduced pressure and the residue was purified by silica gel column chromatography (DCM:MeOH 9.5:0.5) to get compound **5** (E:Z

isomers). Yield: 0.08 g (82%).   ESI-MS *m/z* 878.2 (M+Na)$^{+}$; HRMS (ESI^{+}) *m/z*: [M+Na]$^{+}$ calcd for C$_{43}$H$_{41}$N$_{3}$O$_{16}$Na 878.2385, found 878.2396.

3.2.2.10   *Synthesis of 2-(3-methoxy-4-((4-(((benzyloxycarbonyl) doxorubicinmethyl) phenyl) diazenyl) phenoxy) acetic acid* (**10**)

Compound **8** (0.040 g, 0.004 mmol) was dissolved in THF:water (1.5:1 = 3 mL) and 1 N NaOH solution (0.1 mL) added at -4 °C and reaction mixture stirred for 20 minutes. The remaining procedure was followed as described for compound **9** to obtain compound **10**. Yield: 0.034 g (86%). ^{1}H NMR (500 MHz, CDCl$_{3}$): δ 1.26 (d, 3H, *J* = 7.5 Hz, H$_{m}$), 1.76 (dt, 2H, *J* = 3.0, 7.0 Hz, H$_{h,i}$), 1.88 (dt, 2H, *J* = 3.0, 7.0 Hz, H$_{h,i}$), 2.01-2.07 (m, 1H, H$_{l}$), 2.13-2.20 (m, 2H, H$_{p}$), 2.26-2.34 (m, 1H, H$_{n}$), 2.92-3.06 (m, 2H, H$_{q}$), 3.23 (bs, 1H, -OH), 3.26 (bs, 1H, -OH), 3.60-3.72 (m, 2H, H$_{j,k}$), 3.79-3.90 (m, 4H, OMe & OH), 3.97 (s, 3H, OMe), 4.10-4.18 (m, 1H, H$_{o}$), 4.54 (d, 1H, *J* = 2.5 Hz, -OH), 4.68 (s, 2H, H$_{r}$), 4.75 (s, 2H, H$_{g}$), 5.06 (s, 2H, H$_{f}$), 5.22 (d, 1H, *J* = 4.0 Hz, -OH), 5.26 (bs, 1H, phenolic-OH), 5.52 (d, 1H, *J* = 4.0 Hz, -OH), 6.42-6.52 (m, 1H, H$_{b}$), 6.64-6.68 (m, 1H, H$_{c}$), 7.34-7.44 (m, 3H, H$_{e}$, H$_{v}$), 7.60-7.82 (m, 5H, H$_{a}$, H$_{d}$, H$_{u}$, H$_{w}$), 8.01 (d, 1H, *J* = 7.5 Hz, -NH), 13.21 (bs, 1H, OH), 13.96 (bs, 1H, OH). ESI-MS: [M+H]$^{+}$ C$_{45}$H$_{46}$N$_{3}$O$_{16}$ calcd 884.2878, obsd 884.26.

3.2.2.11   *Coupling of compound **9** to G5-(NH$_{2}$)$_{128}$ dendrimers to prepare G5-L1-DOX* (**11**)

To a solution of compound **9** (86.5 mg, 0.101 mmol, 120 eq.) dissolved in 15 ml DMF:DMSO (3:1) was added EDC (0.195 g, 1.012 mmol, 1200 eq.) as a solid at room temperature, and the reaction mixture stirred for 1 hour. A solution of G5-(NH$_{2}$)$_{128}$

PAMAM dendrimers (24.3 mg, 0.0008 mmol) in 5 mL water was added and reaction mixture stirred for 2 days at room temperature. The mixture was then concentrated under reduced pressure and the residue was dissolved in water and purified by dialysis (10kDa MWCO) for 2 days to produce **G5-L1-DOX**. Yield: 28 mg (0.0007 mmol, 84.3%). MALDI-TOF analysis of compound **G5-L1-DOX** showed a molecular weight of 38,260 Da.

*3.2.2.12   Coupling of compound **10** to G5-(NH$_2$)$_{128}$ dendrimers to prepare G5-L2-DOX (**12**)*

To a solution of compound **10** (126 mg, 0.114 mmol, 100 eq.) dissolved in 16 mL DMF:DMSO (3:1) was added EDC (218 mg, 1.14 mmol, 1000 eq.) as a solid at room temperature and reaction mixture stirred for 1 hour at room temperature. A solution of G5-(NH$_2$)$_{128}$ PAMAM dendrimers (32.8 mg, 0.0011 mmol) in 5 mL of water was added and reaction mixture stirred for 2 days at room temperature. The mixture was then concentrated under reduced pressure and the residue was dissolved in water and purified by dialysis (10kDa MWCO) for 2 days to produce **G5-L2-DOX**. Yield: 25.0 mg (0.0006 mmol, 84%). MALDI-TOF analysis of compound **G5-L2-DOX** showed a molecular weight of 38,010 Da.

3.2.3 Synthesis of G5-L3-DOX and G5-L4-DOX Conjugates

3.2.3.1 *Synthesis of G5-alkyne* (**13**)

G5-(NH$_2$)$_{128}$ PAMAM dendrimers (0.060 g, 0.002 mmol) and 1-pentynoic acid (0.003 g, 0.03 mmol) were dissolved in anhydrous DMSO (6 mL), to which PyBOP (0.016 g,

Scheme 3.2A: Synthesis of G5-alkyne intermediate utilized for a click reaction in the synthesis of G5-L3-DOX and G5-L4-DOX conjugates.
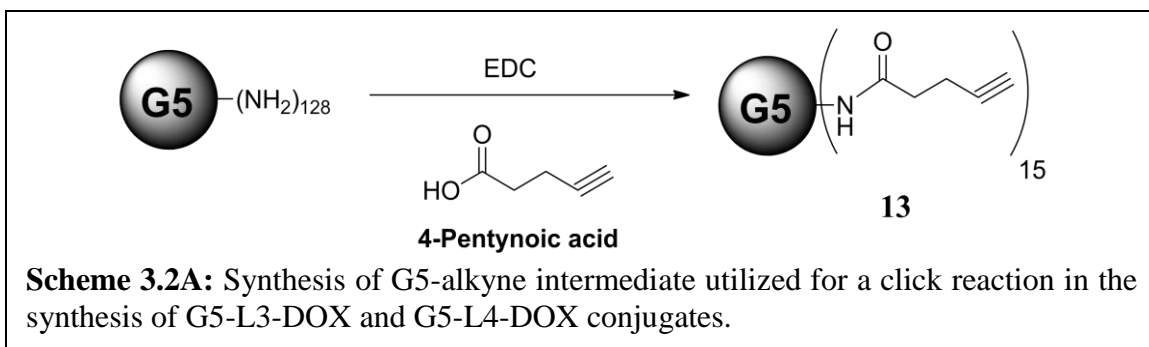
0.032 mmol) and DIPEA (base, 0.020 mL) were added and reaction mixture stirred 36 hours at room temperature. Reaction mixture was purified by dialysis (10kDa MWCO) for 2 days, followed by lyophilization to afford compound **13**. Yield: 0.06 g (96%). ^{1}H NMR (500 MHz, D$_2$O): δ 2.18-2.34 (m, 48H, G5-H), 2.40-2.50 (m, 22H, G5-H), 2.56 (s, 2.5H, pentyne-H), 2.58-2.74 (m, 58H, G5-H), 2.97(t, 2H, *J* = 6.0 Hz, pentyne-H), 3.03-3.24 (m, 44H, G5-H), 3.24 (bs, 0.5H,).

3.2.3.2 *Synthesis of N-(3-bromopropyl)-N-methylaniline* (**14**)

N-methylaniline (300 mg, 2.80 mmol), 1,3-dibromopropane (0.568 mL, 5.6 mmol), K$_2$CO$_3$ (1.16 g, 8.40 mmol) and 18-crown-6 (49.8 mg, 0.30 mmol) were dissolved in 20 mL of anhydrous DMF and mixture stirred for 24 hours at 35 °C. The reaction mixture was filtered and washed with DCM, and filtrate dissolved in DCM (100 mL) before extraction in water. The organic layer was washed with water (2×50 ml), brine (50 ml), and dried over Na$_2$SO$_4$, followed by evaporation of solvents under reduced pressure and the residue purified by silica gel column chromatography (EtOAc:*n*-hexane 1:20 to 1:10) to obtain compound **14**. Yield: 0.260 g (74%). ^{1}H NMR (500 MHz, CDCl$_3$): δ 2.16 (tt, 2H, *J* = 6.5 and 13.5 Hz, H$_c$), 2.99 (s, 3H, NCH$_3$, H$_a$), 3.46-3.55 (m, 4H, H$_b$ and H$_d$),

Scheme 3.2B: Synthetic strategy for G5-L3-DOX and G5-L4-DOX conjugates prepared by coupling azo-bond containing enzyme-activated linkages to G5 dendrimers through a 'clicked' triazole spacer.
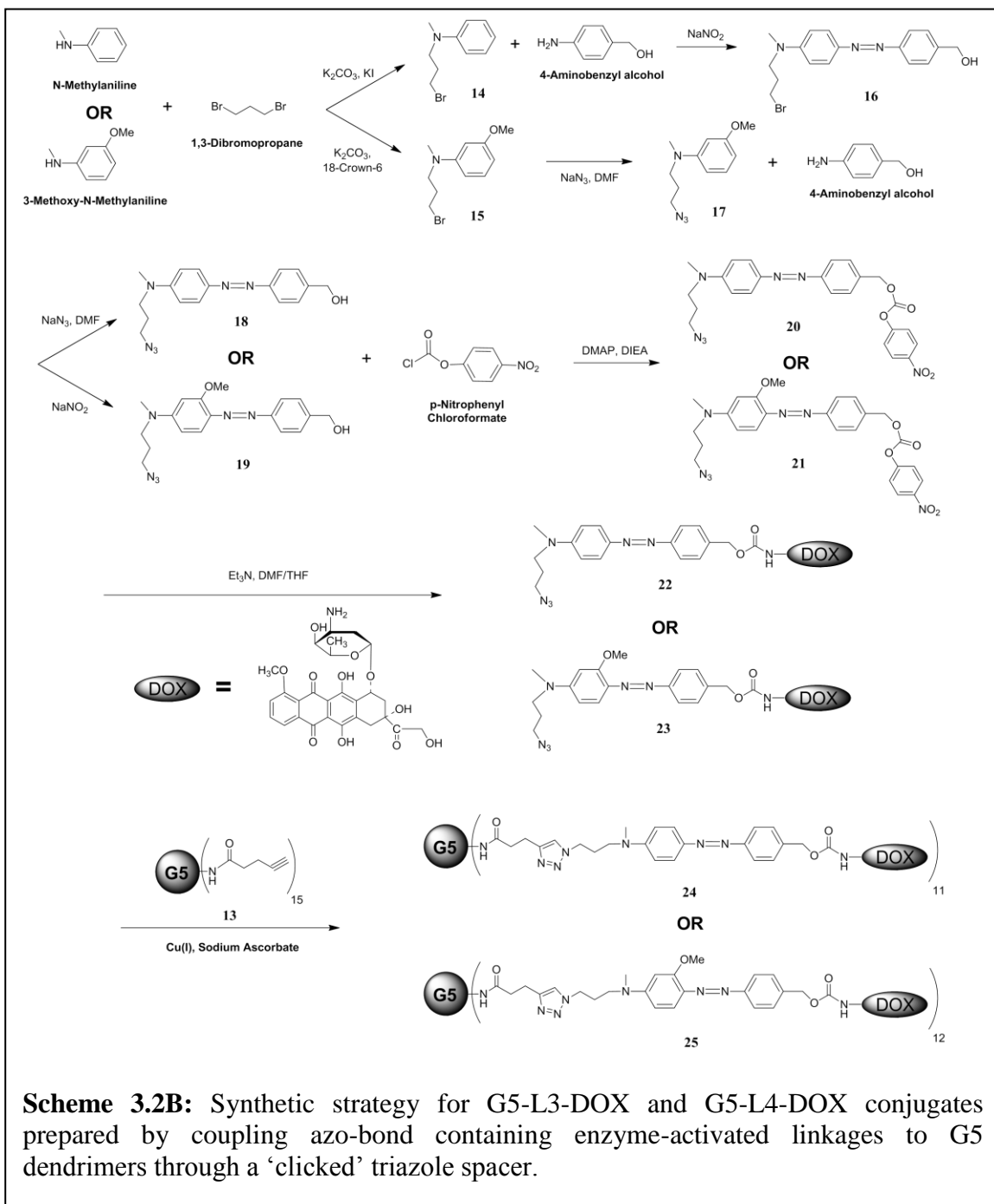
6.71-6.79 (m, 2H, H_e and H_g), 7.24-7.29 (m, 2H, H_f). EI-MS: $[M+H]^+$ $C_{10}H_{15}BrN$ calcd 228.03, obsd 228.04.

3.2.3.3 Synthesis of N-(3-bromopropyl)-3-methoxy-N-methylaniline (**15**)

N-methyl-3-methoxyaniline (1.0 g, 7.294 mmol) was dissolved in anhydrous DMF (20 mL), to which 1,3-dibromopropane (1.48 mL, 14.589 mmol), K_2CO_3 (3.018 g, 21.884 mmol) and 18-crown-6 (0.24 g, 1.458 mmol) were added at room temperature, and reaction mixture stirred at 35°C for 24 hours. The remaining procedure was followed as described for compound **14** to obtain compound **15.** Yield: 0.760 g (75%). ^{1}H NMR (500 MHz, CDCl$_3$): δ 2.16 (tt, 2H, J = 6.5, 13.5 Hz, H$_c$), 2.98 (s, 3H, NCH$_3$, H$_a$), 3.46-3.54 (m, 4H, H$_b$ and H$_d$), 3.83 (s, 3H, OMe), 6.32-6.66 (m, 2H, H$_g$ and H$_i$), 6.38-6.42 (m, 1H, H$_a$), 7.16-7.21 (m, 1H, H$_f$); ^{13}C NMR (125 MHz, CDCl$_3$): δ 29.90 (C$_c$), 31.34 (C$_d$), 38.65 (C$_a$), 50.79 (C$_b$), 55.02 (OC̲H$_3$), 98.77 (C$_i$), 101.26 (C$_e$), 105.31 (C$_g$), 129.81 (C$_f$), 150.32 (C$_j$), 160.72 (C$_h$). EI-MS: [M+H]$^+$ C$_{11}$H$_{17}$BrNO calcd 258.05, obsd 258.04.

3.2.3.4 *Synthesis of 4-((4-((3-bromopropyl) (methyl) amino) phenyl) diazenyl) phenyl)methanol* (**16**)

4-Aminobenzyl alcohol (80 mg, 0.65 mmol) and NaNO$_2$ (47 mg, 0.68 mmol) were dissolved in 2.5mL of EtOH:water (1.5:1), and added to 3 mL of 2 N HCl solution at 0 °C. The reaction mixture was then stirred at 0 °C for 1 hour followed by dropwise addition of compound **14** (0.152 g, 0.66 mmol) in EtOH and reaction mixture stirred overnight at 0 °C. The remaining procedure was followed as described for compound **3** to obtain compound **16** which was used as a crude mixture for the next step. Yield: 0.126 g (99%). EI-MS: [M+H]$^+$ C$_{17}$H$_{21}$BrN$_3$O calcd 362.0868, obsd 362.10.

3.2.3.5 *Synthesis of N-(3-azidopropyl)-3-methoxy-N-methylaniline* (**17**)

Compound **15** (0.5 g, 1.94 mmol) was dissolved in anhydrous DMF (20 mL) and sodium azide (1.26 g, 19.43 mmol) was added, followed by stirring of the reaction mixture at 70 °C for 16 hours. The remaining procedure was followed as described for compound **16** to obtain compound **17**. Yield: 0.340 g (80%). ^{1}H NMR (500 MHz, CDCl$_3$): δ 1.86 (tt, 2H, J = 6.5, 13.5 Hz, H$_c$), 2.93 (s, 3H, NCH$_3$, H$_a$), 3.36 (t, 2H, J = 6.5 Hz, H$_d$), 3.40 (t, 2H, J = 7.5 Hz, H$_b$), 3.79 (s, 3H, OMe), 6.20-6.25 (m, 1H, H$_i$), 6.26-6.30 (m, 1H, H$_g$), 6.33-6.38 (m, 1H, H$_e$), 7.10-7.18 (m, 1H, H$_f$); ^{13}C NMR (125 MHz, CDCl$_3$): δ 26.32 (C$_c$), 38.56 (C$_a$), 49.14 (C$_d$), 49.77 (C$_b$), 55.10 (OC$\underline{\text{H}}_3$), 98.90 (C$_i$), 101.16 (C$_e$), 105.39 (C$_g$), 129.91 (C$_f$), 150.47 (C$_j$), 160.81 (C$_h$). EI-MS: [M+H]$^+$ C$_{11}$H$_{17}$N$_4$O calcd 221.14, obsd 221.12.

3.2.3.6 *Synthesis of 4-((4-((3-azidopropyl)(methyl) amino)phenyl) diazenyl) phenyl) methanol* (**18**)

Compound **16** (0.060 g, 0.166 mmol) was dissolved in 4 mL of anhydrous DMF followed by addition of sodium azide (0.043 g, 0.665 mmol) and reaction mixture stirred at 80 °C for 48 hours. After completion of the reaction (monitored by TLC) the product was filtered and DMF removed under reduced pressure at 40 °C, and residue dissolved in DCM (100 mL) and extracted with water. The organic layer was washed with water, brine and dried over Na$_2$SO$_4$, followed by evaporation of solvents the residue under reduced pressure and residue was purified by silica gel column chromatography (EtOAc:*n*-hexane 3:10 to 3:6) to obtain compound **18.** Yield: 0.046 g (86%). ^{1}H NMR (500 MHz, CDCl$_3$): δ 1.82 (m, 3H, H$_c$ and -OH), 3.05 (s, 3H, NCH$_3$, H$_a$), 3.42 (t, 2H, J = 6.5 Hz, H$_d$), 3.54 (t, 2H, J = 7.5 Hz, H$_b$), 4.78 (s, 2H, H$_j$), 6.72-6.79 (m, 2H, H$_e$), 7.42-7.50 (m, 2H, H$_h$), 7.82-7.92 (m, 4H, H$_f$, H$_g$); ^{13}C NMR (125 MHz, CDCl$_3$): δ 26.41 (C$_c$),

38.8 (C_a), 48.9 (C_d), 49.5 (C_b), 65.0 (C_j), 1114 (C_e), 122.4 (C_g), 125.1 (C_f), 127.4 (C_h), 142.1 (C_k), 143.7 (C_m), 151.1 (C_j), 152.6 (C_l). EI-MS: $[M+H]^+$ $C_{17}H_{21}N_6O$ calcd 325.1777, obsd 325.16.

3.2.3.7 Synthesis of (4-((4-((3-azidopropyl)(methyl) amino)-2-methoxyphenyl) diazenyl) phenyl) methanol (**19**)

4-aminobenzylalcohol (0.275 g, 2.24 mmol) and NaNO$_2$ (0.16 g, 2.35 mmol) were dissolved in EtOH/water (4.5 + 3.0 mL = 7.5 mL), to which 2 N HCl solution (4.5 mL) was added at 0 °C and reaction mixture stirred at 0 °C for 1 hour. Compound **17** (0.45 g, 2.04 mmol) in EtOH was added followed by addition of NaOAc (0.15 g) at 0 °C and mixture stirred for 6 hours at room temperature. The remaining procedure was followed as described for compound **1** to obtain compound **19**. Yield: 0.58 g (81%). ^{1}H NMR (500 MHz, CDCl$_3$): δ 1.87 (tt, 2H, J = 6.5, 13.0 Hz, H_c), 2.31 (bs, 1H, OH), 3.03 (s, 3H, NCH$_3$, H_a), 3.36 (tt, 2H, J = 3.0 & 6.5 Hz, H_d), 3.49 (tt, 2H, J = 3.0 & 7.5 Hz, H_b), 4.00 (s, 3H, OMe), 4.67 (s, 2H, H_j), 6.20-6.25 (m, 1H, H_g), 6.30-6.33 (m, 1H, H_e), 7.35-7.42 (m, 2H, H_i), 7.70-7.80 (m, 3H, H_h, H_f); ^{13}C NMR (125 MHz, CDCl$_3$): δ 26.46 (C_c), 38.62 (C_a), 48.82 (C_d), 49.45 (C_b), 55.20 (O$\underline{C}$H$_3$), 64.77 (C_j), 94.94 (C_g), 104.65 (C_e), 118.18 (C_f), 122.33 (C_i), 127.29 (C_h), 133.54 (C_l), 141.85 (C_n), 152.85 (C_m), 152.91 (C_k), 159.19 (C_o). EI-MS: $[M+H]^+$ $C_{18}H_{23}N_6O_2$ calcd 355.18, obsd 355.16.

3.2.3.8 Synthesis of 4-((4-((3-azidopropyl)(methyl)amino)phenyl)diazenyl)benzyl (4-nitrophenyl) carbonate (**20**)

Compound **18** (0.020 g, 0.0512 mmol) was dissolved in 3 mL of DCM and freshly activated 4°A M.S (0.1 g) was added and reaction mixture stirred for 10 minutes. DIPEA (0.038 ml, 0.220 mmol) and DMAP (cat) were then added at 0 °C. *p*-Nitrophenyl chloroformate (0.023 g, 0.116 mmol) in DCM was added dropwise and the reaction mixture stirred at 0 °C for 10 minutes, followed by stirring at room temperature for an additional 30 minutes. The remaining procedure was followed as described for compound **5** to obtain compound **20**. Yield: 0.024 g (80%). ^{1}H NMR (500 MHz, CDCl$_3$): δ 1.93 (tt, 2H, *J* = 6.5, 13.0 Hz, H$_c$), 3.07 (s, 3H, NCH$_3$, H$_a$), 3.39 (t, 2H, *J* = 6.5 Hz, H$_d$), 3.56 (t, 2H, *J* = 7.0 Hz, H$_b$), 5.34 (s, 2H, H$_i$), 6.72-6.78 (m, 2H, H$_e$), 7.32-6.40 (m, 2H, H$_j$), 7.50-7.58 (m, 2H, H$_h$), 7.81-7.92 (m, 4H, H$_f$ and H$_k$), 8.22-8.28 (m, 2H, H$_g$); ^{13}C NMR (125 MHz, CDCl$_3$): δ 25.46 (C$_c$), 38.2 (C$_a$), 49.1 (C$_d$), 49.6 (C$_b$),70.2 (C$_i$), 111.4, 121.8, 131.2, 125.6, 129.2, 134.4, 143.4, 145.3, 151.2, 152.3, 153.6, 155.6. EI-MS: [M+H]$^+$ C$_{24}$H$_{24}$N$_7$O$_5$ calcd 490.1839, obsd 490.17.

*3.2.3.9 Synthesis of 4-((4-((3-azidopropyl)(methyl)amino)-2-methoxyphenyl) diazenyl) benzyl (4-nitrophenyl) carbonate (**21**)*

Compound **19** (0.470 g, 1.32 mmol) was dissolved in DCM (15 mL) and freshly activated 4°A M.S (0.1 g) was added and reaction mixture stirred for 10 minutes. DIPEA (0.925 mL, 5.30 mmol) and DMAP (0.05 g) were then added and reaction mixture cooled to 0 °C. *p*-Nitrophenyl chloroformate (0.535 g, 2.65 mmol) in DCM (2 mL) was added slowly and mixture stirred at 0°C for 1 hour, followed by an additional 2 hours at room temperature. The remaining procedure was followed as described for compound **6** to obtain compound **21**. Yield: 0.48 g (75%).

^{1}H NMR (500 MHz, CDCl$_3$): δ 1.93 (tt, 2H, J = 6.5, 13.0 Hz, H$_c$), 3.10 (s, 3H, NCH$_3$, H$_a$), 3.43 (t, 2H, J = 3.5 Hz, H$_d$), 3.56 (t, 2H, J = 7.0 Hz, H$_b$), 4.05 (s, 3H, OMe), 5.22 (s, 2H, H$_j$), 6.25-6.30 (m, 1H, H$_g$), 6.32-6.38 (m, 1H, H$_e$), 7.00-7.10 (m, 2H, H$_i$), 7.46-7.52 (m, 2H, H$_k$), 7.74-7.90 (m, 3H, H$_l$, H$_f$), 8.12-8.26 (m, 2H, H$_h$); ^{13}C NMR (125 MHz, CDCl$_3$): δ 26.46 (C$_c$), 38.62 (C$_a$), 48.82 (C$_d$), 49.45 (C$_b$), 55.20 (O$\underline{C}$H$_3$), 64.77 (C$_j$), 94.94 (C$_g$), 104.65 (C$_e$), 118.18 (C$_f$), 122.33 (C$_i$), 127.29 (C$_h$), 133.54 (C$_l$), 141.85 (C$_n$), 152.85 (C$_m$), 152.91 (C$_k$), 159.19 (C$_o$). EI-MS: [M+H]$^+$ C$_{25}$H$_{26}$N$_7$O$_6$ calcd 520.19, obsd 520.17.

3.2.3.10   *Synthesis of 4-((4-((3-azidopropyl)(methyl)amino)phenyl)diazenyl)benzyl-Doxorubicin carbonate* (**22**)

Compound **20** (0.020 g, 0.04 mmol) was dissolved in 2 mL of anhydrous DMF and freshly activated 4°A M.S (0.1 g) was added and reaction mixture for 10 minutes. Neutralized Doxorubicin-HCl (0.035 g, 0.061 mmol) in DIPEA (0.075 mL) was added and reaction mixture stirred at 32 °C for 24 hours. The reaction mixture was concentrated under reduced pressure and residue purified by silica gel column chromatography (DCM:MeOH 9.5:0.5) to produce compound **22**. Yield: 0.03 g (82%). ^{1}H NMR (500 MHz, CDCl$_3$) δ 1.26 (t, 3H, J = 7.5 Hz, CH$_3$, H$_o$), 1.72-1.92 (m, 4H, H$_c$, H$_k$, H$_j$), 2.06-16 (m, 3H, H$_n$,H$_j$, H$_k$), 2.23-2.34 (m, 2H, H$_q$), 2.86 (bd, 1H, J = 7.5 Hz, -OH), 3.00-3.04 (m, 4H, -OH, NCH$_3$, H$_a$), 3.18 (d, 1H, J = 7.5 Hz, -OH), 3.35 (t, 2H, J = 6.5 Hz, H$_d$), 3.49 (t, 2H, J = 7.0 Hz, H$_b$), 3.65 (m, 1H, -OH), 3.80-3.90(m, 1H, H$_l$), 4.02 (s, 3H, OMe), 4.10-4.20 (m, 2H, H$_m$, H$_r$), 4.52 (bs, 1H, OH), 4.73 (s, 2H, H$_s$), 5.02 (s, 2H, H$_i$), 5.18-5.29 (m, 3H, OH, H$_r$), 5.46 (bs, 1H, OH), 6.64-6.74 (m, 2H, H$_e$), 7.27-7.40 (m, 4H, H$_u$, H$_v$, H$_w$,

H$_g$), 7.64-7.82 (m, 5H, H$_f$, H$_g$, H$_h$), 7.94 (m, 1H, NH), 13.14 (bs, 1H, OH, H$_t$), 13.98 (bs, 1H, OH, H$_t$). ESI-MS: [M+H]$^+$ C$_{46}$H$_{50}$N$_7$O$_{13}$ calcd 908.3467, obsd 908.27.

3.2.3.11 *Synthesis of 4-((4-((3-azidopropyl)(methyl)amino)-2-methoxyphenyl) diazenyl) benzyl (4-Doxorubisine) carbonate* (**23**)

Compound **21** (0.020 g, 0.038 mmol) was dissolved in anhydrous DMF (2 mL) and freshly activated 4°A M.S (0.1 g) was added and reaction mixture stirred for 10 minutes. Neutralized Doxorubicin-HCl (0.033 g, 0.057 mmol) in DIPEA (0.015 mL) was added and reaction mixture stirred at room temperature for 24 hours. After completion of the reaction (monitored by TLC) the solvents were evaporated under reduced pressure and residue purified by silica gel column chromatography (EtOAc:*n*-hexane 3.5:6.5) affording compound **23**. Yield: 0.028 g (76%). ^{1}H NMR (500 MHz, CDCl$_3$): δ 0.94 (t, 3H, *J* = 7.5 Hz, H$_q$), 1.56 (dt, 2H, *J* = 3.0, 7.5 Hz, H$_{k,l}$), 1.62 (dt, 2H, *J* = 3.0, 7.5 Hz, H$_{k,l}$), 1.81 (m, 1H, H$_o$), 1.93 (tt, 2H, *J* = 7.5 Hz, H$_c$), 2.18 (t, 2H, *J* = 10.5 Hz, H$_s$), 2.36 (m, 2H, H$_p$), 3.00-3.12 (m, 5H, H$_t$, NCH$_3$, H$_a$), 2.28 (d, 1H, *J* = 1.5 Hz, OH), 3.31 (d, 1H, *J* = 1.5 Hz, OH), 3.41 (t, 2H, *J* = 6.0 Hz, H$_d$), 3.54 (t, 2H, *J* = 7.0 Hz, H$_b$), 3.62-3.72 (m, 2H, H$_m$, OH), 3.86-3.94 (m, 2H, H$_n$, OH), 4.02 (s, 3H, OMe, H$_w$), 4.08 (s, 3H, OMe), 4.10-4.20 (m, 2H, H$_r$, OH), 4.57 (bs, 1H, OH), 4.77 (d, 2H, *J* = 2.5 Hz, H$_u$), 5.04-5.20 (m, 3H, H$_j$, OH), 5.30 (bs, 1H, OH), 5.52 (bs, 1H, OH), 6.22-6.29 (m, 1H, H$_g$), 6.32-6.37 (m, 1H, H$_e$), 7.35-7.44 (m, 3H, H$_y$, H$_i$), 7.74-7.84 (m, 4H, H$_f$, H$_h$, H$_x$, H$_z$), 8.03-8.06 (m, 1H, H$_h$), 13.26 (bs, 1H, OH, H$_v$), 13.99 (bs, 1H, OH, H$_v$). EI-MS: [M+H]$^+$ C$_{46}$H$_{51}$N$_7$O$_{14}$ calcd 925.34, obsd 925.16.

3.2.3.12 *Coupling of compound* **22** *to G5-alkyne* (**13**) *to prepare G5-L3-DOX* (**24**)

Sodium Ascorbate (0.002 g, 0.002 mmol), bathophenonthroline sulfonated sodium salt (SBP, 0.0055 g, 0.002 mmol) and Cu(I) (0.001 g, 0.001 mmol) were dissolved in THF:water (1:1= 3 mL) and bubbled with nitrogen for 10 minutes. In a separate flask compound **22** (0.0043 g, 0.0003 mmol) and compound **13** (0.012 g, 0.0003 mmol) in THF were combined and solution bubbled with nitrogen for 10 minutes. The flask was then heated to 75 °C for 3-4 minutes, during which time the solution became red in color, followed by cooling to room temperature. The mixture of compounds **13** and **22** were then removed via syringe and added to the catalytic flask dropwise, after which the vessel was capped with a septum, flushed with nitrogen and stirred slowly (~300rpm) in the dark for 48 hours at room temperature. The reaction mixture was then purified by dialysis (10kDa MWCO) for 2 days to afford **G5-L3-DOX**. Yield: 0.014g (82%). MALDI-TOF analysis of compound **G5-L3-DOX** showed a molecular weight of 37,900 Da.

3.2.3.13 *Coupling of compound* **23** *to G5-(NH$_2$)$_{128}$ dendrimers to prepare G5-L4-DOX* (**25**)

Sodium Ascorbate (0.002 g, 0.002 mmol), bathophenonthroline sulfonated sodium salt (SBP, 0.0055 g, 0.002 mmol) and Cu(I) (0.001 g, 0.001 mmol) were dissolved in THF:water (1:1= 3 mL) and bubbled with nitrogen for 10 minutes. In a separate flask compound **23** (0.0043 g, 0.0003 mmol) and compound **13** (0.012 g, 0.0003 mmol) in THF were combined and solution bubbled with nitrogen for 10 minutes. The flask was then heated to 75 °C for 3-4 minutes, during which time the solution became red in color, followed by cooling to room temperature. The mixture of compounds **13** and **23** were

then removed by syringe added to the catalytic flask dropwise, after which the vessel was capped with a septum, flushed with nitrogen at stirred slowly (~300rpm) in the dark for 48 hours at room temperature. The reaction mixture was then purified by dialysis (10kDa MWCO) for 2 days to afford **G5-L4-DOX**. Yield: 0.016g (85%). MALDI-TOF analysis of compound **G5-L4-DOX** showed a molecular weight of 35,670 Da.

3.2.4 Characterization of G5-L(x)-DOX Conjugates

G5-L(x)-DOX conjugates were dissolved in deionized water at a concentration of 1 μM followed by measuring the size and zeta potential of each conjugate using a 90Plus particle size analyzer with ZetaPALS capability (Brookhaven Instruments Corporation, Holtsville, NY). G5-L(x)-DOX conjugates were dissolved in anhydrous DMF containing 0.1M tetrabutylammonium perchlorate at a concentration of 3mM of the incorporated azo-linker and the solution was bubbled with nitrogen for 10 minutes before starting cyclic voltammetry (CV) measurements. CV measurements were performed using an Ag-AgCl reference electrode and a platinum wire as both the counter and working electrode. Scans were performed from 0 to +2V at a 0.05 V/s scan rate and data was recorded using an electrochemical potentiostat/ galvanostat (Autolab PGSTAT12, Eco Chemie, Urtecht, Netherlands). Analysis of 4-HAB and dimethylaminoazobenzene (DAB) azobenzenes standards using CV measurements was done to compare our results to published work,[28] validate our experimental setup, and determine whether the G5 carrier or attached DOX molecules mask the potential peaks characteristic of the azo-linkers.

3.2.3.1 Calculation of DOX Loading per G5 dendrimer (n):

91

Number of DOX molecules attached per G5 carriers (n) in each G5-L(x)-DOX conjugate was quantified by measuring the UV absorbance of an aqueous solution of different conjugates (λ_{max} = 500 nm) in deionized water at a 1 mg/mL conjugate concentration. The peak absorbance for each G5-L(x)-DOX conjugate was compared against a DOX concentration versus absorbance calibration curve following Beers Lambert Law[29] to calculate n as described in Eq. 1:

$$DOX\ Conc = 1\ \tfrac{mg\ G5\text{-}L(x)\text{-}DOX}{ml} * \left[G5\ MW + n\big(MW\ of\ L(x)\text{-}DOX\big)\right]^{-1} \tfrac{mmoles\ G5\text{-}L(x)\text{-}DOX}{mg\ G5\text{-}L(x)\text{-}DOX} * \tfrac{n}{1}\ \tfrac{mmoles\ DOX}{mmoles\ G5\text{-}L(x)\text{-}DOX} \qquad (1)$$

Which is simplified to calculate n as described in Eq. 2:

$$n = \frac{DOX\ Conc\ *\ G5\ MW}{1-(MW\ of\ L(x)\text{-}DOX\ *\ DOX\ Conc)} \qquad (2)$$

The number of L(x)-DOX attached per G5 dendrimer was also calculated by measuring the increase in molecular weight using MALDI-TOF analysis compared to free G5 analyzed at the same time as each G5-L(x)-DOX conjugates. Molecular weight of G5-L(x)-DOX conjugates from MADLI-TOF analysis was calculated as the geometric mean of the curve, and number of attached DOX per dendrimer (n) calculated as described in Eq. 3.

$$n = \frac{G5\text{-}DOX_{(geo\ mean)} - G5\ Dendrimer_{(geo\ mean)}}{MW\ of\ L(x)\text{-}DOX} \qquad (3)$$

Each analysis was performed in triplicate for each G5-L(x)-DOX conjugate and the calculated DOX loading per G5 dendrimer was averaged for the two methods to calculate n.

3.2.5 Cell Culture

HepG2 and Hep3B cells were cultured in T-75 flasks using MEM supplemented with 10% FBS, 1% penicillin/streptomycin/amphotericin (antibiotic-antimycotic), 1% sodium pyruvate and 1% non-essential amino acids. HepG2 and Hep3B cells were culture at 37 °C, 5% CO_2 and 95% relative humidity with medium change every 48 hours. Cells were passaged at 80-90% confluency using a 0.25% trypsin-EDTA solution. Adult rat cardiomyocytes were isolated from Sprague-Dawley rats following establish protocols[30,31] and used immediately either as a cell suspension in DMEM (1×10^6 cells/mL) or plated in laminin coated 24-well plates at a seeding density of 10×10^3 - 20×10^3 cells/well.

3.2.6 Preparation of S9 Fractions

To prepare the S9 fraction, which are the cytosolic and/or microsomal subcellular fraction of lysed cells,[32] from HepG2 hepatic cancer cells or rat cardiomyocytes cells were pelleted by spinning at 1000 rpm for 5 minutes, followed by re-suspending the cell pellet in 500 µL fractionation buffer (250 mM sucrose, 20 mM HEPES, 10 mM KCl, 1.5 mM $MgCl_2$ and 1 mM EDTA in deionized water containing 0.1% 1 mM dithiothreitol and 0.5% v/v of protease inhibitor cocktail (Sigma Aldrich, St. Louis, MO)). Cell suspension was passed 20 times through a 27G needle and kept on ice for 20 minutes to

ensure complete cell lysis before centrifuging the lysate at 9,000 x g for 20 minutes to separate the S9 fraction in the supernatant. All S9 fractions isolated from a particular cell type were pooled together and total protein content was determined using the BCA protein assay (Thermo Fisher Scientific, Rockford, IL). S9 fractions were divided into 100 µL aliquots and stored at -80 °C till used.

3.2.7 Enzymatic Cleavage of G5-L(x)-DOX Conjugates

Cleavage of G5-L(x)-DOX conjugates upon incubation with HLM, S9 fractions isolated from HepG2 cells or rat cardiomyocytes, or control insect protein solution was investigated by monitoring the cleavage of the azo-linker and the associated DOX release as a function of time. Briefly, G5-L(x)-DOX conjugates were dissolved in 0.1M KH_2PO_4 buffer (pH = 7.4) at a concentration of 100 µM equivalent DOX, followed by mixing 300 µL of conjugate's solution with HLM, S9 fraction, or control insect protein solution to achieve 0.5 mg/mL in polypropylene tubes. This solution was treated with 5 µL NADPH regenerating solution A and 1 µL NADPH regenerating solution B following manufacturer's specifications (Becton-Dickinson, Franklin Lakes, NJ), followed by incubation at 37 °C while shaking at 200 rpm to initiate the enzymatic cleavage of G5-L(x)-DOX conjugates. We collected 200 µL of the G5-L(x)-DOX solution at selected time points (0 – 240 minutes) and mixed it with 300 µL of 0.1 M KH_2PO_4 buffer (pH = 7.4) in a quartz cuvette, added 20 µL of 6N HCl to eliminate NADPH absorbance (λ_{max} = 340nm) which masks the characteristic absorbance of L1 and L2 azo-linkers, and measured solution's absorbance (λ_{L1} = 346 nm; λ_{L2} = 374 nm) on a DU 730 UV/Vis Spectrophotometer (Beckman Coulter, Indianapolis, IN). The % intact azo-linker was

calculated for G5-L1-DOX and G5-L2-DOX by dividing the absorbance peak value of the azo-linker at each time point by the initial peak absorbance. We simultaneously mixed 100 µL of the G5-L(x)-DOX solution with 1 mL chloroform to extract free DOX released in solution in response to different treatments, followed by extensive vortexing of this mixture and discarding the aqueous layer. The chloroform fraction was dried under nitrogen and the collected residue dissolved in 100 µL acetonitrile for HPLC analysis. Concentration of free DOX was quantified by measuring its absorbance in the collected fractions at 500 nm using a Symmetry300 C4 5µm (4.6 x 250mm) column connected to a Waters HPLC system equipped with a Waters UV dual λ absorbance detector. A mixture of water:acetonitrile containing 0.14% v/v trifluoroacetic acid was used as a mobile phase to separate free DOX on the C4 column using a solvent gradient of 76:24 for 7 minutes, 48:52 for 7 minutes, and 5:95 for 16 minutes at a flow rate of 1 mL/min. Amount of free DOX present in each sample was quantified by integrating its absorbance intensity at 500 nm versus elution volume using the Waters Breeze software compared to a series of DOX standards with concentrations of 100, 50, 25 and 10 µM. We determined the extraction efficiency of free DOX from the enzyme solutions following the same extraction procedure and HPLC analytical method in parallel with every enzymatic cleavage assay, which was routinely >90%. Percentage of DOX release from G5-L(x)-DOX conjugates in response to different treatments was normalized to the corresponding DOX extraction efficiency. Reduction of G5-L(x)-DOX conjugates by different treatments was investigated in triplicate and results show the average ± standard error of the mean (SEM).

3.2.8 Uptake of G5-L(x)-DOX Conjugates and Intracellular DOX Release

HepG2 or Hep3B hepatic cancer cells were seeded in 24-well plates at a seeding density of 5×10^5 cells/well and allowed to adhere overnight before incubating with 0.5 mL of G5-L(x)-DOX conjugates dissolved in OPTI-MEM at a concentration of 100 µM equivalent DOX. Uptake of G5-L(x)-DOX conjugates into HepG2 and Hep3B cells was examined after incubation for 1 hour, whereas the intracellular concentration of released DOX was quantified after incubation for 24 hours. Similarly, uptake of free DOX and G5-L4-DOX conjugates dissolved in Hank's Balanced Salt Solution (HBSS) at a concentration of 100 µM equivalent DOX into plated rat cardiomyocytes was assayed after incubation for 4 and 8 hours. Briefly, cells were washed with cold PBS, trypsinized and centrifuged at 1,000 rpm for 5 minutes before re-suspending the cell pellet in 1 mL of PBS and measuring the number of cells that internalized free DOX or G5-L(x)-DOX conjugates using flow cytometry (λ_{ex} = 488 nm, λ_{em} = 617 nm) following published protocols.[15] Cleavage of G5-L(x)-DOX conjugates and release of the attached DOX molecules upon incubation with HepG2 and Hep3B cells was investigated by measuring the concentration of free DOX in the culture medium and in cell lysates. Free DOX present in the culture medium was extracted by mixing 250 µL of the medium with 2.5 mL of chloroform followed by vigorous vortexing, discarding the medium layer, drying the chloroform fraction under nitrogen, and dissolving the collected residue in 100 µL of acetonitrile to prepare for HPLC analysis. Treated HepG2 and Hep3B cell monolayers were washed with cold PBS, trypsinized, and centrifuged at 1,000 rpm for 5 minutes before re-suspending the cell pellet in 250 µL of the lysis buffer (10mM borate buffer, pH 9.7, 0.5% v/v Triton X-100), tip-sonicating cell suspension for 10 seconds on ice, and

incubating for 30 minutes at 37 °C. Cell lysates were mixed with 10 folds its volume of chloroform followed by vigorous mixing and placing this mixture in a sonicating water bath at 37 °C for 30 minutes to separate the aqueous and organic layers. The aqueous layer was discarded while the chloroform layer was dried under nitrogen to obtain a dry residue that was dissolved in 250 µL acetonitrile before analysis by HPLC. Amount of free DOX present in culture medium and cell lysates was quantified by HPLC analysis using a Symmetry300 C4 5µm (4.6 x 250mm) column connected to a Hewlett Packard 1090 HPLC system equipped with an HP 1046 fluorescence detector set at λ_{ex} of 486 nm, λ_{em} of 560 nm, and photo multiplier gain of 16. A 60:40 water:acetonitrile mixture containing 0.14% v/v trifluoroacetic acid was used at a flow rate of 1 mL/min as a mobile phase to separate free DOX on the C4 column for 15 minutes. Amount of free DOX present in each sample was quantified by integrating its fluorescence intensity versus elution volume using the HP Chemstation software compared to a series of DOX standards with concentrations of 100, 10 and 1 µM. We determined the extraction efficiency of free DOX following the same extraction procedure and HPLC analytical method, which was routinely >85%. Percentage of free DOX present in the culture medium or cell lysate was normalized to the corresponding DOX extraction efficiency. Intracellular cleavage of G5-L(x)-DOX conjugates and the associated DOX release profile was investigated in triplicate for each conjugate in each cell line and results show the average ± SEM.

3.2.9   Clonogenic Survival of Hepatic Cancer Cells

We compared the anticancer activity of G5-L(x)-DOX conjugates to free DOX as a function of concentration by measuring their effect on clonogenic survival of HepG2 and Hep3B hepatic cancer cells. Briefly, HepG2 and Hep3B cells were seeded at a density of 2.5×10^5 cells/T-25 flask and allowed to adhere overnight before incubating with different concentrations (1 nM – 100 μM equivalent concentration of DOX) of free DOX or G5-L(x)-DOX conjugates dissolved in OPTI-MEM solution. HepG2 and Hep3B cells were also incubated with acetylated G5-$(Ac)_{11}$ dendrimers (at equivalent polymer concentrations to G5-L(x)-DOX conjugates) prepared via partial acetylation of the dendrimer surface amine groups following published protocols,[33] and fresh culture medium as negative controls. After 72 hours HepG2 and Hep3B cells were washed with cold PBS, trypsinized using a 0.25% trypsin-EDTA solution and centrifuged at 1,000 rpm for 5 minutes. Cell pellets were suspended in fresh culture medium, counted, and plated in 6-well plates at a seeding density of 500 – 10,000 cells/well and allowed to grow undisturbed for 14 days under normal culture conditions. The formed colonies were gently washed with cold PBS, treated with 1mL methanol/glacial acetic acid (75/25) and 0.04% w/v trypan blue for 5 minutes and counted. Plating efficiency (PE) for each cell line was calculated by dividing the number of colonies by the cell seeding density for cells incubated with fresh culture medium (negative control). The surviving fraction (SF) represents the number of hepatic cancer cells that can replicate after treatment with different concentration of free DOX and G5-L(x)-DOX conjugates and is calculated by normalizing the number of counted colonies to the product of the original seeding density and plating efficiency (PE). All samples were prepared in triplicate for each seeding density and treatment condition, and results expressed as the average %SF ± SEM.

Cytotoxicity curves were fit by a log(conc.) vs. response(% survival) model and IC_{50} (dotted horizontal line) calculated using Graphpad Prism software.

3.2.10 Cardiac Toxicity of Free DOX and G5-L4-DOX Conjugates

Toxicity of G5-L4-DOX conjugates and free DOX in rat cardiomyocytes was evaluated using the lactate dehydrogenase (LDH) leakage cell viability assay. Briefly, each well was counted for total number of cardiomyocytes before an 8 hour treatment with free DOX or G5-L4-DOX (100µM eq. DOX) conjugates dissolved in 0.5mL HBSS. The amount of LDH released to the medium was assayed by mixing 100 µL of the treatment solution in a 96-well plate with the enzyme substrate (1:1) included in the assay kit following the manufacturer's guidelines. The plate was then measured at $\lambda = 490$ nm using a Multiskan microplate reader (Thermo Scientific, Waltham, MA), and results compared to cardiomyocytes incubated with blank HBSS and 10% v/v Triton X-100 solution as negative and positive controls, respectively. Amount of LDH leakage for treatment solution and controls were normalized to the number of seeded cells, and all values compared to the positive control (set as 100% LDH leakage reference) to obtain the percentage of LDH leakage as a function of treatment. Treatments resulting in statistically higher LDH leakage versus the negative control were considered cytotoxic.

3.3   Results

3.3.1   Synthesis of G5-L(x)-DOX Conjugates

Synthesis of the azo-linkers incorporated into G5-L(x)-DOX conjugates was performed via diazotization of different aromatic compounds, with yields of each intermediate matching similar reactions described in the literature,[18,27] to produce the desired azo-dyes with a characteristic red color distinguishable by UV (see λ_{max} in **Table 3.1**). A *p*-Nitrophenyl chloroformate group was installed on ring B of the azo-molecules to create the 1'6 self-elimination spacer and allow for coupling of DOX based on published protocols,[34] with L(x)-DOX yields of 76%-82%. Covalent attachment of the L(x)-DOX carboxylic acid to G5-$(NH_2)_{128}$ dendrimers through a stable amide bond was accomplished via facile EDC coupling to produce G5-L1-DOX and G5-L2-DOX conjugates. This coupling strategy resulted in poor yields (<50%) during the synthesis of G5-L3-DOX and G5-L4-DOX conjugates due to intermolecular azo-DOX reactions of the aniline derivatives during EDC activation. To enhance the specificity for coupling of azo-DOX to the G5 carrier, and avoid side reactions, a triazole "click" spacer was employed to synthesize G5-L3-DOX and G5-L4-DOX conjugates resulting in improved yields (>80%). G5-L(x)-DOX conjugates were synthesized with an equal number of DOX molecules (11-12) per dendrimer as confirmed by UV and molecular weight analysis (**Table 3.1**).

Table 3.1: Characterization of G5-L(x)-DOX conjugates.

Conjugate	X, Y Substitution	Substitution σ Value	Hammett Sigma Value (σ)	Positive Potential Peak[a] [V]	Azo-linker λ_{max} [nm]	Molecular Weight[b] [Da]	n[c]	Size[d] [nm]	Zeta Potential [mV]
G5-L1-DOX	**X** = O **Y** = H	σ_X = -0.27 σ_Y = 0.00 σ_C = -0.17	-0.44	+1.18	346	38,260	12 ± 1	18.6 ± 2.9	0.97 ± 0.26
G5-L2-DOX	**X** = O **Y** = O-CH$_3$	σ_X = -0.27 σ_Y = -0.27 σ_C = -0.17	-0.71	+1.29	374	38,010	12 ± 2	18.0 ± 1.4	0.70 ± 0.27
G5-L3-DOX	**X** = N-CH$_3$ **Y** = H	σ_X = -0.83 σ_Y = 0.00 σ_C = -0.17	-1.00	+1.07	485	37,900	11 ± 1	24.6 ± 1.3	0.61 ± 0.28
G5-L4-DOX	**X** = N-CH$_3$ **Y** = O-CH$_3$	σ_X = -0.83 σ_Y = -0.27 σ_C = -0.17	-1.27	+1.09	480	36,710	12 ± 3	22.4 ± 5.8	1.02 ± 0.20

[a]*Determined by Cyclic Voltammetry (Appendix Figure S35)*
[b]*Determined by MALDI-TOF analysis (Appendix Figures S15, S16, S33 and S34)*
[c]*Calculated as average from UV and MALDI-TOF results (Eq. 2 and Eq.3)*

[d]*Determined by Dynamic Light Scattering*.

3.3.2 Characterization of G5-L(x)-DOX Conjugates

G5-L(x)-DOX conjugates were synthesized with different O (σ = -0.27) and/or N (σ = -0.83) substitutions in the *para* and *ortho* position of the azo-linker, with the σ value for each substituent obtained from published constants.[22,23] To calculate the cumulative σ value of the azo-linkers each substituents σ value was added to the contribution of the R-CH-R' group (σ_C = -0.17) in the *para* position of the opposite benzyl moiety, resulting in σ values for G5-L(x)-DOX conjugates calculated as -0.44, -0.71, -1.00 and -1.27 for G5-L1-DOX, G5-L2-DOX, G5-L3-DOX and G5-L4-DOX, respectively (**Table 3.1**). CV analysis showed all conjugates had a single positive potential peak that fell between 1.00V - 1.60V (**Table 3.1**; **Appendix Figure S35**). Attachment of DOX molecules to the G5 carriers resulted in molecular weights of G5-L(x)-DOX conjugates between 36 – 38 kDa as determined by MALDI-TOF analysis, and particle sizes of 18.6 nm for G5-L1-DOX, 18.0 nm for G5-L2-DOX, 24.6 nm for G5-L3-DOX and 22.4 nm for G5-L4-DOX. All G5-L(x)-DOX conjugates had an approximately neutral charge (0.61 – 1.02 mV) determined by zeta potential analysis.

3.3.3 Enzymatic Activation of G5-L(x)-DOX Conjugates by Azoreductase Enzymes

In order to achieve therapeutic activity G5-L(x)-DOX conjugates must release free DOX molecules to the cytoplasm of hepatic cancer cells after reduction of the azo-linkers by azoreductase enzymes. The selectivity of G5-L(x)-DOX cleavage and subsequent DOX release in the presence of azoreductase enzymes was quantified via UV and HPLC analysis, respectively, upon incubation of the conjugates with HLM enzymes,

S9 cytoplasmic enzyme fractions from human hepatic cancer cells, and non-enzymatic

control proteins for 4 hours. Results show G5-L1-DOX conjugates were not cleaved by

HLM enzymes as ~100% of the azo-linkages were intact after the 4 hour incubation

period as determined by UV monitoring (**Figure 3.3**; Panel **A**). G5-L2-DOX showed a

linear increase in cleavage by HLM enzymes resulting in 85% of the conjugate intact

after 1.5 hours of incubation, which remained at this level for the remainder of the 4 hour

incubation period. Cleavage of G5-L3-DOX and G5-L4-DOX conjugates could not be

Figure 3.3: Enzymatic cleavage and DOX release from G5-L(x)-DOX Conjugates. (**A**) % intact G5-L(x)-DOX conjugates and corresponding (**B**) % DOX released upon incubation with HLM or (**C,D**) HepG2 S9 enzyme solutions. Data are expressed as mean (n = 3) ± SEM., *P < 0.05, **P < 0.01. P values were determined for L2, L3 and L4 G5-DOX conjugates as compared to G5-L1-DOX results following a two-tailed Student's *t*-test. Curves were fit by a Michaelis-Menten model using Graphpad Prism software.

monitored by UV because of the λ_{max} for these linkers (480-485 nm) falling within the UV absorbance peak of the attached DOX molecules (500 nm).The cleavage of G5-L(x)-DOX conjugates was correlated to DOX release upon reduction and self-elimination of the azo-linkers as determined by HPLC analysis. Results show 4% DOX was released from G5-L1-DOX conjugates after a 4 hour incubation with HLM enzymes (**Figure 3.3**; Panel **B**). Incubation of G5-L2-DOX with HLM enzymes resulted in a linear increase in DOX release which plateaued at 17% after 2 hours of incubation. G5-L3-DOX and G5-L4-DOX conjugates incubated with HLM enzymes also showed a linear drug release profile achieving 60% and 100% total DOX release after 2 hours of incubation, respectively.

While HLM enzymes represent an *in situ* system containing the azoreductase enzymes to validate the enzymatic activation of G5-L(x)-DOX, they are isolated from healthy human hepatocytes and do not represent the enzymatic composition of hepatic cancer cells. To evaluate the cleavage of G5-L(x)-DOX in the cytoplasm of human hepatic cancer cells the S9 cytoplasmic enzyme fraction was isolated from HepG2 cells and incubated with each conjugate for 4 hours. UV monitoring of G5-L1-DOX conjugate cleavage by HepG2 S9 enzymes showed 96% of the azo-linkers intact after 4 hours of incubation (**Figure 3.3**; Panel **C**), while 82% of G5-L2-DOX conjugates remained under the same conditions. These results closely matched the total DOX released from G5-L(x)-DOX conjugates in the presence of HepG2 S9 enzymes (**Figure 3.3**; Panel **D**). G5-L1-DOX and G5-L2-DOX conjugates displayed a linear increase in DOX release over the 4 hour incubation period resulting in 8% and 17% total DOX released, respectively. Similarly, incubation of G5-L3-DOX conjugates with HepG2 S9 enzymes resulted in a

linear release profile totaling 37% DOX release after 4 hours. G5-L4-DOX conjugates showed 89% total DOX release after 2 hours of incubation, and remained at this value for the remainder of the 4 hour incubation period.

To confirm that cleavage of G5-L(x)-DOX and DOX release was selective for the azoreductase enzymes each conjugate was incubated with non-enzymatic control proteins and the NADPH cofactors. Results show ~100% of G5-L1-DOX and G5-L2-DOX conjugates were intact after the 4 hour incubation period with control proteins (**Figure 3.4**; Panel **A**). This correlated to <1% DOX release for both G5-L1-DOX and G5-L2-DOX conjugates over the same incubation time as deteremined by HPLC analysis (**Figure 3.4**; Panel **B**). G5-L3-DOX conjugates showed 4% DOX release in the presence of control proteins, while G5-L4-DOX released 16% of the loaded DOX after 4 hours. To evaluate the influence of the NADPH cofactor on non-specific DOX release from G5-L4-

Figure 3.4: Control azo-linker reduction and DOX release from G5-L(x)-DOX conjugates. (**A**) % intact G5-L(x)-DOX conjugates and corresponding (**B**) % DOX released upon incubation of conjugates with non-enzymatic control protein. Data are expressed as mean (n = 3) ± SEM, *P < 0.05. P values were determined for L2, L3 and L4 G5-L(x)-DOX conjugates as compared to G5-L1-DOX results following a two-tailed Student's *t*-test. Curves were fit by a Michaelis-Menten model using Graphpad Prism software.

DOX in the presence of the non-enzymatic control proteins the conjugate was incubated with the NADPH regenerating solution without the presence of protein for 4 hours, resulting in 18% total DOX release (**Appendix Figure S37**).

3.3.4   Uptake of G5-L(x)-DOX Conjugates and Intracellular DOX Release

To confirm that the enzymatic activation of G5-L(x)-DOX conjugates translated to cytoplasmic delivery of free DOX in whole hepatic cancer cells the uptake and intracellular DOX release of each conjugate in HepG2 and Hep3B human hepatic cancer cells was investigated. Uptake studies showed G5-L(x)-DOX conjugates were internalized by 100% of the treated HepG2 and Hep3B cells after only 1 hour of incubation. By normalizing the average fluorescence intensity of cells treated with G5-L(x)-DOX conjugates to the fluorescence of cells treated with free DOX we deteremined the folds DOX fluorescence as a function of treatment and cell type (**Figure 3.5**; Panels **A** & **C**). Uptake results show nearly all G5-L(x)-DOX conjugates delivered higher concentrations of DOX to the cytoplasm of hepatic cancer cells compared to incubation with free DOX. Specifially, G5-L1-DOX and G5-L2-DOX conjugates achieved 4.4 – 4.5 folds the intracellular concentration of DOX in HepG2 cells compared to cells treated with free DOX after a 1 hour incubation period (**Figure 3.5**; Panel **A**). Relative uptake of G5-L3-DOX and G5-L4-DOX conjugates into HepG2 cells showed 1.0 and 1.6 folds the intracellular concentration of DOX compared to cells treated with free DOX for 1 hour.

Figure 3.5: Uptake of G5-L(x)-DOX conjugates and intracellular DOX release. Internalization of G5-L(x)-DOX conjugates into (**A**) HepG2 or (**C**) Hep3B human hepatic cancer cells after a 1 hour incubation. Intracellular DOX release from G5-L(x)-DOX conjugates upon a 24 hour incubation with (**B**) HepG2 or (**D**) Hep3B cells. Data are expressed as mean (n = 3) ± SEM., *P<0.05, **P < 0.01. P values were determined for L2, L3 and L4 G5-DOX conjugates as compared to G5-L1-DOX results following a two-tailed Student's *t*-test

Despite this differential uptake profile between the G5-L(x)-DOX conjugates intracellular release of free DOX to hepatic cancer cells after 24 hours of incubation (**Figure 3.5**, Panels **B** & **D**) matched the same rank order of DOX release as observed during azoreductase enzymatic reduction of each conjugate (**Figure 3.3**, Panel **B**). Specifically, incubation of HepG2 cells with G5-L1-DOX resulted in 1% of the loaded DOX released to both the medium and intracellular lysate, totaling 2% release of the loaded DOX after 24 hours of incubation (**Figure 3.5**; Panel **B**). Approximately 3% of the loaded DOX was released to the medium for L2-L4 G5-L(x)-DOX conjugates, while

107

intracellularly released DOX assayed in the lysate increased from 3% for G5-L2-DOX, to 14% and 37% for G5-L3-DOX and G5-L4-DOX, respectively. This resulted in 7%, 17% and 39% total DOX release from G5-L2-DOX, G5-L3-DOX and G5-L4-DOX conjugates, respectively, after 24 hours of incubation with HepG2 cells.

Uptake and intracellular DOX release from G5-L(x)-DOX conjugates in Hep3B cells matched results obtained for HepG2 cells under similar conditions. G5-L1-DOX and G5-L2-DOX conjugates showed a 3.7-fold increase in the intracellular DOX concentrations in Hep3B cells relative to cells treated with free DOX after a 1 hour incubation (**Figure 3.5**; Panel **C**). Incubation of Hep3B cells with G5-L3-DOX conjugates for 1 hour resulted in equivalent intracellular DOX concentrations as compared to the free DOX, while G5-L4-DOX achieved 1.4 folds the intracellular drug concentration. Intracellular DOX release from G5-L(x)-DOX conjugates in Hep3B cells showed 1-2% DOX release to the medium for all the conjugates tested after a 24 hour incubation period (**Figure 3.5**; Panel **D**). Similarly to HepG2 cells, intracellularly released DOX from G5-L(x)-DOX conjugates assayed in the lysate of treated Hep3B cells followed a rank order of release which matched the affinity of the azo-linker to azoreductase reduction, achieving 0%, 2%, 9% and 27% DOX released to the cytoplasm of Hep3B cells after a 24 hour incubation with G5-L1-DOX, G5-L2-DOX, G5-L3-DOX and G5-L4-DOX conjugates, respectively. This resulted in 1%, 3%, 10% and 28% total DOX released from G5-L1-DOX, G5-L2-DOX, G5-L3-DOX and G5-L4-DOX conjugates, respectively, after 24 hours of incubation with Hep3B cells

3.3.5 Anticancer Activity of G5-L(x)-DOX Conjugates

Enzymatic activation of G5-L(x)-DOX conjugates and selective DOX release to the cytoplasm of hepatic cancer cells is expected to result in significant anticancer activity of these conjugates *in vitro*. We tested this by performing a clonogenic survival assay on HepG2 and Hep3B cells incubated with G5-L(x)-DOX conjugates or free DOX at different equivalent DOX concentrations, and compared the percentage of surviving colonies after treatment to cells incubated with G5-(Ac)$_{11}$ or blank medium as negative controls (**Figure 3.6**). Results showed a concentration dependant decline in the %SF of HepG2 cells treated with free DOX for 72 hours (**Figure 3.6**; Panel **A**), resulting in an IC$_{50}$ and IC$_{90}$ of 10 nM and 105 nM, respectively (**Table 3.2**). To determine the contribution of the dendrimer carrier to G5-L(x)-DOX conjugate cytotoxicity HepG2 cells were treated with the G5-(Ac)$_{11}$ polymer control for 72 hours, resulting in an IC$_{50}$ of

Figure 3.6: Clonogenic survival of hepatic cancer cells treated with G5-L(x)-DOX conjugates. (**A**) HepG2 and (**B**) Hep3B cytotoxicity profiles upon treatment with 1 nM - 100 μM concentrations of free DOX, G5-L(x)-DOX conjugates or an equivalent concentration of the G5-(Ac)$_{11}$ polymer control. Data are expressed as the mean for all seeding densities (n = 3) ± SEM. Curves were fit by a log(conc.) vs. response(% survival) model and IC$_{50}$ (dotted horizontal line) calculated using Graphpad Prism software.

Table 3.2: Clonogenic Survival of G5-L(x)-DOX Treated Hepatic Cancer Cells

Treatment	HepG2		Hep3B	
	IC_{50} [nM]	IC_{90} [nM]	IC_{50} [nM]	IC_{90} [nM]
Free DOX	10 ± 4	105 ± 4	2 ± 1	8 ± 1
G5-L4-DOX	13 ± 5	$2,818 \pm 5**$	$63 \pm 1**$	$3,311 \pm 1**$
G5-L3-DOX	$158 \pm 3**$	$1,202 \pm 3**$	$48 \pm 1**$	$398 \pm 1**$
G5-L2-DOX	$2,042 \pm 5**$	$33,884 \pm 5**$	$17,782 \pm 3**$	N.D.
G5-L1-DOX	$12,303 \pm 3**$	$53,703 \pm 3**$	$33,113 \pm 1**$	$43,651 \pm 1**$
G5-Ac (Control)	$12,882 \pm 6**$	$54,954 \pm 6**$	$67,608 \pm 1**$	N.D.

$**P < 0.01$. P values were determined for the IC_{50} and IC_{90} value of each G5-L(x)-DOX conjugate, or G5-Ac polymer control, as compared to free DOX results following a paired two-tailed t-test.

12,882 nM which is a >1,000-fold reduction in toxicity compared to free DOX. Similarly, G5-L1-DOX conjugates were found to be non-toxic after a 72 hour incubation with HepG2 cells due to limited DOX release observed during the *in vitro* intracellular release studies (**Figure 3.5**; Panel **B**), resulting in an IC_{50} and IC_{90} similar to the G5-$(Ac)_{11}$ polymer control of 12,303 nM and 53,703 nM, respectively. G5-L2-DOX, which released 7% of the loaded DOX molecules after a 24 hour incubation with HepG2 cells, showed an increase in cytotoxicity compared to G5-L1-DOX with an IC_{50} of 2,042 nM after a 72 hour incubation with the cells. Similarly, a shift in HepG2 cytotoxicity was observed for G5-L3-DOX and G5-L4-DOX conjugates with IC_{50} values of 158 nM and 13 nM, as well as IC90 values of 1,202 nM and 2,818 nM, respectively. This led to IC_{50} of the most labile G5-L4-DOX conjugates which was not statistically different from free DOX after a 72 hour incubation with HepG2 cells. The decreasing IC_{50} values of L1-L4 G5-L(x)-

DOX conjugates confirms their cytotoxicity profiles match the rank order of DOX release observed from enzymatic and intracellular release studies.

Incubation of Hep3B cells with G5-L(x)-DOX conjugates showed a similar cytotoxicity profile to that of HepG2 cells (**Figure 3.6**; Panel **B**). Incubation of Hep3B cells with free DOX for 72 hours resulted in an IC_{50} and IC_{90} of 2nM and 8 nM, respectively, which is a 5-13 fold reduction in cytotoxicity of the free drug compared to the HepG2 cells. Treatment of Hep3B cells with the $G5-(Ac)_{11}$ polymer control resulted in limited toxicity with IC_{50} values of 67,608nM, a >6,000-fold reduction in toxicity compared to free DOX. Both G5-L1-DOX and G5-L2-DOX conjugates showed limited cyototixicty towards Hep3B cells due to their limited intracellular release to these cells (**Figure 3.5**; Panel **D**), resulting in IC_{50} values of 17,782 nM and 33,113 nM, respectively. Similar HepG2 cells, a shift in cytotoxicity of G5-L3-DOX and G5-L4-DOX was observed in Hep3B cells after a 72 hour incubation, resulting in IC_{50} values of 48 nM and 63 nM, as well as IC_{90} values of 398 nM and 3,311 nM, respectively.

3.3.6   Cardiac Toxicity of G5-L(x)-DOX Conjugates

Due to the well-documented cardiomyopathy associated with the clinical use of free DOX[26] the intracellular DOX release, uptake and toxicity of G5-L(x)-DOX conjugates towards cardiac cells was studied using isolated primary adult rat cardiomyocytes. Intracellular DOX release from G5-L3-DOX and G5-L4-DOX conjugates in the presence of cardiomyocyte S9 cytoplasmic enzyme fractions and the NADPH enzyme cofactor was investigated resulting in 6% of the loaded DOX molecules released from G5-L3-DOX conjugates after 4 hours of incubation, while G5-L4-DOX

conjugates released 16% under the same conditions (**Figure 3.7**; Panel **A**). Based on this

profile G5-L4-DOX conjugates were selected for to study the uptake of G5-L(x)-DOX

conjugates in rat cardiomyocytes after 4 and 8 hours of incubation. Results showed a 1.8

Figure 3.7: Cardiac toxicity of G5-L(x)-DOX conjugates. (**A**) % DOX release from L3 and L4 G5-L(x)-DOX conjugates in the presence of adult rat cardiomyocyte S9 enzymes. (**B**) 4 and 8 hour uptake and (**C**) 8 hour LDH toxicity of G5-L4-DOX conjugates in adult rat cardiomyocytes compared to an equivalent dose of free DOX. Data are expressed as mean (n = 3) ± SEM. **P < 0.01. P values were determined for free DOX and G5-L4-DOX conjugates compared to negative control (blank medium) following a two-tailed Student's *t*-test.

fold reduction in the intracellular concentration of DOX upon incubation of

cardiomyocytes with G5-L4-DOX conjugates for 4 hours, while a 2 fold reduction was

observed at 8 hours, compared to cell treated with an equivalent concentration of free

DOX (**Figure 3.7**; Panel **B**). To determine whether the internalization and intracellular

DOX release profiles of G5-L4-DOX conjugates in cardiomyocytes translated to

cardiotoxicity an LDH leakage cell viability assay was performed (**Figure 3.7**; Panel **C**).

This assay method allows for the quantification of the LDH toxicity marker released to

the medium from cardiomycoytes as a function of treatment, and results compared to

cells lysed with Triton X-100 or incubated with blank medium as positve and negative

controls, respectively, to determine toxicity. Results showed no statistical difference in

the amount of the LDH toxicity marker released to the medium from rat cardiomyocytes

after an 8 hour incubation with G5-L4-DOX conjugates and blank medium (negative

control). Free DOX, however, was found to nearly double the % of LDH leakage compared to G5-L4-DOX treated cells at an equivalent DOX concentration and incubation time, and as a result showed a statistical increase in toxicity compared to cells incubated with blank medium (negative control).

3.4 Discussion

3.4.1 Synthesis and Characterization of G5-L(x)-DOX Conjugates

G5-$(NH_2)_{128}$ PAMAM dendrimers, a class of water soluble hyperbranched nano-polymers capable of high loading capacities of chemotherapeutic moleucles,[35-37] were utilized to prepare G5-L(x)-DOX conjugates. DOX was selected as the chemotherapeutic agent due to its established clinical use in systemic[38] and loco-regional[39] chemotherapy of HCC patients. G5-L1-DOX and G5-L2-DOX conjugates were successfully synthesized via amide coupling, while G5-L3-DOX and G5-L4-DOX incorporated triazole 'clicked' linkages connecting L(x)-DOX molecules to the G5 carrier. This difference in the linkage chemistry utilized to prepare G5-L(x)-DOX conjugates resulted in a small increase in the particle sizes for G5-L3-DOX and G5-L4-DOX conjugates (22-24 nm) compared to G5-L1-DOX and G5-L2-DOX (~18 nm). This is due to the increase in spacer length from a 2 atom bond coupling the dendrimer amine and azo-molecule for L1 and L2 G5-L(x)-DOX conjugates, to a 9 atom spacer of the triazole linked L3 and L4 G5-L(x)-DOX conjugates. However, it is expected this difference in the coupling strategy will not affect linkage accessibility of G5-L(x)-DOX conjugates to the azoreductase enzymes since an equivalent number of DOX molecules were attached per dendrimer. This ensures that

each conjugate has equal water-solubility, as well as similar surface steric properties which is well known to affect the metabolic activity of hepatic enzymes.[40]

All G5-L(x)-DOX conjugates had an approximately neutral surface charge, which in combination with their small size, results in favorable biodistribution, toxicity and cellular uptake profiles.[41] Specifically, it has been shown that neutral polymeric nanoparticles ≤150nm in diameter retain effective internalization into hepatic cancer cells, while showing decreased phagocytosis by macrohpages and lower non-specific accumulation to liver and lung tissue *in vivo* compared to both cationic and large diameter (>150nm) nanoparticles.[41] In addition, neutralization of the cationic surface charge characteristic of PAMAM dendrimers has been shown to improve their biocompatability *in vitro*[42] and *in vivo*[43]. The molecular weight of all G5-L(x)-DOX conjugates was found to be below the renal excretion limit of ~50kDa,[44] indicating these conjugates will be excreted into the urine after intravenous administration to avoid long-term residence *in vivo* known to cause systemic toxicity of non-biodegradable polymeric nanoparticles.[45] Finally, all G5-L(x)-DOX conjugates displayed a positive potential peak during cyclic voltammetry analysis within 1.00 − 1.60V (**Appendix Figure S35**), a range previously shown to be characteristic for azo-dyes known to be substrates for the azoreductase enzymes.[28] These results confirm synthesized azo-linkers retain the electrochemical properties necessary for azoreductase reduction after covalent conjugation to DOX molecules and the G5 dendrimer carrier.

3.4.2 Cleavage and DOX Release from G5-L(x)-DOX Conjugates by Azoreductase Enzymes

Enzyme-activated G5-L(x)-DOX conjugates represent a novel drug release strategy able to achieve selective DOX delivery to hepatic cancer cells with tunable release based on azo-linker affinity to azoreductase enzymes. To determine the extent and rate of DOX release from these conjugates in the presence of azoreductase enzymes we incubated G5-L(x)-DOX with HLM. This led to an increase in the rate of cleavage and DOX release from G5-L(x)-DOX conjugates as a function of decreasing σ value beyond the -0.37 threshold, similar to the profile observed for azo-dyes studied during Zbaida's experiments.[19-21] Specifically, incubation of G5-L1-DOX conjugates with HLM enzymes resulted in limited cleavage of the azo-linker and DOX release due to the linkage σ value (-0.44) approaching the substrate σ threshold necessary for azoreductase binding. G5-L2-DOX, G5-L3-DOX and G5-L4-DOX conjugates followed an expected increase in DOX release rate due to azoreductase cleavage as a function of decreasing azo-linker σ value, resulting in 100% DOX release from G5-L4-DOX after a 4 hour incubation with HLM enzymes.

To determine the extent of DOX release from G5-L(x)-DOX conjugates in the cytoplasm of hepatic cancer cells conjugates were incubated with S9 cytoplasmic enzymes isolated from HepG2 cells. This resulted in a rank order of DOX release from G5-L(x)-DOX conjugates which matched HLM results. However, L3 and L4 G5-L(x)-DOX conjugates showed a ~10%-20% reduction in the total DOX released after a 4 hour incubation with S9 enzymes prepared from hepatic cancer cells as compared to HLM isolated from normal human hepatocytes. This is likely due to the reduction in expression levels of common metabolic enzymes characteristic of malignant transformation of hepatocytes to hepatic cancer phenotypes.[46-48] This difference in enzymatic reduction

between HepG2 S9 and HLM enzymes was not observed for G5-L1-DOX and G5-L2-DOX conjugates due to their low affinity to azoreductase enzymes resulting in saturation of the reduction rate despite a decrease in enzyme expression levels.

DOX release from G5-L(x)-DOX conjugates was confirmed to be selective for the azoreductase enzymes with limited reduction of the azo-linker for G5-L1-DOX and G5-L2-DOX conjugates after a 4 hour incubation period with non-enzymatic control proteins. This correlated to negligible DOX release from L1-L3 G5-L(x)-DOX conjugates in the presence of the control protein solution, while G5-L4-DOX conjugates released 16% of the loaded DOX molecules under the same conditions. Incubation of G5-L4-DOX conjugates in the NADPH generating system without protein confirmed that this non-specific DOX release was a result of azo-linker reduction by the NADPH enzyme cofactor (**Appendix Figure S37**). The non-specific reduction of azo-dyes by NADPH has been previously reported,[20] and is expected to increase as a function of azo-linker electronegativity resulting in the greatest cleavage observed for the highly labile G5-L4-DOX conjugates.

3.4.3   Uptake of G5-L(x)-DOX Conjugates and Intracellular DOX Release

To confirm G5-L(x)-DOX can achieve selective release of DOX to the cytoplasm of hepatic cancer cells *in vitro* uptake and intracellular drug release of each conjugate in HepG2 and Hep3B cells was studied. Results showed a substantial increase in intracellular DOX concentrations after a 1 hour of incubation with G5-L1-DOX and G5-L2-DOX conjugates compared to an equivalent concentration of free DOX. This is due to the ability of the loaded DOX molecules on G5-L(x)-DOX conjugates to avoid

116

recognition and efflux by the P-glycoprotein (Pgp) multi-drug transport protein overexpressed in cancer cells[49] when bound to macromolecules like polymeric carriers.[50,51] In addition, L1 and L2 G5-L(x)-DOX conjugates showed a 2-4 fold increase in intracellular DOX concentrations after a 1 hour incubation with HepG2 and Hep3B cells compared to an equivalent concentration of G5-L3-DOX and G5-L4-DOX conjugates. This extensive internalization of G5-L1-DOX and G5-L2-DOX is likely caused by precipitation of the amphilic conjugates out of solution via particle aggregation as a result of the displayed hydrophobic DOX corona. This dissolution results in rapid contact of the particles with the cell surface increasing the potential for both fluid-phase pinocytosis as well as partitioning of drug-loaded nanoparticles through the cellular lipid membrande via fusion of the hydrophobic DOX corona.[52] This is supported by the observation that L1 and L2 G5-L(x)-DOX conjugates formed visible precipitations after a two week storage period at room temperature in deionized water, while L3 and L4 G5-L(x)-DOX conjugates were found to be stable for months at similar storage conditions. We believe this difference in aqeuous stability is due to the increased distance of DOX molecules from the G5 carriers for G5-L3-DOX and G5-L4-DOX conjugates which incoporate triazole 'clicked' linkages covalently coupling azo-DOX molecules to the dendrimer, while G5-L1-DOX and G5-L2-DOX are prepared through shorter peptide-bonds. This architecture may allow for improved solvency of the particles and therefore explain the reduced internalization profile of L3 and L4 G5-L(x)-DOX conjugates as compared to L1 and L2 G5-L(x)-DOX formulations into both HepG2 and Hep3B cells.

Despite this differential uptake profile for G5-L(x)-DOX conjugates intracellular drug release studies found the rank order for the amount of DOX released from the

117

conjugates correlated to results from HLM and HepG2 S9 enzymatic reduction studies. This resulted in the greatest intracellular amount of DOX release observed from G5-L4-DOX conjugates with 37% and 27% total DOX released after a 24 hour incubation with HepG2 and Hep3B hepatic cancer cells, respectively. The difference in extent of DOX release from each G5-L(x)-DOX conjugates between HepG2 and Hep3B cell lines is due to the reported variance in their expression of drug-metabolizing enzymes.[53,54] Studies are currently underway to further investigate this difference in DOX release from G5-L(x)-DOX conjugates between the tested hepatic cancer cell lines by identifying the key hepatic enzymes responsible for conjugate cleavage.

A small fraction of DOX was assayed in the medium of treated HepG2 (1-3%) and Hep3B cells (1-2%) due to recognition and efflux of the intracellularly released DOX from G5-L(x)-DOX conjugates by the Pgp. In addition, the total percentage of DOX effluxed by Pgp to the medium for both cell lines was similar for all the tested G5-L(x)-DOX conjugates despite a large increase in intracellular DOX released, indicating the rate of DOX effluxed by Pgp after liberation from G5-L(x)-DOX conjugates was saturated at a relatively low intracellular drug concentration. This minimal amount of DOX efflux highlights the advantage of cell-specific drug delivery using polymeric carriers to achieve high intracellular drug concetrations in hepatic cancer cells.[49,50]

3.4.4 Anticancer Activity of G5-L(x)-DOX Conjugates

Cytotoxicity of G5-L(x)-DOX conjugates towards hepatic cancer cells was assessed via the clonogenic survival assay,[25] which measures both the viability of treated cancer cells similar to standard cytotoxicity assays (e.g. MTT and trypan blue exlusion) as

well as the inability of living cells to proliferate after DNA damage triggered by the chemotherapeutic agent. Results of the clonogenic survival study showed the rank order of anticancer activity for G5-L(x)-DOX matches the corresponding decrease in azo-linker σ value, and confirms that intracellular activation and release of free DOX from G5-L(x)-DOX corresponds to effective apoptosis *in vitro*. Specifically, G5-L(x)-DOX conjugates were found to be non-toxic in their parent form towards HepG2 and Hep3B cells (G5-L1-DOX), until activated by the azoreductase enzymes resulting in a shift in cytotoxicity of G5-L(x)-DOX conjugates based on azo-linker σ value and subsequently their relative affinity to azoreductase cleavage. This resulted in a cytotoxicity profile for G5-L4-DOX conjugates which matched the free drug in HepG2 cells.

Treatment of Hep3B cells with free DOX resulted in a 5-fold reduction in IC_{50} values compared to HepG2 cells which is a due to the increased sensitivity of Hep3B cells to DOX-meadiated DNA damage due to a *p53* deletion while HepG2 has retained wild-type *p53*.[55] Though G5-L2-DOX conjugates were toxic in HepG2 cells, both G5-L1-DOX and G5-L2-DOX were found to be relatively non-toxic in Hep3B cells due to the lack of intracellular DOX release. This difference is attributed to the differential expression of metabolic enzymes between the HepG2 and Hep3B hepatic cancer cell lines.[53,54] Interestingly, G5-L3-DOX and G5-L4-DOX conjugates had similar IC_{50} values in Hep3B cells (48nM and 63nM, respectively) after a 72 hour incubation period, indicating a threshold toxicity in these cells was achieved by the activated G5-L(x)-DOX conjugates. This is likely due to the reported *p53*-independent modulation of p27, a potent cell-cycle arrest protein, after exposure of Hep3B cells to DOX resulting in a potential dose-dependant DOX apoptotic threshold.[55] Furthermore, G5-L3-DOX

conjugates were found to have lower IC_{90} values towards HepG2 and Hep3B cells compared to G5-L4-DOX conjugates. The reason for this observation is not clear and is likely dependant on expression and relative kinetics of the enzyme responsbile for azoreductase activity as a function of conjugate composition and exposure time, further highlighting the necessity of studies to identify and characterize this enzyme species.

While these G5-L(x)-DOX conjugates show effective anticancer activity *in vitro*, the most signifcant advantage of polymer-based nanoparticles is their ability to enhance the water solubility of the loaded chemotherapeutic agents *in vivo*,[14,51,56] leading to preferential tumor tissue distribution,[57,58] and the ability to achieve cancer cell-specific drug delivery leading to high anticancer activity while avoiding non-specific toxicity.[50,61,62]

3.4.5   Cardiac Toxicity of G5-L(x)-DOX Conjugates

The major dose-limiting toxicity of DOX administration in the clinic is acute and chronic cardiomyopathy at high cumulative doses.[26] In order for G5-L(x)-DOX conjugates to be cardiotoxic the conjugates must be internalized and release free DOX to the cytoplasm of cardiac cells. To study the relative intracellular DOX release from G5-L(x)-DOX conjugates in cardiac cells G5-L3-DOX and G5-L4-DOX were incubated with S9 cytoplasmic enzyme fractions isolated from primary rat cardiomyocytes. Results showed G5-L3-DOX conjugates released a negligible amount of DOX over the 4 hour incubation period, while G5-L4-DOX conjugates had a similar DOX release profile in the presence of cardiomyocyte S9 enzymes to incubation with only the NADPH cofactor (**Appendix Figure S37**). This confirms that G5-L(x)-DOX conjugates show limited

DOX release to normal cardiomyocytes due to low expression of metabolic enzymes in cardiac tissue.[59]

Coupling of DOX to G5 dendrimers to prepare G5-L4-DOX conjugates resulted in a 1.8-2 fold reduction of the intracellular DOX concentration in rat cardiomyocytes compared to an equivalent dose of free DOX up to 8 hours of incubation. This is due to the requirement of macromolecular G5-L4-DOX conjugates to be internalized into cardiac cells by endocytosis, while free DOX can passively diffuse through the cellular lipid membrane and into the cytoplasm, where they are retained due to the lack of Pgp expression in cardiac tissue.[60] The limited uptake of G5-L(x)-DOX conjugates and negligible DOX release in the presence of rat cardiomyocyte cytoplasmic enzymes resulted in G5-L4-DOX conjugates being non-toxic towards plated rat cardiomyocytes after an 8 hour incubation as determined by the LDH leakage cell viability assay, while an equivalent dose of free DOX was found to be toxic. These results highlight the ability of G5-L(x)-DOX to utilize the presence of the liver-specific azoreductase enzymes as a switch to control DOX release, and as a result achieve selective DOX delivery and cytotoxicity towards hepatic cancer cells. As a result G5-L(x)-DOX conjugates have the potential to achieve high anticancer activity towards hepatic cancer cells while limiting the delivery of free DOX to heart tissue and thereby reducing the cardiotoxicity associated with DOX administration in the clinic.[26]

3.5 Conclusions

G5-L(x)-DOX conjugates were synthesized incorporating four different azo-linkers (L1-L4) to achieve selective DOX release in the presence of the liver-specific

azoreductase enzyme. By modulating the σ values of the engineered azo-linkers, and subsequently changing its affinity to azoreductase cleavage, G5-L(x)-DOX conjugates were able to achieve tunable DOX release in the presence of azoreductase enzymes and the cytoplasm of whole hepatic cancer cells. This resulted in effective hepatic cancer cell apoptosis upon incubation with G5-L(x)-DOX conjugates, with cytotoxicity profiles that followed a similar rank order of DOX release as observed during enzymatic reduction and *in vitro* drug release studies. Limited DOX release, uptake and non-specific toxicity of G5-L(x)-DOX conjugates towards isolated rat cardiomyocytes confirmed delivery of free DOX was selective for hepatic cancer cells upon activation by azoreductase enzymes. As a result G5-L(x)-DOX nano-conjugates show potential as a novel therapeutic alternative to loco-regional chemotherapy techniques in the treatment of unresectable HCC, which will preferentially accumulate in tumor tissue and selectively release the loaded DOX molecules to hepatic cancer cells to achieve high anticancer activity with reduced DOX-mediated cardiotoxicity in the clinic. Furthermore, the flexibility in the design of the descibed azo-linkers offers the opportunity to incorporate a variety of linker compositions into a single G5-L(x)-DOX molecule to achieve differential activation and DOX release rates in the presence of azoreductase enzymes to design personalized medicines for HCC therapy.

Acknowledgments

References

1   ACS. Vol. Cancer Facts & Figures 2011 . (American Cancer Society, Atlanta, 2011).

2   Vol. . (American Cancer Society, Atlanta, 2011).

3   Bosch, F. X., Ribes, J., Díaz, M. & Cléries, R. Primary liver cancer: worldwide incidence and trends. *Gastroenterology* **127**, S5-S16 (2004).

4   El-Serag, H. B., Marrero, J. A., Rudolph, L. & Reddy, K. R. Diagnosis and treatment of hepatocellular carcinoma. *Gastroenterology* **134**, 1752-1763 (2008).

5   Poon, R. T.-P., Fan, S.-T. F., Tsang, F. H.-F. & Wong, J. Locoregional therapies for hepatocellular carcinoma: a critical review from the surgeon's perspective. *Ann. Surg.* **235**, 466-486 (2002).

6   Yamada, R. *et al.* Transcatheter arterial chemoembolization (TACE) in the treatment of unresectable liver cancer. *World J. Surg.* **19**, 795-800 (1995).

7   Skitzki, J. J. & Chang, A. E. Hepatic artery chemotherapy for colorectal liver metastases: technical considerations and review of clinical trials. *Surg. Oncol.* **11**, 123-135 (2002).

8   Li, L. *et al.* In vivo delivery of silica nanorattle encapsulated docetaxel for liver cancer therapy with low toxicity and high efficacy. *ACS Nano* **4**, 6874-6882 (2010).

9   Liu, S.-Y., Liang, Z.-S., Gao, F., Luo, S.-F. & Lu, G.-Q. In vitro photothermal study of gold nanoshells functionalized with small targeting peptides to liver cancer cells. *J. Mater. Sci.* **21**, 665-674 (2010).

10   Maeng, J. H. *et al.* Multifunctional doxorubicin loaded superparamagnetic iron oxide nanoparticles for chemotherapy and magnetic resonance imaging in liver cancer. *Biomaterials* **31**, 4995-5006 (2010).

11   Na, K., Park, K.-H., Kim, S. W. & Bae, Y. H. Self-assembled hydrogel nanoparticles from curdlan derivatives: characterization, anti-cancer drug release and interaction with a hepatoma cell line (HepG2). *J. Control. Release* **69**, 225-236 (2000).

12   Maeda, H. SMANCS and polymer-conjugated macromolecular drugs: advantages in cancer chemotherapy. *Adv. Drug Deliver. Rev.* **46**, 169-185 (2001).

13   Duncan, R. *et al.* Preclinical evaluation of polymer-bound doxorubicin. *J. Control. Release* **19**, 331-346 (1992).

14   Kopeček, J., Kopečková, P., Minko, T. & Lu, Z.-R. HPMA copolymer–anticancer drug conjugates: design, activity, and mechanism of action. *Eur. J. Pharm. Biopharm.* **50**, 61-81 (2000).

15   Tang, A., Kopečková, P. & Kopeček, J. Binding and cytotoxicity of HPMA copolymer conjugates to lymphocytes mediated by receptor-binding epitopes. *Pharm. Res.* **20**, 360-367 (2003).

16   David, A., Kopečková, P., Rubinstein, A. & Kopeček, J. Enhanced biorecognition and internalization of HPMA copolymers containing multiple or multivalent carbohydrate side-chains by human hepatocarcinoma cells. *Bioconjugate Chem.* **12**, 890-899 (2001).

17   Lammers, T. *et al.* Effect of physicochemical modification on the biodistribution and tumor accumulation of HPMA copolymers. *J. Control. Release* **110**, 103-118 (2005).

18   Gao, S.-Q., Lu, Z.-R., Petri, B., Kopečková, P. & Kopeček, J. Colon-specific 9-aminocamptothecin-HPMA copolymer conjugates containing a 1,6-elimination spacer. *J. Control. Release* **110**, 323-331 (2006).

19   Zbaida, S. in *Enzyme Systems that Metabolise Drugs and Other Xenobiotics*   555-566 (John Wiley & Sons, Ltd, 2002).

20   Zbaida, S., Brewer, C. F. & Levine, W. G. Substrates for microsomal azoreductase. Hammett substituent effects, NMR studies, and response to inhibitors. *Drug Metab. Dispos.* **20**, 902-908 (1992).

21   Zbaida, S., Brewer, C. F. & Levine, W. G. Hepatic microsomal azoreductase activity. Reactivity of azo dye substrates is determined by their electron densities and redox potentials. *Drug Metab. Dispos.* **22**, 412-418 (1994).

22   Hammett, L. P. The effect of structure upon the reactions of organic compounds. Benzene derivatives. *J. Am. Chem. Soc.* **59**, 96-103 (1937).

23   McDaniel, D. H. & Brown, H. C. An extended table of hammett substitutent constants based on the ionization of substituted benzoic acids. *J. Org. Chem.* **23**, 420-427 (1958).

24   de Groot, F. M. H. *et al.* Elongated multiple electronic cascade and cyclization spacer systems in activatible anticancer prodrugs for enhanced drug release. *J. Org. Chem.* **66**, 8815-8830 (2001).

25   Franken, N. A. P., Rodermond, H. M., Stap, J., Haveman, J. & van Bree, C. Clonogenic assay of cells in vitro. *Nat. Protoc.* **1**, 2315-2319 (2006).

26   Saltiel, E. & McGuire, W. Doxorubicin (adriamycin) cardiomyopathy - a critical review. *Western J. Med.* **139**, 332-341 (1983).

27   Kim, J.-H., El-Khouly, M. E., Araki, Y., Ito, O. & Kay, K.-Y. Photoinduced processes of subphthalocyanine-diazobenzene-fullerene triad as an efficient excited energy transfer system. *Chem. Lett.* **37**, 544-545 (2008).

28   Zbaida, S. & Levine, W. G. A novel application of cyclic voltammetry for direct investigation of metabolic intermediates in microsomal azo reduction. *Chem. Res. Toxicol.* **4**, 82-88 (1991).

29   Fuwa, K. & Valle, B. L. The physical basis of analytical atomic absorption apectrometry. The pertinence of the Beer-Lambert law. *Anal. Chem.* **35**, 942-946 (1963).

30   Westfall, M. V., Rust, E. M., Albayya, F. & Metzger, J. M. in *Methods in Cell Biology* Vol. Volume 52 (eds P. Emerson Charles & H. Lee Sweeney) Ch. 15, 307-322 (Academic Press, 1997).

31   Wahr, P. A., Michele, D. E. & Metzger, J. M. Effects of aging on single cardiac myocyte function in Fischer 344 x Brown Norway rats. *Am. J. Physiol.-Heart. C.* **279**, H559-H565 (2000).

32   van de Kerkhof, E. G., de Graaf, I. A. M. & Groothuis, G. M. M. In vitro methods to study intestinal drug metabolism. *Curr. Drug Metab.* **8**, 658-675 (2007).

33   Medina, S. H. *et al.* N-acetylgalactosamine-functionalized dendrimers as hepatic cancer cell-targeted carriers. *Biomaterials* **32**, 4118-4129 (2011).

34   Yoo, H. S. & Park, T. G. Biodegradable polymeric micelles composed of doxorubicin conjugated PLGA–PEG block copolymer. *J. Control. Release* **70**, 63-70 (2001).

35   Svenson, S. & Tomalia, D. A. Dendrimers in biomedical applications--reflections on the field. *Adv. Drug Deliver. Rev.* **57**, 2106-2129 (2005).

36   Medina, S. H. & El-Sayed, M. E. H. Dendrimers as carriers for delivery of chemotherapeutic agents. *Chem. Rev.* **109**, 3141-3157 (2009).

37   Tomalia, D. A., Reyna, L. A. & Svenson, S. Dendrimers as multi-purpose nanodevices for oncology drug delivery and diagnostic imaging. *Biochem. Soc. Trans.* **035**, 61-67 (2007).

38   Nowak, A. K., Chow, P. K. H. & Findlay, M. Systemic therapy for advanced hepatocellular carcinoma: a review. *Eur. J. Cancer* **40**, 1474-1484 (2004).

39   Kalva, S. P. *et al.* Transarterial cemoembolization with doxorubicin-eluting microspheres for inoperable hepatocellular carcinoma. *Gastrointest. Cancer Res.* **4**, 2-8 (2011).

40   Langowski, J. & Long, A. Computer systems for the prediction of xenobiotic metabolism. *Adv. Drug Deliver. Rev.* **54**, 407-415 (2002).

41   He, C., Hu, Y., Yin, L., Tang, C. & Yin, C. Effects of particle size and surface charge on cellular uptake and biodistribution of polymeric nanoparticles. *Biomaterials* **31**, 3657-3666 (2010).

42   Sadekar, S. & Ghandehari, H. Transepithelial transport and toxicity of PAMAM dendrimers: Implications for oral drug delivery. *Adv. Drug Deliver. Rev.* **64**, 571-588 (2012).

43   Greish, K. *et al.* Size and surface charge significantly influence the toxicity of silica and dendritic nanoparticles. *Nanotoxicology* **28**, 1-11 (2011).

44   Fox, M. E., Szoka, F. C. & Fréchet, J. M. J. Soluble polymer carriers for the treatment of cancer: the importance of molecular architecture. *Accounts Chem. Res.* **42**, 1141-1151 (2009).

45   Alexis, F., Pridgen, E., Molnar, L. K. & Farokhzad, O. C. Factors affecting the clearance and biodistribution of polymeric nanoparticles. *Mol. Pharm.* **5**, 505-515 (2008).

46   Aninat, C. *et al.* Expression of cytochromes P450, conjugated enzymes and nuclear receptors in human hepatoma HepaRG cells. *Drug Metab. Dispos.* **34**, 75-83 (2006).

47   Wilkening, S. & Bader, A. Influence of culture time on the expression of drug-metabolizing enzymes in primary human hepatocytes and hepatoma cell line HepG2. *J. Biochem. Mol. Toxic.* **17**, 207-213 (2003).

48   Wilkening, S., Stahl, F. & Bader, A. Comparison of primary human hepatocytes and hepatoma cell line HepG2 with regard to their biotransformation properties. *Drug. Metab. Dispos.* **31**, 1035-1042 (2003).

49   Bao, L. *et al.* Increased expression of P-glycoprotein is associated with doxorubicin chemoresistance in the metastatic 4T1 breast cancer model. *Am. J. Pathol.* **178**, 838-852 (2011).

50   Shen, F. *et al.* Quantitation of doxorubicin uptake, efflux, and modulation of multidrug resistance (MDR) in MDR human cancer cells. *J. Pharmacol. Exp. Ther.* **324**, 95-102 (2008).

51   Duncan, R. Polymer conjugates as anticancer nanomedicines. *Nat. Rev. Cancer* **6**, 688-701 (2006).

52   Verma, A. & Stellacci, F. Effect of surface properties on nanoparticle–cell interactions. *Small* **6**, 12-21 (2010).

53   Guo, L. *et al.* Similarities and differences in the expression of drug-metabolizing enzymes between human hepatic cell lines and primary human hepatocytes. *Drug Metab. Dispos.* **39**, 528-538 (2011).

54   Majer, B. J. *et al.* Genotoxic effects of dietary and lifestyle related carcinogens in human derived hepatoma (HepG2, Hep3B) cells. *Mutat. Res.-Fund. Mol. M.* **551**, 153-166 (2004).

55   Lee, T. K.-W., Lau, T. C.-M. & Ng, I. O.-L. Doxorubicin-induced apoptosis and chemosensitivity in hepatoma cell lines. *Cancer Chemoth. Pharm.* **49**, 78-86 (2002).

56   Greco, F. & Vicent, M. J. Polymer-drug conjugates: current status and future trends. *Front. Biosci.* **13**, 2744-2756 (2008).

57   Maeda, H. The enhanced permeability and retention (EPR) effect in tumor vasculature: the key role of tumor-selective macromolecular drug targeting. *Adv. Enzyme Regul.* **41**, 189-207 (2001).

58   Maeda, H., Bharate, G. Y. & Daruwalla, J. Polymeric drugs for efficient tumor-targeted drug delivery based on EPR-effect. *Eur. J. Pharm. Biopharm.* **71**, 409-419 (2009).

59   Anzenbacher, P. & Anzenbacherová, E. Cytochromes P450 and metabolism of xenobiotics. *Cell Mol. Life Sci.* **58**, 737-747 (2001).

60   Cordon-Cardo, C. *et al.* Expression of the multidrug resistance gene product (P-glycoprotein) in human normal and tumor tissues. *J. Histochem. Cytochem.* **38**, 1277-1287 (1990).

Appendix

General Experimental Procedures

All reactions were carried out with anhydrous solvents in flame-dried glassware and under nitrogen unless otherwise noted. Chemicals used were reagent grade as supplied except where noted. Analytical thin-layer chromatography was performed using silica gel 60 F254 glass plates. Compound spots were visualized by UV light (254 nm) and by staining with a yellow solution containing $Ce(NH_4)_2(NO_3)_6$ (0.5 g) and $(NH_4)_6Mo_7O_{24}\cdot 4H_2O$ (24.0 g) in 6% H_2SO_4 (500 mL). Flash column chromatography was performed on silica gel 60 (230–400 Mesh). NMR spectra were referenced using Me_4Si (0 ppm), residual $CDCl_3$ (δ ^{1}H-NMR 7.26 ppm, ^{13}C-NMR 77.0 ppm), CD_3SOCD_3 (δ ^{1}H-NMR 2.49 ppm, ^{13}C-NMR 39.5 ppm), CD_3OD (δ ^{1}H-NMR 3.30 ppm, ^{13}C-NMR 49.00 ppm), D_2O (δ ^{1}H-NMR 4.56 ppm). Peak and coupling constant assignments are based on ^{1}H-NMR, ^{1}H–^{1}H gCOSY and (or) [1]H–[13]C gHMQC experiments. ESI-MS measurements were performed according to the published procedures2 on a Q-TOF Ultima API LC-MS instrument with Waters 2795 Separation Module (Waters Corporation, Milford, MA). All samples passed through an EagleEye HPLC C18 column, 3 mm × 150 mm, 5 μm at a flow rate of 0.5 mL/min with a linear gradient from 10% eluent B to 26% eluent B over eight minutes with the column temperature maintained at 45°C. All injections were performed in the full-loop injection mode using a 10 μL sample loop. Eluent A consisted of a pure aqueous solution and eluent B contained 75% acetonitrile/25% aqueous solution (v/v). The following instrument settings were common for analyses S16 performed in both positive and negative ion modes: source temperature 120°C, desolvation

temperature 400°C, collision energy 10 eV. When operated in negative ion mode, the mass spectrometer used the following instrument settings: capillary voltage 2.0 kV, cone voltage 35 V, extraction cone 4 V. The following instrumental parameters were used for data acquisition in positive ion mode: capillary voltage 3.5 kV, cone voltage 35 V. Sample concentrations were 1 mg/mL. MALDI-TOF analysis of G5-DOX conjugates, as well as the parent G5 dendrimer, was performed at the University of Michigan Mass Spectrometry Core or the Michigan State University Mass Spectrometry Facility. Briefly, 1 mg of sample was diluted in 50:50 water:methanol before mixing with the 2,5-dihydroxybenzoic acid matrix solution prepared at 10 mg/mL in an acetonitrile:water (1:1) mixture containing 0.1% TFA. Sample solutions were evaporated to dryness on the target plate and analyzed by either a Waters Tofspec-2E or Shimadzu Biotech Axima CFR MALDI-TOF instrument; both calibrated using BSA in sinapinic acid

Synthesis of G5 –L1-DOX and G5-L2-DOX conjugates
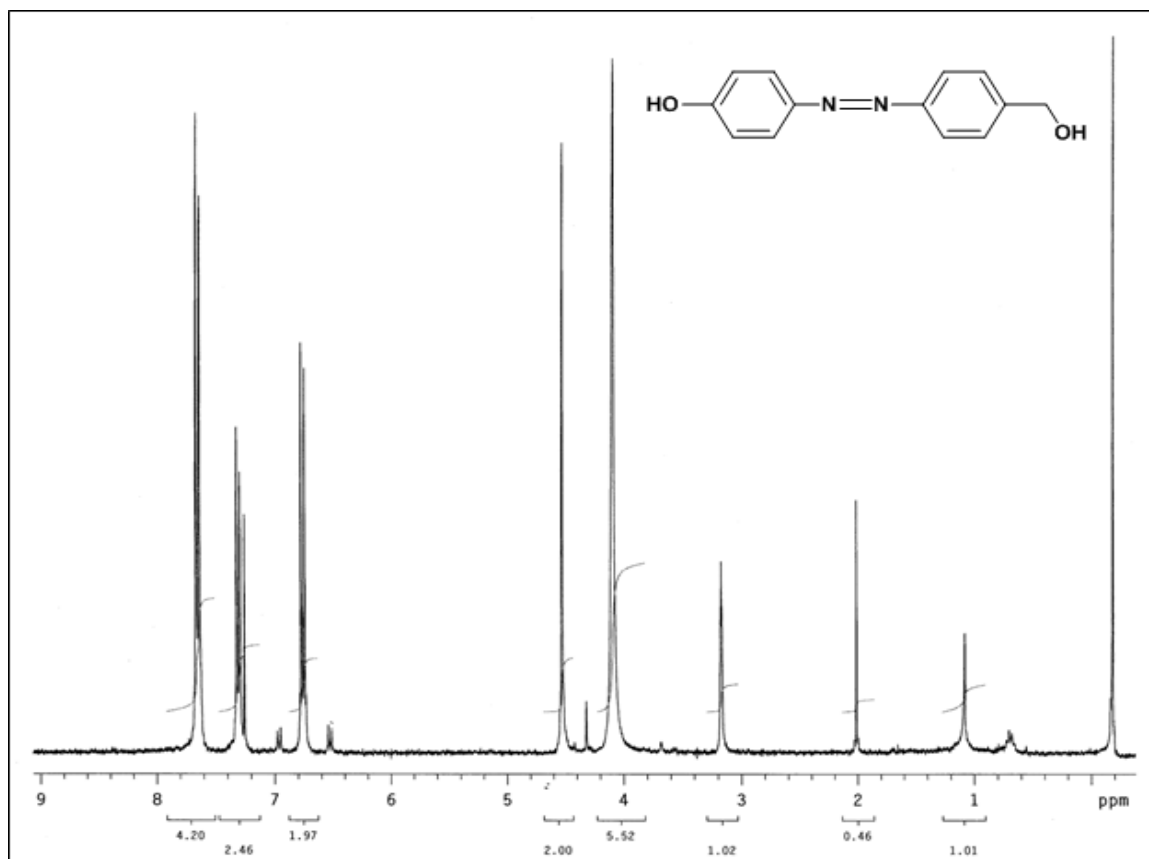
Figure S1. ^{1}H NMR of 4-((4-(hydroxymethyl)phenyl)diazenyl)phenol (**1**) dissolved in DMSO-d$_6$ on a Varian 500 MHz system (Palo Alto, CA).
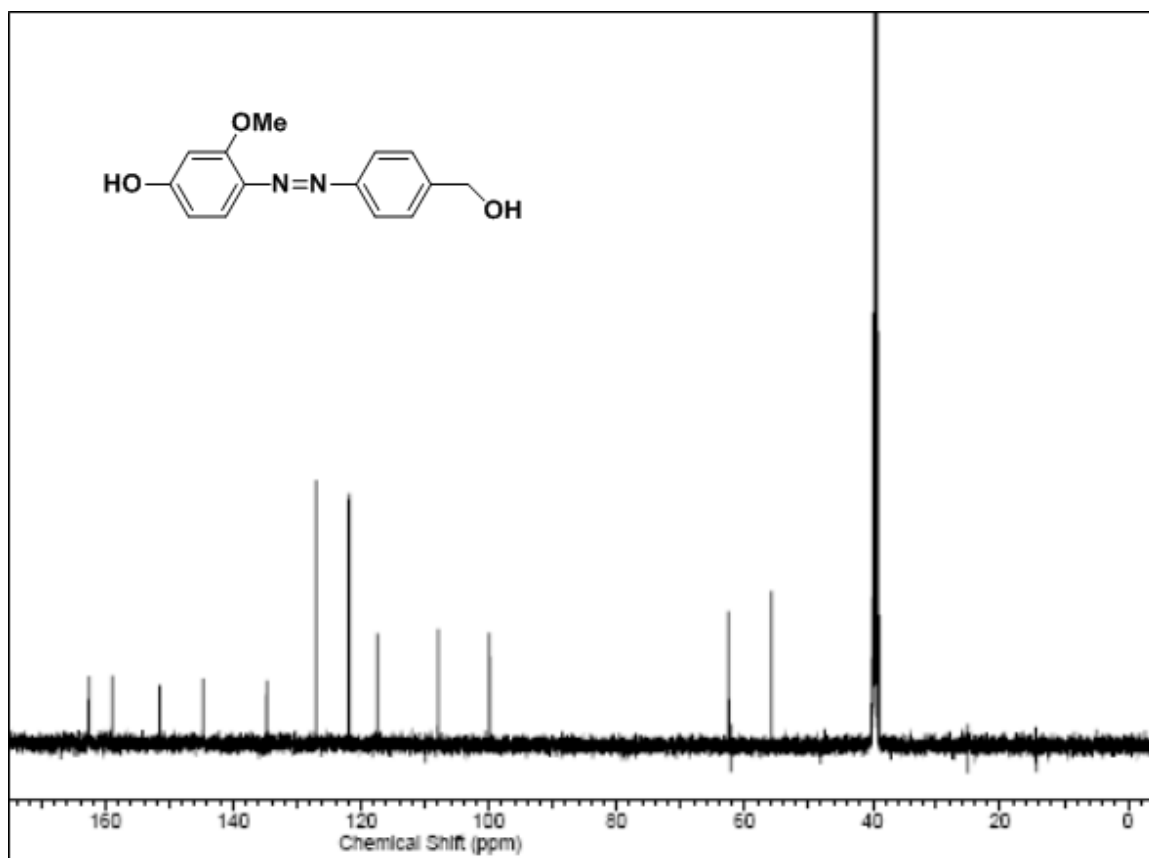
Figure S2. ^{13}C NMR of **4-((4-(hydroxymethyl)phenyl)diazenyl)-3-methoxyphenol (2)** dissolved in CD$_3$SOCD$_3$ on a Varian 125 MHz system (Palo Alto, CA).
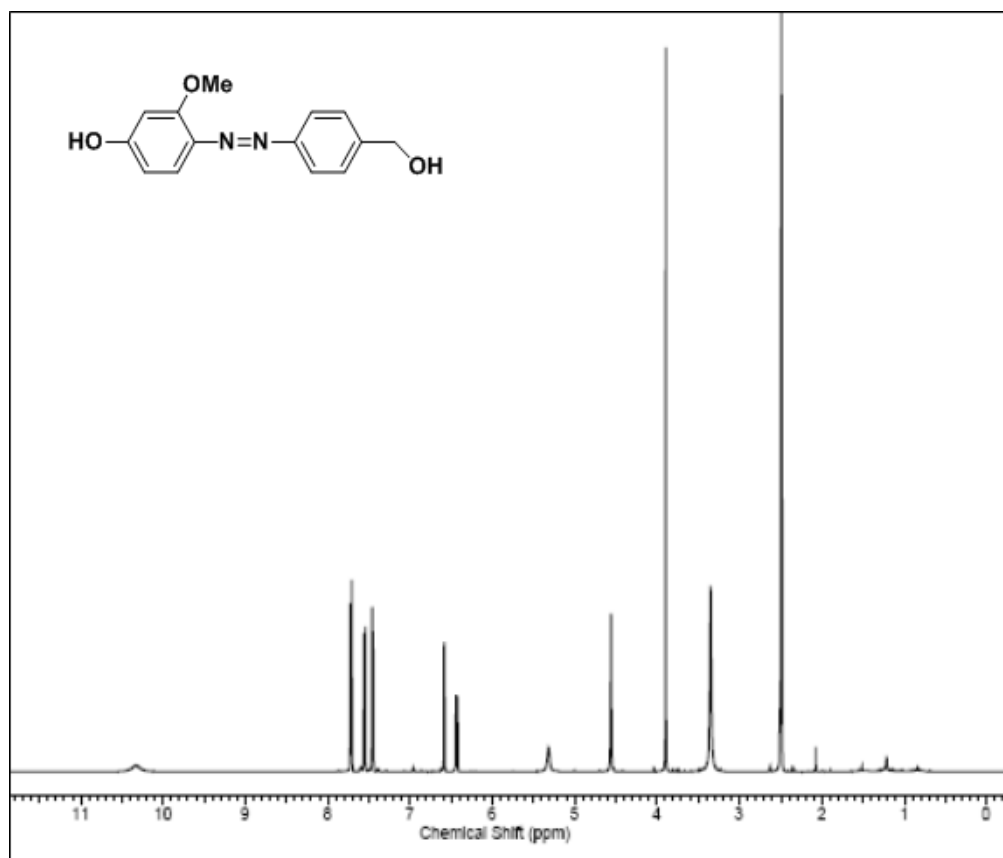
Figure S3. ^{1}H NMR of **4-((4-(hydroxymethyl)phenyl)diazenyl)-3-methoxyphenol (2)** dissolved in CD$_3$SOCD$_3$ on a Varian 400 MHz system (Palo Alto, CA).
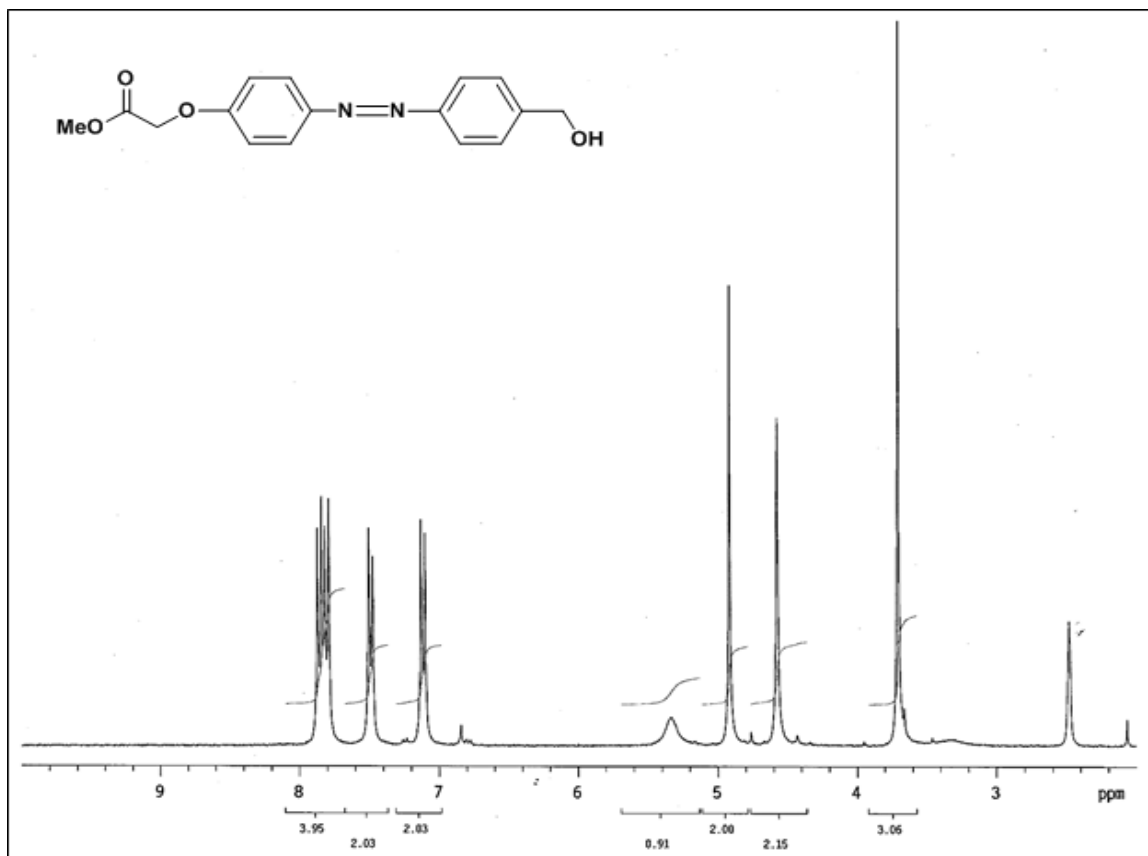
Figure S4. ^{1}H NMR of **4-(4-(carbomethoxy)methoxyphenylazo)benzyl alcohol** (**3**) dissolved in DMSO- d_6 on a Varian 400 MHz system (Palo Alto, CA).
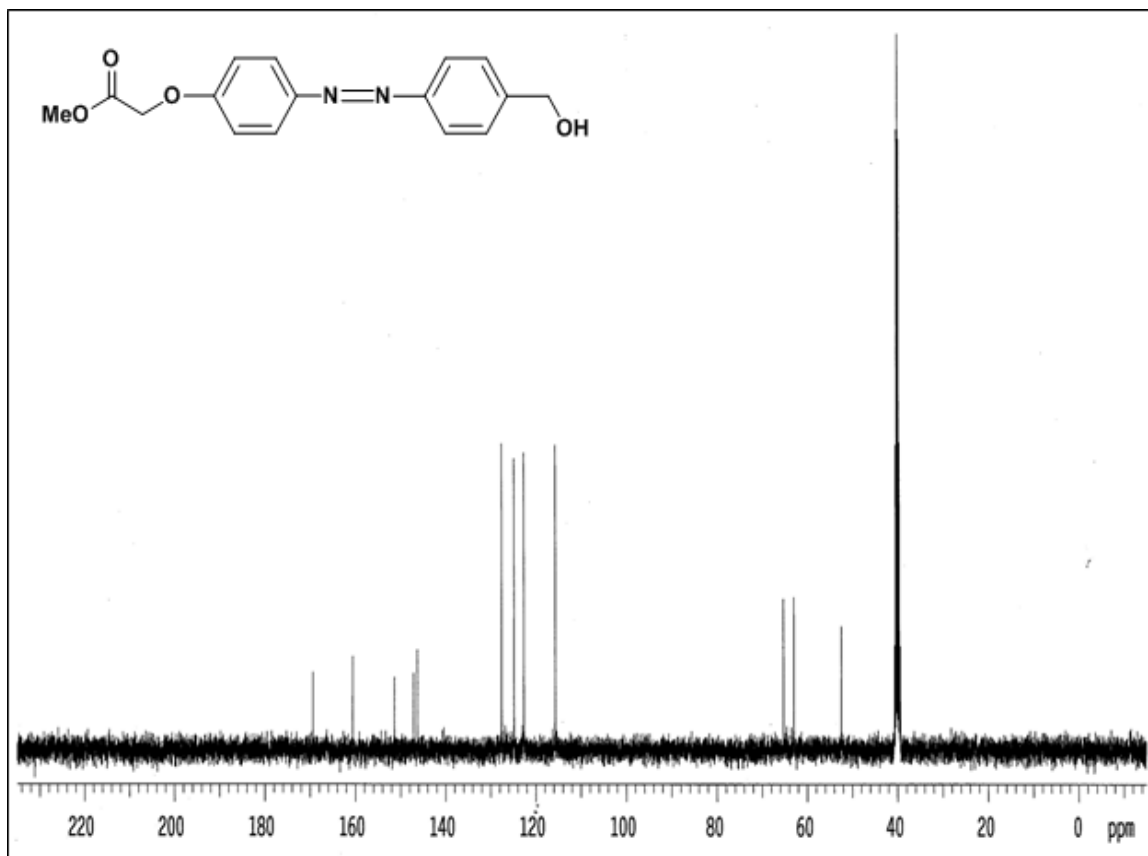
Figure S5. ^{13}C NMR of **4-(4-(carbomethoxy)methoxyphenylazo)benzyl alcohol (3)** dissolved in DMSO- d_6 on a Varian 100 MHz system (Palo Alto, CA).
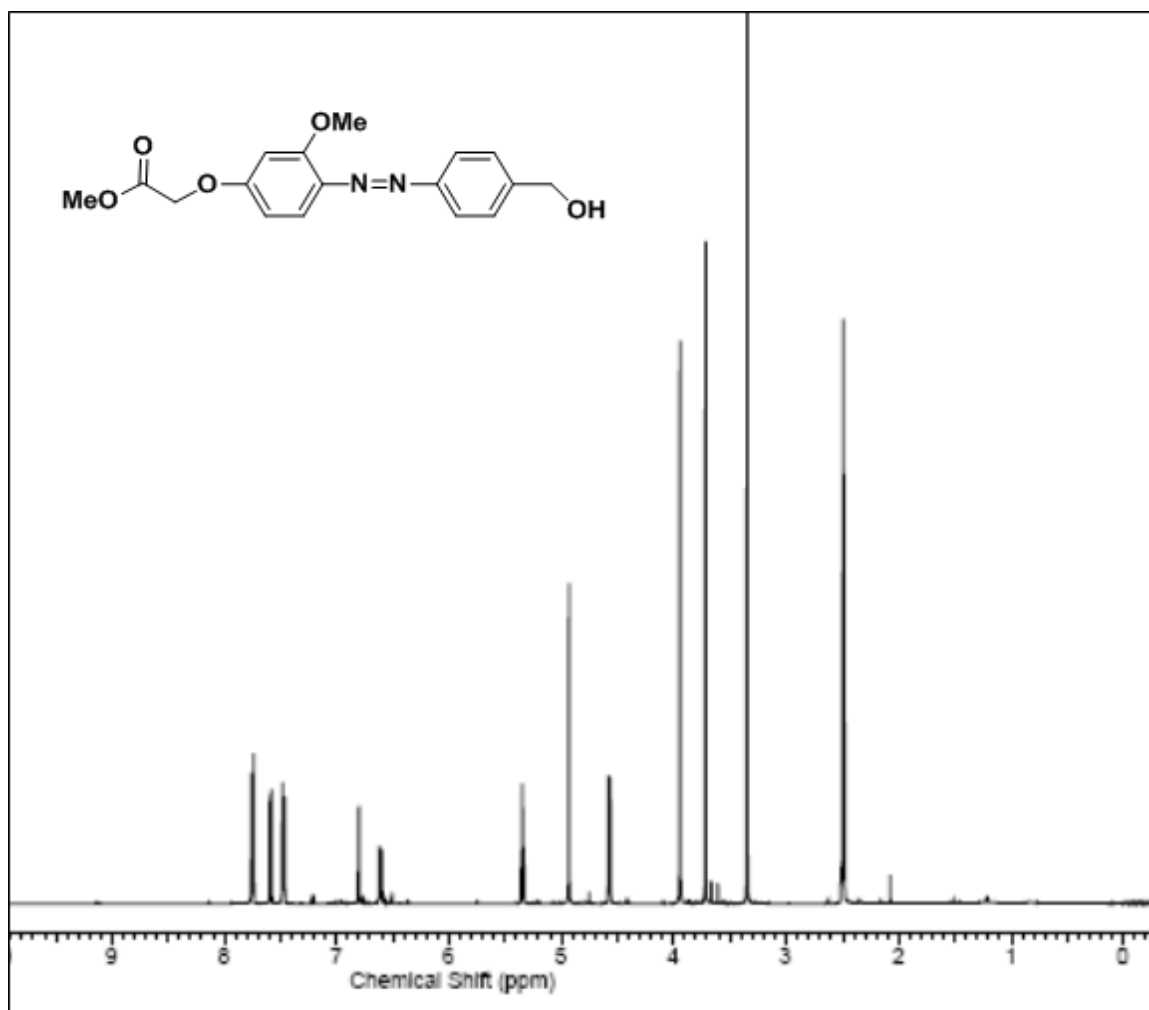
Figure S6. ^{1}H NMR of **methyl 2-(4-((4-(hydroxymethyl)phenyl)diazenyl)-3-methoxyphenoxy)acetate (4)** dissolved in CD_3SOCD_3 on a Varian 500 MHz system (Palo Alto, CA).

134
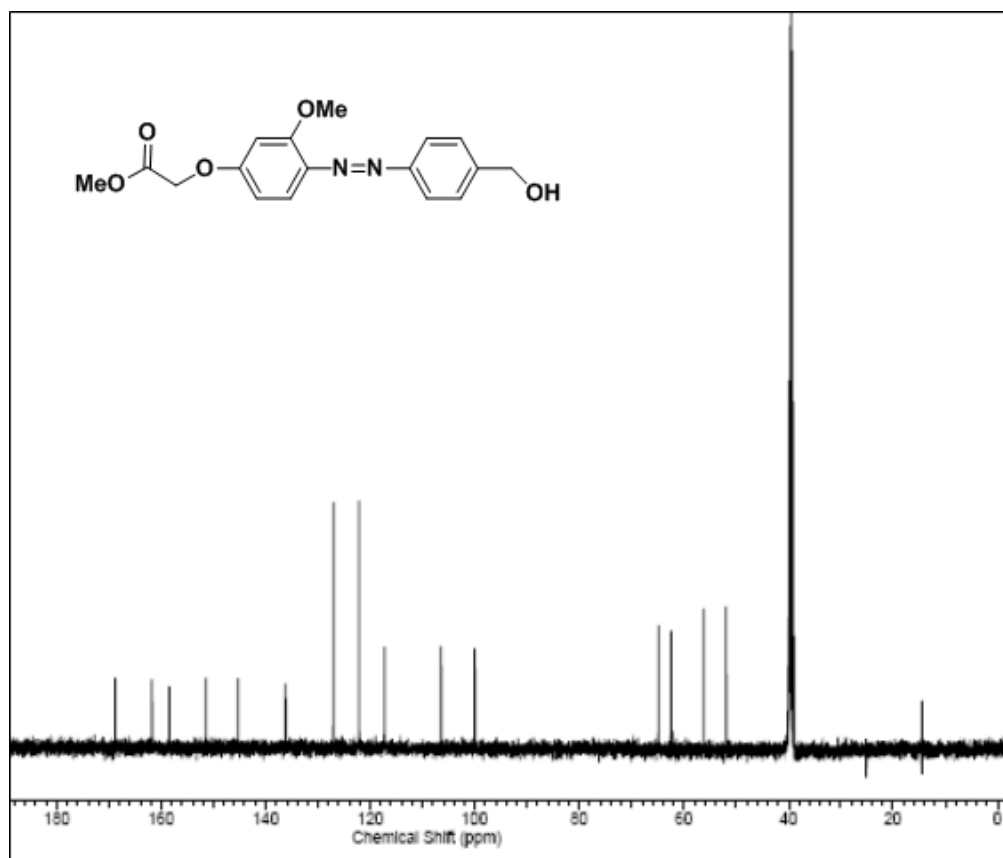
Figure S7. ^{13}C NMR of **methyl 2-(4-((4-(hydroxymethyl)phenyl)diazenyl)-3-methoxyphenoxy)acetate (4)** dissolved in CD$_3$SOCD$_3$ on a Varian 125 MHz system (Palo Alto, CA).
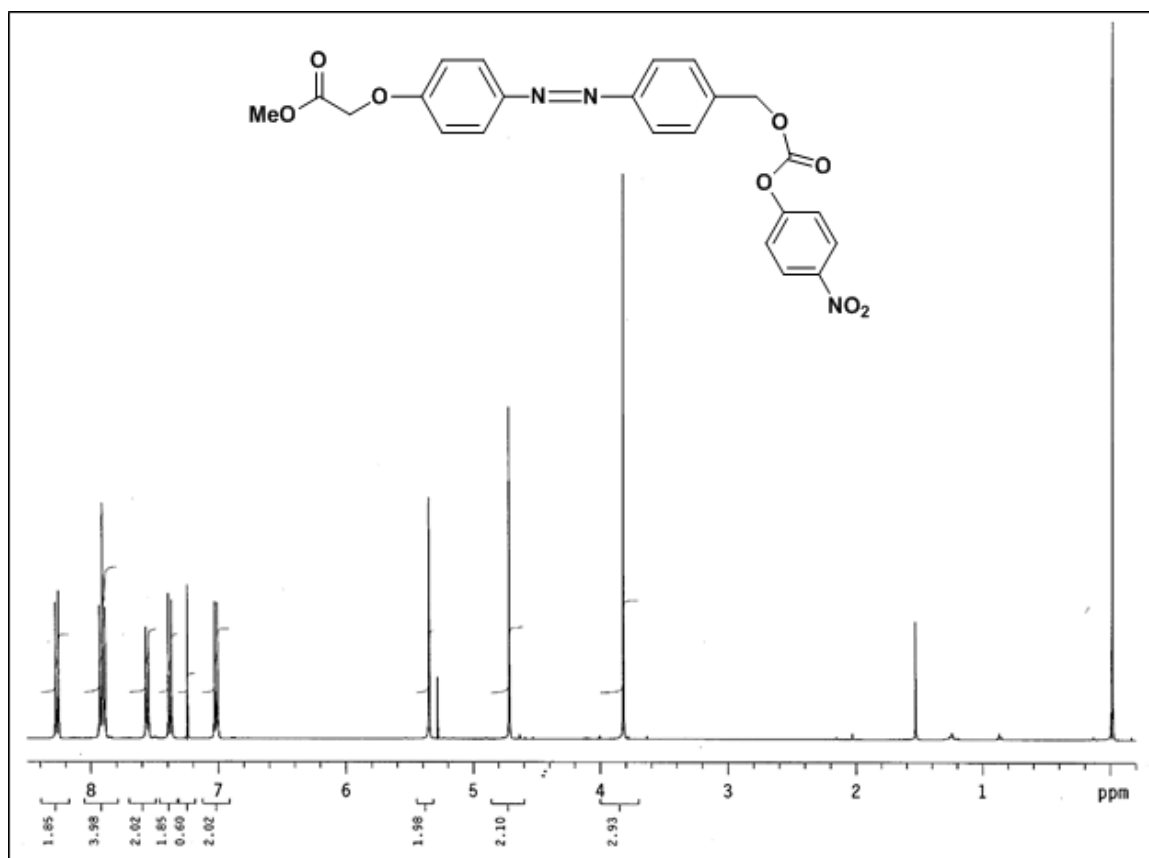
Figure S8. ^{1}H NMR of **4-(4-(carbomethoxy)methoxyphenylazo)benzyl-4'-nitrophenyl carbonate (5)** dissolved in CDCl$_3$ on a Varian 400 MHz system (Palo Alto, CA).
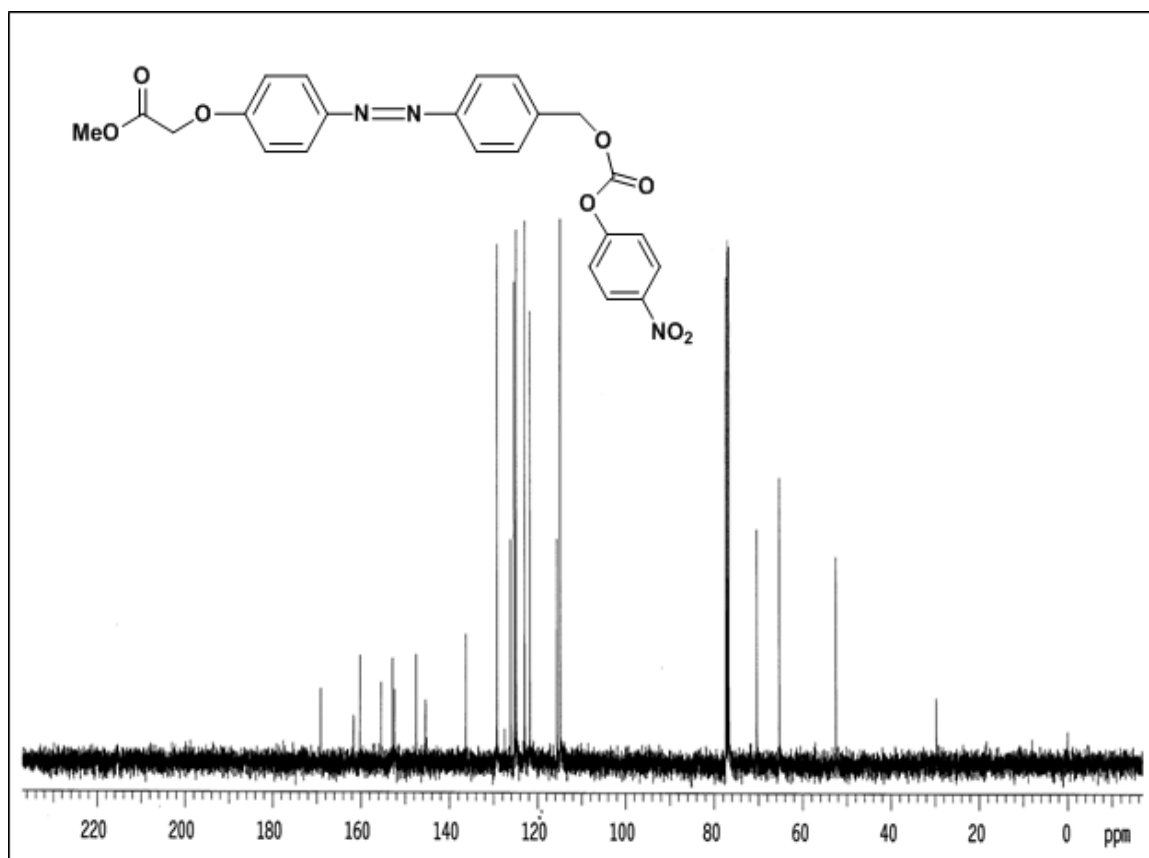
Figure S9. ^{13}C NMR of **4-(4-(Carbomethoxy)methoxyphenylazo)benzyl-4'-nitrophenyl carbonate (5)** dissolved in CDCl$_3$ on a Varian 100 MHz system (Palo Alto, CA).
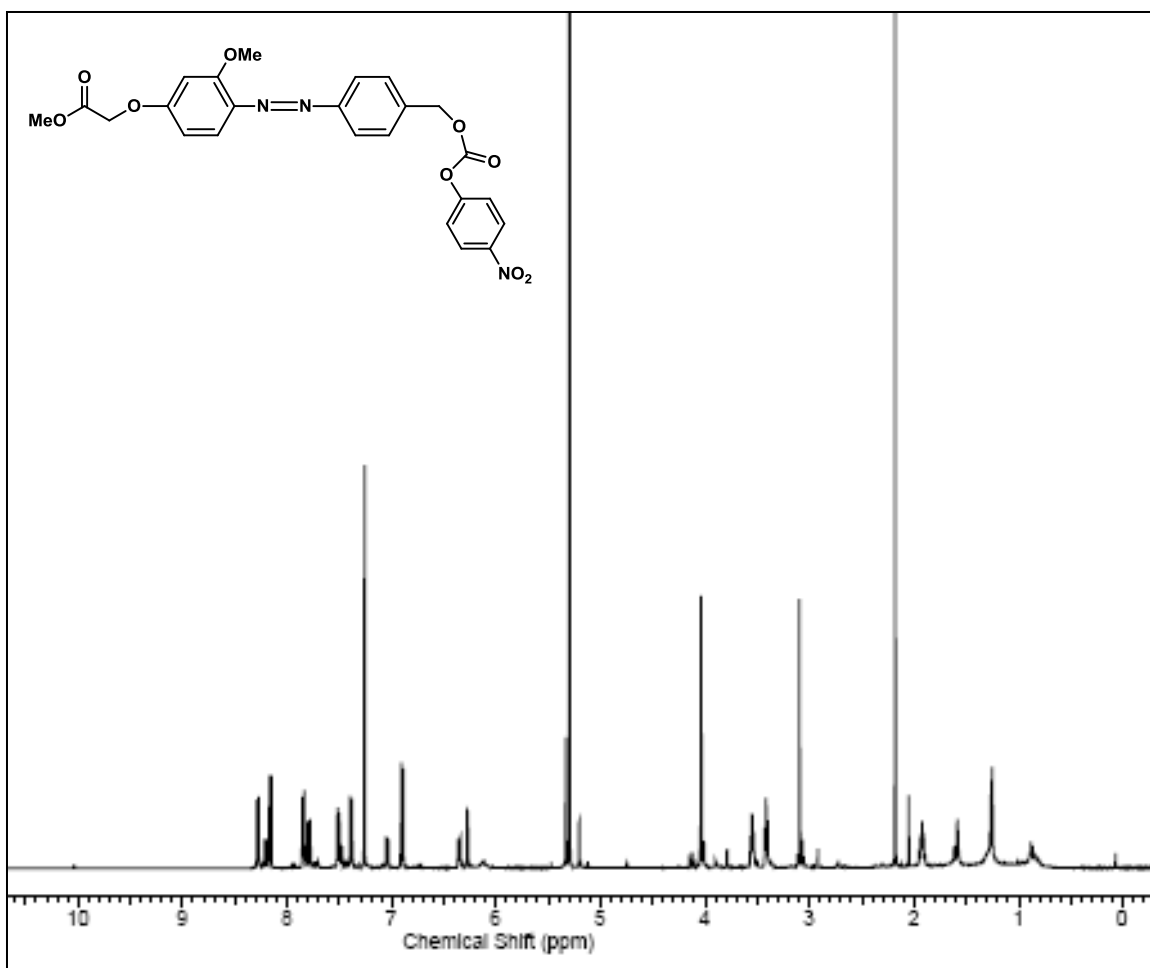
Figure S10. ^{1}H NMR of **methyl 2-(3-methoxy-4-((4-((((4-nitrophenoxy)c arbonyl)oxy) methyl) phenyl) diazenyl) phenoxy) acetate (6)** dissolved in CDCl$_3$ on a Varian 500 MHz system (Palo Alto, CA).
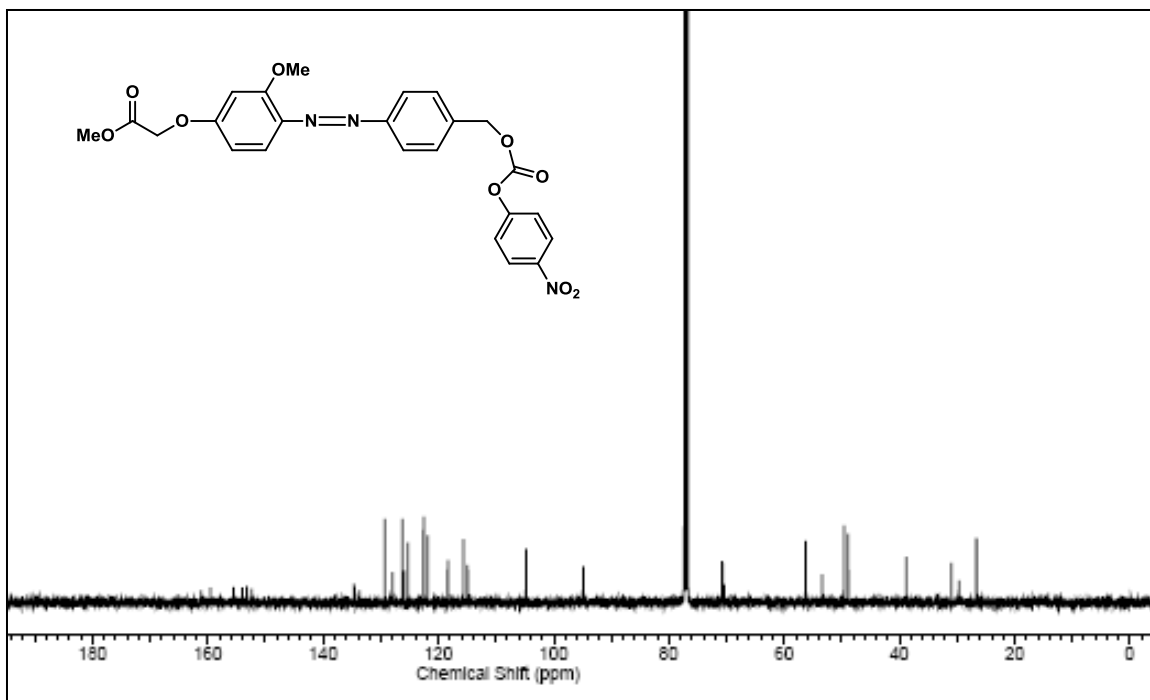
Figure S11. ^{13}C NMR of **methyl 2-(3-methoxy-4-((4-((((4-nitrophenoxy) carbonyl)oxy) methyl) phenyl) diazenyl) phenoxy) acetate (6)** dissolved in CD_3SOCD_3 on a Varian 125 MHz system (Palo Alto, CA).

139
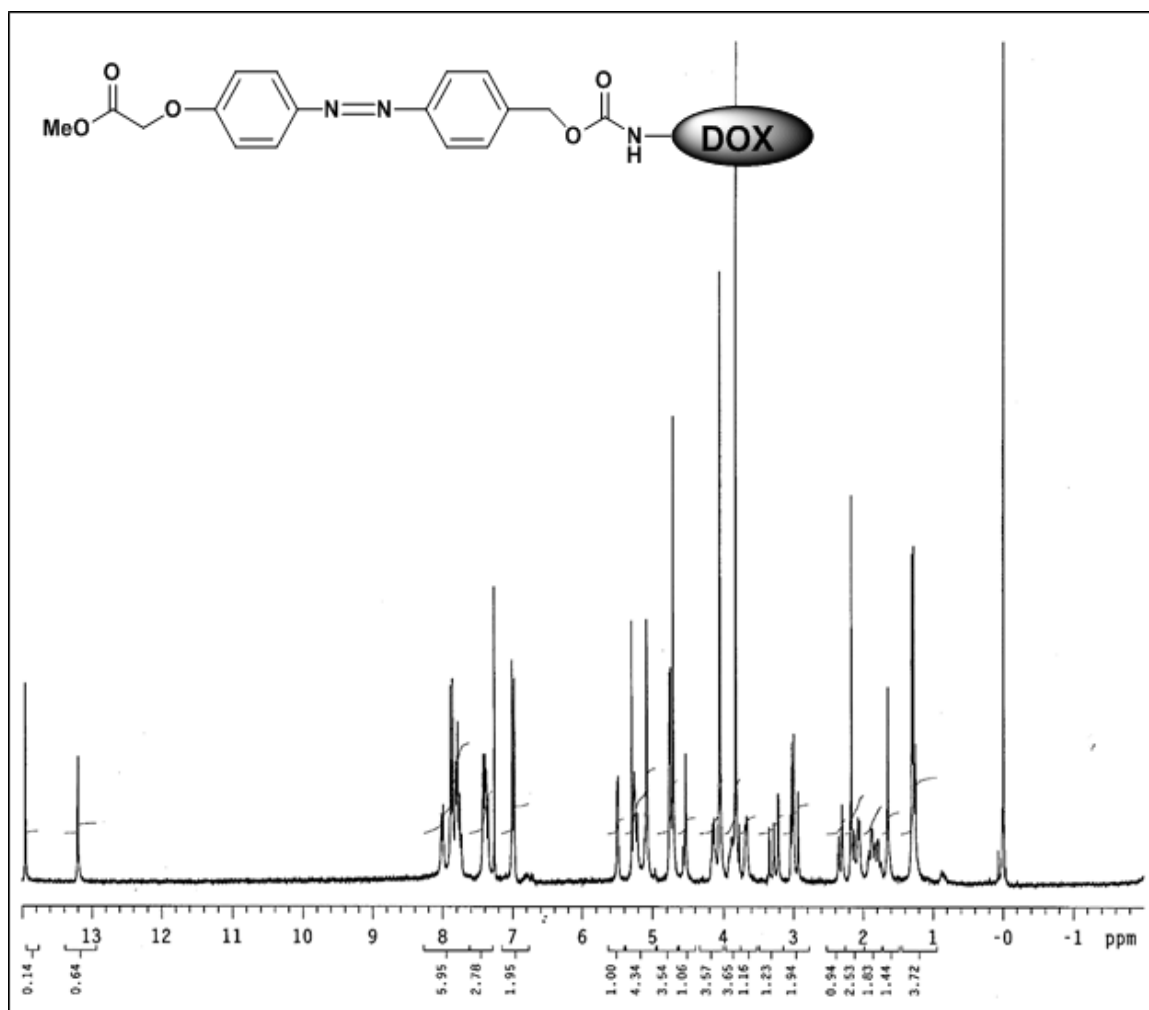
Figure S12. ^{1}H NMR of *N*-(4-(4-(carbomethoxy) methoxyphenylazo) benzyloxycarbonyl) doxorubicin (7)** dissolved in CDCl$_3$ on a Varian 400 MHz system (Palo Alto, CA).
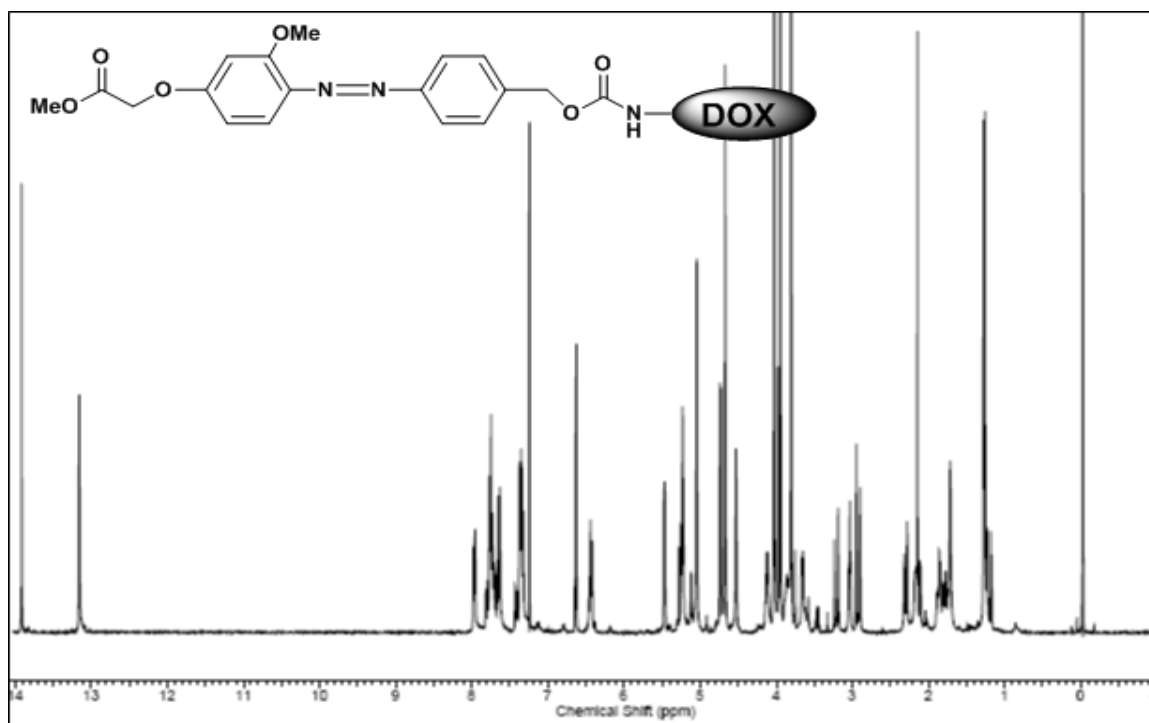
Figure S13. ^{1}H NMR of **methyl 2-(3-methoxy-4-((4-(((carbonyl) oxy) methyl) phenyl) diazenyl) phenoxy) acetate doxorubicin (8)** dissolved in CDCl$_3$ on a Varian 500 MHz system (Palo Alto, CA).
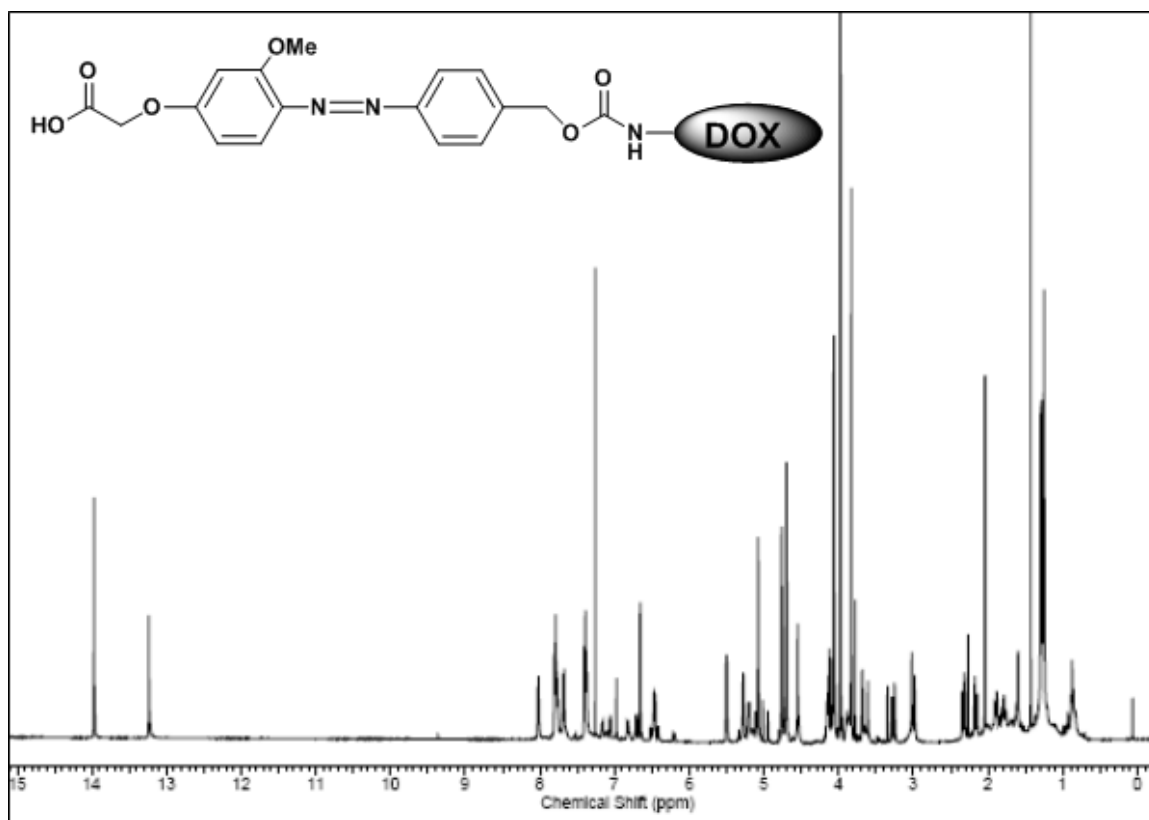
Figure S14. ¹H NMR of **2-(3-methoxy-4-((4-(((benzyloxycarbonyl) doxorubicinmethyl) phenyl) diazenyl) phenoxy) acetic acid (10)** dissolved in CDCl₃ on a Varian 500 MHz system (Palo Alto, CA).

142
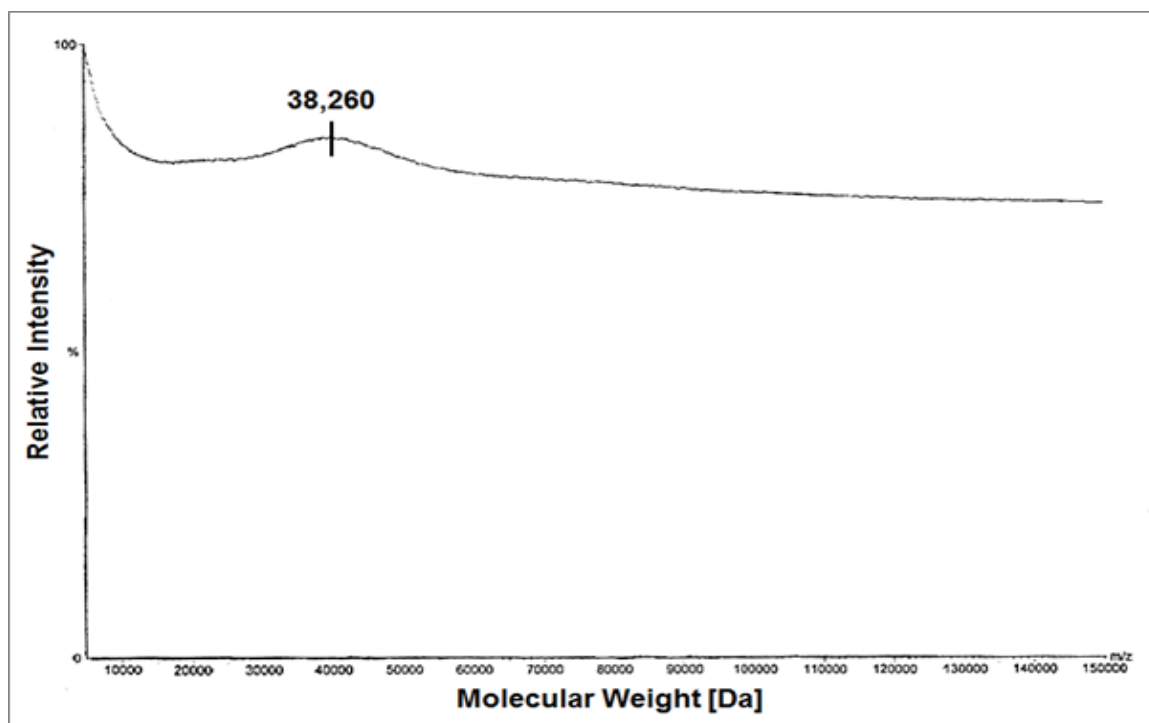
Figure S15. MALDI-TOF results of **G5-L1-DOX (11)** analyzed on a Waters Tofspec-2E (Milford, MA).
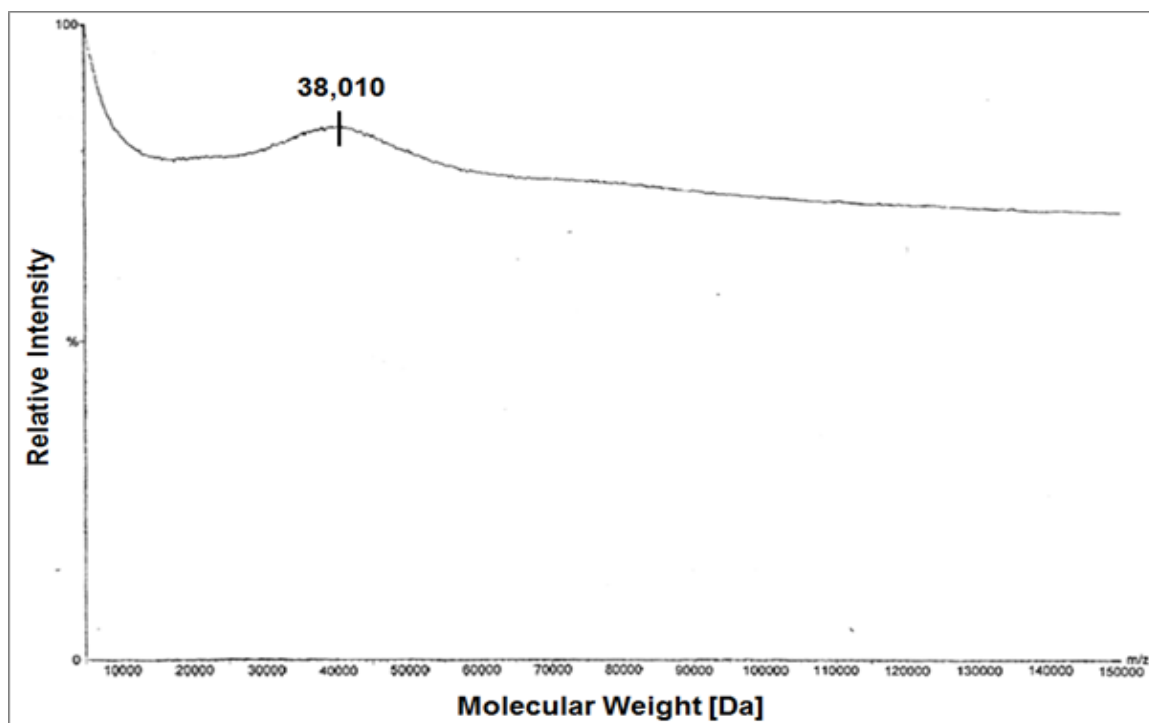
Figure S16. MALDI-TOF results of **G5-L2-DOX (12)** analyzed on a Waters Tofspec-2E (Milford, MA).

Synthesis of G5 –L3-DOX and G5-L4-DOX conjugates
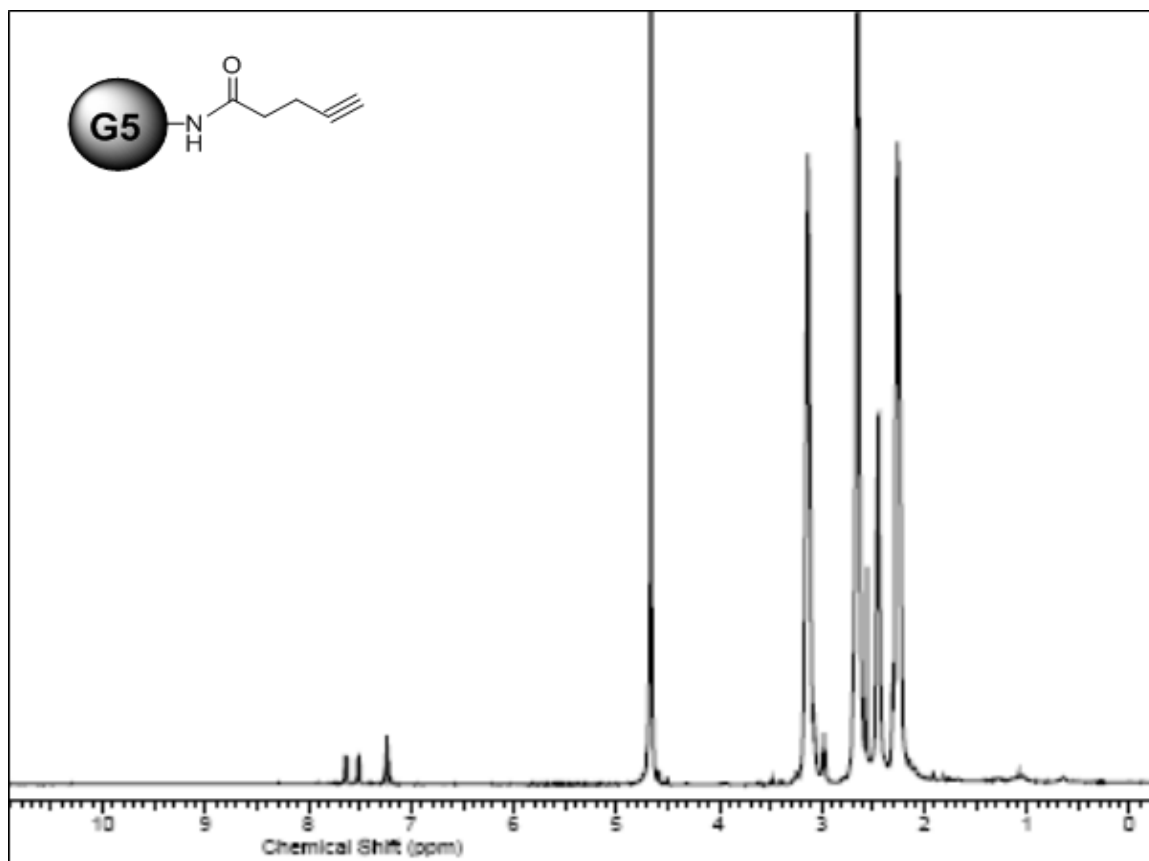
Figure S17. ^{1}H NMR of **G5-alkyne (13)** dissolved in D$_2$O on a Varian 500 MHz system (Palo Alto, CA).
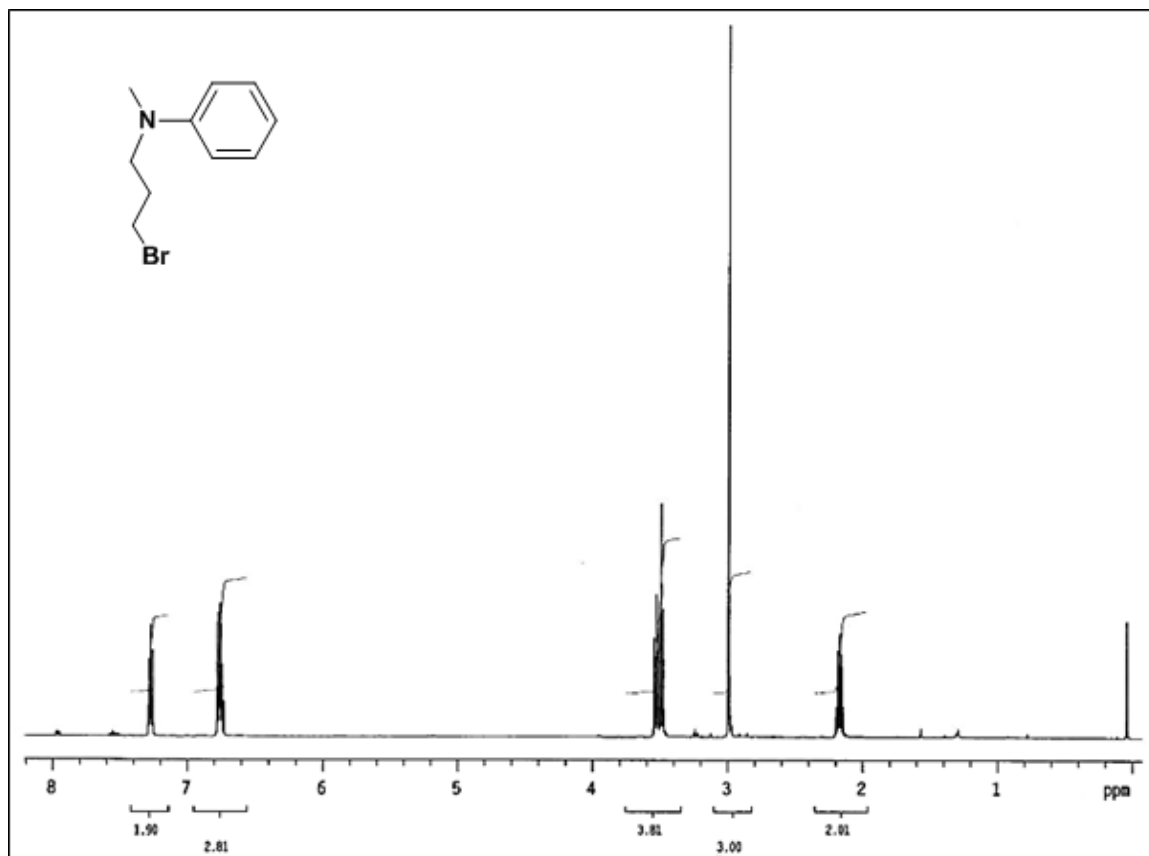
Figure S18. ^{1}H NMR of ***N*-(3-bromopropyl)-*N*-methylaniline (14)** dissolved in CDCl$_3$ on a Varian 500 MHz system (Palo Alto, CA).

146
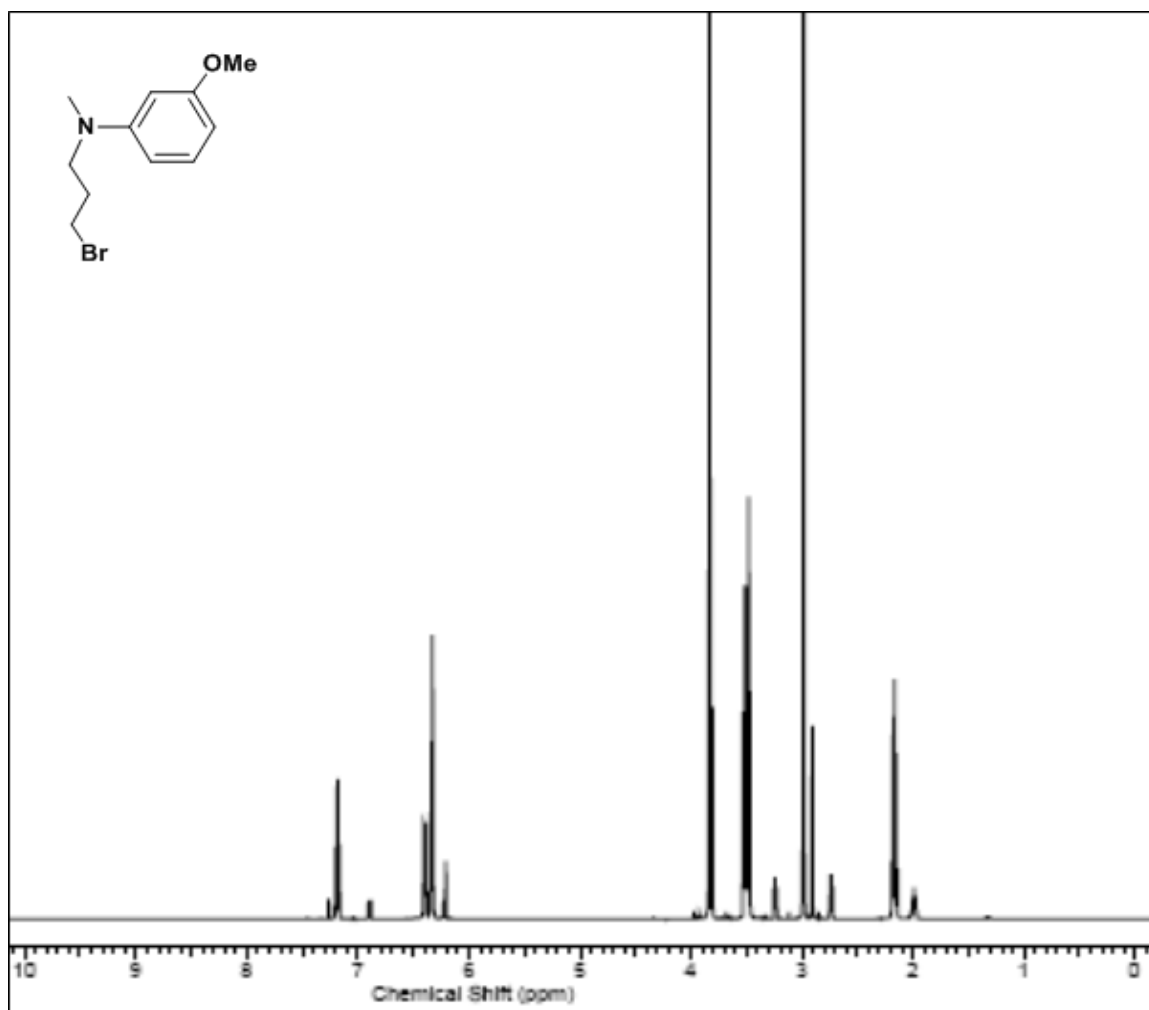
Figure S19. ^{1}H NMR of *N*-(3-bromopropyl)-3-methoxy-*N*-methylaniline (**15**) dissolved in CDCl$_3$ on a Varian 500 MHz system (Palo Alto, CA).
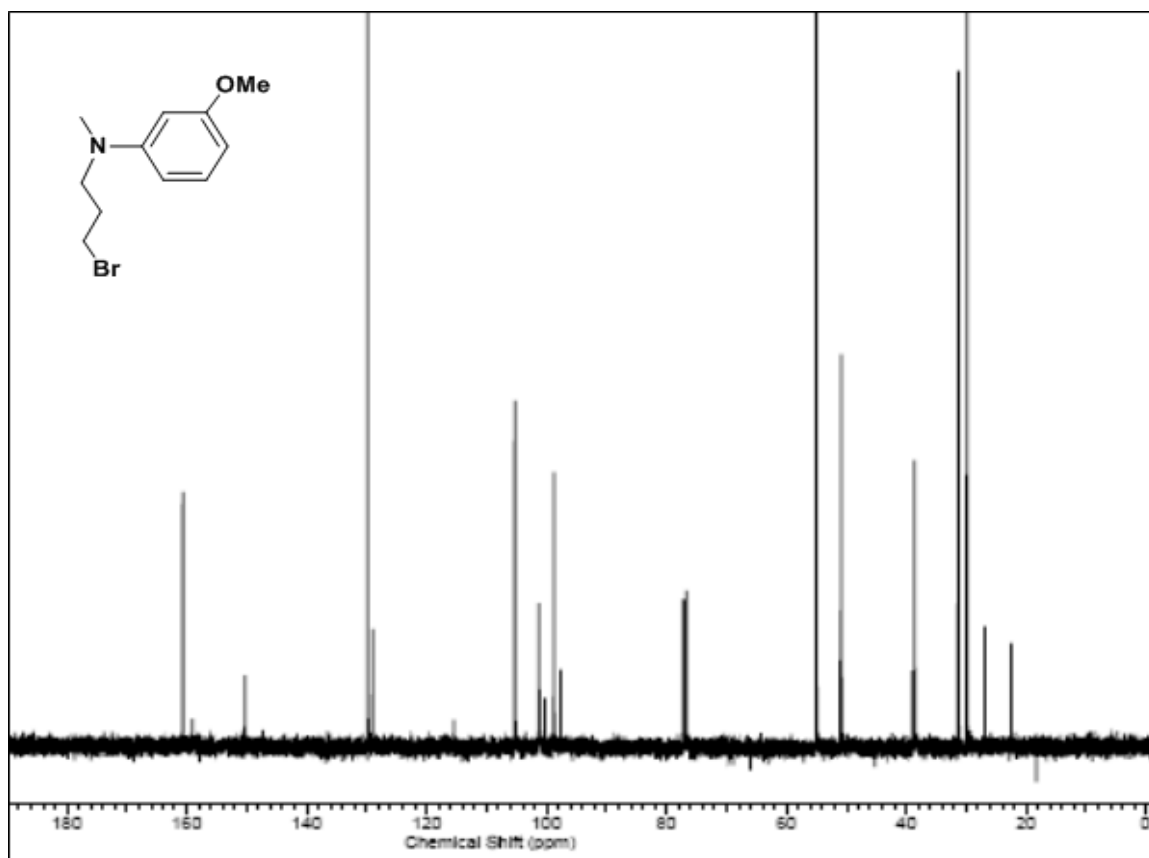
Figure S20. ^{13}C NMR of ***N*-(3-bromopropyl)-3-methoxy-*N*-methylaniline (15)** dissolved in CDCl$_3$ on a Varian 125 MHz system (Palo Alto, CA).
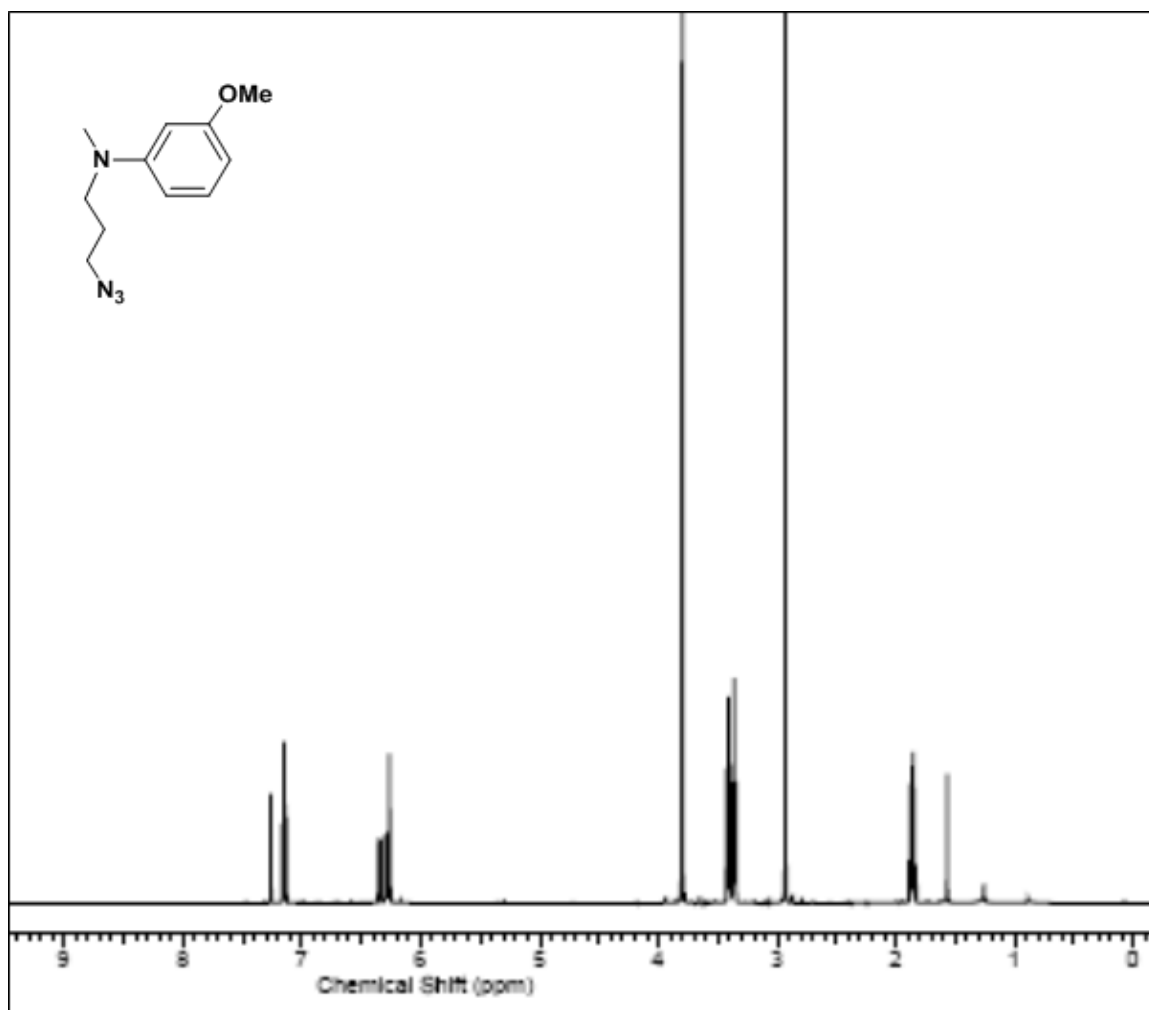
Figure S21. ¹H NMR of *N*-(3-azidopropyl)-3-methoxy-*N*-methylaniline (**17**) dissolved in CDCl₃ on a Varian 500 MHz system (Palo Alto, CA).
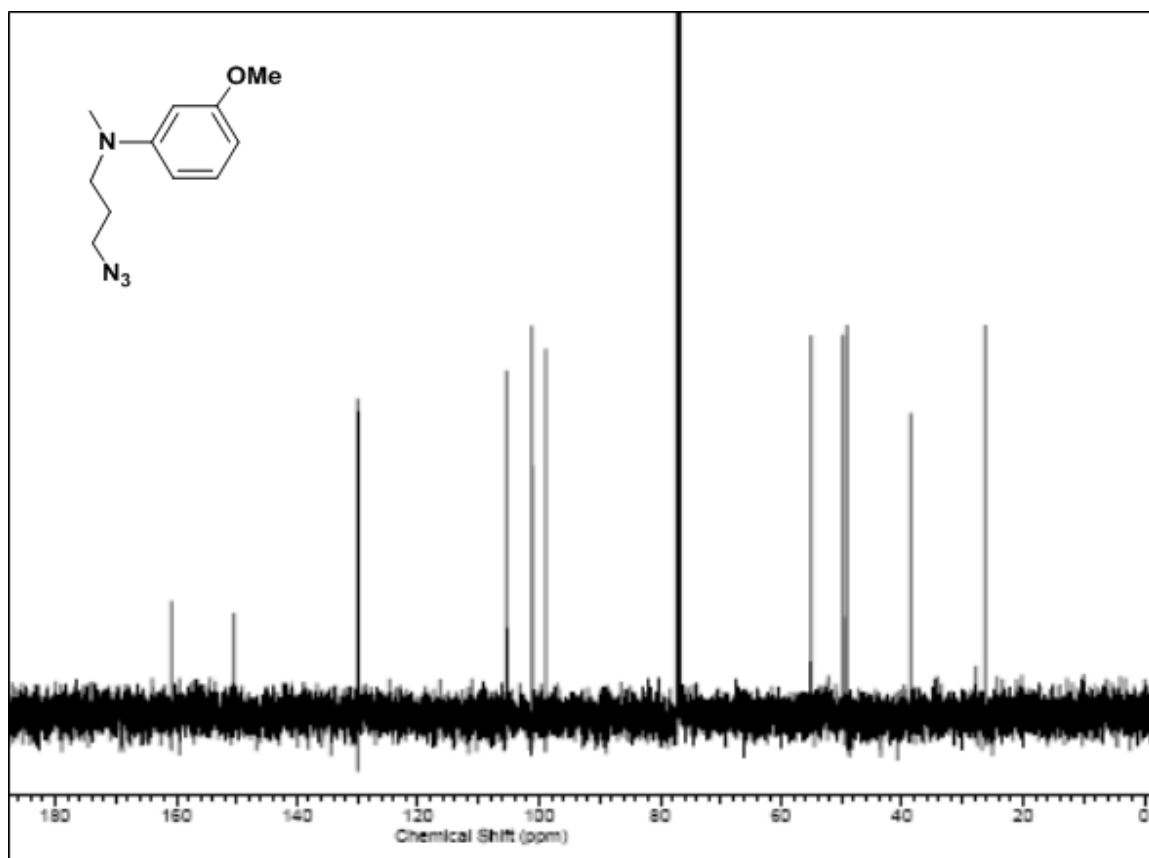
Figure S22. ^{13}C NMR of *N*-(3-bromopropyl)-3-methoxy-*N*-methylaniline (**17**) dissolved in CDCl$_3$ on a Varian 125 MHz system (Palo Alto, CA).
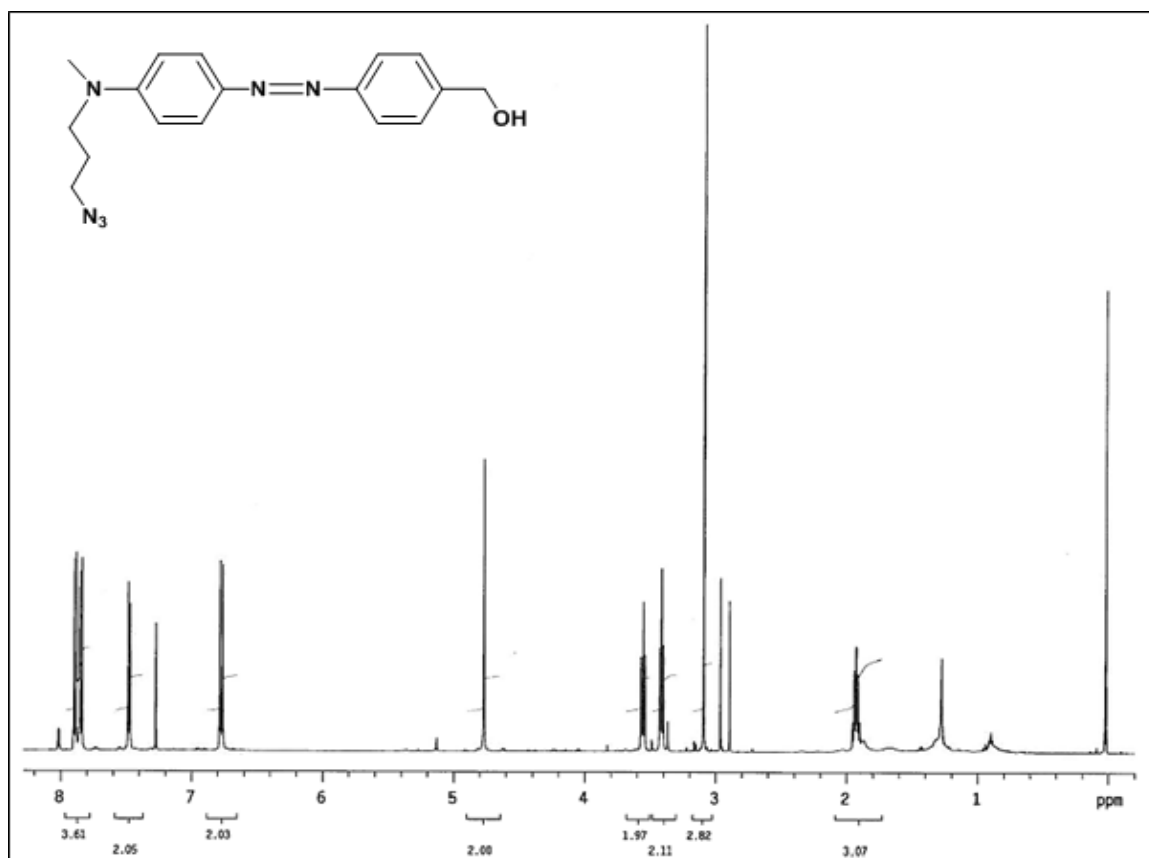
Figure S23. ^{1}H NMR of **4-((4-((3-azidopropyl)(methyl) amino) phenyl) diazenyl) phenyl) methanol (18)** dissolved in CDCl$_3$ on a Varian 500 MHz system (Palo Alto, CA).
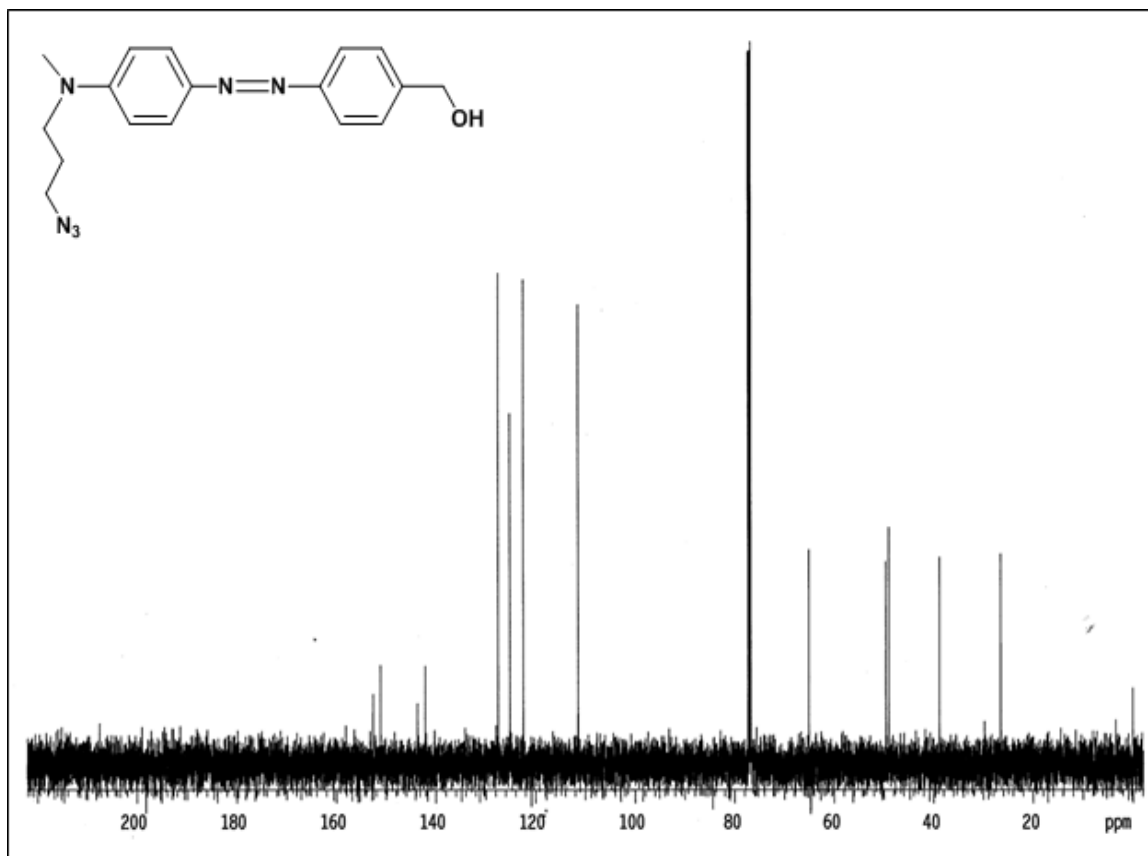
Figure S24. ^{13}C NMR of **4-((4-((3-azidopropyl)(methyl) amino) phenyl) diazenyl) phenyl) methanol (18)** dissolved in CDCl₃ on a Varian 125 MHz system (Palo Alto, CA).

152
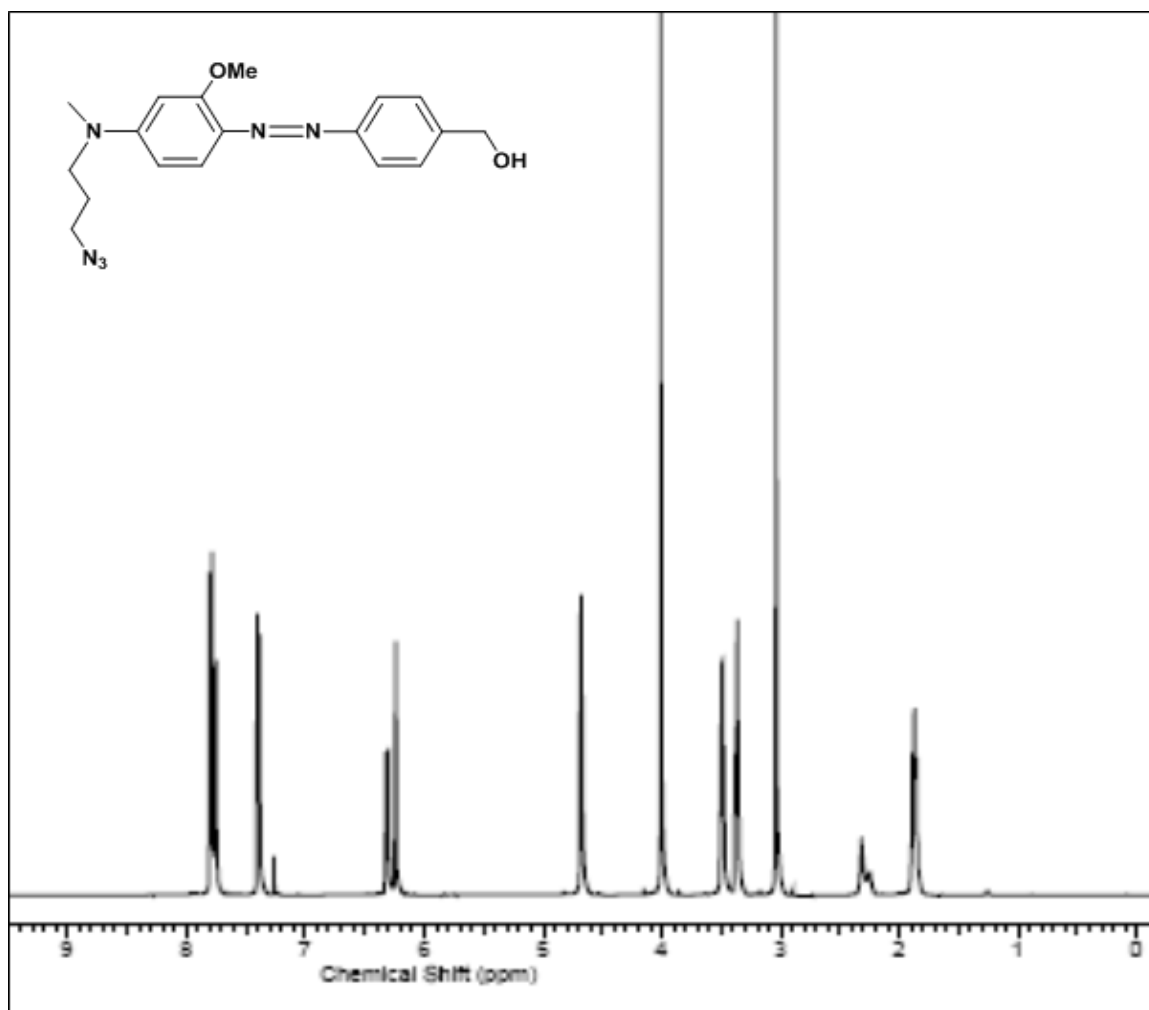
Figure S25. ¹H NMR of **(4-((4-((3-azidopropyl)(methyl)amino)-2-methoxyphenyl)diazenyl)phenyl)methanol (19)** dissolved in CDCl₃ on a Varian 500 MHz system (Palo Alto, CA).
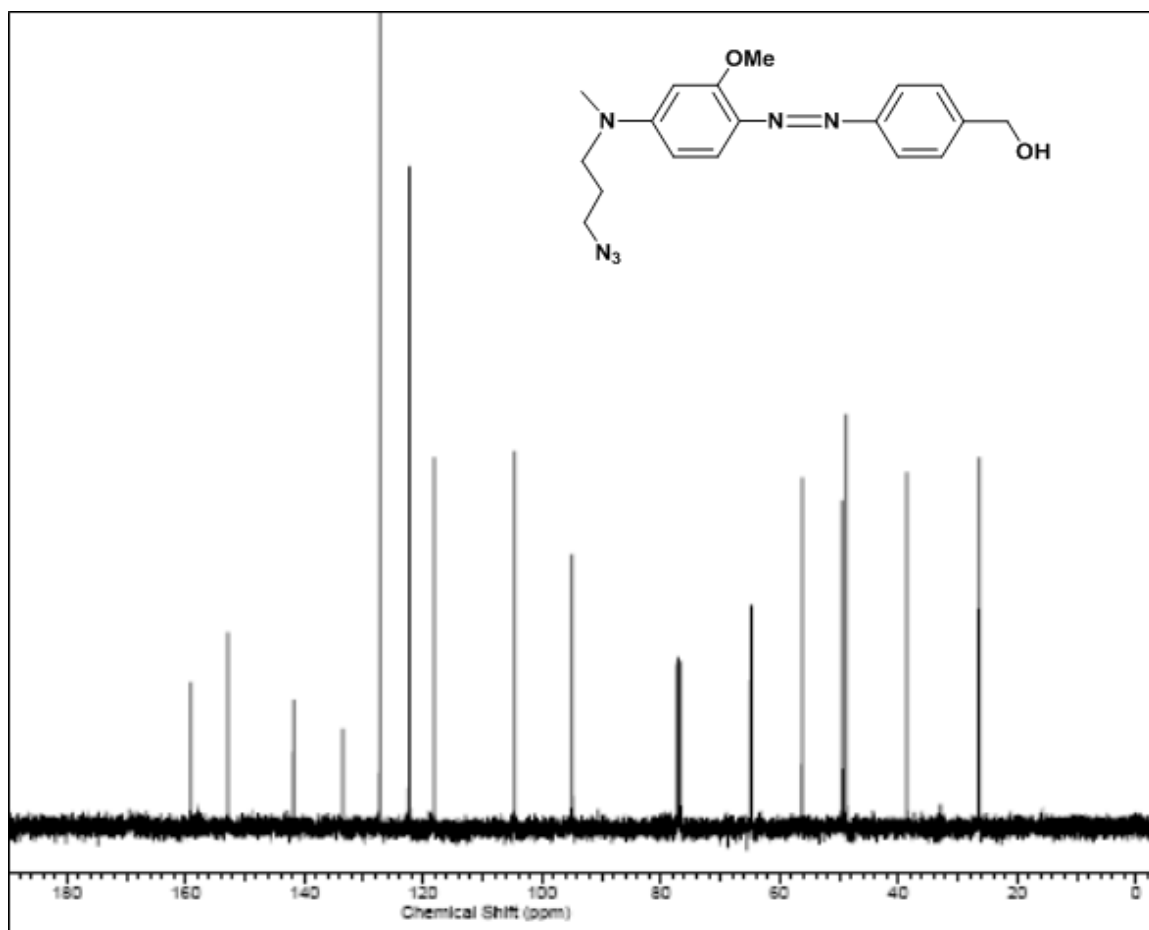
Figure S26. ^{13}C NMR of **(4-((4-((3-azidopropyl)(methyl)amino)-2-methoxyphenyl)diazenyl)phenyl)methanol (19)** dissolved in CDCl$_3$ on a Varian 125 MHz system (Palo Alto, CA).
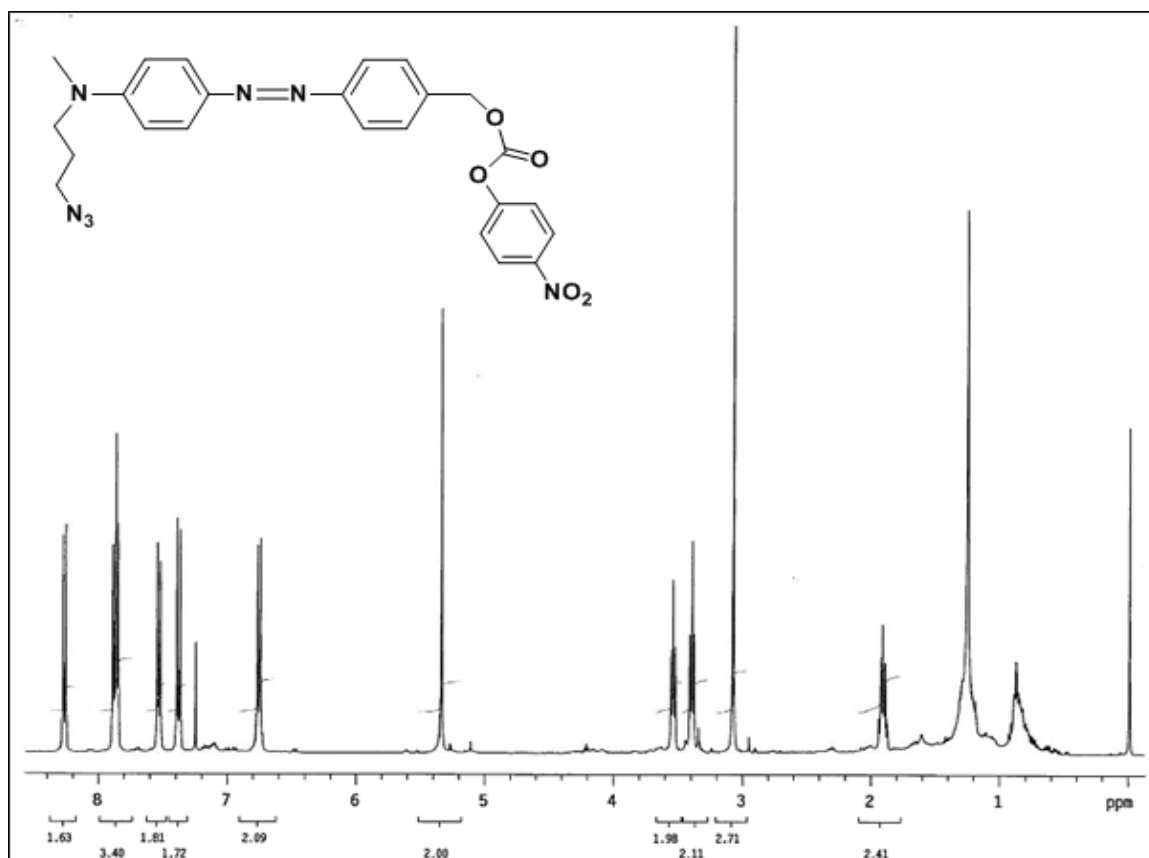
Figure S27. ^{1}H NMR of **4-((4-((3-azidopropyl)(methyl)amino)phenyl)diazenyl)benzyl (4-nitrophenyl) carbonate (20)** dissolved in CDCl$_3$ on a Varian 500 MHz system (Palo Alto, CA).
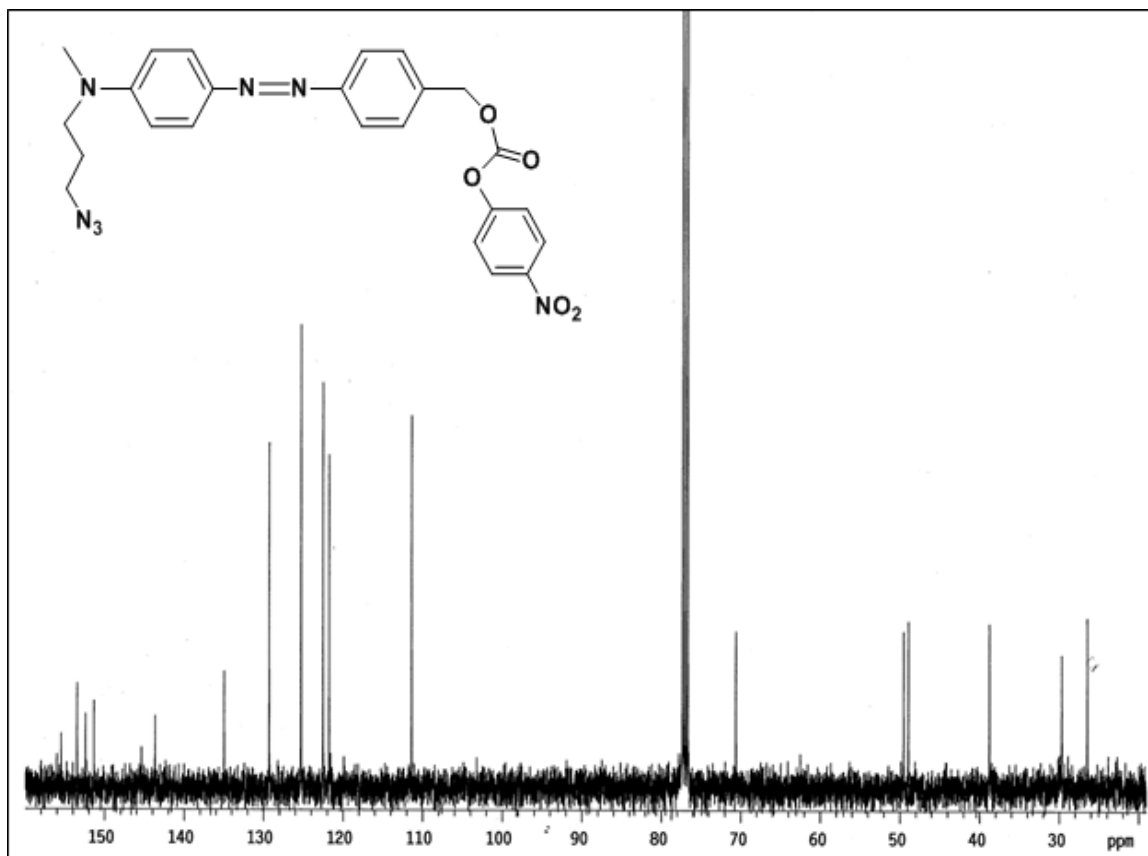
Figure S28. ^{13}C NMR **4-((4-((3-azidopropyl)(methyl)amino)phenyl)diazenyl)benzyl (4-nitrophenyl) carbonate (20)** dissolved in CDCl$_3$ on a Varian 125 MHz system (Palo Alto, CA).
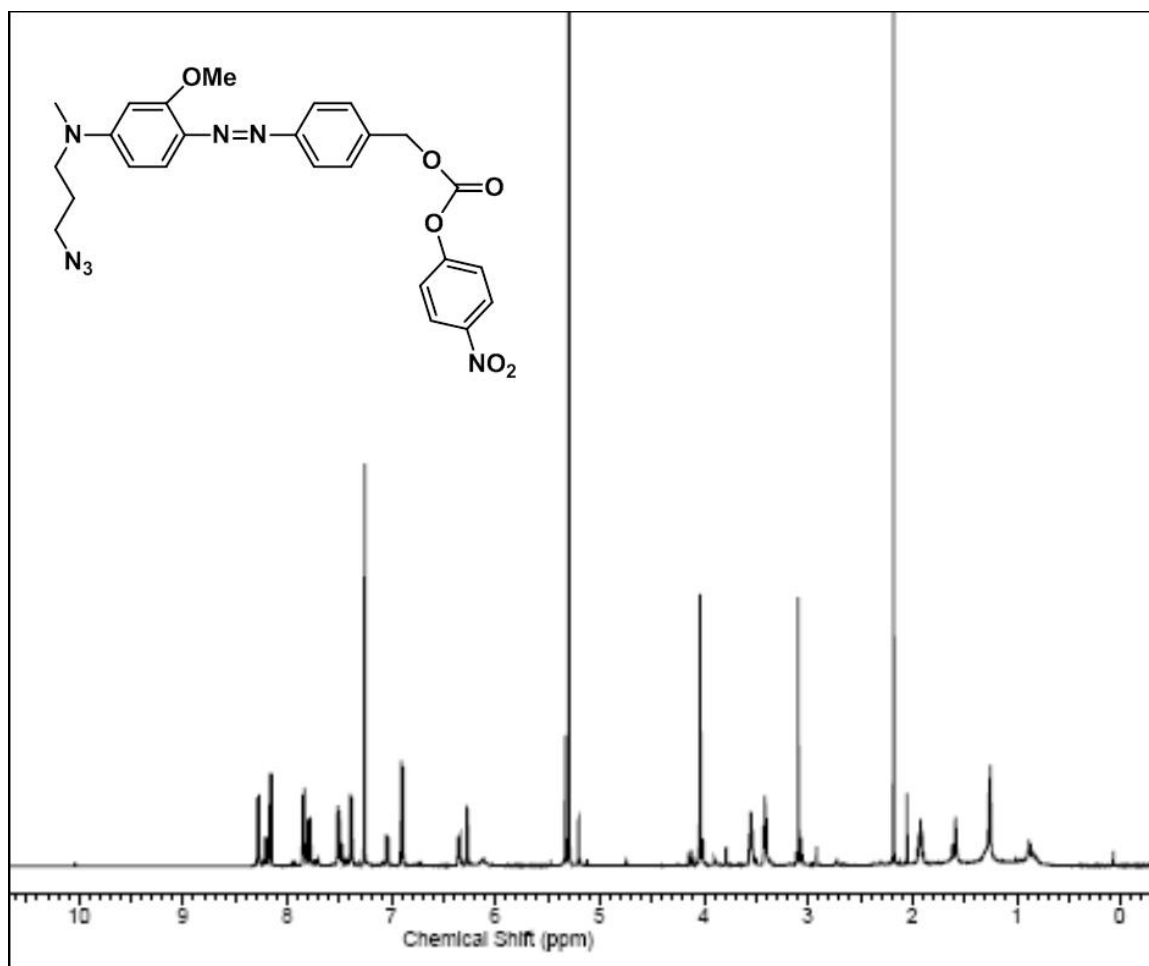
Figure S29. ^{1}H NMR of **4-((4-((3-azidopropyl)(methyl)amino)-2-methoxyphenyl) diazenyl) benzyl (4-nitrophenyl) carbonate (21)** dissolved in CDCl$_3$ on a Varian 500 MHz system (Palo Alto, CA).

157
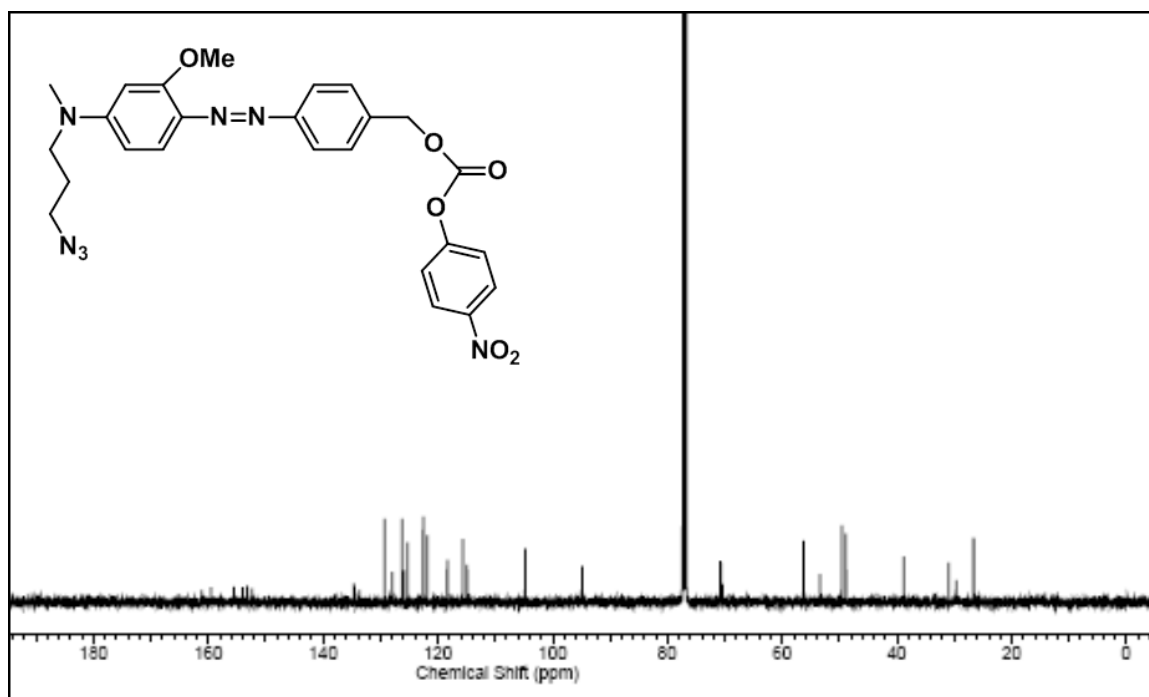
Figure S30. ^{13}C NMR of **4-((4-((3-azidopropyl)(methyl)amino)-2-methoxyphenyl) diazenyl) benzyl (4-nitrophenyl) carbonate (21)** dissolved in CDCl$_3$ on a Varian 125 MHz system (Palo Alto, CA).

158
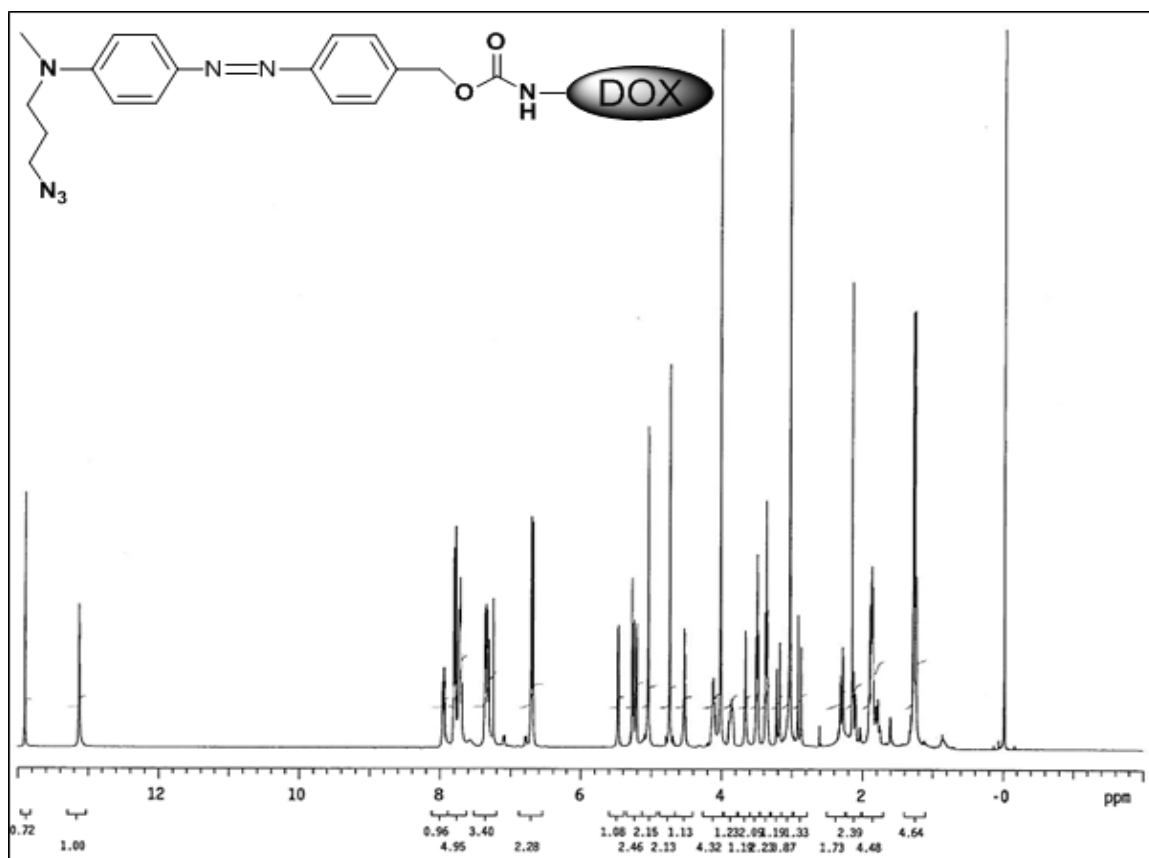
Figure S31. [^1]H NMR of **4-((4-((3-azidopropyl)(methyl)amino)phenyl)diazenyl)benzyl -Doxorubicin carbonate (22)** dissolved in CDCl$_3$ on a Varian 500 MHz system (Palo Alto, CA).
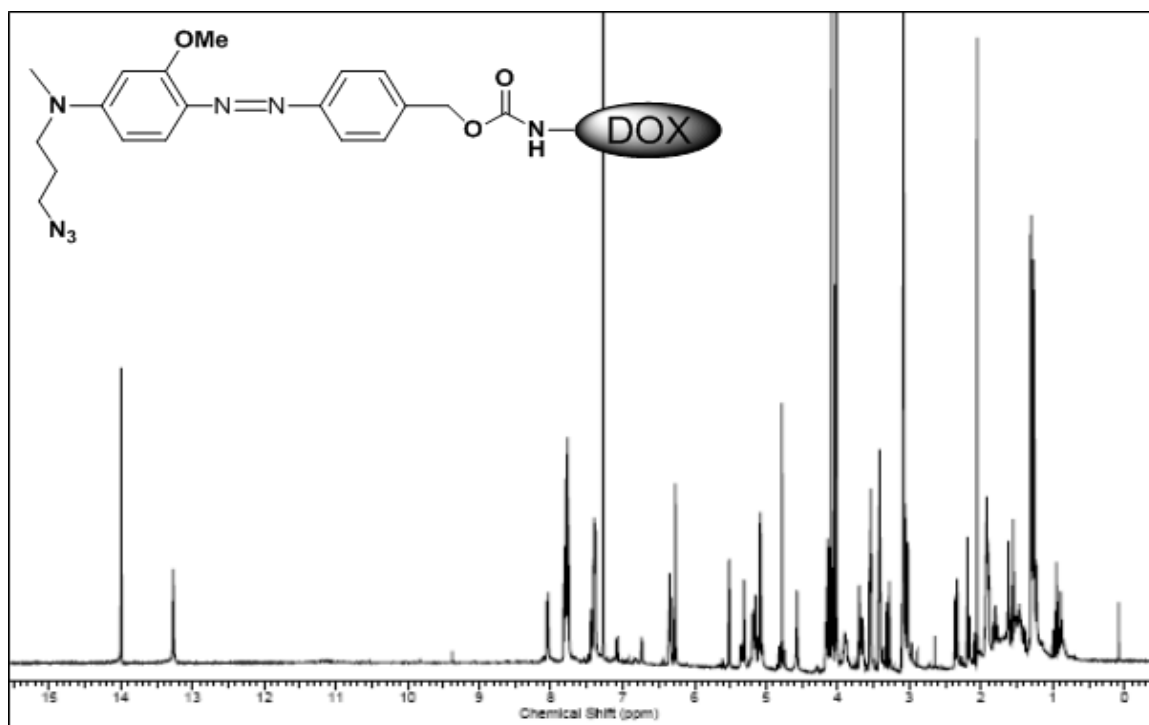
Figure S32. ^{1}H NMR of **4-((4-((3-azidopropyl)(methyl)amino)-2-methoxyphenyl)diazenyl)benzyl (4-Doxorubisine) carbonate (23)** dissolved in CDCl$_3$ on a Varian 500 MHz system (Palo Alto, CA).
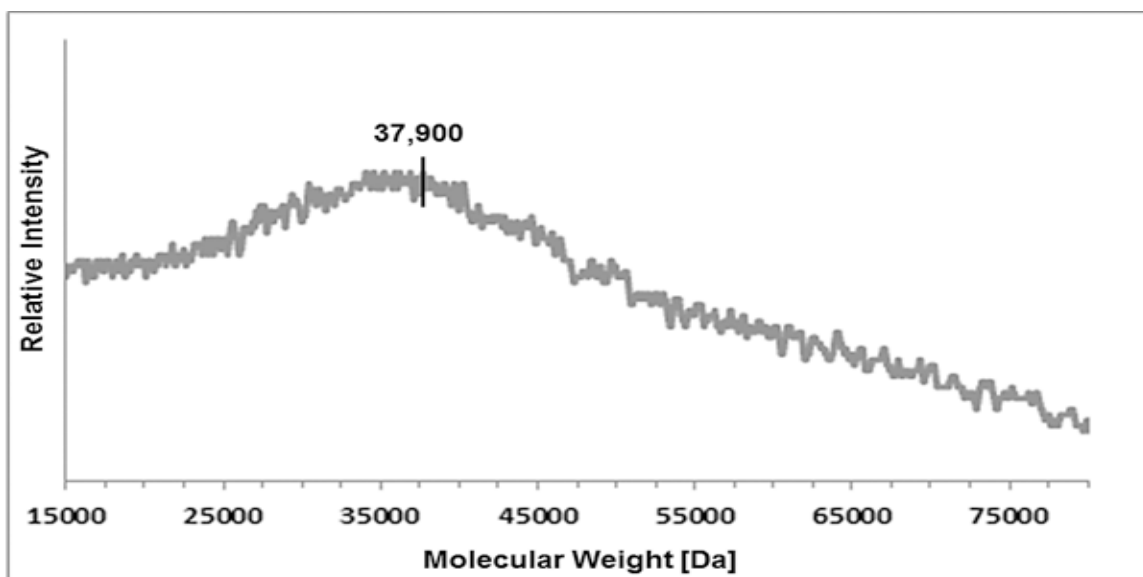
Figure S33. MALDI-TOF results of **G5-L3-DOX (24)** analyzed on a Shimadzu Biotech Axima CFR (Kyoto, Japan).
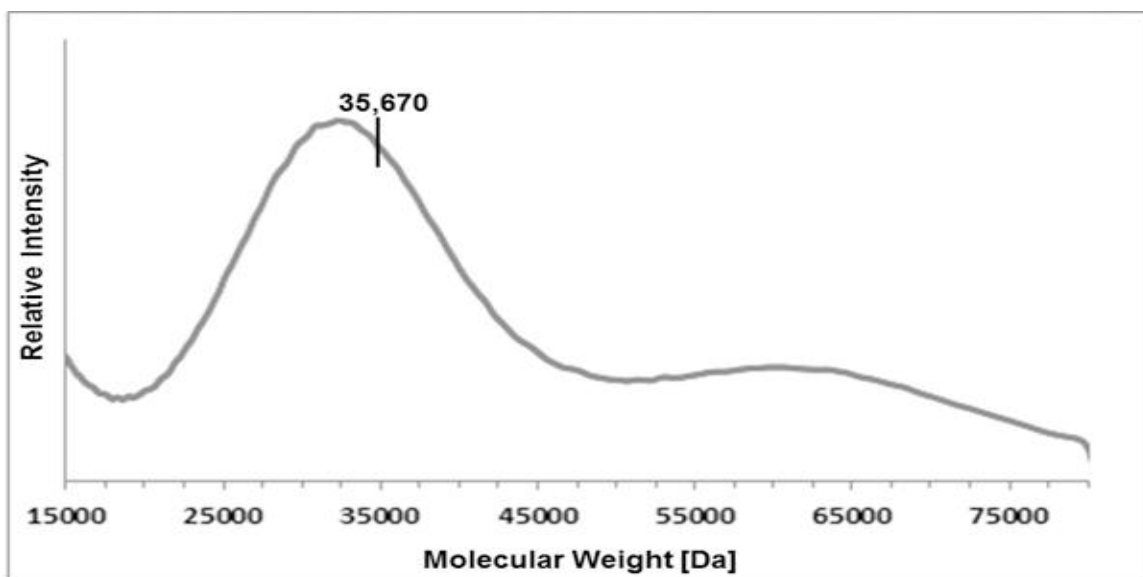
Figure S34. MALDI-TOF results of **G5-L4-DOX** analyzed on a Shimadzu Biotech Axima CFR (Kyoto, Japan).
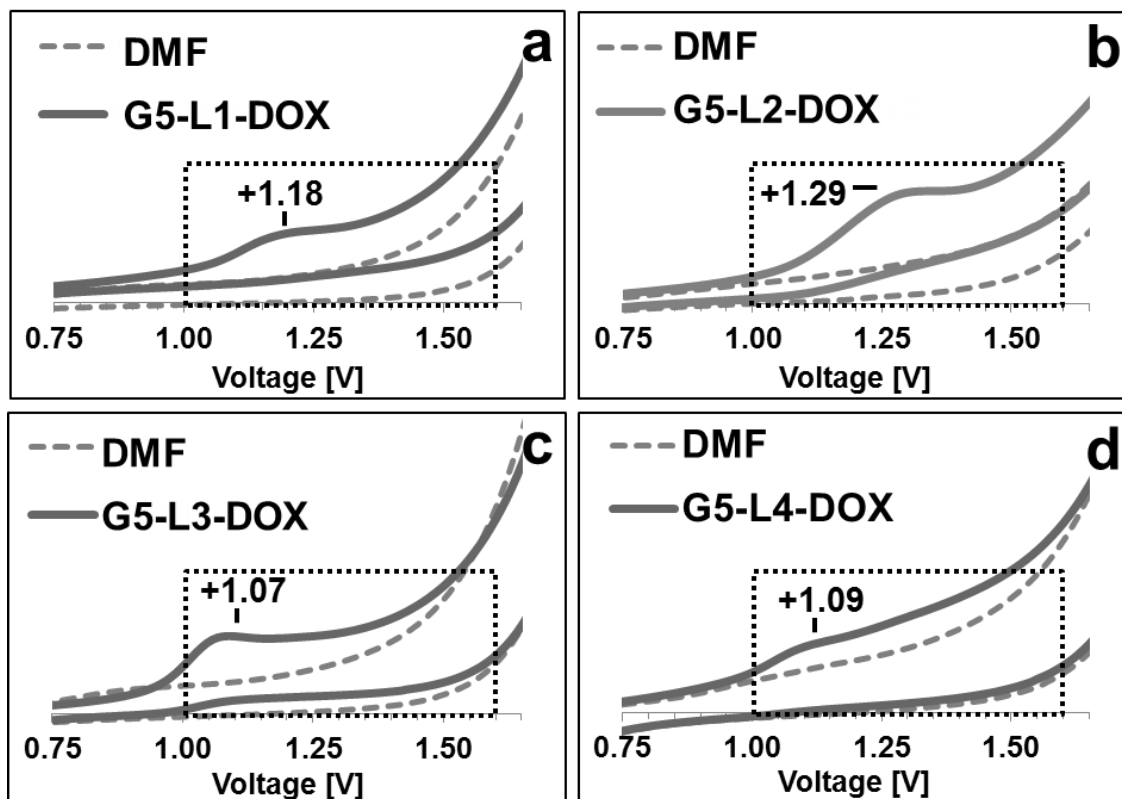
Figure S35. CV analysis of G5-L(x)-DOX conjugates. (**a**) G5-L1-DOX, (**b**) G5-L2-DOX, (**c**) G5-L3-DOX and (**d**) G5-L4-DOX conjugates positive potential peaks. Relative current (y-axis) was plotted versus voltage (V).
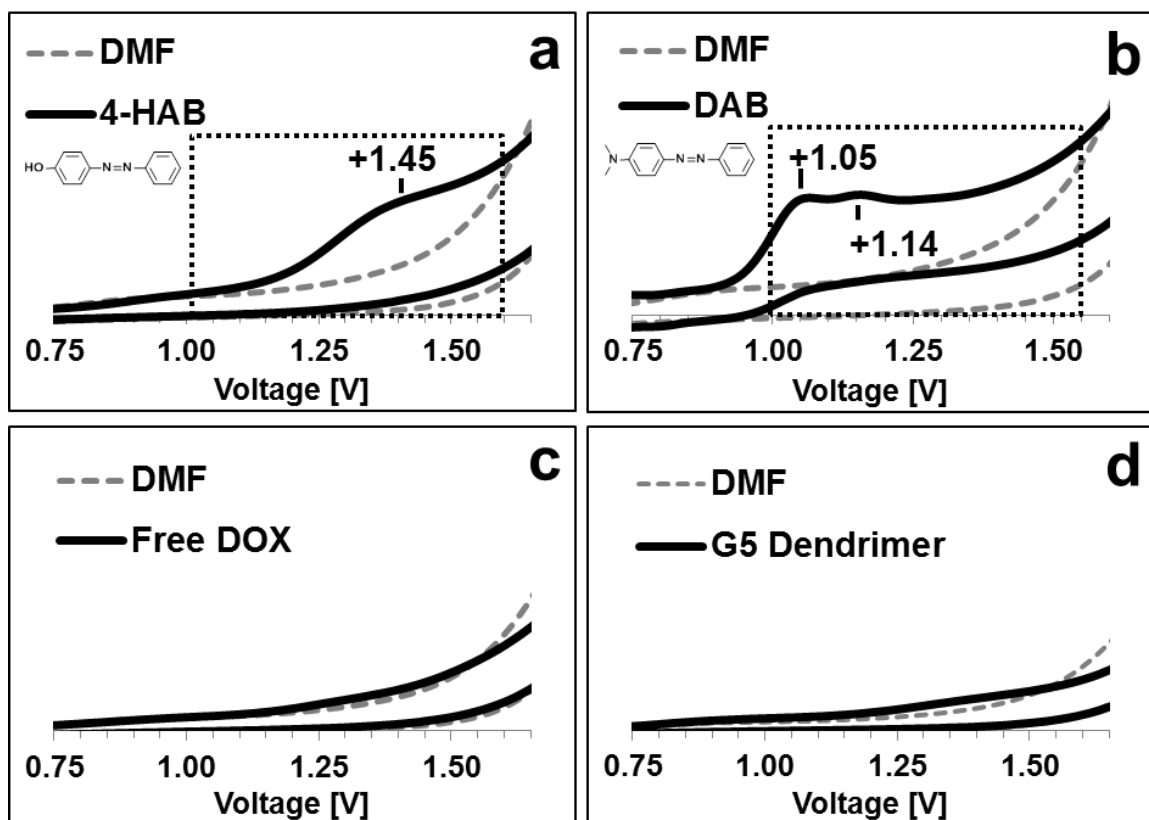
Figure S36. CV standards and controls. Positive potential peaks of (**a**) 4-HAB and (**b**) DAB azobenzene standards correlated well with previous work indicating equivalency of experimental setup. (**c**) Free DOX and (**d**) G5 dendrimer controls showed no contribution to signal during CV analysis of conjugates. Relative current (y-axis) was plotted versus voltage (V).
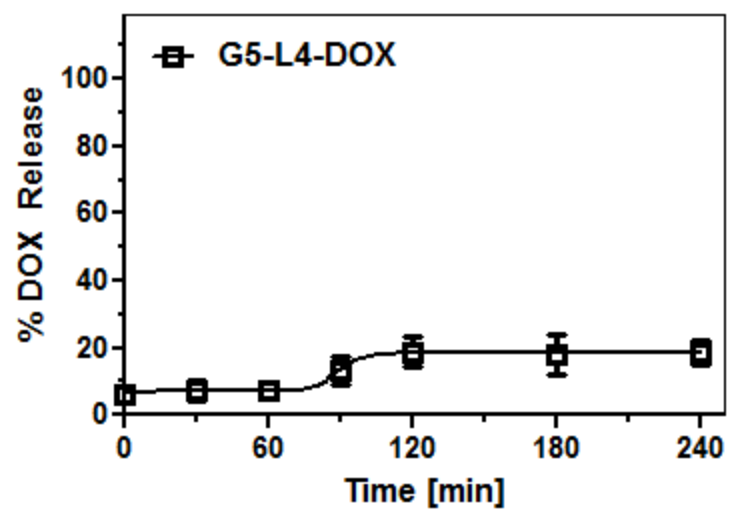
Figure S37. % of DOX released from G5-L4-DOX conjugates upon incubation with NADPH enzyme cofactor. Data are expressed as mean (n = 3) ± SEM. Curve was fit by a Michaelis-Menten model using Graphpad Prism software.

Chapter 4

N-acetylgalactosamine-functionalized Dendrimers as Hepatic Cancer Cell-targeted Carriers

4.1   Introduction

Tomalia and co-workers first reported the synthesis of poly(amidoamine) (PAMAM) dendrimers as a new class of branched, water-soluble polymers in 1985.[1] PAMAM dendrimers are characterized by a unique tree-like branching architecture and exhibit a characteristic increase in size, molecular weight and number of surface functional groups with the increase in generation number.[2] Aqueous solubility, monodispersity and large number of surface groups of PAMAM dendrimers available for conjugation of therapeutic molecules, targeting ligands and imaging agents has made these polymers ideal carriers for both diagnostic and therapeutic applications.[2-7] For example, PAMAM dendrimers have been used as gene[8-10] and anticancer drug carriers[2,3] that may display an antibody for cell or tissue targeting.[11,12]

Here we report the synthesis of PAMAM-sugar conjugates that can target hepatic cancer cells for selective drug delivery. We selected generation 5 (G5) PAMAM-NH_2 dendrimers as a carrier due to the large number of primary amine surface groups suitable for direct attachment of drug, imaging molecules and targeting ligands. To developed a

carrier that can selectively target hepatic cancer, we utilized G5 dendrimers with a diaminobutane (DAB) core to construct the *N*-acetylgalactosamine-functionlized carriers due to their intrinsic ability to accumulate in the liver compared to dendrimers with ethylenediamine cores (EDA).[5,6] In addition, G5 dendrimers with a DAB core proved to preferentially extravasate across the leaky tumor vasculature while exhibiting insignificant extravasation across normal blood vessles,[13] which allows effective *in vivo* targeting of these carriers to tumor tissue.[12,14-17] We envision that conjugation of *N*-acetylgalactosamine (NAcGal) molecules to G5 dendrimers will provide an additional strategy to increase their accumulation and retention in liver tumor tissue and warrant their use as carriers for targeted delivery of chemotherapeutic agents

We report the conjugation of *N*-acetylgalactosamine (NAcGal) sugar molecules to the primary amine surface groups of G5-$(NH_2)_{128}$ dendrimers via peptide and thiourea linkages to prepare G5-NAcGal conjugates with various sugar density. These G5-NAcGal conjugates are designed to achieve selective binding to the asialoglycoprotein receptor (ASGPR) that is highly expressed on the surface of hepatic cancer cells,[18] which will trigger their receptor-mediated endocytosis of these conjugates into hepatic cancer cells (**Figure 4.1**). We evaluated the effect of surface charge, concentration, incubation time, number of conjugated NAcGal molecules, and linkage chemistry on the uptake of G5-NAcGal conjugates into human hepatic cancer cells (HepG2). Selectivity of G5-NAcGal conjugates towards hepatic cancer cells and the contribution of ASGPR to conjugate's internalization was also evaluated using a competitive inhibition assay and assessing conjugate's uptake into MCF-7 breast cancer cells, which lack the ASGPR. MCF-7 breast cancer cells were selected for this comparison due to their high endocytic

capacity and their reported use as a control cell line to test selectivity of galactosylated carriers toward the ASGPR.[19]
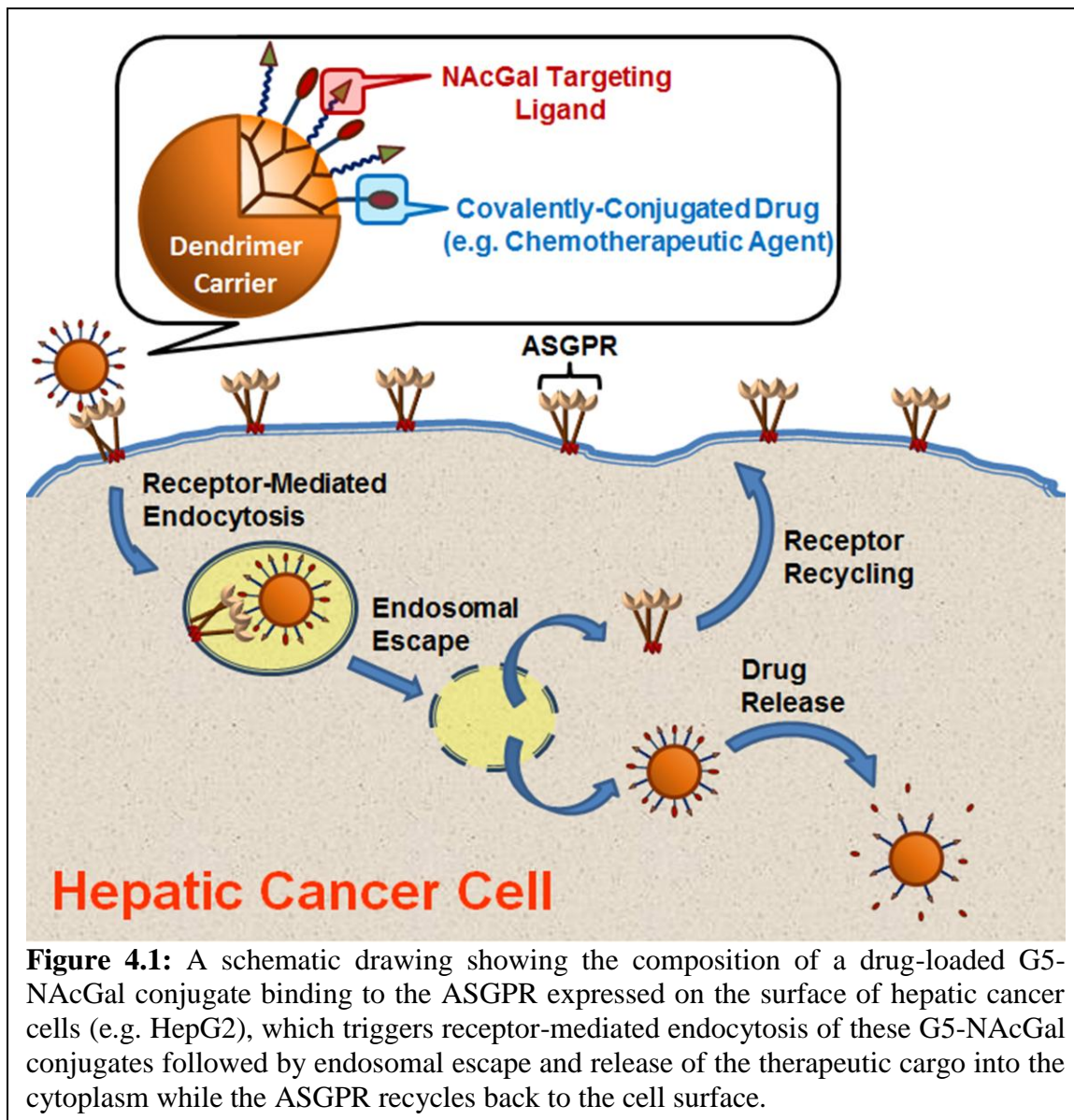
Figure 4.1: A schematic drawing showing the composition of a drug-loaded G5-NAcGal conjugate binding to the ASGPR expressed on the surface of hepatic cancer cells (e.g. HepG2), which triggers receptor-mediated endocytosis of these G5-NAcGal conjugates followed by endosomal escape and release of the therapeutic cargo into the cytoplasm while the ASGPR recycles back to the cell surface.

4.2   Materials and Methods

4.2.1   Materials

G5-(NH$_2$)$_{128}$ PAMAM dendrimers with DAB core, *N*-acetylgalactosamine, fluorescein isothiocyanate (Fl) and bovine insulin were purchased from Sigma-Aldrich Inc. (St. Louis, MO). Minimum essential medium (MEM), OPTI-MEM reduced serum medium, fetal bovine serum (FBS), 0.25% trypsin / 0.20% ethylene diamine teraacetic acid (EDTA) solution, phosphate buffered saline (PBS), penicillin/streptomycin/amphotericin solution, sodium pyruvate, and non-essential amino acid solutions were purchased from Invitrogen Corporation (Carlsbad, CA). Cytotoxicity Detection Kit (Lactate Dehydrogenase; LDH) was purchased from Roche, Inc. (Indianapolis, IN). T-75 flasks, Costar 24-well plates, and cell culture supplies were purchased from Corning Inc. (Corning, NY). HepG2 cell line was provided by Dr. Donna Shewach and the MCF-7 cell line was a generous gift from Dr. Sofia Merajver.

4.2.2 Synthesis of Fluorescently-labeled G5-NAcGal Conjugates via Peptide Linkages

*4.2.2.1 Synthesis of 3-(carbo-t-butoxymethyl)-2-(acetylamino)-2-deoxy-D-galactopyranoside (**1**)*

NAcGal (486 mg, 2.2 mmoles) was dissolved in 10 ml of dimethylformamide (DMF) and NaH (88 mg, 2.2 mmoles) was added as a solid followed by the addition of tert-butyl bromoacetate (429.1 mg, 2.2 mmoles) in 2 ml of DMF. After stirring at room temperature for 72 hours, DMF was removed under reduced pressure and the reaction mixture was purified on a silica gel column using an consecutive eluent system of CH$_2$Cl$_2$ (100%), CH$_2$Cl$_2$:methanol (15:1), CH$_2$Cl$_2$:methanol (10:1) and finally CH$_2$Cl$_2$:methanol (8:1) to produce 400 mg (54% yield) of product 1 as a white solid. ^{1}H NMR of compound 1 in

Scheme 4.1: Protocol for synthesis of fluorescently-labeled G5-NAcGal conjugates through a peptide linkage connecting the NAcGal ligands to the G5 carrier
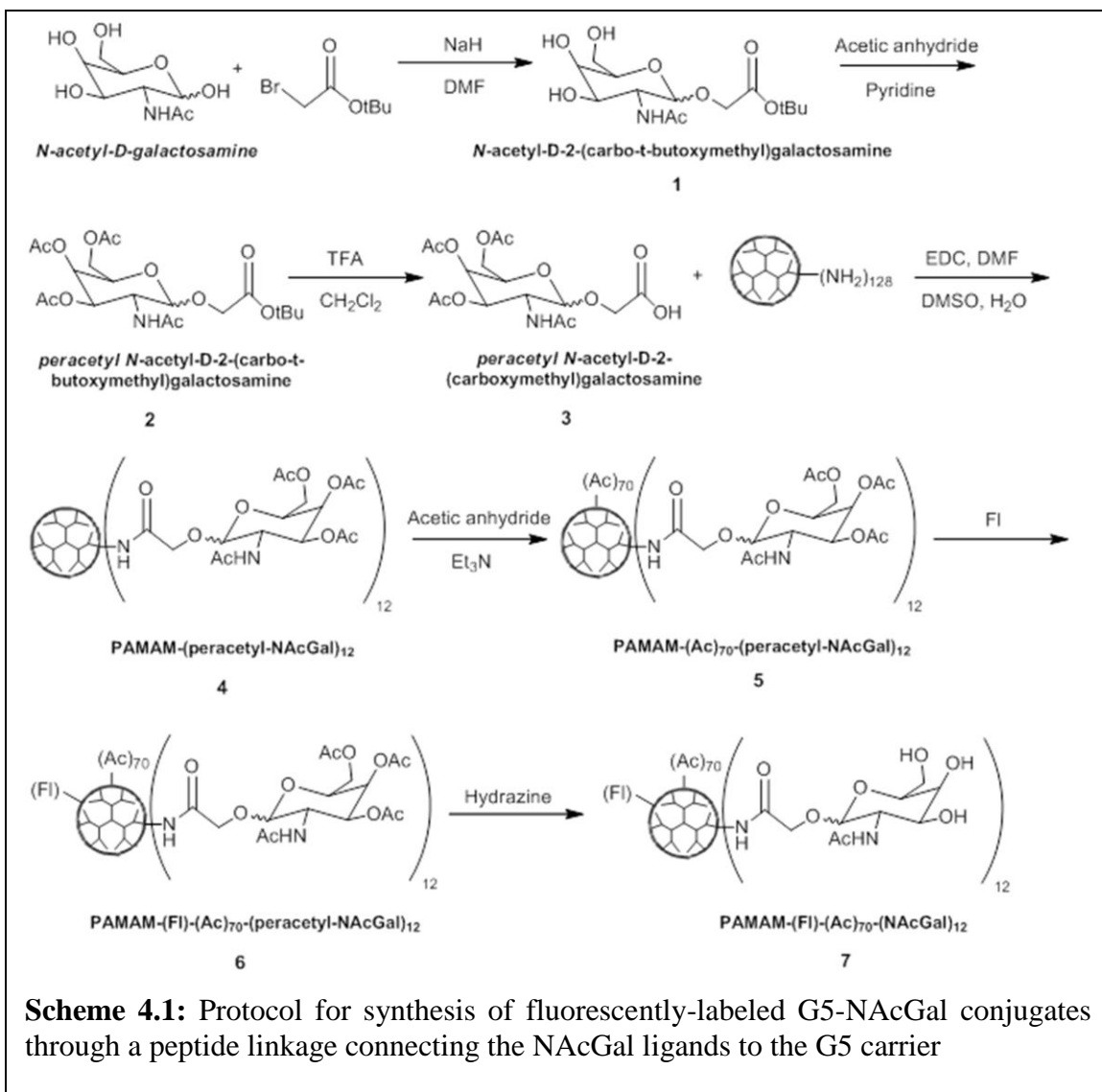
CD$_3$OD (400 MHz Varian, Palo Alto, CA) shows δ 4.92 (d, *J*=4.8 Hz, 1H), 4.36 (dd, *J$_1$*=9.2 Hz, *J$_2$*=4.8 Hz, 1H), 4.26 (dd, *J$_1$*=9.2 Hz, *J$_2$*=7.2 Hz, 1H), 4.15 (s, 2H), 3.82 (dd, *J$_1$*=7.6 Hz, *J$_2$*=3.6 Hz, 1H), 3.62-3.52 (m, 3H), 3.29 (m, 1H), 2.00 (s, 3H), 1.45 (s, 9H); ESI Mass of compound 1 is 358 [M+Na]$^+$

*4.2.2.2 Synthesis of 3-(carbo-t-butoxymethyl)-2-(acetylamino)-2-deoxy-D-galactopyranoside-3,4,6-triacetate (**2**)*

Excess of pyridine (0.145 ml, 1.79 mmoles) and acetic anhydride (0.34 ml, 3.58 mmoles) was added to compound 1 (67 mg, 0.179 mmoles) dissolved in 2 ml of anhydrous dichloromethane and the reaction mixture was stirred at room temperature for 16 hours. The reaction mixture was diluted with 50 ml CH_2Cl_2, washed twice with 20 ml of 0.1 N HCl followed by an additional wash with 20 ml DI water. The organic layer was dried over $MgSO_4$ and concentrated providing 57 mg (69% yield) of product 2 as a colorless oil which was used as the crude product in the next step without any further purification. ^{1}H NMR of compound 2 in $CDCl_3$ (500 MHz Varian, Palo Alto, CA) shows δ 6.48 (d, J=9.0 Hz, 1H), 5.36 (t, J=7.0 Hz, 1H), 5.17 (q, J=5.5 Hz, 1H), 4.97 (m, 1H), 4.66 (m, 1H), 4.23 (dd, J_1=12.0 Hz, J_2=4.5 Hz, 1H), 4.17 (m, 2H), 4.10 (dd, J_1=12.0 Hz, J_2=6.0 Hz, 1H), 3.98 (d, J=16.5 Hz, 1H), 2.08 (s, 3H), 2,04 (s, 3H), 2.03 (s, 3H), 1.97 (s, 3H), 1.46 (s, 9H); ESI Mass of compound 2 is 462 [M+H]$^+$

*4.2.2.3 Synthesis of 3-(carboxymethyl)-2-(acetylamino)-2-deoxy-D-galactopyranoside-3,4,6-triacetate (**3**)*

Trifluoroacetic acid (1 ml) was added to a solution of 2 (55 mg, 0.119 mmoles) dissolved in 2 ml of CH_2Cl_2 and the reaction mixture was stirred at room temperature for 12 hours. The reaction mixture was concentrated by co-evaporation with toluene and was purified on a silica gel column using CH_2Cl_2:methanol:ethanol (10:1:0.01) as an eluent to produce 35 mg (0.086 mmoles, 73% yield) of product 3 as a colorless oil. ^{1}H NMR of compound 3 in $CDCl_3$ (400 MHz Varian, Palo Alto, CA) shows δ 6.85 (br d, J=8.0 Hz, 1H), 5.39 (t, J=8.0 Hz, 1H), 5.20 (q,), 5.02 (d, J=5.0 Hz, 1H), 4.63 (m, 1H), 4.33-4.03 (m, 5H), 2.07 (s, 3H), 2,04 (s, 3H), 2.02 (s, 3H), 1.97 (s, 3H); ESI Mass of compound 3 is 428 [M+Na]$^+$

*4.2.2.4 Synthesis of 3-(PAMAM-carbamidomethyl)-2-(acetylamino)-2-deoxy-D-galactopyranoside-3,4,6-triacetate (**4**)*

1-ethyl-3-(3-dimethylaminopropyl) carbodiimide (156.2 mg, 0.815 mmoles) was added to a solution of compound 3 (33.0 mg, 0.082 mmoles) dissolved in a 6 ml of dimethylformamide:dimethylsulfoxide (3:1) mixture and the reaction solution was stirred at room temperature for 1 hour. G5-$(NH_2)_{128}$ dendrimer (58.5 mg, 0.00203 mmoles) was added to the reaction mixture and stirred at room temperature for 72 hours. The reaction was concentrated by rotary evaporation, purified by dialysis against pure water and dried by lyophilization to produce 57 mg (0.00175 mmoles, 86% yield) of compound 4 as a white solid. MALDI-TOF analysis shows that the mass for 4 is 32,573 gm/mole.

*4.2.2.5 Synthesis of 3-(acetyl-PAMAM-carbamidomethyl)-2-(acetylamino)-2-deoxy-D-galactopyranoside-3,4,6-triacetate (**5**)*

Compound 4 (55 mg, 0.00169 mmoles) was dissolved in 3 ml anhydrous methanol and triethylamine (0.035 ml, 0.253 mmoles) was added to the solution, followed by addition of acetic anhydride (0.0016 ml, 0.170 mmoles) and stirring the reaction mixture for 20 hours at room temperature. The reaction mixture was concentrated by rotary evaporation, purified by dialysis against pure water, and dried by lyophilization to produce 47 mg (0.00133 mmol, 78% yield) of product 5 as a white solid. MALDI-TOF analysis shows that the mass for 5 is 35,469 gm/mole.

4.2.2.6 Synthesis of 3-(fluorescene-acetyl-PAMAM-carbamidomethyl)-2-(acetylamino)-2-deoxy-D-galactopyranoside-3,4,6-triacetate (6)

Fluorescein isothiocyanate (5 mg, 0.0133 mmoles) was dissolved in 1 ml acetone and added to a solution of compound 5 (47 mg, 0.00133 mmoles) dissolved in 3 ml DI water and the reaction mixture was stirred at room temperature for 24 hours. The reaction mixture was concentrated by rotary evaporation, purified by dialysis against pure water, and dried by lyophilization to produce 45 mg (0.00125 mmoles, 93% yield) of product 6 as an orange solid. MALDI-TOF analysis shows that the mass for 6 is 35,997 gm/mole.

4.2.2.7 Synthesis of 3-(fluorescene-acetyl-PAMAM-carbamidomethyl)-2-(acetylamino)-2-deoxy-D-galactopyranoside (7)

Hydrazine monohydrate (0.4 ml, 8.24000 mmoles) was added to a solution of compound 6 (45 mg, 0.00125 mmoles) dissolved in 3ml anhydrous methanol and the reaction mixture was stirred at room temperature for 36 hours. The reaction solution was concentrated by rotary evaporation, purified by dialysis against pure water and dried by lyophilization to produce 40 mg (0.00111 mmoles, 89% yield) of fluorescently-labeled G5-NAcGal conjugates (7) as an orange solid. MALDI-TOF analysis shows that the mass for 7 is 35,857 gm/mole.

4.2.3   Synthesis of Fluorescently-labeled G5-NAcGal Conjugates via Thiourea Linkages

4.2.3.1 Synthesis of 3-bromopropyl-2-(acetylamino)-2-deoxy-D-galactopyranoside (8)

Scheme 4.2: Protocol for synthesis of fluorescently-labeled G5-NAcGal conjugates through a thiourea linkage connecting the NAcGal ligands to the G5 carrier
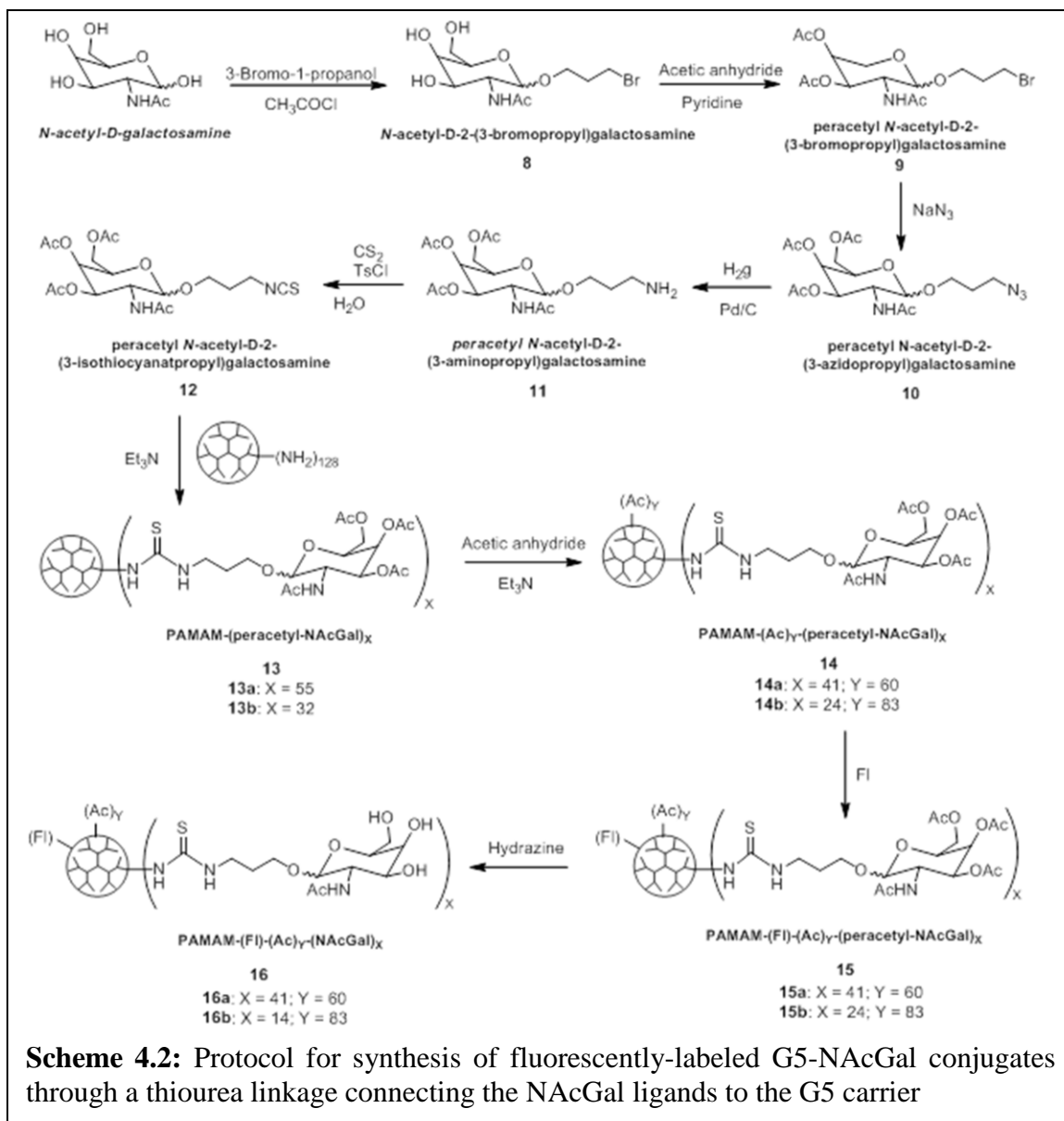
Acetyl chloride (1.68 ml) was added dropwise to a solution of NAcGal (2.0 g, 9.0 mmoles) in 3-bromo-l-propanol (30 ml) at 0 °C. The reaction mixture was stirred for 5.5 hours at 70 °C before neutralizing the reaction mixture with Dowex-OH resin. The reaction mixture was filtered and the filtrate was purified on a silica gel column using CH$_2$Cl$_2$:methanol (3:2) as an eluent to isolate pure compound 8 (2.6 g, 7.6 mmoles, 84% yield). ^{1}H NMR of compound 8 in CD$_3$OD (300 MHz Varian, Palo Alto, CA) shows δ 1.98 (s, 3H); 2.07-2.18 (m, 2H); 3.47-3.67 (m, 3H), 3.68-3.98 (m, 6H), 4.26 (dd, 1H,

J_1=3.5 Hz, J_2=11.1 Hz); 4.83 (d, 1H, J=3.5 Hz); ESI Mass for compound 8 is 364 [M+Na] [+]

*4.2.3.2 Synthesis of 3-bromopropyl-2-(acetylamino)-2-deoxy-D-galactopyranoside-3,4,6-triacetate (**9**)*

Excess pyridine (5 ml, 61.89 mmoles) and acetic anhydride (10 ml, 105.88 mmoles) were added to compound 8 (2 g, 5.84 mmoles) dissolved in 20 ml anhydrous dichloromethane and the reaction mixture was stirred at room temperature for 16 hours. The reaction mixture was washed with saturated copper sulfate solution followed by another wash with saturated sodium bicarbonate solution to neutralize the acetic acid byproduct. The organic layer was dried over Na_2SO_4 and concentrated by rotary evaporation before loading onto a silica gel column and fractionated using CH_2Cl_2:methanol (98:2) mixture to isolate pure compound 9 (2.36 g, 5.04 mmoles, 86% yield). ^{1}H NMR of compound 9 in $CDCl_3$ (300 MHz Varian, Palo Alto, CA) shows δ 1.97 (s, 3H), 2.00 (s, 3H), 2.05 (s, 3H), 2.12-2.19 (m, 2H; s, 3H), 3.47-3.67 (m, 3H), 3.84-3.97 (m, 1H), 4.04-4.22 (m, 3H), 4.53-4.64 (m, 1H), 4.91 (d, 1H, J=3.5), 5.15 (dd, 1H, J_1=2.9, J_2=11.1), 5.38 (d, 1H, J=3.5), 5.59 (d, 1H, J=9.9); ESI Mass of compound 9 is 490 [M+Na] [+]

*4.2.3.3 Synthesis of 3-azidopropyl-2-(acetylamino)-2-deoxy-D-galactopyranoside-3,4,6-triacetate (**10**)*

Sodium azide (0.41 g, 6.30 mmoles) was added as a solid to a solution of compound 9 (1.47 g, 3.14 mmoles) in 20 ml DMF and stirred for 3 hours at 50 °C followed by diluting the reaction mixture with ethyl acetate, washing with ice cold water, drying over Na_2SO_4

and concentrating by rotary evaporation. The reaction mixture was purified on a silica gel column using CH_2Cl_2:acetone (9:1) mixture to produce pure compound 10 (1.33 g, 3.09 mmoles, 98% yield). ^{1}H NMR of compound 10 in $CDCl_3$ (300 MHz Varian, Palo Alto, CA) shows δ 1.97 (s, 3H), 2.00 (s, 3H), 2.05 (s, 3H), 2.12-2.19 (m, 2H; s, 3H), 3.28-3.60 (m, 3H), 3.73-3.88 (m, 1H), 4.02-4.21 (m, 3H), 4.49-4.66 (m, 1H), 4.88 (d, 1H, J=3.5 Hz), 5.14 (dd, 1H, J_1=5.36, J_2 =5.66); ESI Mass for compound 10 is 453 [M+Na] [+]

4.2.3.4 *Synthesis of 3-isothiocyanopropyl-2-(acetylamino)-2-deoxy-D-galactopyranoside-3,4,6-triacetate (*12*)*

Compound 10 (0.8 g, 1.86 mmoles) was dissolved in 30 ml ethanol and a catalytic amount of Pd/C was added to the reaction mixture and left stirring under a hydrogen blanket for 24 hours. The reaction mixture was filtered and concentrated to produce the crude compound 11 (0.735 g, 1.81 mmoles) that was directly used in the next reaction. Triethylamine (0.61 ml, 4.45 mmoles) and carbon disulfide (0.089 ml, 1.48 mmoles) were added under nitrogen to a solution of compound 11 (0.4 g, 0.99 mmoles) dissolved in 20 ml tetrahydrofuran and stirred for 1 hour at room temperature, followed by cooling the reaction mixture in an ice bath and adding *p*-toluenesulfonyl chloride (0.3 g, 1.58 mmoles) as a solid. The reaction mixture was allowed to warm up to room temperature in 1 hour followed by addition of 1 N HCl and extracting the reaction mixture using ethyl acetate. Ethyl acetate layers were dried over Na_2SO_4 and concentrated by rotary evaporation before loading on a silica gel column and isolating compound 12 (0.182 g, 0.40 mmoles, 22% yield over 2 steps) using ethyl acetate:hexanes (3:2) mixture as an eluent. ^{1}H NMR of compound 12 in $CDCl_3$ (300 MHz Varian, Palo Alto, CA) shows δ

1.22-1.26 (2H, d); 1.97 (3H, s); 1.98 (3H, s); 2.02 (3H, s); 2.03 (3H, s); 3.52-3.70 (3H, m); 3.80-3.89 (1H, m); 4.04-4.16 (3H, m); 4.53-4.63 (1H, m); 4.91 (1H, d, J=3.5); 5.16 (1H, dd, J_1=3.5, J_2=11.1); 5.38 (1H, d, J=2.9); 5.76 (1H, d,=J 9.3); ESI Mass of compound 12 is 469 [M+Na] $^+$

4.2.3.5 *Synthesis of 3-((PAMAM-thioureido)propyl-2-(acetylamino))-2-deoxy-D-galactopyranoside-3,4,6-triacetate (***13a/b***)*

G5-$(NH_2)_{128}$ dendrimer (13a: 80 mg, 0.00277 mmoles; 13b: 60 mg, 0.00208 mmoles) was dissolved in 2 ml of DI water and triethylamine (13a: 49.7 µL, 0.354 mmoles; 13b: 37 µL, 0.2649 mmoles) was added to the reaction flask. Compound 12 (13a: 79 mg, 0.1774 mmoles; 13b: 29 mg, 0.0666 mmoles) was dissolved in 2 ml acetone and added dropwise to the reaction mixture and stirred for 48 hours at room temperature. The reaction mixture was concentrated by rotary evaporation, purified by dialysis against pure water and lyophilized to produce 139 mg (0.0026 mmoles, 94% yield) of compound 13a and 89 mg (0.0021 mmoles, 99% yield) of compound 13b. MALDI-TOF analysis shows that the mass for 13a is 53,468 gm/mole and is 43,185gm/mole for 13b.

4.2.3.6 *Synthesis of 3-((acetyl-PAMAM-thioureido)propyl-2-(acetylamino))-2-deoxy-D-galactopyranoside-3,4,6-triacetate (***14a/b***)*

Compounds 13a/b (13a: 130 mg, 0.00243 mmoles; 13b: 80 mg, 0.00185 mmoles) were dissolved in 3ml of anhydrous methanol followed by addition of triethylamine (14a: 0.0493 ml, 0.354 mmoles; 14b: 0.0494 ml, 0.355 mmoles) via a syringe and acetic anhydride (14a: 0.0137 ml, 0.145 mmoles; 14b: 0.0145 ml, 0.153 mmoles) at room

temperature. The reaction mixture was stirred at room temperature for 20 hours, concentrated by rotary evaporation, purified by dialysis against pure water, and lyophilized to yield 130 mg of 14a and 85 mg of 14b. MALDI-TOF analysis shows that the mass for 14a is 49,717 gm/mole and is 46,671 gm/mole for 14b.

*4.2.3.7 Synthesis of 3-((flourescene-acetyl-PAMAM-thioureido)propyl-2-(acetylamino))-2-deoxy-D-galactopyranoside-3,4,6-triacetate (***15a/b***)*

Fluorescein isothiocyanate (Fl) (14a: 5.8 mg, 0.0149 mmoles; 14b: 4 mg, 0.01042 mmoles) was dissolved in 0.5 ml acetone and added to an aqueous solution of compound 14a/b (15a: 124 mg, 0.002494 mmoles; 15b: 75 mg, 0.001736 mmoles) and kept stirring for 20 hours at room temperature. The reaction mixture was concentrated by rotary evaporation and the fluorescently-labeled conjugates were purified by dialysis against pure water followed by lyophilization to yield 130 mg (0.002490 mmoles, 99% yield) of compound 15a and 77 mg (0.001635 mmoles, 94% yield) of compound 15b. MALDI-TOF analysis shows that the mass for 15a is 52,024 gm/mole and is 47,071 gm/mole for 15b.

*4.2.3.8 Synthesis of 3-((fluorescene-acetyl-PAMAM-thioureido)propyl-2-(acetylamino))-2-deoxy-D-galactopyranoside (***16a/b***)*

Compound 15a/b (15a: 125 mg, 0.00240 mmoles; 15b: 71 mg, 0.00150 mmoles) was dissolved in 3 ml of methanol and mixed with hydrazine monohydrate (16a: 1.16 ml, 24.02 mmoles; 16b: 0.73 ml, 15.08 mmoles) was stirred for 24 hours at room temperature. The reaction mixture was concentrated by rotary evaporation, purified by

dialysis against pure water and lyophilized to obtain 115 mg (0.0024 mmoles, 99% yield) and 57 mg (0.00139 mmoles, 93% yield) of fluorescently-labeled G5-NAcGal conjugates (16a & 16b), respectively. MALDI-TOF analysis shows that the mass for 16a is 46,867 gm/mole and is 40,934 gm/mole for 16b.

4.2.4 Characterization of Fluorescently-labeled G5-NAcGal Conjugates

Non-acetylated $G5-(Fl)-(NH_2)_{122}$, acetylated $G5-(Fl)-(Ac)_{110}$, NAcGal-targeted $G5-(Fl)-(Ac)_{70}-(NAcGal)_{12}$ conjugates with a peptide linkage, or $G5-(Fl)-(Ac)_{83}-(NAcGal)_{14}$ and $G5-(Fl)-(Ac)_{60}-(NAcGal)_{41}$ conjugates with thiourea linkages were dissolved in deionized water at a concentration of 1 μM. The size and zeta potential of each conjugate were measured using a 90Plus particle size analyzer with ZetaPALS capability (Brookhaven Instruments Corporation, Holtsville, NY).

4.2.5 Culture of HepG2 and MCF-7 Cells

HepG2 cells were cultured in T-75 flasks using MEM supplemented with 10% FBS, and 1% penicillin/streptomycin/amphotericin, sodium pyruvate and non-essential amino acids. Similarly, MCF-7 cells were cultured using the same medium composition with the addition of 0.1% insulin solution. HepG2 cells (passages 20-25) and MCF-7 cells (passages 90-95) were incubated at 37 °C, 5% CO_2 and 95% relative humidity while changing the culture medium every 48 hours. Cells were passaged at 80-90% confluency using a 0.25% trypsin-EDTA solution.

4.2.6 Uptake of Fluorescently-labeled Dendrimers into HepG2 and MCF-7 Cells

179

HepG2 and MCF-7 cells were seeded in 24-well plates at seeding density of 5×10^5 cells/well and allowed to adhere overnight. The culture medium was aspirated and the cells were incubated for 2 or 24 hours at regular culture conditions with different concentrations (5-100 nM) of non-acetylated G5-(Fl)-$(NH_2)_{122}$, acetylated G5-(Fl)-$(Ac)_{110}$, NAcGal-targeted G5-(Fl)-$(Ac)_{70}$-$(NAcGal)_{12}$ conjugates with a peptide linkage, or G5-(Fl)-$(Ac)_{83}$-$(NAcGal)_{14}$ and G5-(Fl)-$(Ac)_{60}$-$(NAcGal)_{41}$ conjugates with thiourea linkages dissolved in OPTI-MEM solution. After the selected incubation period HepG2 and MCF-7 cells were washed with cold PBS, trypsinized and centrifuged at 1000 rpm for 5 minutes to pellet the cells before resuspending them in 1 mL of fresh PBS and analyzing them using a Beckman Coulter FACsCalibur flow cytometer with a 488 nm excitation laser. Gating during flow analysis was based on normalized fluorescence of untreated cells to evaluate cellular internalization of each treatment as a function of conjugate's chemical composition, concentration, and incubation time. Uptake of each conjugate was evaluated in three independent experiments using four replicates for each experimental condition.

Uptake of non-acetylated G5-(Fl)-$(NH_2)_{122}$, acetylated G5-(Fl)-$(Ac)_{110}$, and NAcGal-targeted G5-(Fl)-$(Ac)_{83}$-$(NAcGal)_{14}$ conjugates into HepG2 cells (1×10^5 cells/well) upon incubation with 200 nM solution of each conjugate for 4 hours was visualized using a Nikon Eclipse TE2000-U inverted microscope equipped with a photometrics EMCCD camera and an EXFO fluorescent lamp (λ_{ex} = 488 nm, λ_{em} =512 nm). Uptake of NAcGal-targeted G5-(Fl)-$(Ac)_{83}$-$(NAcGal)_{14}$ conjugates into HepG2 cells was evaluated as a function of conjugate's concentration (5-100 nM) upon co-incubation

with 100 mM of free NAcGal ligands using flow cytometry to determine the role of the ASGPR in the internalization of NAcGal-targeted conjugates into hepatic cancer cells.

4.2.7 Cytotoxicity of Fluorescently-labeled Dendrimers Towards HepG2 Cells

Toxicity of non-acetylated G5-(Fl)-(NH$_2$)$_{122}$, acetylated G5-(Fl)-(Ac)$_{110}$, NAcGal-targeted G5-(Fl)-(Ac)$_{70}$-(NAcGal)$_{12}$ conjugates with a peptide linkage, or G5-(Fl)-(Ac)$_{83}$-(NAcGal)$_{14}$ and G5-(Fl)-(Ac)$_{60}$-(NAcGal)$_{41}$ conjugates with thiourea linkages was evaluated using the lactate dehydrogenase (LDH) leakage assay (Roche Diagnostics Corporation, Indianapolis, IN) at a concentration of 100 nM, which is the highest concentration using in the uptake studies. Briefly, HepG2 cells were seeded in 24-well plates at a seeding density of 5x10^5 cells/well and allowed to adhere overnight before replacing the culture medium with OPTI-MEM solution containing different conjugates and incubating for 2 and 24 hours under normal culture conditions. The amount of LDH enzyme present in the culture medium after incubation with each conjugate was quantified by mixing 100 μL of the culture medium with 100 μL of the enzyme substrate included in the assay kit following the manufacturer's guidelines, and measuring the absorbance of this mixture at 490 nm using a Multiskan microplate reader (Thermo Fisher Scientific, Inc., Walham, MA). Contribution of the fluorescent and sugar molecules to the absorbance of each conjugate was eliminated by subtracting the absorbance of a 100 nM solution of each conjugates at 490 nm. LDH leakage observed upon incubation of HepG2 cells with OPTI-MEM culture medium and 2% v/v Triton X-100 solution were used as negative and positive controls, respectively. The amount of LDH enzyme present in the culture medium upon incubation of each conjugate with

HepG2 cells was normalized to the amount of LDH observed upon incubation of HepG2 cells with 2% v/v Triton X-100 solution. G5-NAcGal conjugates that result in statistically higher LDH leakage compared to the negative control (blank OPTI-MEM culture medium) were considered cytotoxic.

4.3   Results

4.3.1   Synthesis of Fluorescently-labeled G5-NAcGal Conjugates

Coupling of NAcGal-COOH ligands to G5-$(NH_2)_{128}$ dendrimers via peptide linkages yielded G5-$(NAcGal)_{12}$ conjugates (**Scheme 4.1**; Compound **4**) with 9.4 mole% of NAcGal molecules as determined by MALDI-TOF analysis. To evaluate the effect of linkage chemistry on the internalization of G5-NAcGal conjugates, NAcGal molecules were functionalized with an isothiocyanate group to allow their coupling to G5-$(NH_2)_{128}$ dendrimers via a thiourea linkage following the synthesis scheme shown in **Scheme 4.2**. We varied the amount of NAcGal molecules used in the coupling reaction to achieve 10 mole% and 40 mole% capping of the NH_2 surface groups, which yielded G5-(Fl)-$(Ac)_{83}$-$(NAcGal)_{14}$ and G5-(Fl)-$(Ac)_{60}$-$(NAcGal)_{41}$ conjugates (**Scheme 4.2**, Compounds **16a** and **16b**) containing 10.9 mole% and 32.0 mole% NAcGal ligands, respectively. G5-NAcGal conjugates were reacted with acetic anhydride yielding acetylated G5-NAcGal conjugates (**Scheme 4.1**; Compound **5**, **Scheme 4.2**; Compounds **14a** and **14b**). Approximately 4 ± 2 fluorescein isothiocyanate molecules were attached per G5-NAcGal conjugate, which matches the reported values and provide sufficient fluorescence signals for analysis of conjugate's uptake into HepG2 and MCF-7 cells. The acetyl groups used

182

to cap the hydroxyl groups of the coupled NAcGal molecules were removed after the fluorescence labeling of all G5-NAcGal conjugates using hydrazine to yield the final fluorescently-labeled G5-NAcGal conjugates (**Scheme 4.1**; Compound **7**, **Scheme 4.2**, Compounds **16a** and **16b**) used in all the uptake studies.

4.3.2 Size and Surface Charge of Fluorescently-labeled G5-NAcGal Conjugates

Our results show that the average size of G5-$(Fl)_6$-$(NH_2)_{122}$ is 4.75 ± 0.73 nm (**Figure 4.2**; Panel **A**), and carry a net positive charge of 7.14 ± 1.02 mV (**Figure 4.2**; Panel **B**). Acetylation of 110 (86%) of the primary amine surface groups slightly increased the average size of G5-$(Fl)_6$-$(Ac)_{110}$ dendrimers to 5.00 ± 1.44 nm and completely abolished the positive surface charge of this carrier as shown by the drop in zeta potential to -0.17 ± 0.64 mV (**Figure 4.2**). Acetylation of 70 (55%) of the primary amine surface groups, coupling of 12 NAcGal molecules (9.4%), and fluorescence-labeling of G5-$(NH_2)_{128}$ dendrimers yields G5-$(Fl)_6$-$(Ac)_{70}$-$(NAcGal)_{12}$ conjugates with
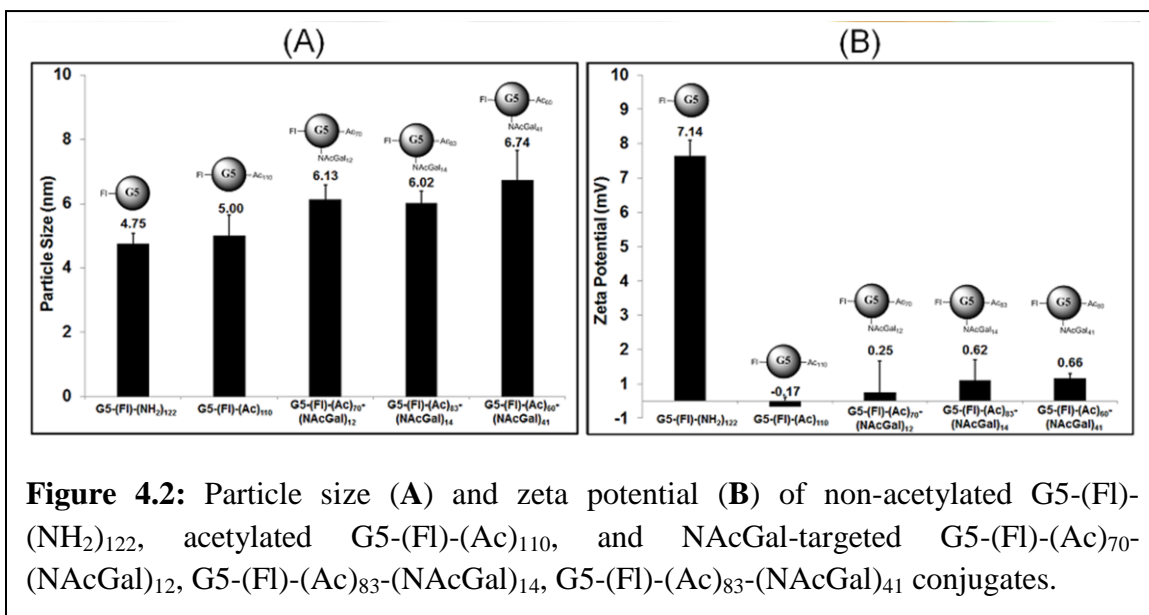
Figure 4.2: Particle size (**A**) and zeta potential (**B**) of non-acetylated G5-(Fl)-$(NH_2)_{122}$, acetylated G5-(Fl)-$(Ac)_{110}$, and NAcGal-targeted G5-(Fl)-$(Ac)_{70}$-$(NAcGal)_{12}$, G5-(Fl)-$(Ac)_{83}$-$(NAcGal)_{14}$, G5-(Fl)-$(Ac)_{83}$-$(NAcGal)_{41}$ conjugates.

an average size of 6.13 ± 1.00 nm and average zeta potential of 0.25 ± 2.08 mV. Similarly, acetylation of 83 (65%) of the primary amine surface groups, coupling of 14 NAcGal molecules (11%), and fluorescence-labeling of G5-$(NH_2)_{128}$ dendrimers yields G5-$(Fl)_6$-$(Ac)_{83}$-$(NAcGal)_{14}$ conjugates with an average size of 6.02 ± 0.83 nm and an average zeta potential of 0.62 ± 1.32 mV. Increasing the number of NAcGal molecules conjugated to G5-$(NH_2)_{128}$ dendrimers to 41 (32%) along with acetylation of 60 (47%) primary amine surface groups yields G5-$(Fl)_6$-$(Ac)_{60}$-$(NAcGal)_{41}$ conjugates with an average size of 6.74 ± 2.05 nm and an average zeta potential of 0.66 ± 0.33 mV.

4.3.3   Uptake of Cationic G5-(Fl)-(NH$_2$) Dendrimers into HepG2 and MCF-7 Cells

Results show that uptake of cationic G5-(Fl)-$(NH_2)_{122}$ dendrimers by HepG2 and MCF-7 cells increases with the increase in carrier concentration and incubation time (**Figure 4.3**). Specifically, the fraction of HepG2 and MCF-7 cells that internalized G5-(Fl)-$(NH_2)_{122}$ particles after 2 h of incubation increased linearly with the increase in

Figure 4.3: Uptake of cationic G5-(Fl)-$(NH_2)_{122}$ conjugates into HepG2 and MCF-7 upon incubation for 2 (**A**) and 24 h (**B**). Results are the average of four samples + standard error of the mean. Statistical difference between groups is denoted by **, which indicates that $p \leq 0.01$.
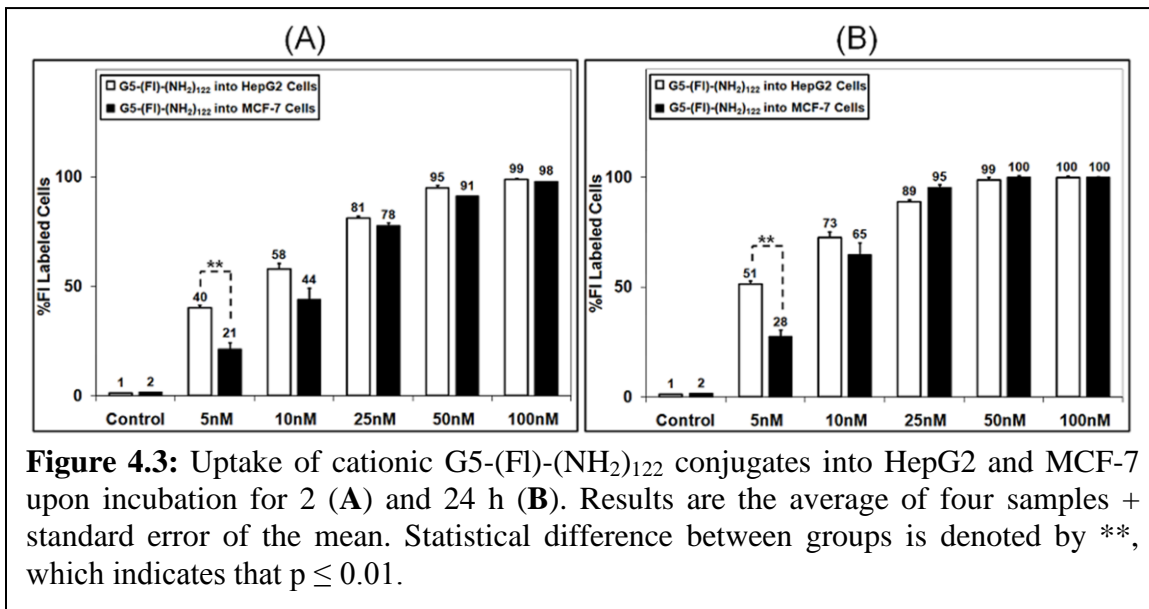
carrier concentration reaching 90-100% of the cell population at 50 nM particle concentration (**Figure 4.3**; Panel **A**). Incubation with a higher concentration (100 nM) of G5-(Fl)-$(NH_2)_{122}$ particles produced a statistically insignificant increase in the fraction of HepG2 and MCF-7 cells internalizing these particles. Increasing the incubation time to 24 h produced a corresponding increase in the fraction of HepG2 and MCF-7 cells taking up G5-(Fl)-$(NH_2)_{122}$ particles at 5, 10, and 25 nM concentrations compared to shorter incubation time (**Figure 4.3**; Panel **B**). Incubation of HepG2 and MCF-7 cells with 50 and 100 nM solutions of G5-(Fl)-$(NH_2)_{122}$ particles for 24 h led to their uptake by almost 100% of the cell population.

4.3.4 Uptake of G5-NAcGal Conjugates into HepG2 Cells

We compared the uptake of acetylated, non-targeted, G5-(Fl)-$(Ac)_{110}$ to NAcGal-targeted G5-(Fl)-$(Ac)_{70}$-$(NAcGal)_{12}$ conjugates prepared through peptide coupling, and G5-(Fl)-$(Ac)_{83}$-$(NAcGal)_{14}$ and G5-(Fl)-$(Ac)_{60}$-$(NAcGal)_{41}$ conjugates incorporating a thiourea linkage (**Figure 4.4**). Results show that acetylated, non-targeted, G5-(Fl)-$(Ac)_{110}$ conjugates were internalized by only 10% of HepG2 cells after incubation with a 100 nM solution of the particles for 2 hours (**Figure 4.4**; Panel **A**). Incubation of HepG2 cells with 100 nM solution of neutral G5-(Fl)-$(Ac)_{110}$ dendrimers for 24 h led to internalization of these particles by 86% of HepG2 cells. Despite the similarity in size and surface charge, all G5-NAcGal conjugates exhibited higher uptake into HepG2 cells compared to non-targeted G5-(Fl)-$(Ac)_{110}$ dendrimers at all concentrations and incubation times (**Figure 4.4**). For example, the fraction of HepG2 taking up G5-(Fl) $(Ac)_{70}$-$(NAcGal)_{12}$ conjugates increased from 15% to 95% with the increase in conjugate concentration from

185

Figure 4.4: Uptake of acetylated G5-(Fl)-(Ac)$_{110}$ dendrimers, G5-(Fl)-(Ac)$_{70}$-(NAcGal)$_{12}$ conjugates incorporating peptide linkages, and G5-(Fl)-(Ac)$_{83}$-(NAcGal)$_{14}$ and G5-(Fl)-(Ac)$_{83}$-(NAcGal)$_{41}$ conjugates incorporating thiourea linkages into HepG2 cancer cells upon incubation for 2 (**A**) and 24 hours (**B**). Results are the average of four samples þ standard error of the mean. Statistical difference between groups is denoted by **, which indicates that p $\leq$ 0.01.

5 nM to 100 nM compared to non-targeted G5-(Fl)-(Ac)$_{110}$ dendrimers, which was internalized by 10% of HepG2 cells at the highest tested concentration, 100 nM (**Figure 4.4**; Panel **A**). After incubation for 24 h, G5-(Fl)-(Ac)$_{70}$-(NAcGal)$_{12}$ conjugates showed a much higher uptake into HepG2 cells reaching 78% of the cell population at a 5 nM concentration (**Figure 4.4**; Panel **B**). Increasing the concentration of G5-(Fl)-(Ac)$_{70}$-(NAcGal)$_{12}$ conjugates to 10 nM saturates the internalization process with more than 92% of HepG2 cells taking up this NAcGal-targeted conjugate compared to only 14% of the non-targeted G5-(Fl)-(Ac)$_{110}$ dendrimers.

We compared the uptake of G5-(Fl)-(Ac)$_{70}$-(NAcGal)$_{12}$ conjugates synthesized via peptide coupling to that of G5-(Fl)-(Ac)$_{83}$-(NAcGal)$_{14}$ and G5-(Fl)-(Ac)$_{60}$-(NAcGal)$_{41}$ conjugates incorporating a thiourea linkage as a function of conjugate's concentration and incubation time to evaluate the effect of linkage chemistry on the internalization of NAcGal-targeted conjugates into HepG2 cells. After 2 h of incubation with HepG2 cells, uptake of peptide-linked G5-(Fl)-(Ac)$_{70}$-(NAcGal)$_{12}$ conjugates was similar to conjugates

incorporating a thiourea linkage at 5 nM, 50 nM and 100 nM concentrations, but was lower by 40% at 10 nM and 25 nM concentrations (**Figure 4.4**; Panel **A**). After 24 hours of incubation with HepG2 cells, uptake of peptide-linked $G5-(Fl)-(Ac)_{70}-(NAcGal)_{12}$ conjugates was equivalent to the G5-NAcGal conjugates incorporating a thiourea linkage at almost all the tested concentrations.

NAcGal-targeted conjugates containing a thiourea linkage showed much higher internalization into HepG2 cells compared to non-targeted $G5-(Fl)-(Ac)_{110}$ conjugates at 10-100 nM and 5-100 nM concentration for $G5-(Fl)-(Ac)_{83}-(NAcGal)_{14}$ and $G5-(Fl)-$ $(Ac)_{60}-(NAcGal)_{41}$ conjugates, respectively (**Figure 4.4**). $G5-(Fl)-(Ac)_{83}-(NAcGal)_{14}$ and $G5-(Fl)-(Ac)_{60}-(NAcGal)_{41}$ conjugates showed similar uptake into HepG2 cells at all concentrations and incubation times.

We visualized the uptake and intracellular distribution of cationic $G5-(Fl)-$ $(NH_2)_{122}$, acetylated $G5-(Fl)-(Ac)_{110}$, and NAcGal targeted $G5-(Fl)-(Ac)_{83}-(NAcGal)_{14}$ conjugates into HepG2 cells using fluorescence microscopy (**Figure 4.5**). After a 4 hour incubation of HepG2 cells with a 200 nM solution of each conjugate, fluorescence images show that cationic $G5-(Fl)-(NH_2)_{122}$ conjugates are readily internalized by HepG2 cells while neutral $G5-(Fl)-(Ac)_{110}$ conjugates are poorly taken up into the cells. HepG2 cells incubated with $G5-(Fl)-(Ac)_{83}-(NAcGal)_{14}$ conjugates showed high fluorescence intensity in membrane-bound vesicles such as the endosomes and lysosomes, along with diffuse distribution throughout the cytoplasm (**Figure 4.5**).

Figure 4.5: Phase contrast and fluorescence images showing the internalization and intracellular distribution of cationic G5-(Fl)-$(NH_2)_{122}$, acetylated G5-(Fl)-$(Ac)_{110}$, and G5-(Fl)-$(Ac)_{83}$-$(NAcGal)_{14}$ conjugates into HepG2 cells visualized at a 20x magnification (scale bar = 100 μm) using a Nikon Eclipse TE2000-U inverted microscope with a Photometrics EMCCD camera and EXFO fluorescent lamp (λ_{ex} = 488 nm, λ_{em} = 512 nm).
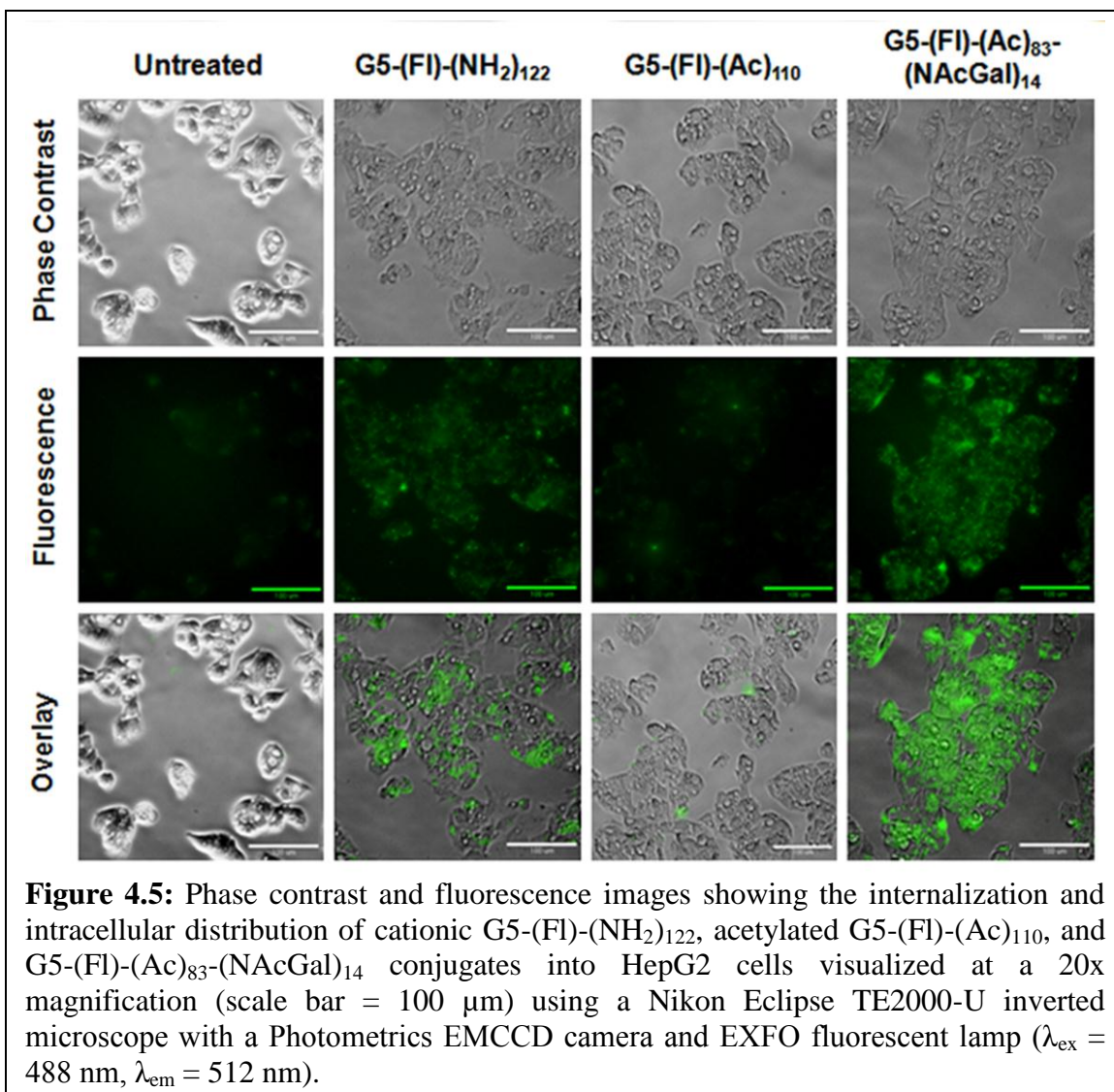
4.3.5   Role of ASGPR in HepG2 Uptake of G5-NAcGal Conjugates

We carried out a competitive uptake study to confirm the contribution and specificity of the ASGPR to the internalization of G5-NAcGal conjugates into HepG2 cells. In this study, we compared the uptake of G5-(Fl)-$(Ac)_{83}$-$(NAcGal)_{14}$ conjugates into HepG2 cells in the presence of excess (100 mM) free NAcGal molecules in the culture medium to the conjugates uptake in the absence of free sugar molecules as a function of G5-NAcGal conjugate concentration and incubation time (**Figure 4.6**). In the

188

absence of free NAcGal molecules uptake of G5-(Fl)-(Ac)$_{83}$-(NAcGal)$_{14}$ conjugates into

HepG2 cells increase with the increase in conjugate concentration, reaching maximum

uptake upon incubation with 100 nM and 10 nM conjugate solutions for 2 and 24 hours,

respectively (**Figure 4.6**). However, co-incubation of free NAcGal with G5-(Fl)-(Ac)$_{83}$-

(NAcGal)$_{14}$ conjugates led to a statistically significant (p $\leq$ 0.01) reduction in conjugate's

uptake in HepG2 cells with only 14% of the HepG2 cells taking up the conjugates after

24 hours of incubation (**Figure 4.6**; Panel **B**).
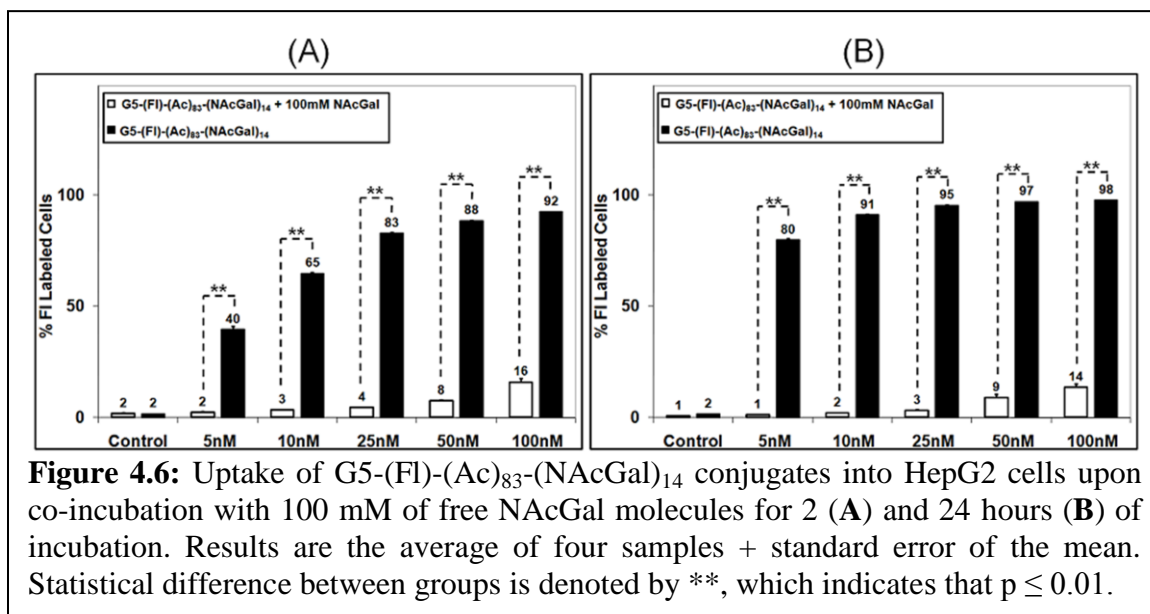
Figure 4.6: Uptake of G5-(Fl)-(Ac)$_{83}$-(NAcGal)$_{14}$ conjugates into HepG2 cells upon co-incubation with 100 mM of free NAcGal molecules for 2 (**A**) and 24 hours (**B**) of incubation. Results are the average of four samples + standard error of the mean. Statistical difference between groups is denoted by **, which indicates that p $\leq$ 0.01.

Selectivity of G5-NAcGal for hepatic cancer cells was investigated by incubating

non-targeted G5-(Fl)-(Ac)$_{110}$, G5-(Fl)-(Ac)$_{83}$-(NAcGal)$_{14}$ and G5-(Fl)-(Ac)$_{60}$-(NAcGal)$_{41}$

conjugates with MCF-7 breast cancer cells, which do not express the ASGPR essential

for internalization of NAcGal-targeted conjugates. Results show that MCF-7 cells exhibit

negligible uptake ($\leq$ 3%) of both the NAcGal-targeted and non-targeted G5 conjugates

for all the evaluated concentrations upon incubation for 2 hours at all the tested

concentrations (**Figure 4.7**; Panel **A**). Incubation of MCF-7 cells with NAcGal-targeted

and non-targeted G5 conjugates for 24 h also showed limited conjugate uptake with only 19% of the MCF-7 cells internalizing G5-(Fl)-(Ac)$_{83}$-(NAcGal)$_{14}$ conjugates, which can be attributed to non-specific fluid-phase endocytosis (**Figure 4.7**; Panel **B**).

Figure 4.7: Uptake of acetylated G5-(Fl)-(Ac)$_{110}$, G5-(Fl)-(Ac)$_{83}$-(NAcGal)$_{14}$, and G5-(Fl)-(Ac)$_{83}$-(NAcGal)$_{41}$ conjugates into MCF-7 breast cancer cells upon incubation for 2 (**A**) and 24 hours (**B**). Results are the average of four samples + standard error of the mean.
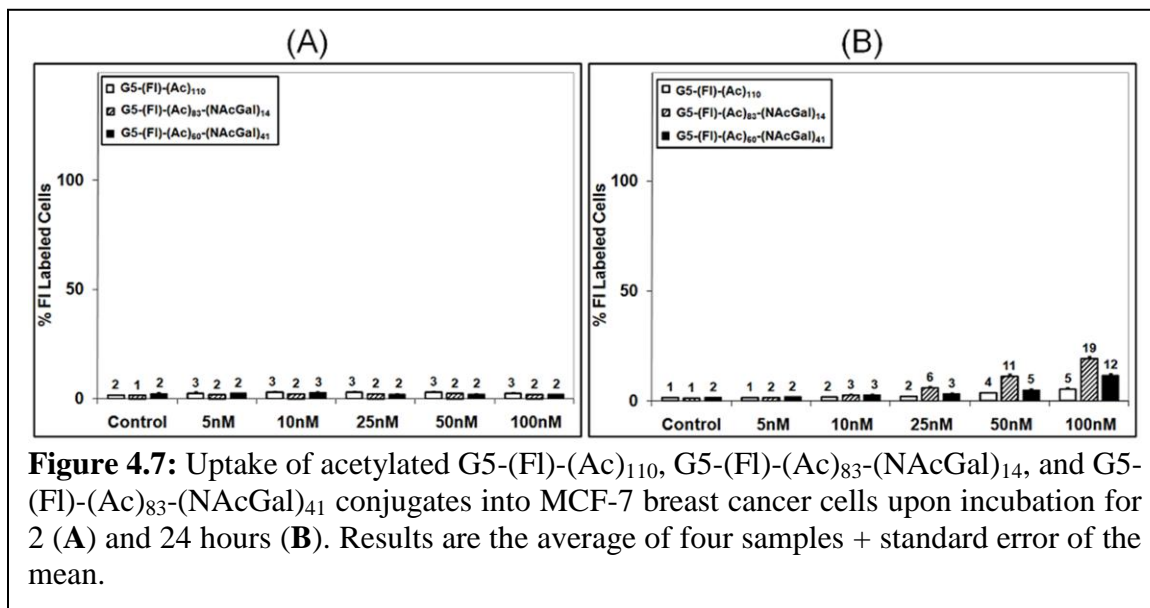
4.3.6   Cytotoxicity of Fluorescently-labeled G5-NAcGal Conjugates

Biocompatibility and lack of cellular toxicity are essential requirements for successful use of G5-NAcGal conjugates as carriers for targeted drug delivery into hepatic cancer cells. Consequently, we examined the toxicity of cationic G5-(Fl)-(NH$_2$)$_{122}$, acetylated G5-(Fl)-(Ac)$_{110}$, and NAcGal-targeted G5-(Fl)-(Ac)$_{70}$-(NAcGal)$_{12}$, G5-(Fl)-(Ac)$_{83}$-(NAcGal)$_{14}$, and G5-(Fl)-(Ac)$_{60}$-(NAcGal)$_{41}$ conjugates upon incubation with HepG2 cells at the highest tested concentration, 100 nM, for 2 and 24 hours using the lactate dehydrogenase (LDH) leakage assay following established protocols.[46,47] Results show that all G5-based conjugates tested in this study produced insignificant

190

LDH leakage compared to that observed upon incubation of HepG2 cells in regular culture medium for 2 and 24 hours (**Figure 4.8**).

Figure 4.8: Percentage of LDH leakage observed after incubation of 100 nM solutions of cationic G5-(Fl)-(NH$_2$)$_{122}$, acetylated G5-(Fl)-(Ac)$_{110}$, G5-(Fl)-(Ac)$_{70}$-(NAcGal)$_{12}$, G5-(Fl)-(Ac)$_{83}$-(NAcGal)$_{14}$, and G5-(Fl)-(Ac)$_{83}$-(NAcGal)$_{41}$ conjugates with HepG2 cells for 2 (**A**) and 24 hours (**B**). LDH leakage for each treatment is normalized to that observed upon incubation of HepG2 cells with 2% (v/v) Triton X-100 solution. Results are the average of four samples + standard error of the mean.
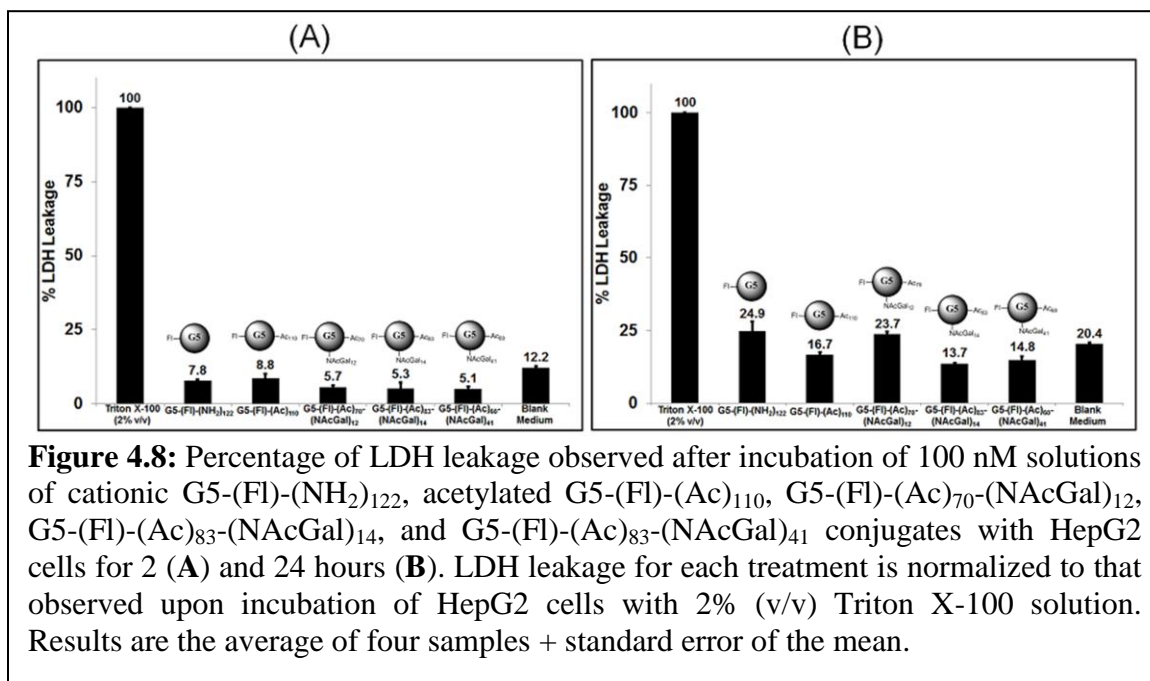
4.4 Discussion

4.4.1 Synthesis of Fluorescently-labeled G5-NAcGal Conjugates

One successful strategy to target drug carriers to hepatic cancer cells is to covalently conjugates NAcGal sugar molecules to the polymer backbone[20,21] or to the surface of the polymeric particle.[22,23] Earlier reports showed that conjugation of 10 mole% NAcGal molecules to N-(2-hydroxypropyl)methacrylamide (HPMA) polymers increased their uptake into HepG2 cells compared to non-targeted carriers.[20] Consequently, we reacted NAcGal molecules functionalized with a carboxylic acid group with G5-(NH$_2$)$_{128}$ dendrimers at a COOH-to-NH$_2$ of 13:128 following the synthesis

scheme shown in **Scheme 4.1**. To evaluate the effect of linkage chemistry on the internalization of G5-NAcGal conjugates, NAcGal molecules were functionalized with an isothiocyanate group to allow their coupling to G5-$(NH_2)_{128}$ dendrimers via a thiourea linkage following the synthesis scheme showing in **Scheme 4.2**. G5-NAcGal conjugates were reacted with acetic anhydride to neutralize a major fraction of the primary surface groups and minimize the contribution of non-specific absorptive-mediated endocytosis to the internalization of these conjugates yielding acetylated G5-NAcGal conjugates (**Scheme 4.1**; Compound **5**, **Scheme 4.2**; Compounds **14a** and **14b**). To quantify the amount of each conjugates internalized by HepG2 and MCF-7 cells and visualize their intracellular distribution, we fluorescently labeled all G5-NAcGal conjugates by reacting with fluorescein isothiocyanate (Fl) following published protocols.[24,25]

4.4.2 Size and Surface Charge of Fluorescently-labeled G5-NAcGal Conjugates

Earlier research showed that internalization of PAMAM-NH_2 dendrimers is mediated by electrostatic interaction between the cationic primary amine surface groups and the negatively charged proteoglycans displayed on the surface of mammalian cells, which triggers macropinocytosis[26] and clathrin-mediated endocytosis[26-28] of these particles into different cell lines. Internalization of PAMAM-NH_2 dendrimers into mammalian cells proved to increase with the increase in their size and positive charge density.[26-31] To achieve selective drug delivery into hepatic cancer cells using G5-NAcGal conjugates as carriers, it is critical to neutralize the free primary amine surface groups thus limiting the internalization of these conjugates to receptor-mediated endocytosis through the interaction of the NAcGal ligands and the ASGPR expressed on

the surface of hepatic cancer cells while minimizing the contribution of non-specific adsorptive-mediated endocytosis to conjugate's uptake. Further, G5-NAcGal conjugates should be 5-8 nm in size to reduce their diffusion across the endothelial lining of normal blood vessels, increase their extravasation across tumor vasculature, and diminish their recognition and entrapment by the reticular endothelial system.[32-34] Our results show that the average size of G5-$(Fl)_6$-$(NH_2)_{122}$ (4.75 nm) closely matches the reported size (5 nm) of non-labeled G5-$(NH_2)_{128}$ dendrimers.[35] Covalent coupling of NAcGal molecules to G5-$(NH_2)_{128}$ dendrimers with variable degrees of acetylation caused a gradual increase in conjugate size with the increase in the number of attached NAcGal ligands (**Figure 4.2**, Panel **A**) particularly for conjugates incorporating thiourea linkages, which have a longer spacer between the sugar molecule and the dendrimer surface compared to the spacer used in peptide coupling (**Schemes 4.1 and 4.2**). However, the average size of all the synthesized G5-NAcGal conjugates remained within the desirable size range (5-8 nm). Coupling of NAcGal and Fl molecules to G5 dendrimers along with variable degrees of acetylation resulted in capping 69%-84% of the primary amine surface groups in G5-NAcGal conjugates, which successfully reduced the cationic nature of these conjugates shown by the statistically significant drop in zeta potential of G5-$(Fl)_6$-$(Ac)_{70}$-$(NAcGal)_{12}$, G5-$(Fl)_6$-$(Ac)_{83}$-$(NAcGal)_{14}$, and G5-$(Fl)_6$-$(Ac)_{60}$-$(NAcGal)_{41}$ conjugates compared to G5-$(Fl)_6$-$(NH_2)_{122}$ dendrimers (**Figure 4.2**; Panel **B**). Reduction in positive surface charge of G5-NAcGal conjugates will minimize their in vivo opsonization and nonspecific uptake into non-targeted cells. It is important to note that fluorescence labeling, acetylation, and coupling of NAcGal molecules to G5-$(NH_2)_{128}$ dendrimers did not affect its intrinsic aqueous solubility. All the fluorescently-labeled G5-NAcGal

conjugates were freely soluble in water, buffers, and cell culture medium at all the concentrations used in the reported uptake studies.

4.4.3 Uptake of Cationic G5-(Fl)-(NH$_2$) Dendrimers into HepG2 and MCF-7 Cells

Results show that uptake of cationic G5-(Fl)-(NH$_2$)$_{122}$ dendrimers by HepG2 and MCF-7 cells increases with the increase in carrier concentration and incubation time (**Figure 4.3**). HepG2 and MCF-7 cells exhibited similar uptake of G5-(Fl)-(NH$_2$)$_{122}$ dendrimers at both incubation time points except at the lowest concentration (5 nM) where the fraction of HepG2 cells that internalized these cationic particles was twice as much as the fraction of MCF-7 cells that internalized the same particle under similar conditions, which can be attributed to the higher endocytic capacity of hepatic cells toward synthetic particles.[39] This difference in uptake between HepG2 and MCF-7 cells was not observed at higher concentrations of G5-(Fl)-(NH$_2$)$_{122}$ dendrimers because the number of particles present in solution is no longer a limiting factor. The inability of G5-(Fl)-(NH$_2$)$_{122}$ dendrimers to discriminate between HepG2 and MCF-7 cells is a result of the protonation of 99% of the NH$_2$ surface groups (pKa of 10.8) at physiologic pH, which confers a high positive charge density on the particle surface leading to electrostatic interaction with the negatively charged proteoglycans displayed on the surface of HepG2 and MCF-7 cells that triggers adsorptive-mediated endocytosis of these particles. These results are in agreement with earlier reports showing non-selective internalization of cationic dendrimers by Caco-2,[27,30] A592 lung epithelium,[40] and B16f10 melanoma[41] cells via adsorptive-mediated endocytosis. We conjugated NAcGal molecules and acetylated the free NH$_2$ surface groups to switch the internalization mechanism of these

carriers from non-specific adsorptive-mediated endocytosis to selective uptake by receptor-mediated endocytosis into hepatic cells.

4.4.4 Uptake of G5-NAcGal Conjugates into HepG2 Cells

We compared the uptake of acetylated, non-targeted, G5-(Fl)-(Ac)$_{110}$ to NAcGal-targeted G5-(Fl)-(Ac)$_{70}$-(NAcGal)$_{12}$ conjugates prepared through peptide coupling, and G5-(Fl)-(Ac)$_{83}$-(NAcGal)$_{14}$ and G5-(Fl)-(Ac)$_{60}$-(NAcGal)$_{41}$ conjugates incorporating a thiourea linkage (**Figure 4.4**). Uptake of the neutral G5-(Fl)-(Ac)$_{110}$ dendrimers into HepG2 cells was reduced by 50-fold compared to cationic G5-(Fl)-(NH$_2$)$_{122}$ particles as a result of 7.5-fold reduction in the number of free NH$_2$ surface groups, which clearly confirms the role of positive surface charge in the internalization of G5-(Fl)-(NH$_2$)$_{122}$ conjugates into hepatic cancer cells. Incubation of HepG2 cells with 100 nM solution of neutral G5-(Fl)-(Ac)$_{110}$ dendrimers for 24 hours led to internalization of these particles by 86% of HepG2 cells, which is a result of the higher particle concentration and longer incubation time leading to fluid-phase endocytosis of these particles as shown in earlier reports.[42]

Despite the similarity in size and surface charge (**Figure 4.2**), all G5-NAcGal conjugates exhibited higher uptake into HepG2 cells compared to non-targeted G5-(Fl)-(Ac)$_{110}$ dendrimers at all concentrations and incubation times (**Figure 4.4**). These results clearly show the significantly enhanced uptake of NAcGal-functionalized G5 dendrimers into hepatic cancer cells over non-targeted G5 dendrimers. Furthermore, we compared the uptake of G5-(Fl)-(Ac)$_{70}$-(NAcGal)$_{12}$ conjugates synthesized via peptide coupling to that of G5-(Fl)-(Ac)$_{83}$-(NAcGal)$_{14}$ and G5-(Fl)-(Ac)$_{60}$-(NAcGal)$_{41}$ conjugates

incorporating a thiourea linkage as a function of conjugate's concentration and incubation time to evaluate the effect of linkage chemistry on the internalization of NAcGal-targeted conjugates into HepG2 cells. The results clearly show a difference in uptake between peptide- and thiourea-linked G5-NAcGal conjugates at short incubation times likely due to the longer spacer arms (5 atoms) connecting the NAcGal ligands to the G5 carrier in the thiourea linkage compared to the peptide linkage (3 atoms), which will results in a better display and recognition of the anchored NAcGal ligands. Finally, G5-(Fl)-(Ac)$_{83}$-(NAcGal)$_{14}$ and G5-(Fl)-(Ac)$_{60}$-(NAcGal)$_{41}$ conjugates showed similar uptake into HepG2 cells at all concentrations and incubation times despite the difference in their NAcGal content, which suggests that conjugation of 10 mole% of NAcGal molecules per G5 dendrimer is sufficient to achieve maximal internalization into hepatic cancer cells. In addition, results show that G5-NAcGal conjugates are efficiently internalized into HepG2 cells compared to linear polymers like HPMA-NAcGal conjugates incorporating 14.8 mole%, which are internalized by only 25% of HepG2 cells after 2 hours of incubation at a much higher concentration of 667 nM.[20] For example, incubation of a 50 nM solution of G5-NAcGal conjugates with HepG2 cells for 2 hours results in conjugate internalization by 95% of HepG2 cells, which is 4-fold higher than the reported uptake of linear HPMA-NAcGal conjugates incubated at a 13-fold higher concentration indicating the higher affinity and selectivity of G5-NAcGal conjugates toward hepatic cancer cells compared to linear carriers.

Further, we visualized the uptake and intracellular distribution of cationic G5-(Fl)-(NH$_2$)$_{122}$, acetylated G5-(Fl)-(Ac)$_{110}$, and NAcGal targeted G5-(Fl)-(Ac)$_{83}$-(NAcGal)$_{14}$ conjugates into HepG2 cells using fluorescence microscopy (**Figure 4.5**).

196

Fluorescence images show that cationic G5-(Fl)-(NH$_2$)$_{122}$ conjugates are readily internalized by HepG2 cells while neutral G5-(Fl)-(Ac)$_{110}$ conjugates are poorly taken up into the cells, which provides a clear visual evidence on the effect of positive charge on triggering nonspecific adsorptive-mediated endocytosis of cationic dendrimers into hepatic cancer cells. HepG2 cells incubated with G5-(Fl)-(Ac)$_{83}$-(NAcGal)$_{14}$ conjugates showed high fluorescence intensity in membrane-bound vesicles such as the endosomes and lysosomes, along with diffuse distribution throughout the cytoplasm (**Figure 4.5**). These images provide additional evidence that NAcGal ligands enhance the cellular uptake of G5-NAcGal conjugates through receptor-mediated endocytosis. The combination of punctuate and diffuse fluorescence in HepG2 cells incubated with G5-(Fl)-(Ac)$_{83}$-(NAcGal)$_{14}$ conjugates show the ability of the G5 carrier to escape the endosomal membrane and enter the cytoplasm through the proton sponge mechanism.[8,43,44] The ability of G5-NAcGal conjugates to escape the endosomal/lysosomal trafficking pathway and enter the cytoplasm indicates their ability to function as vehicles for efficient delivery of anticancer drugs into the cytoplasm of hepatic cancer cells.

4.4.5 Role of ASGPR in HepG2 Uptake of G5-NAcGal Conjugates

We carried out a competitive uptake study to confirm the contribution and specificity of the ASGPR to the internalization of G5-NAcGal conjugates into HepG2 cells. In this study, we compared the uptake of G5-(Fl)-(Ac)$_{83}$-(NAcGal)$_{14}$ conjugates into HepG2 cells in the presence of excess (100 mM) free NAcGal molecules in the culture medium to the conjugates uptake in the absence of free sugar molecules as a

function of G5-NAcGal conjugate concentration and incubation time (**Figure 4.6**). The observed reduction in the uptake of G5-(Fl)-(Ac)$_{83}$-(NAcGal)$_{14}$ conjugates into HepG2 upon co-incubation with free NAcGal molecules is explained by previous studies showing that the binding and internalization of the ASGPR follow Michaelis-Menten kinetics.[45] Presence of excess free NAcGal that can effectively compete for and bind to the ASGPR will saturate the receptors and reduce their availability to bind and internalize the G5-(Fl)-(Ac)$_{83}$-(NAcGal)$_{14}$ conjugates present in solution, which will reduce their net uptake into HepG2 cells. This clearly demonstrates that uptake of G5-NAcGal conjugates into hepatic cancer cells occurs through the ASGPR via receptor-mediated endocytosis. Our results are supported by a previous study where uptake of NAcGal-targeted HPMA conjugates into HepG2 cells was inhibited by co-incubation with excess lactose molecules.[20]

Selectivity of G5-NAcGal for hepatic cancer cells was investigated by incubating non-targeted G5-(Fl)-(Ac)$_{110}$, G5-(Fl)-(Ac)$_{83}$-(NAcGal)$_{14}$ and G5-(Fl)-(Ac)$_{60}$-(NAcGal)$_{41}$ conjugates with MCF-7 breast cancer cells (**Figure 4.7**), which do not express the ASGPR essential for internalization of NAcGal-targeted conjugates. The limited uptake of G5-NAcGal conjugates into MCF-7 cells compared to HepG2 cells confirms the selectivity of these targeted polymers towards hepatic cancer cells and suggests their potential as targeted drug carriers.

4.4.6 Cytotoxicity of Fluorescently-labeled G5-NAcGal Conjugates

Biocompatibility and lack of cellular toxicity are essential requirements for successful use of G5-NAcGal conjugates as carriers for targeted drug delivery into

hepatic cancer cells. To examine the toxicity of cationic G5-(Fl)-(NH$_2$)$_{122}$, acetylated G5-(Fl)-(Ac)$_{110}$, and NAcGal-targeted G5-(Fl)-(Ac)$_{70}$-(NAcGal)$_{12}$, G5-(Fl)-(Ac)$_{83}$-(NAcGal)$_{14}$, and G5-(Fl)-(Ac)$_{60}$-(NAcGal)$_{41}$ conjugates upon incubation with HepG2 we utilized the lactate dehydrogenase (LDH) leakage assay following established protocols.[46,47] Toxic interaction of cationic dendrimers with mammalian cells proved to destabilize the cell membrane and increase the leakage of LDH enzyme into the culture medium, which is used as a measure for particle toxicity compared to baseline LDH leakage observed under normal culture conditions.[46,47] Results show that all G5-based conjugates tested in this study produced insignificant LDH leakage compared to that observed upon incubation of HepG2 cells in regular culture medium for 2 and 24 hours (**Figure 4.8**), which indicates that these G5-NAcGal conjugates are nontoxic and can be used as drug carriers for targeted delivery into hepatic cancer cells.

4.5   Conclusion

We have successfully synthesized G5-NAcGal conjugates using two different coupling strategies, which allows for tuning of the number of NAcGal molecules attached per single G5 carrier. Cationic G5-(Fl)-(NH$_2$)$_{122}$ dendrimers showed similar internalization into both HepG2 and MCF-7 cells via adsorptive-mediated endocytosis, which is a fast and efficient internalization route but it fails to discriminate between cancer cell types and should not be exploited for cell-specific drug delivery. Conjugation of 12 NAcGal molecules to G5 dendrimers yielded G5-NAcGal conjugates that were selectively internalized by almost 100% of hepatic cancer cells within a short period of time. The low number of NAcGal molecules required to trigger receptor-mediated

endocytosis of G5-NAcGal conjugates into hepatic cancer leaves approximately 90% of the NH$_2$ surface groups available for loading of drug and imaging molecules, which expands the therapeutic utility of the proposed carrier. Results clearly show that NAcGal-targeted G5 dendrimers present a highly efficient carrier for selective delivery of therapeutic molecules into the cytoplasm of hepatic cancer cells for a wide range of therapeutic applications.

Acknowledgements

References

1   Tomalia, D. A. *et al.* A new class of polymers: starburst-dendritic macromolecules. *Polym. J.* **17**, 117 (1985).
2   Patri, A. K., Majoros, I. J. & Baker, J. R. Dendritic polymer macromolecular carriers for drug delivery. *Curr. Opin. Chem. Biol.* **6**, 466-471 (2002).
3   Tomalia, D. A., Reyna, L. A. & Svenson, S. Dendrimers as multi-purpose nanodevices for oncology drug delivery and diagnostic imaging. *Biochem. Soc. T.* **035**, 61-67 (2007).
4   Svenson, S. & Tomalia, D. A. Dendrimers in biomedical applications--reflections on the field. *Adv. Drug Deliver. Rev.* **57**, 2106-2129 (2005).
5   Kobayashi, H. & Brechbiel, M. W. Nano-sized MRI contrast agents with dendrimer cores. *Adv. Drug Deliver. Rev.* **57**, 2271 (2005).

6   Kobayashi, H. *et al.* Macromolecular MRI contrast agents with small dendrimers: pharmacokinetic differences between sizes and cores. *Bioconjugate Chem.* **14**, 388-394 (2003).

7   Medina, S. H. & El-Sayed, M. E. H. Dendrimers as carriers for delivery of chemotherapeutic agents. *Chem. Rev.* **109**, 3141-3157 (2009).

8   Zhou, J. *et al.* PAMAM dendrimers for efficient siRNA delivery and potent gene silencing. *Chem. Commun.*, 2362-2364 (2006).

9   Zhong, H. *et al.* Studies on polyamidoamine dendrimers as efficient gene delivery vector. *J. Biomater. Appl.* **22**, 527-544 (2008).

10   Navarro, G. & Tros de Ilarduya, C. Activated and non-activated PAMAM dendrimers for gene delivery *in vitro* and *in vivo*. *Nanomed.-Nanotechnol.* **5**, 287-297 (2009).

11   Patri, A. K. *et al.* Synthesis and in vitro testing of J591 antibody−dendrimer conjugates for targeted prostate cancer therapy. *Bioconjugate Chem.* **15**, 1174-1181 (2004).

12   Shukla, R. *et al.* HER2 specific tumor targeting with dendrimer conjugated anti-HER2 mAb. *Bioconjugate Chem.* **17**, 1109-1115 (2006).

13   Sato, A., Takagi, M., Shimamoto, A., Kawakami, S. & Hashida, M. Small interfering RNA delivery to the liver by intravenous administration of galactosylated cationic liposomes in mice. *Biomaterials* **28**, 1434-1442 (2007).

14   Kukowska-Latallo, J. F. *et al.* Nanoparticle targeting of anticancer drug improves therapeutic response in animal model of human epithelial cancer. *Cancer Res.* **65**, 5317-5324 (2005).

15   Shi, X. *et al.* Dendrimer-functionalized shell-crosslinked iron oxide nanoparticles for *in-vivo* magnetic resonance imaging of tumors. *Adv. Mater.* **20**, 1671-1678 (2008).

16   Swanson, S. D. *et al.* Targeted gadolinium-loaded dendrimer nanoparticles for tumor-specific magnetic resonance contrast enhancement. *Int. J. Nanomed.* **3**, 201-210 (2008).

17   Backer, M. V. *et al.* Vascular endothelial growth factor selectively targets boronated dendrimers to tumor vasculature. *Mol. Cancer Ther.* **4**, 1423-1429 (2005).

18   Schwartz, A. L., Fridovich, S. E., Knowles, B. B. & Lodish, H. F. Characterization of the asialoglycoprotein receptor in a continuous hepatoma line. *J. Biol. Chem.* **256**, 8878-8881 (1981).

19   Jain, V. *et al.* Galactose-grafted chylomicron-mimicking emulsion: evaluation of specificity against HepG-2 and MCF-7 cell lines. *J. Pharm. Pharmacol.* **61**, 303-310 (2009).

20   David, A., Kopeckova, P., Rubinstein, A. & Kopecek, J. Enhanced biorecognition and internalization of HPMA copolymers containing multiple or multivalent carbohydrate side-chains by human hepatocarcinoma cells. *Bioconjugate Chem.* **12**, 890-899 (2001).

21   Seymour, L. W. *et al.* Hepatic drug targeting: phase I evaluation of polymer-bound doxorubicin. *J. Clin. Oncol.* **20**, 1668-1676 (2002).

22　Liang, H.-F. *et al.* Paclitaxel-loaded poly(gamma-glutamic acid)-poly(lactide) nanoparticles as a targeted drug delivery system against cultured HepG2 cells. *Bioconjugate Chem.* **17**, 291-299 (2006).

23　Liang, H.-F., Yang, T.-F., Huang, C.-T., Chen, M.-C. & Sung, H.-W. Preparation of nanoparticles composed of poly(gamma-glutamic acid)-poly(lactide) block copolymers and evaluation of their uptake by HepG2 cells. *J. Control. Release* **105**, 213-225 (2005).

24　El-Sayed, M., Kiani, M. F., Naimark, M. D., Hikal, A. H. & Ghandehari, H. Extravasation of poly(amidoamine) (PAMAM) dendrimers across microvascular network endothelium. *Pharm. Res.* **18**, 23-28 (2001).

25　Quintana, A. *et al.* Design and function of a dendrimer-based therapeutic nanodevice targeted to tumor cells through the folate receptor. *Pharm. Res.* **19**, 1310-1316 (2002).

26　Albertazzi, L., Serresi, M., Albanese, A. & Beltram, F. Dendrimer internalization and intracellular trafficking in living cells. *Mol. Pharm.* **7**, 680-688 (2010).

27　Kitchens, K., Foraker, A., Kolhatkar, R., Swaan, P. & Ghandehari, H. Endocytosis and interaction of poly (amidoamine) dendrimers with Caco-2 cells. *Pharm. Res.* **24**, 2138-2145 (2007).

28　Kitchens, K. M., Kolhatkar, R. B., Swaan, P. W. & Ghandehari, H. Endocytosis inhibitors prevent poly(amidoamine) dendrimer internalization and permeability across Caco-2 cells. *Mol. Pharm.* **5**, 364-369 (2008).

29　Kitchens, K. M., El-Sayed, M. E. H. & Ghandehari, H. Transepithelial and endothelial transport of poly (amidoamine) dendrimers. *Adv. Drug Deliver. Rev.* **57**, 2163-2176 (2005).

30　Kitchens, K., Kolhatkar, R., Swaan, P., Eddington, N. & Ghandehari, H. Transport of poly(amidoamine) dendrimers across Caco-2 cell monolayers: influence of size, charge and fluorescent labeling. *Pharm. Res.* **23**, 2818-2826 (2006).

31　Kolhe, P. *et al.* Preparation, cellular transport, and activity of polyamidoamine-based dendritic nanodevices with a high drug payload. *Biomaterials* **27**, 660-669 (2006).

32　Dong, Q. *et al.* Magnetic resonance angiography with gadomer-17: an animal study. *Invest. Radiol.* **33**, 699-708 (1998).

33　Kobayashi, H. *et al.* Micro-MR angiography of normal and intratumoral vessels in mice using dedicated intravascular MR contrast agents with high generation of polyamidoamine dendrimer core: reference to pharmacokinetic properties of dendrimer-based MR contrast agents. *JMRI-J. Magn. Reson. Im.* **14**, 705-713 (2001).

34　Sato, N. *et al.* Pharmacokinetics and enhancement patterns of macromolecular MR contrast agents with various sizes of polyamidoamine dendrimer cores. *Magn. Reson. Med.* **46**, 1169-1173 (2001).

35　McKendry, R. *et al.* Creating nanoscale patterns of dendrimers on silicon surfaces with dip-pen anolithography. *Nano Lett.* **2**, 713-716 (2002).

36　Cakara, D., Kleimann, J. & Borkovec, M. Microscopic protonation equilibria of poly(amidoamine) dendrimers from macroscopic itrations. *Macromolecules* **36**, 4201-4207 (2003).

37   Gabellieri, E., Strambini, G. B., Shcharbin, D., Klajnert, B. & Bryszewska, M. Dendrimer–protein interactions studied by tryptophan room temperature phosphorescence. *Biochim. Biophys. Acta.* **1764**, 1750-1756 (2006).

38   Diallo, M., Christie, S., Swaminathan, P., Johnson, J. & Goddard, W. Dendrimer enhanced ultrafiltration. 1. Recovery of Cu(II) from aqueous solutions using PAMAM dendrimers with ethylene diamine core and terminal NH_2 groups. *Environ. Sci. Technol.* **39**, 1366-1377 (2005).

39   Lloyd, J. B., Duncan, R. & Kopecek, J. Synthetic polymers as targetable carriers for drugs. *Pure Appl. Chem.* **56**, 1301-1304 (1984).

40   Perumal, O. P., Inapagolla, R., Kannan, S. & Kannan, R. M. The effect of surface functionality on cellular trafficking of dendrimers. *Biomaterials* **29**, 3469-3476 (2008).

41   Seib, F. P., Jones, A. T. & Duncan, R. Comparison of the endocytic properties of linear and branched PEIs, and cationic PAMAM dendrimers in B16f10 melanoma cells. *J. Control. Release* **117**, 291-300 (2007).

42   Hillaireau, H. & Couvreur, P. Nanocarriers' entry into the cell: relevance to drug delivery. *Cell. Mol. Life Sci.* **66**, 2873-2896 (2009).

43   Behr, J.-P. The proton sponge: a trick to enter cells the viruses did not exploit. *Chimia* **51**, 34-36 (1997).

44   Kono, K., Akiyama, H., Takahashi, T., Takagishi, T. & Harada, A. Transfection activity of polyamidoamine dendrimers having hydrophobic amino acid residues in the periphery. *Bioconjugate Chem.* **16**, 208-214 (2004).

45   Schwartz, A. L., Fridovich, S. E. & Lodish, H. F. Kinetics of internalization and recylcing of the asialoglycoprotein receptor in a hepatoma cell line. *J. Biol. Chem.* **257**, 4230-4237 (1982).

46   El-Sayed, M., Ginski, M., Rhodes, C. & Ghandehari, H. Transepithelial transport of poly(amidoamine) dendrimers across Caco-2 cell monolayers. *J. Control. Release* **81**, 355 (2002).

47   El-Sayed, M., Ginski, M., Rhodes, C. A. & Ghandehari, H. Influence of surface chemistry of poly(amidoamine) dendrimers on Caco-2 cell monolayers. *J. Bioact. Compat. Pol.* **18**, 7-22 (2003).

Appendix

Synthesis of Fluorescently-labeled G5-NAcGal Conjugates via Peptide Linkages
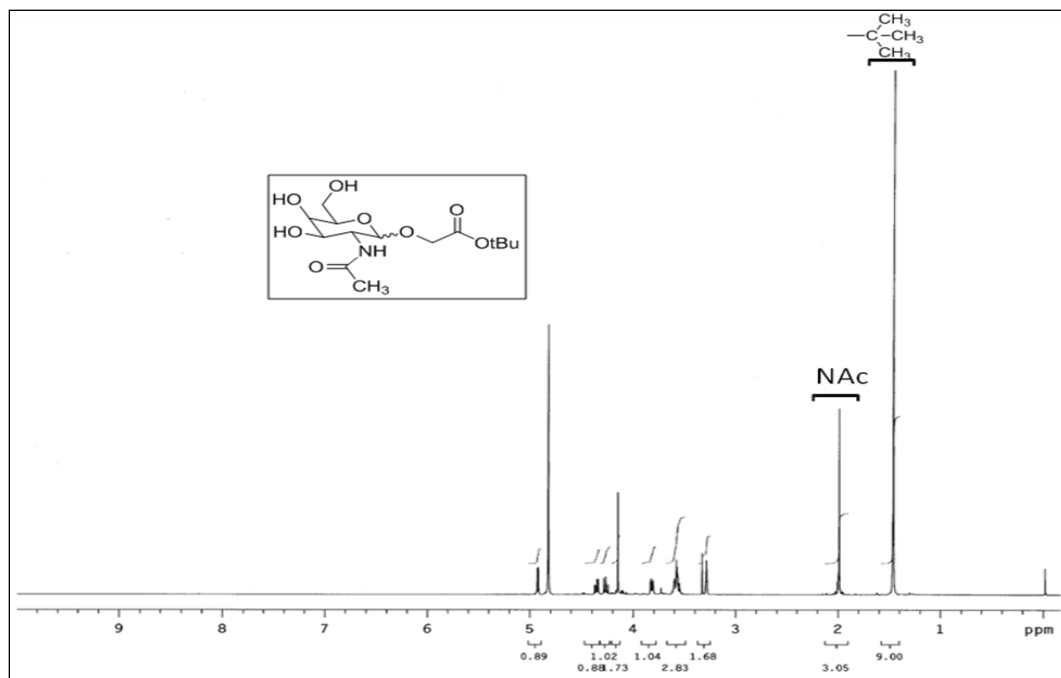
Figure S1: ^{1}H NMR of **3-(carbo-t-butoxymethyl)-2-(acetylamino)-2-deoxy-D-galactopyranoside** (**1**) dissolved in CD$_3$OD on a Varian 400 MHz system (Palo Alto, CA).
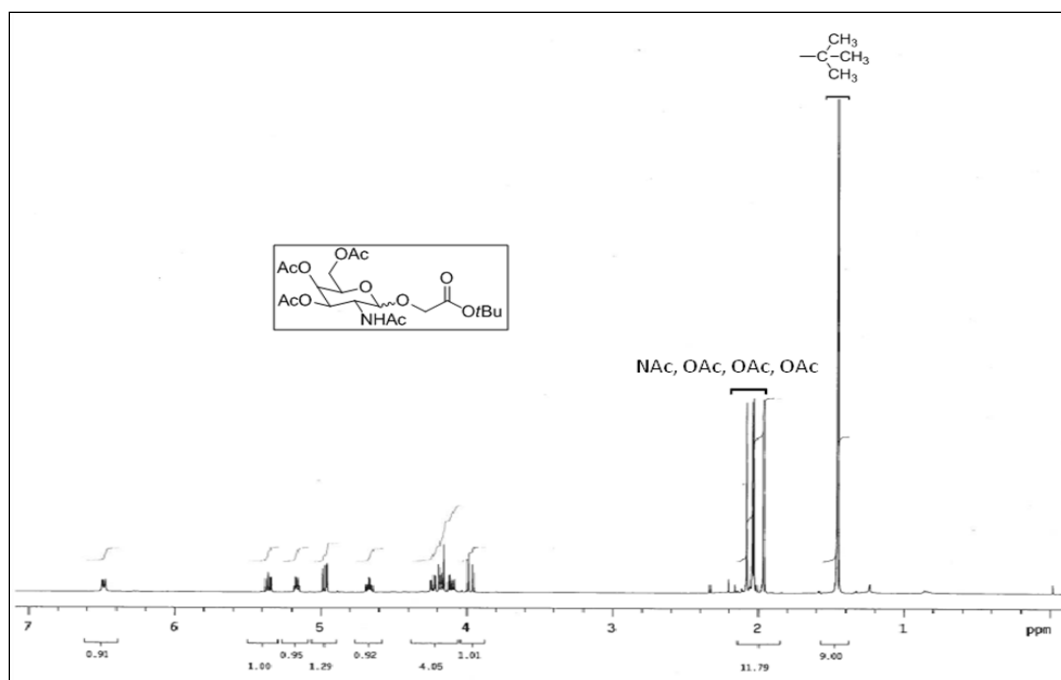
Figure S2: ^{1}H NMR of **3-(carbo-t-butoxymethyl)-2-(acetylamino)-2-deoxy-D-galactopyranoside-3,4,6-triacetate** (**2**) dissolved in CDCl$_3$ on a Varian 500 MHz system (Palo Alto, CA).
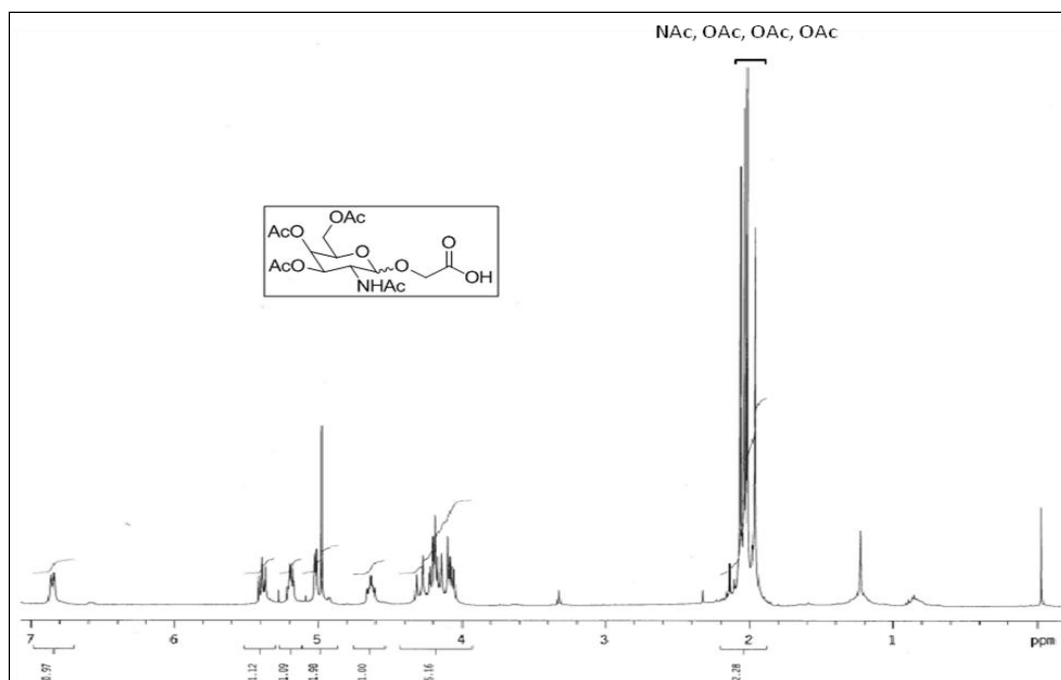
Figure S3: ^{1}H NMR of 3-(carboxymethyl)-2-(acetylamino)-2-deoxy-D-galactopyranoside-3,4,6-triacetate (**3**) dissolved in CDCl$_3$ on a Varian 400 MHz system (Palo Alto, CA).
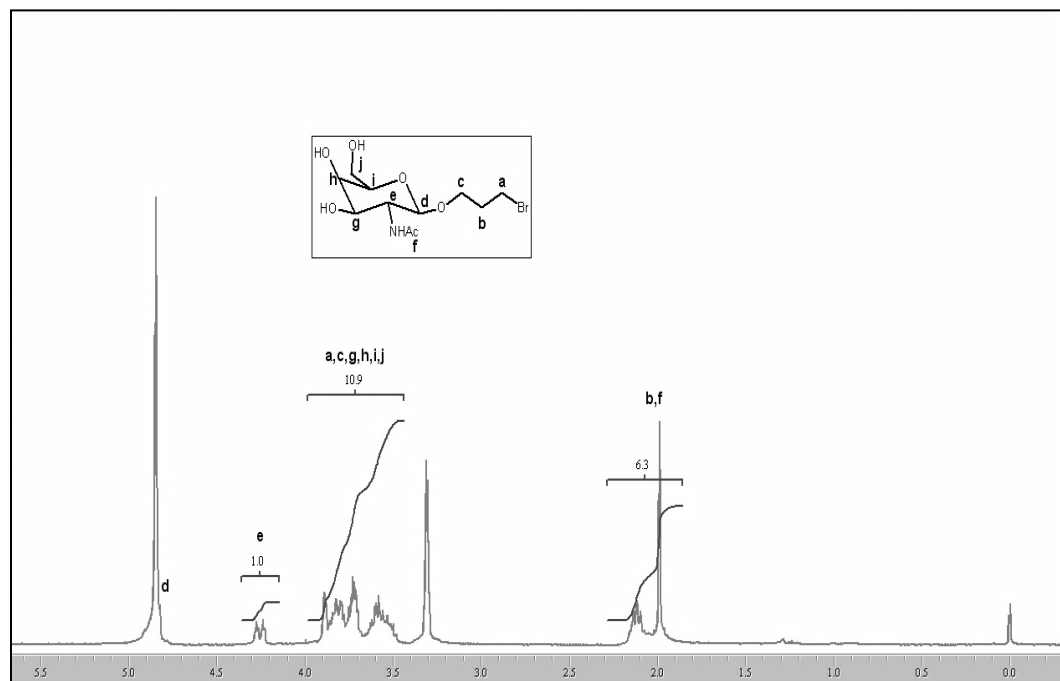
Figure S4: ^{1}H NMR of **3-bromopropyl-2-(acetylamino)-2-deoxy-D-galactopyranoside** (**8**) dissolved in CD₃OD on a Varian 300 MHz system (Palo Alto, CA).
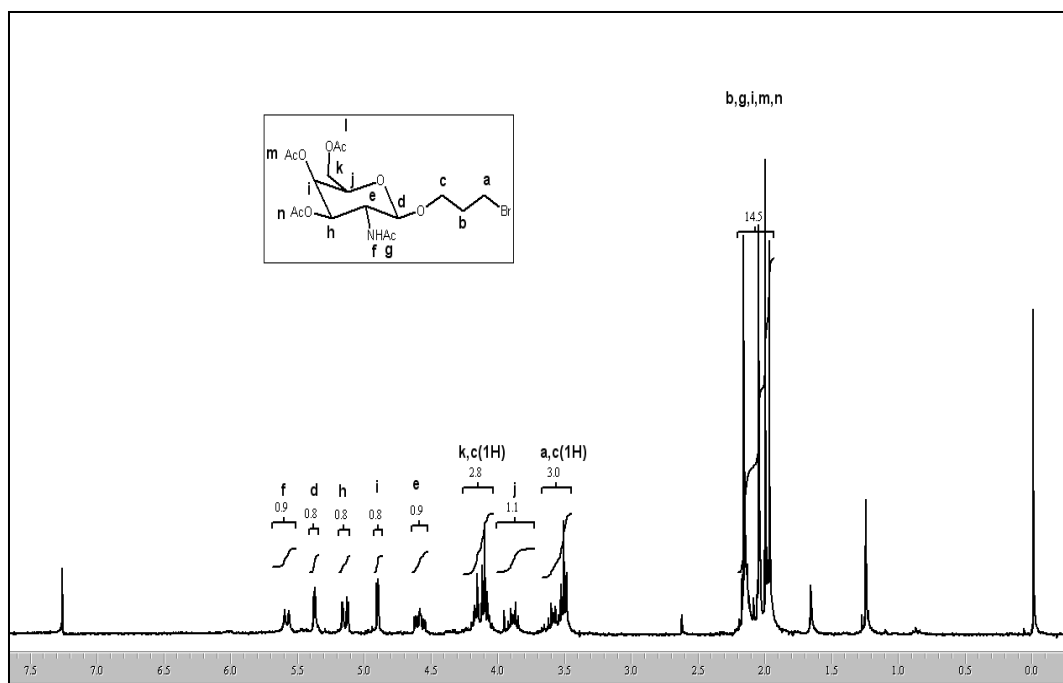
Figure S5: ^{1}H NMR of **3-bromopropyl-2-(acetylamino)-2-deoxy-D-galactopyranoside-3,4,6-triacetate** (**9**) dissolved in CDCl$_3$ on a Varian 300 MHz system (Palo Alto, CA).
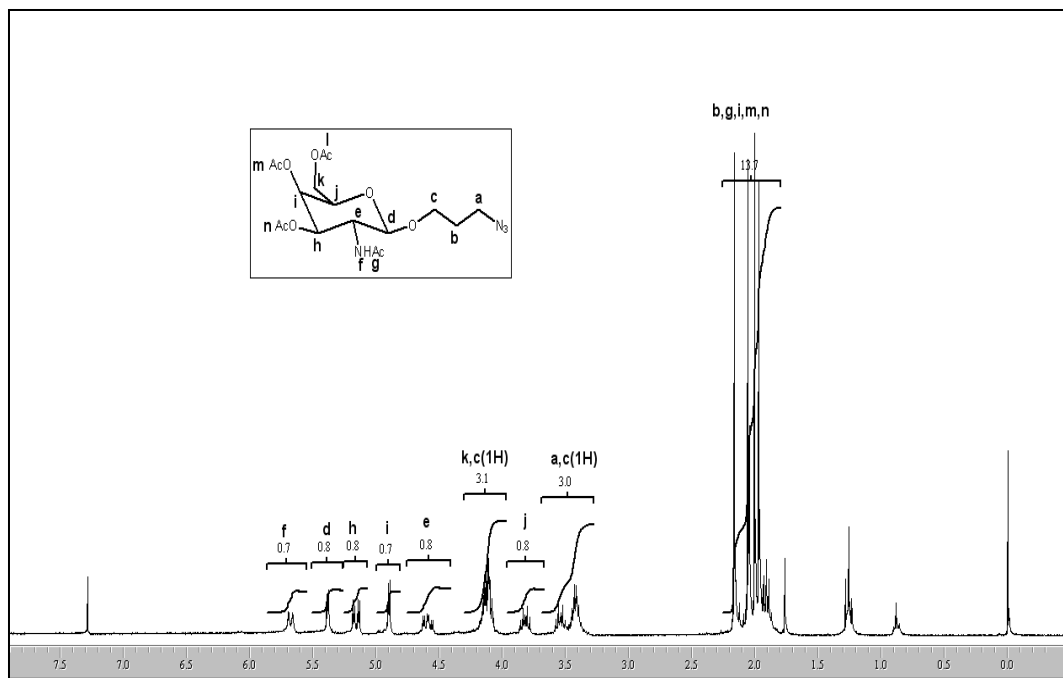
Figure S6: ^{1}H NMR of **3-azidopropyl-2-(acetylamino)-2-deoxy-D-galactopyranoside-3,4,6-triacetate** (**10**) dissolved in CDCl$_3$ on a Varian 300 MHz system (Palo Alto, CA).
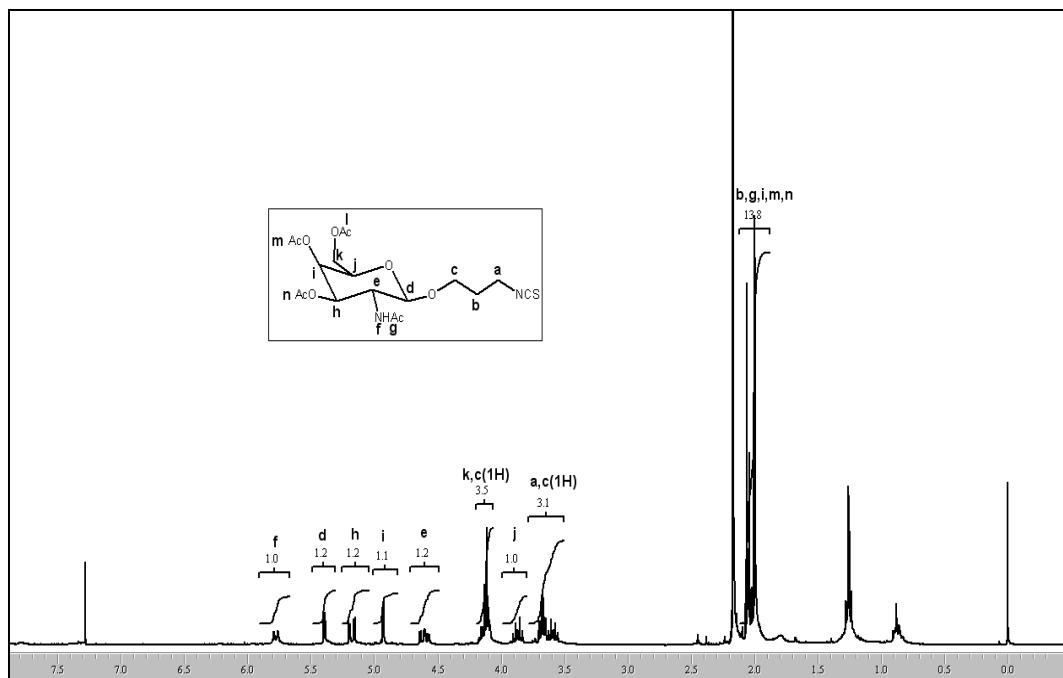
Figure S7: ^{1}H NMR of **3-isothiocyanopropyl-2-(acetylamino)-2-deoxy-D-galactopyranoside-3,4,6-triacetate** (**12**) dissolved in CDCl$_3$ on a Varian 300 MHz system (Palo Alto, CA).

Chapter 5

Development of PEGylated Dendrimers Functionalized with *N*-acetylgalactosamine

and SP94 Peptides as Carriers for Targeted Drug Delivery to Hepatic Cancer Cells

5.1   Introduction

Poly(amidoamine) (PAMAM) dendrimers are a family of water-soluble polymers characterized by a unique tree-like branching architecture, with each branching unit constituting a successive generation (G), resulting in a compact spherical geometry in solution and controlled incremental increase in size, molecular weight, and number of surface amine groups.[1,2] The potential of PAMAM dendrimers in controlled drug delivery has been extensively investigated and arises from the large number of branching arms and a high density of surface amine groups which can be utilized to immobilize therapeutic or imaging agents forming compact nano-conjugates with a high loading of bioactive molecules.[1-3] Different chemotherapeutic agents such as Doxorubicin (DOX),[4,5] Taxol,[6] and Methotrexate[7,8] have been covalently attached to PAMAM dendrimers to enhance the solubility of the loaded anticancer drugs. These conjugates employed hydrolytically cleavable bonds,[6-8] pH-sensitive linkages,[4,5] or triggerable chemical spacers[9] to achieve selective release of the chemotherapeutic agents to the cytoplasm of cancer cells, resulting in enhanced therapeutic activity while minimizing non-specific toxicity. Folic acid,[6,10,11] antibodies[12-14] and RGD peptides[15-17] have been conjugated to

the surface of dendrimer-based conjugates to function as active targeting ligands to achieve selective delivery of the loaded drug molecules to cancer cells via receptor-mediated endocytosis. However, intravenous administration of these targeted dendrimer carriers to tumor-bearing animal models resulted in rapid particle opsonization leading to recognition and clearance by the reticuloendothlial system (RES), as well as retention in the kidneys, causing non-specific toxicity. Specifically, Boswell et al. showed that i.v injection of RGD-targeted ^{111}In-labeled PAMAM-Gadolinium (Gd) complexes to a melanoma nude mouse tumor model resulted in >100% of the injected dose per gram of tissue weight cumulatively distributing to liver, spleen and kidney tissue 1 hour after administration.[15] Similarly, folic acid-targeted, boronated PAMAM dendrimers showed distribution of 25% of the injected dose/g in the liver and spleen of KB-tumor bearing mice 6 hours after i.v. administration, while the kidneys retained 104% of the injected dose/g of the conjugates under the same conditions.[18] In both of these studies <5% of the injected dose/g of the nanoparticles accumulated in tumor tissue for all time points studied due to the extensive RES clearance and kidney retention of the PAMAM dendrimer based-carriers leading to significant hepatic and renal toxicity.[19,20] This non-specific biodistribution profile is a result of rapid opsonization of cationic PAMAM dendrimers by blood proteins (e.g. albumin),[7] leading to recognition and clearance by macrophages *in vivo*.[21,22] To address these issues neutralization of the cationic dendrimer surface amine groups by acetylation (Ac) and attachment of hydrophilic poly(ethylene glycol) (PEG) chains has resulted in enhanced dendrimer biocompatibility.[23] Furthermore, PEGylation of nanoparticles has been shown to inhibit opsonization via

steric repulsion of plasma proteins from the carrier surface by the hydrophilic PEG corona, reducing the recognition and clearance of these carriers by RES organs.[22]

We sought to develop targeted G5 dendrimer carriers that can selectively deliver a large dose of chemotherapeutic agents to hepatic cancer cells while avoiding non-specific distribution to neighboring healthy liver parenchymal cells. We previously reported the covalent coupling of N-acetylgalactosamine (NAcGal) sugar ligands to G5 PAMAM dendrimers via peptide and thiourea linkages forming G5-NAcGal conjugates, which were selectively internalized by HepG2 human hepatic cancer cells.[24] Specifically, binding of NAcGal molecules displayed on the G5 dendrimer surface to the asialoglycoprotein receptor (ASGPR), a hepatocyte-specific lectin highly expressed on the surface of hepatic cancer cells,[25] triggered the internalization of the G5-NAcGal conjugates into HepG2 cells via receptor-mediated endocytosis.

In this article we determine the biodistribution of ^{14}C-labeled G5-(Ac)$_{108}$-(NAcGal)$_{14}$ conjugates as compared to the G5-(NH$_2$)$_{127}$ polymer control and PEGylated G5-(Ac)$_{73}$-(PEG)$_{10}$ conjugates in a liver-tumor animal model established via orthotopic implantation of hepatic cancer cells into the left hepatic lobe of nude mice. These studies evaluated the effect of NAcGal targeting and surface PEGylation on the accumulation of dendrimer carriers in tumor tissue and healthy liver as a function of time. Biodistribution results prompted us to combine the stealth ability of dendrimer PEGylation with the targeting of NAcGal sugar molecules to the ASGPR expressed on the surface of hepatic cancer cells in a single particle to achieve hepatic cancer cell-specific internalization. Specifically, we conjugated PEG (2kDa) chains to the primary amine groups of G5 dendrimers carriers through acid-sensitive *cis*-aconityl linkages (*c*), while functionalizing

the terminal end of the PEG with NAcGal sugar molecules, or the recently reported SP94 hepatic cancer cell-specific peptide,[26] as a targeting ligand. NAcGal ligands were coupled to PEG chains in an α- or β-conformation to confirm that G5-(*c*PEG[NAcGal]) conjugates maintain receptor-mediated endocytosis into hepatic cancer cells specifically by the ASGPR, which shows selective affinity towards β-sugars.[27] After intravenous administration these targeted G5-(*c*PEG) conjugates will escape opsonization in the blood circulation, and preferentially accumulate in tumor tissue due to the Enhanced Permeability and Retention (EPR) effect.[28] The conjugates will then be internalized into hepatic cancer cells via binding of the displayed targeting ligand to the cancer cell surface receptor resulting in receptor-mediated endocytosis. Once located within the acidic endosome the *cis*-aconityl linkages will be reduced allowing for "shedding" of the PEG corona necessary for drug release and facile excretion of the dendrimer into urine after delivery[29-32] (**Figure 5.1**).

To test this hypothesis we synthesized G5-(cPEG) conjugates with and without NAcGal or SP94 targeting ligands in equivalent loading ratios, and measured their size, molecular weight, and surface charge using dynamic light scattering, MALDI-TOF analysis and zeta potential measurements, respectively. Rate of *cis*-aconityl linker reduction and PEG release from the G5 carrier surface in acidic conditions was studied and compared to neutral physiologic buffers using gel permeation chromatography (GPC). We investigated the internalization of NAcGal-targeted G5-(*c*PEG[NAcGal]) carriers into HepG2 hepatic cancer cells as a function of sugar conformation, incubation time and ligand concentration. These results were compared to the uptake of SP94-targeted G5-(*c*PEG[SP94]) conjugates in HepG2 cells under similar conditions to identify
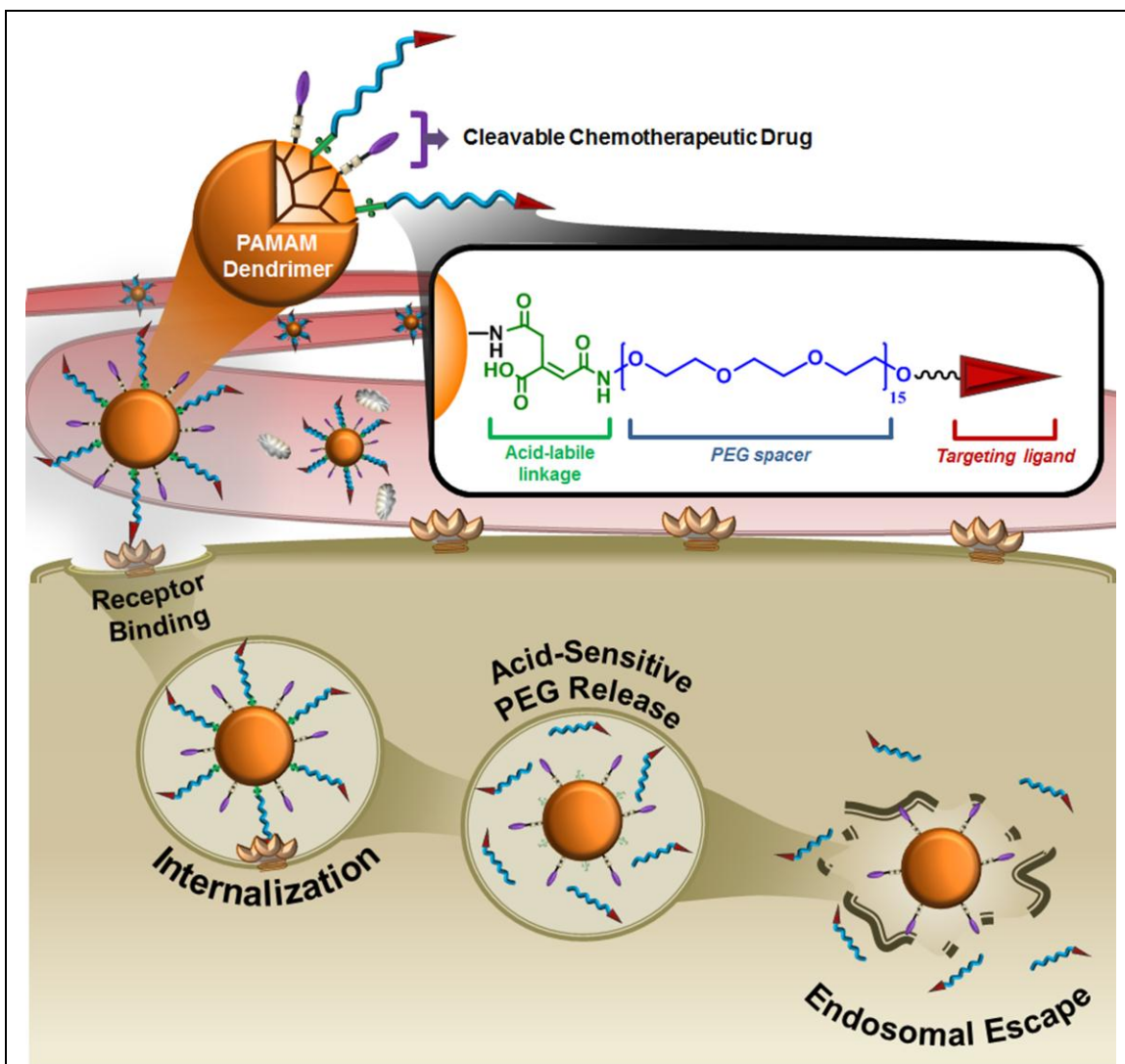
Figure 5.1: A schematic drawing showing the composition of a drug-loaded targeted G5-(*c*PEG) conjugates which will preferentially distribute to liver tumor tissue via the EPR effect while avoiding opsonization in the systemic circulation due to the PEG corona. The displayed targeting ligand is recognized by the hepatic-cell surface receptor expressed on hepatic cancer cells (e.g. HepG2) triggering receptor-mediated endocytosis of these conjugates into the cancer cells, followed by reduction of the *cis*-aconityl linker by the acidic endosome and endosomal escape of the dendrimer carrier.

the targeting strategy which results in efficient internalization of targeted G5-(*c*PEG) carriers into hepatic cancer cells. Opsonization of carriers with and without PEGylation was studied using a bovine serum albumin binding assay, and the phagocytosis of these opsonized particles into liver macrophage Kupffer cells determined as a function of G5 carrier surface properties using flow cytometry. We evaluated the selective

internalization of targeted G5-(cPEG) conjugates into hepatic cancer cells by incubating conjugates with plated rat hepatocytes as a function of incubation time and ligand concentration.

5.2   Materials and Methods

5.2.1   Materials

G5-$(NH_2)_{128}$ PAMAM dendrimers with a dimethylaminobutane core were purchased from Dendritic Nanotechnologies Inc. (Midland, MI) and purified by dialysis against deionized water using Slide-A-Lyzer dialysis cassettes (MWCO 10kDa, Thermo Fisher Scientific, Rockford, IL) to remove imperfect dendrimers and polymer debris. *N*-acetylgalactosamine, HCl solution (35%) and fluorescein isothiocyanate (Fl) were purchased from Sigma-Aldrich Inc. (St. Louis, MO). *N*-hydroxysuccinimide-activated Boc-poly(ethylene glycol) (2kDa) (BocHN-PEG-CONHS) was purchased from NOF Corporation (Cibitung-Bekasi, Indonesia). [^{14}C]Iodoacetamide was purchased from American Radiolabeled Chemicals, Inc. (St. Louis, MO), and SOLVABLE^{TM} digestion reagent and ULTIMA-FLO^{TM} AP flow scintillation cocktail fluid purchased from Perkin-Elmer (Waltham, MA). EcoLume^{TM} analytical liquid scintillation fluid was purchased from MP Biomedical (Solon, OH). SP94 peptide (H_2N-SFSIIHTPILPLGGC-COOH) was custom synthesized by GenScript Inc (Piscataway, NJ) with a GGC spacer at the C-terminus. Minimum essential medium (MEM), OPTI-MEM reduced serum medium, Rosewell Park Memorial Institute-1640 (RPMI) medium, Hanks Balanced Salt Solution (HBSS), fetal bovine serum (FBS), 0.25% trypsin / 0.20% ethylene diamine teraacetic

acid (EDTA) solution, phosphate buffered saline (PBS), penicillin/streptomycin/amphotericin solution, sodium pyruvate and non-essential amino acid solutions were purchased from Invitrogen Corporation (Carlsbad, CA). Pronase from *Streptomyces griseus* and DNase I grade II from bovine pancreas were purchased from Roche, Inc. (Indianapolis, IN). Bovine Serum Albumin (BSA) and dialysis cassette (MWCO 1-10kDa) were purchased from Thermo Fisher Scientific Inc. (Rockford, IL). Phagocytosis assay kit was purchased from Cayman Chemicals Co. (Ann Arbor, MI). Primary hepatocytes isolated from the livers of Sprague-Dawley rats plated in 24-well plates at 5×10^5 cells/well and complete hepatocyte culture media (K2300) were purchased from Xenotech LLC (Lenexa, KS).

5.2.2 Synthesis of [^{14}C]G5-(NH$_2$), [^{14}C]G5-(Ac)-(NAcGal), and [^{14}C]G5-(Ac)-(PEG) Conjugates

G5-(NH$_2$)$_{128}$ PAMAM dendrimers (113.1 mg, 0.0039 mmoles) were dissolved in 6 mL 0.1M sodium bicarbonate solution (pH 10) followed by addition of 1.2 molar equivalents of [^{14}C]Iodoacetamide dissolved in DI water, and the reaction was stirred in the dark at room temperature. Radio-labeling progress was monitored daily by removing 100 µL of reaction solution and analyzed by GPC using a Superdex^{TM} 75 size exclusion column connected to a Hewlett Packard Series II 1050 liquid chromatography system equipped with a Packard 500TR flow scintillation detector run at a 2 mL/min flow rate of ULTIMA-FLO^{TM} AP flow scintillation cocktail (Perkin-Elmer, Waltham, MA) during detection. 0.1M sodium bicarbonate solution (pH 10) was used as a mobile phase to separate free [^{14}C]Iodoacetamide from the radio-labeled [^{14}C]G5-NH$_2$ conjugates at a

flow rate of 1 mL/min. The radio-labeling efficiency was determined by integrating the peak intensity of [^{14}C]G5-(NH$_2$) conjugates and dividing by the free [^{14}C]Iodoacetamide peak area. Once ≥ 90% of the [^{14}C]Iodoacetamide radio-labels had reacted with the G5 dendrimer (72 hours) the reaction was stopped and [^{14}C]G5-(NH$_2$) conjugates purified by dialysis (MWCO 10kDa) against deionized water for 2 days and dried by lyophilization to yield 108.6 mg of [^{14}C]G5-(NH$_2$) (0.0038 mmoles, 97% yield). To determine the average number of [^{14}C]-labels attached per dendrimer 1 mg of the [^{14}C]G5-(NH$_2$) conjugate was mixed with 5 mL EcoLume^{TM} scintillation cocktail and analyzed by a LS6500 liquid scintillation counter (Beckman Coulter, Indianapolis, IN), and results compared to a series of [^{14}C]Iodoacetamide standards.

Coupling of NAcGal sugar ligands and acetylation of [^{14}C]G5-(NH$_2$) dendrimers was performed following published protocols[24] yielding [^{14}C]G5-(Ac)-(NAcGal) conjugates as a white solid (23.9 mg, 97% yield). Molecular weight of [^{14}C]G5-(Ac)-(NAcGal) conjugates was estimated by performing MALDI-TOF analysis on a non-radioactive G5-(Ac)-(NAcGal) analogue synthesized in an identical manner, resulting in a molecular weight of 38,180 gm/mole. [^{14}C]G5-(Ac)-(PEG) conjugates were synthesized by dissolving [^{14}C]G5-(NH$_2$) (47.8 mg, 0.0017 mmoles) in 3 mL anhydrous MeOH followed by addition of NHS-PEG (65.0 mg, 0.0306 mmoles), and reaction mixture stirred at room temperature for 24 hours. Solvents were removed under reduced pressure, and [^{14}C]G5-(PEG) conjugates acetylated as previously described,[24] before purification by dialysis (MWCO 10kDa) against deionized water for 2 days and dried by lyophilization to produce [^{14}C]G5-(Ac)-(PEG) as a white solid (88.0 mg, 99% yield).

MALDI-TOF analysis of un-labeled G5-(Ac)-(PEG) conjugates showed a molecular weight of 51,962 gm/mole.

5.2.3 *In Vivo* Biodistribution of [14C]G5-(NH₂), [14C]G5-(Ac)-(NAcGal), and [14C]G5-(Ac)-(PEG) Conjugates in Tumor-Bearing Mice

We developed an orthotopic hepatic cancer model by injection of HepG2 cells suspended in matrigel in the left lobe of the mouse model. Briefly, 4-5 week old female NCr nude mice were in UCUCA approved pathogen-free animal housing facility with unrestricted access to food and water. Mice received 100 mg/kg cyclophosphamide via intraperitoneal injection 24 hours prior to xenograft surgery, then 1 hour before surgery mice receive 0.24 mg/kg dexamethasone, and again 24 hours post-surgery. At the time of the surgery mice were anesthetized by injecting i.p. a mixture of ketamine:xylazine 70:10 mg/kg, followed by exposing of the liver via laparotomy and injecting 1×10^7 HepG2 cells suspended in 100 µL matrigel into the left median hepatic lobe. Each mouse received 15 mg/kg ampicillin by i.p. before suturing the incision. Dimensions of the implanted tumor was measured 4 weeks after implantation using a caliper to calculate the tumor volume using the ellipsoidal volume formula ($V = \frac{\pi}{6} * W^2 * L$).[33] Once tumor volume reached 75-100 mm³ mice were used in subsequent biodistribution studies.

[14C]G5-(NH₂), [14C]G5-(Ac)-(NAcGal) or [14C]G5-(Ac)-(PEG) conjugates were dissolved in 250 µL of sterile saline at a dose of 0.322 µmole/kg to achieve sufficient radioactivity to resolve a ≤1000 fold reduction in the injected dose. Tumor-bearing mice were given 0.5 mL sterile saline administered i.p. 24 hours prior to treatment, followed by administration of the radio-labeled conjugates via tail-vein injection. 2, 24 and 48

hours post administration animals were anesthetized, euthanized by intracardiac blood draw, and plasma immediately separated via centrifugation at 9,000 rpm for 10 minutes. Tumor tissue, vital organs, including the brain, heart, lungs, kidneys, liver, spleen, pancreas, intestine and lymph nodes (peyer's patches), bone marrow and waste (feces and urine absorbed onto filter paper) were collected, weighed and snap frozen in liquid nitrogen until used. Before processing, samples were thawed and an equal volume of PBS was added, followed by extensive homogenization via a Polytron PT 1600 E homogenizer for 10 minutes. SOLVABLE^{TM} tissue digestion reagent was added to each sample at 1 mL/g of tissue (or a minimum of 3 mL) before vigorous vortexing, followed by incubation for 18 hours in a 60 °C in shaking water bath. After this incubation period samples were re-homogenized and incubated for an additional 8 hours in a 60 °C shaking water bath to complete digestion, before addition of 200 µL glacial acetic acid followed by extensive vortexing and an additional 1 hour incubation at 60 °C to precipitate proteins. Samples were centrifuged at 3,000 rpm for 5 minutes to condense solid material and 2 mL of the supernatant was mixed with 5 mL of EcoLume^{TM}, analyzed by liquid scintillation counting and results compared to a series of [^{14}C]Iodoacetamide standards to determine amount of [^{14}C]-labeled conjugate per tissue. We determined the extraction efficiency of each conjugate from tissues by spiking organs and waste collected from untreated control mice with 0.0247 µmole of [^{14}C]-labeled conjugates and samples processed following the same extraction procedure and analytical method. The amount of [^{14}C]-labeled conjugates which distributed each tissue was normalized to the corresponding extraction efficiency. Biodistribution of each conjugates was investigated

220

in quadruplicate and results shown as the average % of the injected dose per tissue ± standard error of the mean (SEM).

5.2.4   Synthesis of G5-(FI)$_6$-(Ac)-(cPEG[NAcGal$_{\alpha/\beta}$]) Conjugates

*5.2.4.1 Synthesis   of   (3aR,5R,6R,7R,7aR)-5-(acetoxymethyl)-2-methyl-5,6,7,7a-tetrahydro-3aH-pyrano[3,2-d]oxazole-6,7-diyl diacetate (**2**):*

D-Gal-NH$_2$.HCl (5.0 g, 23.24 mmol) was dissolved in pyridine (28.15 mL, 348.74 mmol) and acetic anhydride (26.35 mL, 278.88 mmol) was added slowly. DMAP (2.0 g) was added to the reaction mixture before stirring 0 ^{o}C for 1 hour, then at room temperature for an additional 24 hours. The reaction was then quenched with a saturated NaHCO$_3$ solution and extracted into EtOAc, followed by washing with 1N of HCl solution, water, brine and dried over Na$_2$SO$_4$. Solvents were evaporated under reduced pressure and the residue was purified by silica gel column chromatography using DCM:EtOAc:MeOH (7.5:2.0:0.5) as an eluent to obtain compound **1** (7.25 g, 80% yield). ^{1}H NMR (500 MHz, CDCl$_3$): 1:0.33 β: α ratio. δ 1.82 (s, 3H, CH$_3$, OAc, (β)), 1.85 (s, 3H, CH$_3$, OAc, (α)), 1.88 (s, 3H, CH$_3$, OAc, (β)), 1.90 (s, 3H, CH$_3$, OAc, (β)), 1.92 (s, 3H, CH$_3$, OAc, (α)), 1.94(s, 3H, CH$_3$, OAc, (α)), 1.98 (s, 3H, CH$_3$, OAc, (α)), 2.00 (s, 3H, CH$_3$, OAc, (α)), 2.03 (s, 3H, CH$_3$, OAc, (β)), 2.04 (s, 3H, CH$_3$, OAc, (β)), 3.90-4.04 (m, 3H, H$_3$ and 2xH$_6$), 4.06 (m, 3H, H$_6$, 2xH$_3$), 4.55 (dt, 1H, *J* = 3.5 & 9.0 Hz, H$_5$), 4.61 (dt, 1H, *J* = 4.5 & 9.0 Hz, H$_5$), 5.04-5.12 (m, 2H, 2xH$_2$), 5.22 (d, 1H, *J* = 1.5 Hz, H$_4$), 5.30 (d, 1H, *J* = 2.0 Hz, H$_4$), 6.10 (d, 1H, *J* = 3.5 Hz, (α), H$_1$), 6.28 (d, 1H, *J* = 8.5 Hz, (β), H$_1$); ^{13}C NMR (125 MHz, CDCl$_3$): δ 20.30 (OAc, 3C̲H$_3$, (β)), 20.33 (OAc, 3C̲H$_3$, (β)), 20.35 (OAc,
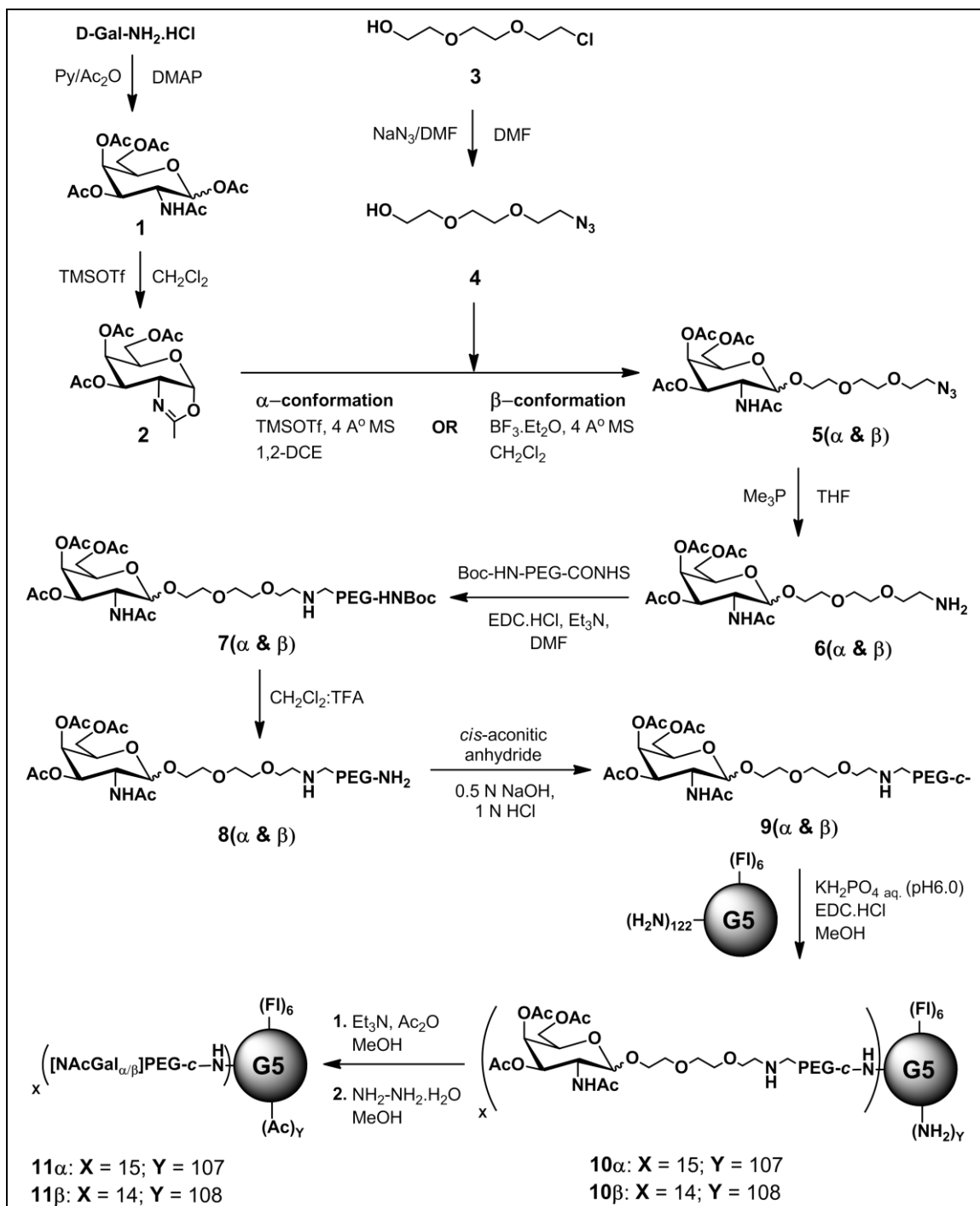
Scheme 5.1: Synthesis of α- or β-conformation NAcGal-targeted G5-PEG carriers through *cis*-aconityl linkages to prepare G5-(Fl)$_6$-(Ac)$_{107}$-(*c*PEG[NAcGal$_α$])$_{15}$ and G5-(Fl)$_6$-(Ac)$_{108}$-(*c*PEG[NAcGal$_β$])$_{14}$ conjugates.

3$\underline{C}H_3$, (β)), 20.40 (OAc, 3$\underline{C}H_3$, (α)), 20.42 (OAc, 3$\underline{C}H_3$, (α)), 20.52 (OAc, 3$\underline{C}H_3$, (β)), 20.70 (OAc, 3$\underline{C}H_3$, (α)), 20.75 (OAc, 3$\underline{C}H_3$, (α)), 23.51 (OAc, 3$\underline{C}H_3$, (α)), 23.53 (OAc, 3$\underline{C}H_3$, (β)), 46.52 (β, C_2), 55.90 (α, C_2), 61.03 (β, C_6), 61.78 (α, C_6), 66.41 (β, C_3), 67.36 (β, C_4), 68.14 (β, C_5), 70.01 (α, C_3), 73.45 (α, C_4), 78.47 (α, C_5), 90.80 (β, C_1), 93.63 (α, C_1), 168.80 (β, $\underline{C}O$), 169.01 (α, $\underline{C}O$), 169.65 (α, $\underline{C}O$), 169.98 (β, $\underline{C}O$), 170.14 (β, $\underline{C}O$), 170.20 (α, $\underline{C}O$), 170.53 (α, $\underline{C}O$), 170.56 (β, $\underline{C}O$), 170.58 (β, $\underline{C}O$), 173.87 (α, $\underline{C}O$); EI-MS: $[M+H]^+$ $C_{16}H_{24}NO_{10}$ calcd 390.13, obsd 390.12, $[M+Na]^+$ $C_{16}H_{23}NNaO_{10}$ calcd 412.12, obsd 412.11

Compound **1** (2.0 g, 5.139 mmol) was dissolved in DCM (25 mL), TMSOTf (1.85 mL, 10.27 mmol) added and reaction mixture stirred at 40 ^{o}C for 24 hours. The reaction was quenched with Et_3N (0.4 mL, pH 7.5), diluted in DCM and extracted with a saturated $NaHCO_3$ solution. The organic layer was washed with water, brine and dried over Na_2SO_4 before evaporation of solvents under reduced pressure and residue purified by silica gel column chromatography using DCM:EtOAc:MeOH (7.5:2.0:0.5) as an eluent to obtain compound **2** (1.35 g, 82% yield). ^{1}H NMR (500 MHz, $CDCl_3$): δ 2.03 (s, 3H, H_7), 2.064 (s, 3H, CH_3, OAc), 2.067 (s, 3H, CH_3, OAc), 2.08 (s, 3H, CH_3, OAc), 4.12 (dd, 1H, J = 6,5 & 12.0 Hz, H_6), 4.18 (d, 1H, J = 9.0 Hz, H_3), 4.32 (dd, 1H, J = 3.5 & 12.0 Hz, $H_{6'}$), 4.52 (dd, 1H, J = 1.5 & 5.5 Hz, H_2), 5.00 (m, 1H, H_5), 5.14 (s, 1H, H_4), 6.12 (d, 1H, J = 6.5 Hz, H_1); ^{13}C NMR (125 MHz, $CDCl_3$): δ 14.30 (C_7), 20.6, 20.7, 20.75 (OAc, 3$\underline{C}H_3$), 62.8 (C_6), 69.6 (C_2), 76.4 (C_3), 77.6 (C_5), 84.3 (C_4), 107.3 (C_1), 167.05 (C_8), 169.6, 169.8, 170.3 (OAc, $\underline{C}O$); EI-MS: $[M+H]^+$ $C_{14}H_{20}NO_8$ calcd 330.12, obsd 330.11, $[M+Na]^+$ $C_{14}H_{19}NNaO_8$ calcd 352.10, obsd 352.11.

5.2.4.2 Synthesis of 2-(2-(2-azidoethoxy)ethoxy)ethanol (**4**):

Compound **3** (10.0 g, 59.50 mmol) was dissolved in anhydrous DMF (200 mL), to which NaN$_3$ (77.3 g, 119.00 mmol) was added and reaction mixture stirred at 80 ^{o}C or 48 hours. Solvents were removed under reduced pressure and residue dissolved in DCM (200 mL), washed with water (400 mL) and brine (100 mL) before being dried over Na$_2$SO$_4$. Solvent was evaporated under reduced pressures and residue purified by silica gel column chromatography using EtOAc:*n*-hexane (6:4) to obtain **4** as a liquid (7.80 g, 75% yield) .

^{1}H NMR (500 MHz, CDCl$_3$): δ 2.34 (d, 1H, *J* = 5.5 Hz, OH), 3.93 (t, 2H, *J* = 6.0 Hz, H$_a$), 3.61 (t, 2H, *J* = 4.5 Hz, H$_b$), 3.65-3.68 (m, 6H, H$_c$, H$_e$, H$_f$), 3.73 (q, 2H, *J* = 5.5 Hz, H$_d$); ^{13}C NMR (125 MHz, CDCl$_3$): δ 50.62 (C$_a$), 61.73 (C$_f$), 70.02 (C$_b$), 70.36 (C$_e$), 70.63 (C$_c$), 72.45 (C$_d$); EI-MS: [M+Na]$^+$ C$_6$H$_{13}$N$_3$NaO$_3$calcd 198.08, obsd 198.07.

5.2.4.3 Synthesis of (2R,3R,4R,5R,6R)-5-acetamido-2-(acetoxymethyl)-6-(2-(2-(2-azidoethoxy) ethoxy) ethoxy)tetrahydro-2H-pyran-3,4-diyl diacetate (**5α & β**):

(**5α & 5β**): Compound **2** (150 mg, 0.454 mmol) and alcohol **4** (95.5 mg, 0.545 mmol) was dissolved in 1,2-dichloroethane (3 mL), followed by the addition of 4 A^o MS (0.3 g) and reaction mixture stirred at room temperature for 20 minutes under N$_2.$ TMSOTf (50.5 mg, 0.227 mmol) was then added via syringe and mixture stirred at 50 °C for 24 hours, followed by cooling to room temperature and quenching with Et$_3$N (0.4 mL, pH 7.5). The reaction mixture was extracted twice with DCM (60 mL) and saturated NaHCO$_3$ solution (20 mL), and organic layer washed with water, brine and dried over Na$_2$SO$_4$. Solvents were evaporated under reduced pressure and the residue purified by silica gel column

chromatography using DCM:MeOH (9.5:0.5) as an eluent to obtain compound **5α** (40 mg, 15% yield) as the first eluted. **5α** ^{1}H NMR (400 MHz, CDCl$_3$): δ 1.97 (s, 3H, CH$_3$, OAc), 1.98 (s, 3H, CH$_3$, OAc), 2.03 (s, 3H, CH$_3$, OAc), 2.14 (s, 3H, CH$_3$, OAc), 3.46 (t, 2H, J = 5.2 Hz, H$_a$), 3.62-3.76 (m, 8H, H$_{b,c,d,e}$), 3.81-3.92 (m, 2H, H$_f$), 4.09-4.25 (m, 3H, H$_5$, H$_6$), 4.76 (d, 1H, J = 8.5 Hz, H$_3$); 5.04 (dd, 1H, J = 3.0, 11.0 Hz, H$_4$), 5.29-5.31 (m, 2H, H$_2$, H$_6$), 6.18 (d, 1H, J = 4.6 Hz, H$_1$); EI-MS: [M+Na]$^+$ C$_{20}$H$_{32}$N$_4$NaO$_{11}$calcd 527.20, obsd 520.19. Second eluted was **5β**: (1.15 g, 85% yield). **5β** ^{1}H NMR (500 MHz, CDCl$_3$): δ 1.98 (s, 3H, CH$_3$, OAc), 2.04 (s, 3H, CH$_3$, OAc), 2.06 (s, 3H, CH$_3$, OAc), 2.13 (s, 3H, CH$_3$, OAc), 3.38 (t, 2H, J = 5.0 Hz, H$_a$), 3.61-3.67 (m, 8H, H$_{b,c,d,e}$), 3.75-3.82 (m, 1H, H$_f$), 4.18-4.22 (m, 2H, H$_f$, H$_6$), 4.32-4.38 (m, 2H, H$_2$, H$_{6'}$), 4.75 (dd, 1H, J = 2.5 & 5.5 Hz, H$_3$); 5.0 (s, 1H, H$_4$), 5.34 (m, 1H, H$_5$), 6.06 (d, 1H, J = 8.0 Hz, H$_1$), 4.52 (dd, 1H, J = 1.5 & 5.5 Hz, H$_2$), 5.00 (m, 1H, H$_5$), 5.14 (s, 1H, H$_4$), 6.12 (d, 1H, J = 6.5 Hz, H$_1$); **5β** ^{13}C NMR (125 MHz, CDCl$_3$): δ 20.9 (OAc, $\underline{C}$H$_3$), 21.12 (2 OAc, $\underline{C}$H$_3$), 23.39 (OAc, $\underline{C}$H$_3$), 50.87 Ca), 60.54 (C$_2$), 62.87 (C$_6$), 67.21 (C$_f$), 70.13 (C$_b$), 70.23 (C$_c$), 70.55 (C$_d$), 70.88 (C$_e$), 70.91 (C$_5$), 78.03 (C$_3$), 80.04 (C$_4$), 106.90 (C$_1$), 169.72, 170.25, 170.77, 170.82 (4OAc, $\underline{C}$O); EI-MS: [M+Na]$^+$ C$_{20}$H$_{32}$N$_4$NaO$_{11}$calcd 527.20, obsd 520.19.

This protocol was modified to synthesize **5β** exclusively. Briefly, compound **2** (1.0 g, 3.03 mmol) and alcohol **4** (1.60 g, 9.11 mmol) were dissolved in anhydrous DCM (20 mL), followed by addition of dried 4 A^o MS (0.4 g) and reaction mixture stirred at room temperature for 20 minutes under N$_2$. CSA (camphor sulphonic acid, 0.615 g, 9.0 mL, 9.1 mmol) was added at room temperature and 8 hours, followed by heating to 45 ^{o}C for 24 hours. The reaction mixture was cooled to room temperature, neutralized with Et$_3$N (0.2

mL, pH 7.5), diluted with DCM (100 mL) and extracted using saturated $NaHCO_3$ solution. The organic layer was washed with water, brine and dried over Na_2SO_4. Solvents were evaporated under reduced pressure and the residue purified by silica gel column chromatography using DCM:EtOAc:MeOH (8.0:1.5:0.5) to obtain compound **5β** (1.15 g, 85%). The spectral data matched with above compound **5β**.

*5.2.4.4 Synthesis of (2R,3R,4R,5R,6R)-5-acetamido-2-(acetoxymethyl)-6-(2-(2-(2-aminoethoxy) ethoxy)ethoxy)tetrahydro-2H-pyran-3,4-diyl diacetate (**6α & β**):*

Compound **5** (**5α**: 100 mg, 0.574 mmol; **5β**: 150 mg, 0.861 mmol) was dissolved in anhydrous THF (8 mL), followed by addition of Me_3P (**6α**: 180 mg, 0.689 mmol; **6β**: 0.046 g, 0.59 mmol, as a 1M solution in 0.12mL THF) and reaction mixture stirred at room temperature for 16 hours under N_2. Solvents were evaporated under reduced pressure to obtain compound **6α** (240 mg, 83% yield) and **6β** (0.125 g, 90% yield). No further purification was required and compound was used directly for next step. **6α** ^{1}H NMR (500 MHz, $CDCl_3$): δ 1.98 (s, 3H, CH_3, OAc), 2.02 (s, 3H, CH_3, OAc), 2.06 (s, 3H, CH_3, OAc), 2.14 (s, 3H, CH_3, OAc), 3.22-3.34 (m, 2H, $-NH_2$), 3.58-3.80 (m, 8H), 3.80-3.88 (m, 2H), 3.94-4.15 (m, 4H), 4.16-4.24 (m, 1H), 4.70 (d, 1H, J = 8.5 Hz), 5.18 (dd, 1H, J = 3.0 & 11.0 Hz), 5.40 (d, 1H, J = 3.0 Hz, H_1); ESI-MS: $[M+H]^+$ $C_{20}H_{35}N_2O_{11}$ calcd 479.22, obsd 479.20. **6β** ^{1}H NMR (500 MHz, CD_3OD): δ 1.88 (s, 3H, CH_3, OAc), 1.92-1.98 (m, 6H, $2CH_3$, OAc), 2.02 (s, 3H, CH_3, OAc), 2.98-3.07 (m, 2H, H_a), 3.32-3.35 (m, 1H, H_c), 3.48-3.74 (m, 8H), 3.75-3.96 (m, 2H), 4.02-4.42 (m, 4H), 4.96-4.07 (m, 1H), 5.30 (m, 1H, H_1); **6β** ^{13}C NMR (125 MHz, CD_3OD): δ 20.53 (OAc, $\underline{C}H_3$), 20.62 (2OAc, $\underline{C}H_3$), 20.66 (OAc, $\underline{C}H_3$), 50.51 Ca), 61.56 (C_2), 62.71 (C_6), 69.50

(C$_f$), 69.90 (C$_b$), 70.25 (C$_c$), 70.51 (C$_d$), 72.39 (C$_e$), 76.29 (C$_5$), 77.58 (C$_3$), 84.27 (C$_4$), 107.26 (C$_1$), 169.62, 169.74, 170.33, 170.46 (4OAc, <u>C</u>O); ESI-MS: [M+H]$^+$ C$_{20}$H$_{35}$N$_2$O$_{11}$calcd 479.22, obsd 479.20.

5.2.4.5 Synthesis of (2R,3R,4R,5R,6R)-5-acetamido-2-(acetoxymethyl)-6-(2-(2-(2-amino(Boc amino PEG-)ethoxy)ethoxy)ethoxy)tetrahydro-2H-pyran-3,4-diyl diacetate (**7α & β**):

7α : Compound **6α** (30 mg, 0.063 mmol) and BocHN-PEG-CONHS (70 mg, 0.031 mmol) were dissolved in anhydrous DMF (3 mL), followed by addition of Et$_3$N (0.02mL) and reaction mixture stirred at room temperature for 48 hours. The reaction mixture was precipitated by slow dropwise addition of ether (40mL) at 0 °C, and solution stored at -18 °C overnight to complete precipitation. The precipitated portion was filtered through a glass filter at 0 °C, washed twice with DCM (25 mL) and concentrated under reduced pressure to produce compound **7α** as an off-white solid (68 mg, 80% yield). **7α** ^{1}H NMR (500 MHz, CDCl$_3$): δ 1.43 (s, 9H, 3CH$_3$, Boc), 1.94 (s, 3H, CH$_3$, OAc), 1.98 (s, 3H, CH$_3$, OAc), 2.03 (s, 3H, CH$_3$, OAc), 2.14 (s, 3H, CH$_3$, OAc), 3.05-3.15 (m, 4H), 3.32-3.65 (m, 10H, H$_{a,b,c,d,e}$.), 3.40-4.00 (m, 180H, PEG-H), (4.02-4.18 (m, 3H, H$_2$, H$_{6,6'}$), 4.78 (d, 1H, *J* = 3.4 Hz, H$_3$); 5.02-5.16 (m, 2H), 5.34 (d, 1H, *J* = 1.2 Hz), 6.54 (d, 1H, *J* = 3.6 Hz H$_1$); EI-MS: [M+H]$^-$ C$_{20}$H$_{35}$N$_2$O$_{11}$+ PEG-NHBoc calcd 2622.32, obsd 2622.20.

7β: Compound **6β** (0.025 g, 0.053 mmol) and BocHN-PEG-CONHS (0.04 g, 0.017 mmol) were dissolved in anhydrous DMF (3 mL), followed by addition of EDC.HCl (0.005 g, 0.026 mmol), HOBT (0.0035 mg, 0.026 mmol) in DMF (0.5 mL), Et$_3$N

(0.02mL) and stirred for 48 hours at room temperature. The reaction mixture was purified via dialysis (MWCO 1kDa) against deionized water for 36 hours, followed by extraction of the dialysis contents twice with cold Et_2O (5 mL) and lyophilized to obtain compound **7β** as an off-white solid (47 mg, 80% yield). **7β** ^{1}H NMR (500 MHz, D_2O): δ 1.28 (s, 9H, $3CH_3$, Boc), 1.82 (s, 3H, CH_3, OAc), 1.88 (s, 3H, CH_3, OAc), 1.93 (s, 3H, CH_3, OAc), 2.00 (s, 3H, CH_3, OAc), 2.06-2.09 (m, 52H, PEG-H), 3.18 (t, 2H, J = 5.0 Hz, Ha), 3.38-3.46 (m, 3H, $H_{2d,1e}$), 3.48-3.62 (m, 180H, PEG-H), 3.69 (t, 1H, J = 4.5 Hz, H_e), 3.80 (s, 1H, H_f), 4.04-4.21 (m, 4H, H_2, H_5, $H_{6,6'}$), 5.06 (dd, 1H, J = 3.0 & 11.0 Hz, H_3); 5.31 (d, 1H, J = 3.5 Hz H_4), 5.66 (d, 1H, J = 8.5 Hz H_1); EI-MS: $[M+H]^-$ $C_{20}H_{35}N_2O_{11}$+ PEG-NHBoc calcd 2622.32, obsd 2622.20.

5.2.4.6 *Synthesis of (2R,3R,4R,5R,6R)-5-acetamido-2-(acetoxymethyl)-6-(2-(2-(2-amino(amino PEG-)ethoxy)ethoxy)ethoxy)tetrahydro-2H-pyran-3,4-diyl diacetate* (**8α & β**):

Compound **7** (**7α**: 83mg, 0.033 mmol; **7β**: 35 mg, 0.013 mmol) was dissolved in DCM:trifluoroacetic acid (TFA) (1.5:1, 4 mL) and stirred at room temperature for 12 hours, followed by evaporation under reduced pressure. Residue was washed three times with DCM (3 mL) and evaporated to remove all TFA, followed by washing twice with cold Et_2O (4 mL) and decanted before evaporation to obtain compound **8** (**8α**: 75 mg, 90% yield; **8β**: 28 mg, 83% yield) as a crude mixture utilized for the next reaction. **8α** ^{1}H NMR (400 MHz, $CDCl_3$): δ 1.97 (s, 3H, CH_3, OAc), 2.06 (s, 3H, CH_3, OAc), 2.10 (s, 3H, CH_3, OAc), 2.13 (s, 3H, CH_3, OAc), 3.17 (t, 2H, NH_2), 3.32-3.65 (m, 10H, $H_{a,b,c,d,e}$), 3.62 (m, 180H, PEG-H), 3.72-3.80 (m, 4H, H_f, $H_{a'}$), 3.89 (m, 2H, H_a) 4.05-4.17 (m, 3H, H_2,

H$_{6,6'}$), 4.79 (d, 1H, J = 4.4 Hz, H$_3$); 5.15 (d, 1H, J = 5.4 Hz, H$_4$), 5.33 (d, 1H, J = 5.8 Hz

H$_5$), 6.54 (d, 1H, J = 4.2 Hz H$_1$); **8β** ^{1}H NMR (500 MH, CDCl$_3$): δ 1.98 (s, 3H, CH$_3$,

OAc), 2.02 (s, 6H, 2CH$_3$, OAc), 2.03 (s, 3H, CH$_3$, OAc), 2.10-2.24 (m, 52H, PEG-H),

3.17 (s, 2H, Ha), 3.48-3.62 (m, 180H, PEG-H), 3.90-4.58 (m, 6H), 5.16-5.44 (m, 3H),

5.49 (s, 2H), 5.84 (d, 1H, J = 9.0, H$_1$); 6.06-6.30 (m, 2H), 6.46 (s, 1H); EI-MS: [M+H]$^-$

C$_{20}$H$_{35}$N$_2$O11+ PEG-NH$_2$ calcd 2522.3, obsd 2522.20.

5.2.4.7 *Synthesis of (2R,3R,4R,5R,6R)-5-acetamido-2-(acetoxymethyl)-6-(2-(2-(2-amino(cis-aconityl-amino PEG-)ethoxy)ethoxy)ethoxy)tetrahydro-2H-pyran-3,4-diyl diacetate* (**9α & β**):

Compound **8** (**8α**: 75 mg, 0.030 mmol; **8β**: 28 mg, 0.011 mmol) was dissolved in

deionized water (4 mL) followed by addition of *cis*-aconitic anhydride (**9α**: 16 mg, 0.101

mmol; **9β**: 6 mg, 0.038 mmol) dissolved in 0.5 mL of 1,4-dioxane. The pH was adjusted

to 8.5-8.7 by dropwise addition of 0.5 M NaOH and solution stirred for 10 minutes at

room temperature. This was followed by adjustment of the pH to 7.4-7.5 via addition of

ice-cold 1N HCl solution and reaction mixture stirred at 0 ^{o}C for 5 minutes before further

acidification to pH 2.5-3.0 at 0 ^{o}C while stirring for 5 minutes. The reaction mixture was

purified by dialysis (MWCO 1 kDa) against deionized water for 36 hours and lyophilized

to obtain compound **9** as an off-white solid (**9α**: 65 mg; 82% yield; **9β**: 25 mg, 85%

yield). **9α** ^{1}H NMR (400 MHz, CDCl$_3$): δ 1.97 (s, 3H, CH$_3$, OAc), 2.06 (s, 3H, CH$_3$,

OAc), 2.10 (s, 3H, CH$_3$, OAc), 2.13 (s, 3H, CH$_3$, OAc), 3.32-3.62 (m, 12H,*CH$_2$*-COOH,

H$_{a,b,c,d,e.}$), 3.62 (m, 180H, PEG-H), 3.72-3.80 (m, 4H, H$_f$, H$_{a'}$), 3.89 (m, 2H, H$_a$) 4.05-4.17

(m, 3H, H$_2$, H$_{6,6'}$), 4.81 (d, 1H, J = 4.2 Hz, H$_3$); 5.15 (dd, 1H, J = 1.6 & 1 Hz, H$_4$), 5.29

(d, 1H, J = 1.4 Hz H_5), 6.33 (s, 1H, olefin), 6.44 (d, 1H, J = 4.4 Hz H_1), 7.61 (bs, 2H, COOH); **9β** ^{1}H NMR (500 MHz, CDCl$_3$): δ 1.10-2.60 (m, 64H, 4CH$_3$, PEG-H), 3.13 (s, 2H, H$_a$), 3.42-3.90 (m, 180H, PEG-H), 3.96-4.42 (m, 6H), 5.30-5.42 (m, 2H), 6.35 (s, 1H), 6.81 (d, 1H, J = 7.0, olefin); 7.12 (d, 1H, J = 7.0, olefin), 7.54 (dd, 1H, J = 3.0 & 5.5 Hz, olefin), 7.71 (dd, 1H, J = 3.5 & 6.0 Hz, olefin); EI-MS: [M+H]$^-$ C$_{20}$H$_{35}$N$_2$O11+ PEG-NH-cis-Ac calcd 2678.3, obsd 2678.20.

*5.2.4.8 Synthesis of (2R,3R,4R,5R,6R)-5-acetamido-2-(acetoxymethyl)-6-(2-(2-(2-amino(Fl$_6$-G5-cis-aconityl-amino PEG-)ethoxy)ethoxy)ethoxy)tetrahydro-2H-pyran-3,4-diyl diacetate (**10 α & β**):*

Compound **9** (**9α**: 10.7 mg, 0.004 mmol; **9β**: 5.3 mg, 0.002 mmol) was dissolved in 2.5 mL 0.1 M potassium phosphate buffer (pH 6.0) followed by addition of EDC.HCl (**10α**: 4 mg, 0.016 mmol; **10β**: 2 mg, 0.008 mmol; 1:4 with acid) and reaction mixture stirred at room temperature for 30 minutes. Fluorescently-labeled G5-(Fl)$_6$-(NH$_2$)$_{122}$ dendrimers, prepared following published protocols,[24] (**10α**: 12 mg, 0.00039 mmol; **10β**: 5 mg, 0.00016 mmol) were dissolved in 2 mL of MeOH and added to the reaction solution before adjustment of the mixture to pH 8.0 via dropwise addition of 0.5 M NaOH, followed by stirring at room temperature in the dark for 36 hours. The reaction was purified by dialysis (MWCO 10 kDa) against deionized water for 36 hours and lyophilized to obtain compound **10** as a light orange solid (**10α**: 20 mg; 88% yield; **10β**: 10 mg, 97% yield). **10α** ^{1}H NMR (400 MHz, D$_2$O): δ 1.90 (s, 3H, CH$_3$, OAc), 1.96 (s, 3H, CH$_3$, OAc), 1.98 (s, 3H, CH$_3$, OAc), 2.09 (s, 3H, CH$_3$, OAc), 2.32-3.32 (m, G5-H) 3.32-3.56 (m, 10H, H$_{a,b,c,d,e,}$), 3.56 (m, PEG-H), 3.60-3.63 (m, 4H, H$_f$, H$_{a'}$), 3.73-3.76 (m,

230

2H, H$_a$) 4.09-4.17 (m, 3H, H$_2$, H$_{6,6'}$), 4.98 (dd, 1H, J = 1.6 & 1.8 Hz, H$_4$), 5.27 (d, 1H, J =

1.6 Hz H$_5$), 6.42 (bd, 1H, H$_1$); **10β** ^{1}H NMR (500 MHz, D$_2$O): δ 0.40-2.72 (m, 184H,

4CH$_3$, G5-H, PEG-H), 3.13 (s, 2H, H$_a$), 3.22-3.66 (m, 420H, G5-H, PEG-H), 3.68 (s,

1H), 3.79 (s, 2H), 3.84-3.40 (m, 2H), 4.10 (s, 2H), 4.17 (s, 2H), 4.32 (d, 1H, J = 7.5 Hz);

5.09 (s, 1H), 6.76 (d, 1H, J = 7.0, olefin); 7.06 (d, 1H, J = 7.0, olefin), 7.36 (dd, 1H, J =

3.0 & 5.5 Hz, olefin), 7.91 (d, 1H, J = 6.0 Hz, olefin).

5.2.4.9 *Synthesis of (2R,3R,4R,5R,6R)-5-acetamido-2-(acetoxymethyl)-6-(2-(2-(2-amino(FI$_6$-G5(Ac)-cis-aconityl-amino PEG-)ethoxy)ethoxy)ethoxy)tetrahydro-2H-pyran-3,4-diyl diacetate* (**11 α & β**):

Compound **10** (**10α**: 20 mg, 0.0006 mmoles; **10β**: 10 mg, 0.0003 mmoles) was dissolved

in anhydrous MeOH (2 mL), followed by addition of Et$_3$N (0.2 mL), excess of Ac$_2$O

(0.15 mL) and reaction mixture stirred at room temperature for 48 hours. Solvents were

removed under reduced pressure and residue purified by dialysis (MWCO 10kDa) against

sterile water for 48 hours and residue lyophilized. To remove the acetyl groups from the

NAcGal sugar moiety the compound was dissolved in anhydrous MeOH (2 mL)

containing hydrazine hydrate (0.4 mL) and reaction mixture stirred at room temperature

for 48 hours. Solvents were removed under reduced pressure and residue purified by

dialysis (MWCO 10kDa) against deionized water for 48 hours and lyophilized to obtain

compound **11** as a light orange solid (**11α**: 18.5 mg, 93% yield; **11β**: 9 mg, 90 % yield.

11α ^{1}H NMR (500 MHz, D$_2$O): δ 0.40-2.72 (m, 184H, 4CH$_3$, G5-H, PEG-H), 3.13 (s, 2H,

Ha), 3.22-3.66 (m, 420H, G5-H, PEG-H), 3.68 (s, 1H), 3.79 (s, 2H), 3.84-3.40 (m, 2H),

4.10 (s, 2H), 4.17 (s, 2H), 4.34 (d, 1H, J = 7.5 Hz); 5.12 (s, 1H), 6.65 (d, 1H, J = 7.0,

olefin); 7.12 (d, 1H, $J = 7.0$, olefin), 7.34 (dd, 1H, $J = 3.0$ & 5.8 Hz, olefin), 7.98 (d, 1H, $J = 6.4$ Hz, olefin); **11β** ^{1}H NMR (500 MHz, D$_2$O): δ 0.40-2.72 (m, 184H, 4CH$_3$, G5-H, PEG-H), 3.13 (s, 2H, Ha), 3.22-3.66 (m, 420H, G5-H, PEG-H), 3.68 (s, 1H), 3.79 (s, 2H), 3.84-3.40 (m, 2H), 4.10 (s, 2H), 4.17 (s, 2H), 4.32 (d, 1H, $J = 7.5$ Hz); 5.09 (s, 1H), 6.76 (d, 1H, $J = 7.0$, olefin); 7.06 (d, 1H, $J = 7.0$, olefin), 7.36 (dd, 1H, $J = 3.0$ & 5.5 Hz, olefin), 7.91 (d, 1H, $J = 6.0$ Hz, olefin).

5.2.5 Synthesis of G5-(FI)$_6$-(Ac)-(cPEG[SP94]) conjugates

5.2.5.1 *Synthesis of Fmoc-SP94-Mal-tert-butyl(2-(3-(2,5-dioxo-2,5-dihydro-1H-pyrrol-1-yl) propanamido)(polyethylene glycol)ethyl)carbamate* (**13**):

Commercially available MAL-PEG-NH$_2$.TFA (0.010 g, 0.005 mmol) was dissolved in anhydrous DCM and added (Boc)$_2$ (0.0015 g, 0.005 mmol) at room temperature and stirred for 16 hours. The reaction was quenched with water and extracted in DCM (2 x 25 mL). The organic layer was washed with water and dried over Na$_2$SO$_4$ and solvents removed under reduced pressure to obtain compound **12** (0.010 g, 95% yield). The compound was used for next step without further purification. ESI-MS: [M+H]$^+$ MAL-PEG-NH$_{BOC}$ calcd 1892.10, obsd 1892.20

Compound **12** (0.0075 g, 0.0093 mmoles) and Fmoc-SP94-SH peptides (0.0065 g, 0.0093 mmoles) were dissolved in pH 6.5 sodium phosphate buffer:MeOH (1.5:0.5 mL) mixture and reaction solution stirred at room temperature for 36 hours. The solution was then purified by dialysis (MWCO 1 kDa) against deionized water for 36 hours to remove low molecular weight impurities, and lyophilized to obtain compound **13** (0.012 g, 80%

Scheme 5.2: Synthesis of SP94 peptide-targeted G5-PEG carriers through *cis*-aconityl linkages to prepare G5-(Fl)$_6$-(Ac)$_{108}$-(*c*PEG[SP94])$_{14}$ conjugates.
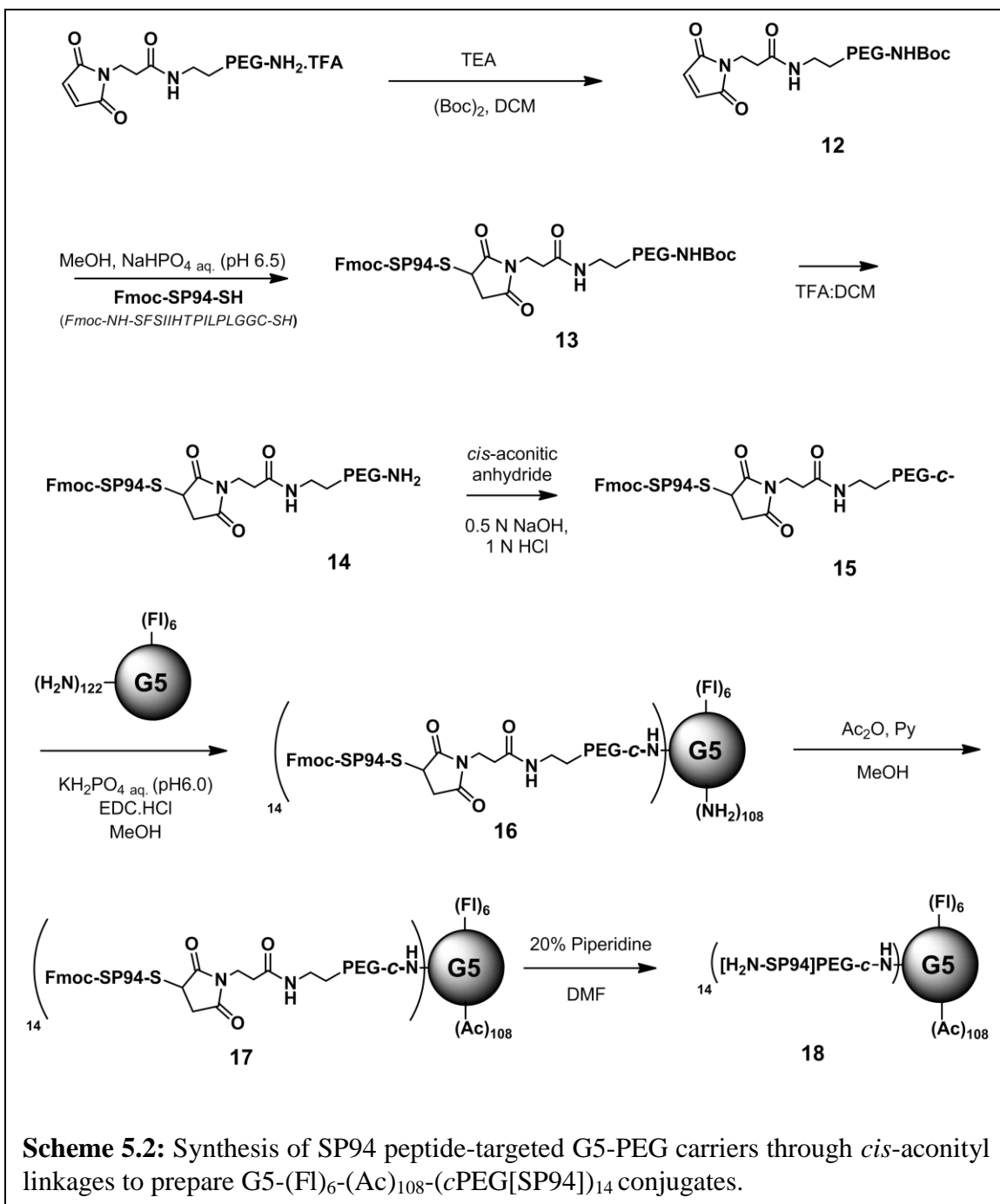
yield). ^{1}H NMR (500 MHz, CDCl$_3$): δ 0.82-1.02 (m, 24H, 8-CH$_3$), 1.12-1.76 (m, 42H), 1.74-2.10 (m, 8H), 2.14-2.24 (m, 3H), 2.47 (t, 4H, *J* = 6.5 Hz), 2.68 (bs, 1H), 2.81 (bs, 1H), 2.88-3.06 (m, 3H), 3.08-3.42 (m, 48H including PEG-H), 3.42-4.08 (m, 242H), 4.09-4.32 (m, 5H), 4.32-4.54 (m, 4H), 4.58-4.80 (m, 5H), 5.13 (bs, 1H), 5.22 (bs, 2H),

5.35 (t, 1H, J = 6.0 Hz), 6.65 (d, 1H, J = 8.0 Hz, -NH), 6.83 (s, 2H), 7.01 (d, 1H, J = 8.5 Hz, -NH), 7.10-7.46 (m, 10H), 7.52-7.78 (m, 2H), 7.78-8.00 (m, 2H), 8.08 (d, 1H, J = 8.5 Hz, -NH), 8.24-8.46 (m, 2H, -NH), 8.70-8.78 (m, 2H); ESI-MS: [M+H]$^+$ FmocNH-SP94-S-MAL-PEG-NHBoc calcd 3669.20, obsd 3669.11.

5.2.5.2 Synthesis of Fmoc-SP94-Mal-(2-(3-(2,5-dioxo-2,5-dihydro-1H-pyrrol-1-yl)

propanamido)(polyethylene glycol)ethyl)carbamate (**14**):

Compound **13** (0.012 g, 0.013 mmoles) was dissolved in DCM:trifluoroacetic acid (TFA) (1.5:1, 2.5mL) and stirred at room temperature for 24 hours, followed by removal of solvents under reduced pressure. The residue was repeatedly diluted in DCM (3 mL) and dried several times to completely remove residual TFA, followed by repeated washing and decanting with cold Et$_2$O (3 x 4 mL) to remove low molecular weight impurities. Solvents were removed under reduced pressure to obtain compound **14** (0.011 g, 85% yield) utilized as the crude mixture for the next reaction. ^{1}H NMR (500 MHz, CDCl$_3$): δ 0.73-1.02 (m, 24H, 8-CH$_3$), 1.10-1.72 (m, 26H), 1.74-2.10 (m, 8H), 2.12-2.24 (m, 3H), 2.42-2.54 (m, 4H), 3.00-3.44 (m, 38H, including PEG-H), 3.42-4.08 (m, 180H), 4.09-4.80 (m, 18H), 5.08 (bs, 1H), 5.30-5.55 (m, 2H), 6.64 (d, 1H, J = 8.0 Hz, -NH), 6.99 (d, 1H, J = 8.0 Hz, -NH), 7.10-7.44 (m, 10H), 7.58-7.84 (m, 2H), 8.22-8.32 (m, 1H), 8.66-8.88 (m, 1H); ESI-MS: [M+H]$^+$ FmocNH-SP94-S-MAL-PEG-NH$_2$ calcd 3569.20, obsd 3569.00.

5.2.5.3 Synthesis of Fmoc-SP94-Mal- (2-(3-(2,5-dioxo-2,5-dihydro-1H-pyrrol-1-yl) propanamido)- 2-amino(cis-aconityl-amino PEG-)- (polyethylene glycol)ethyl)carbamate (**15**):

Compound **14** (0.028 g, 0.011 mmoles) was dissolved in deionized water (4 mL) followed by addition of *cis*-aconitic anhydride (0.006 g, 0.038 mmoles) dissolved in 0.5 mL of 1,4-dioxane. The pH was adjusted to 8.5-8.7 by dropwise addition of 0.5 M NaOH and solution stirred for 10 minutes at room temperature. This was followed by adjustment of the pH to 7.4-7.5 via addition of ice-cold 1N HCl solution and reaction mixture stirred at 0 $^{\circ}$C for 5 minutes before further acidification to pH 2.5-3.0 at 0 $^{\circ}$C while stirring for 5 minutes. The reaction mixture was purified by dialysis (MWCO 1 kDa) against deionized water for 36 hours and lyophilized to obtain compound **15** as an off-white fluffy solid (0.011 g, 65% yield). ^{1}H NMR (500 MHz, CDCl$_3$): δ 0.78-1.02 (m, 24H, 8-CH$_3$), 1.12-1.74 (m, 42H), 1.78-2.10 (m, 8H), 2.20 (t, 4H, $J = 7.5$ Hz), 2.28 (t, 2H, $J = 7.5$ Hz), 2.30-2.54 (m, 6H), 2.90-4.10 (m, 290H, including PEG-H), 4.10-4.24 (m, 8H), 4.28-4.52 (m, 6H), 4.54-4.80 (m, 5H), 5.35 (t, 1H, $J = 5.0$ Hz), 5.38 (bs, 1H), 6.33 (bs, 1H), 6.62-7.00 (m, 4H, -NH), 7.00-7.42 (m, 9H), 7.60-7.84 (m, 5H), 8.11 (bs, 1H, -NH), 8.47 (bs, 1H, -NH), 8.52-8.60 (m, 2H); ESI-MS: [M+H]$^{-}$ FmocNH-SP94-S-MAL-PEG-NH-Cis-Ac-COOH calcd 3725.31, obsd 1862.20 as a doubly charged ion.

5.2.5.4 Synthesis of Fmoc-SP94-Mal-(2-(3-(2,5-dioxo-2,5-dihydro-1H-pyrrol-1-yl) propanamido)-2-amino(Fl$_6$-G5-cis-aconityl-amino PEG-)-(polyethylene glycol) ethyl) carbamate (**16**):

Compound **15** (0.0075 g, 0.002 mmoles, 18 eq.) was dissolved in 2.5mL 0.1 M potassium

phosphate buffer (pH 6.0) followed by addition of EDC.HCl (0.002 g, 0.008 mmoles, 1:4

with acid) and stirred at room temperature for 30 minutes. Fluorescently-labeled G5-

$(Fl)_6$-$(NH_2)_{122}$ dendrimers (0.005 g, 0.0001 mmoles) were dissolved in 2mL MeOH and

the pH of the solution adjusted to 8.0 with 0.5 M Na_2CO_3 solution, followed by stirring of

the reaction mixture for 48 hours in the dark. The reaction solution was purified by

dialysis (MWCO 10 kDa) against sterile water for 36 hours, and lyophilized to obtain

compound **16** as a light orange fluffy solid (0.010 g, 85% yield). ^{1}H NMR (500 MHz,

D_2O): δ 0.58-0.80 (m, 24H, 8-CH_3), 0.92-1.24 (m, 12H), 1.52-4.00 (m, 254H, including

PEG-H), 4.50 (s, 2H), 4.58 (s, 2H), 4.74 (bs, 1H), 5.10 (bs, 1H), 5.15 (bs, 1H), 6.14 (d,

2H, J = 12.0 Hz -NH), 6.30-6.52 (m, 4H), 6.84-7.23 (m, 4H), 7.35 (bs, 1H, -NH), 7.46

(bs, 1H, -NH), 7.72 (bs, 1H, -NH), 7.62-7.82 (m, 2H).

5.2.5.5 Synthesis of Fmoc-SP94-Mal-(2-(3-(2,5-dioxo-2,5-dihydro-1H-pyrrol-1-yl)

propanamido)-2-amino(FT-G5-NHAc-cis-aconityl-amino PEG-)-(polyethylene glycol)

ethyl) carbamate (**17**):

Compound **16** (0.001 g, 0.0003 mmoles) was dissolved in anhydrous MeOH (1.5 mL),

followed by addition of Et_3N (0.2 mL) and Ac_2O (0.1 mL) before stirring of the reaction

mixture at room temperature for 48 hours. Solvents were removed under reduced

pressure and reside dissolved in water (4 mL) and purified by dialysis (MWCO 10 kDa)

against deionized water for 24 hours before lyophilization to obtain compound **17** as a

light orange color fluffy solid (0.008 g, 80 % yield).

5.2.5.6 Synthesis of H₂N-SP94-Mal-(2-(3-(2,5-dioxo-2,5-dihydro-1H-pyrrol-1-yl)propanamido)- 2-amino(FT-G5-NHAc-cis-aconityl-amino PEG-)-(polyethylene glycol)ethyl)carbamate (**18**):

Compound **17** (0.008 g, 0.0003 mmoles) was dissolved in 20% piperidine in DMF (1.5 mL) and mixture stirred at room temperature for 48 hours. Piperidine was removed under reduced pressure, residue dissolved in water and compound purified by dialysis (MWCO 10kDa) against deionized water for 48 hours before lyophilization to obtain compound **18** as a light orange color fluffy solid (0.006 g, 80 % yield). ^{1}H NMR (500 MHz, D₂O): δ 0.58-0.80 (m, 24H, 8-CH₃), 0.92-1.26 (m, 12H), 1.39 (s, 3H), 1.42 (s, 3H), 1.56-1.94 (m, 12H), 2.12-2.42 (m, 12H), 2.50-3.60 (m, 252H, including PEG-H), 3.70-4.01 (m, 12H,), 4.10-4.34 (m, 8H), 4.38 (d, 2H, J = 5.5 Hz), 4.50 (s, 2H), 4.52-4.62 (m, 5H), 5.04 (bs, 1H), 5.10 (bs, 1H), 5.15 (bs, 1H), 6.12 (d, 2H, J = 12.0 Hz -NH), 6.10-6.52 (m, 4H), 6.84-7.30 (m, 5H), 7.14 (bs, 1H, -NH), 7.55 (bs, 1H, -NH), 7.70 (bs, 1H, -NH), 7.75 (bs, 1H, -NH), 7.88 (bs, 1H, -NH), 8.05 (bs, 1H, -NH), 8.20-8.40 (m, 2H).

5.2.6 Characterization of Targeted G5-(FI)₆-(Ac)-(cPEG) Conjugates

The number of PEG chains attached per single G5-(FI)₆-(Ac) dendrimer was determined by gravimetric analysis after sample acidification, dialysis and change in weight measured. Briefly, 2 mg of each targeted G5-(*c*PEG) conjugate was dissolved in 1 mL of HCl-acidified PBS (pH 1.0) and mixture stirred at room temperature for 24 hours, before dialysis (MWCO 5kDa) against deionized water for 48 hours. The remaining G5-(FI)₆-(Ac) dendrimers were lyophilized and dried sample weighed using a semi-micro analytical balance. The change in weight was divided by the molecular weight of the

PEG-R (where R represents, methyl (non-targeted), NAcGal sugar or the SP94 peptide) to determine the number of targeted or non-targeted PEG chains attached per G5-(FI)$_6$-(Ac) dendrimer carrier. This analysis was performed in triplicate for each conjugate with a nominal ± 10% deviation in the mean number of calculated PEG-ligand chains. Results are reported as the average number of PEG chains with or without targeting attached per dendrimer ± standard error of the mean SEM.

Size and surface charge of G5-(FI)$_6$-(Ac)-(cPEG) carriers with and without targeting ligands was determined by dissolving each conjugate in 1 mL deionized water at a particle concentration of 1 μM and analyzed using a 90Plus particle size analyzer with ZetaPALS capability (Brookhaven Instruments Corporation, Holtsville, NY). To investigate the acid-sensitive cleavage of the *cis*-aconityl linker and release of PEG chains from the G5-(FI)$_6$-(Ac) carrier, 0.5 mg/mL of G5-(FI)$_6$-(Ac)-(cPEG) conjugates was dissolved in 2 mL of 1mM citrate buffer prepared at either pH 5.0 or pH 7.4 and samples incubated for 24 hours at 37 °C while shaking. We collected 100 μL of the G5-(FI)$_6$-(Ac)-(cPEG) solution at selected time points (0 – 24 hours) and the concentration of free PEG analyzed using a Ultrahydrogel500 10 μm (7.8 x 300mm) column connected to a Viscotek GPCmax system equipped with a Water refractive index detector. Deionized water was used as a mobile phase at a 0.5 mL/min flow rate, and the concentration of free PEG released as a function of time quantified by measuring the change in solution refractive index versus elution time compared to a series of PEG standards, and results referenced to the calculated initial PEG concentration to determine % PEG release. Results are presented as the average % PEG release of triplicate experiments ± SEM.

5.2.7 Culture of HepG2 and Rat Hepatocyte Cells

HepG2 cells (a gift from Dr. Donna Shewach, Department of Pharmacology, University of Michigan) were cultured in T-75 flasks using MEM supplemented with 10% FBS, and 1% penicillin/streptomycin/amphotericin, sodium pyruvate and non-essential amino acids following published protocols.[24] HepG2 cells (passages 28-32) were incubated at 37 °C, 5% CO2 and 95% relative humidity while changing the culture medium every 48 hours. Cells were passaged at 80-90% confluency using a 0.25% trypsin-EDTA solution. Primary hepatocytes freshly isolated from Sprague-Dawley rats were received 48 hours after isolation and cultured in fresh complete hepatocyte culture media (K2300) for 24 hours before their use in different uptake studies.

5.2.8 Uptake of Targeted $G5\text{-}(Fl)_6\text{-}(Ac)\text{-}(cPEG)$ Conjugates by HepG2 Hepatic Cancer Cells and Primary Rat Hepatocytes

To determine the selectivity of targeted $G5\text{-}(Fl)_6\text{-}(Ac)\text{-}(cPEG)$ carriers towards liver cancer cells the internalization of each conjugate into HepG2 human hepatic cancer cells or rat hepatocytes was evaluated as a function of conjugate's chemical composition, ligand concentration, cell type and incubation time. The studies were performed by seeding cells in 24-well plates at a seeding density of $5\text{x}10^5$ cells/well, and allowed to adhere overnight before a 2 or 24 hour incubation with non-targeted $G5\text{-}(Fl)_6\text{-}(Ac)_{107}\text{-}(cPEG)_{15}$, NAcGal-targeted $G5\text{-}(Fl)_6\text{-}(Ac)_{108}\text{-}(NAcGal)_{14}$, $G5\text{-}(Fl)_6\text{-}(Ac)_{107}\text{-}(cPEG[NAcGal_\alpha])_{15}$ and $G5\text{-}(Fl)_6\text{-}(Ac)_{108}\text{-}(cPEG[NAcGal_\beta])_{14}$, or SP94-targeted $G5\text{-}(Fl)_6\text{-}(Ac)_{108}\text{-}(cPEG[SP94])_{14}$ conjugates at $100 - 4000$ nM equivalent ligand concentration in 0.5 mL of either OPTI-MEM solution for HepG2 cells or hepatocyte

culture media (K2300) for rat hepatocytes. Briefly, after treatment cells were washed with cold PBS, trypsinized with 0.25% trypsin-EDTA solution and centrifuged at 1000 rpm for 5 minutes to pellet the cells before suspending them in 1 mL of fresh PBS and analyzing them using flow cytometry as previously described.[24] Uptake of each conjugate was compared to untreated controls via three independent experiments using four replicates for each experimental condition. Results are expressed as the % of treated cells which displayed fluorescence due to particle internalization ± SEM, as well as intracellular fluorescence intensity normalized to the fluorescent signal of untreated control cells to determine the relative intracellular particle concentration ± SEM as a function of composition, incubation time and cell type.

5.2.9 Isolation of Mouse Liver Macrophage Kupffer Cells

Isolation of primary mouse Kupffer cells was performed as previously described by Su et. al,[34] with minor modification. Briefly, two black-swiss mice were anesthetized via i.p injection of pentobarbital (50 µg/g), abdominal cavity exposed via 'U' shaped celiotomy and inferior vena cava cannulated with a 20 gauge angiocath. The livers were each perfused with 12 mL 37 °C heparin solution (1000U/mL in Hanks Balanced Salt Solution (HBSS)) over 1 minute, followed by infusion of 12 mL 37 °C pronase solution (0.1% w/v in HBSS) over 1 minute. The blanched livers were then excised, gall bladder removed and liver tissue finely minced before a 60 minute digestion in 150 mL pronase solution at 37 °C while spinning. 1 mL of DNase solution (80µg/mL in PBS) was added in 20 minute intervals during digestion to prevent cell clumping, followed by filtration of the slurry through sterile gauze mesh and filtrate centrifuged at 1800 rpm for 5 minutes.

The tissue pellet was then resuspended in 10 mL DNase solution and filtered through a 70 μm cell strainer before centrifugation at 1800 rpm for 5 minutes at 16 °C. The cell pellet was suspended in 1 mL DNase solution and added to the top of a discontinuous Percoll gradient prepared by gently adding 3.75 mL 50% Percoll to 5 mL 25% Percoll (diluted in 10X PBS) in a 15mL falcon tube, ensuring a visible interface is formed before addition of the cell suspension. The gradient mixture was then centrifuged at 1800 rpm for 15 minutes at 0 °C using the lowest acceleration/deceleration settings so as to not disturb the gradient. The debris and 25% Percoll layer were discarded, and the 50% Percoll fraction was washed twice with 20 mL DNase solution to remove Percoll before assessing cell viability by trypan blue exclusion. Following the final washing cells were diluted in serum-free RPMI medium and added to 24-well plates at a seeding density of $1x10^6$ cells/well, followed by incubation 30 minutes at normal culture conditions to allow for differential adhesion of Kupffer cells. After this period the medium was aspirated to remove non-adherent cells and debris, resulting in retention of approximately $5x10^5$ cells/well cultured in 1 mL RPMI medium containing 5% FBS before use. To confirm retained cells were Kupffer liver macrophages a phagocytosis assay kit was utilized, following the manufacturer's guidelines (Cayman Chemicals, Ann Arbor, MI), to assess uptake of FI-labeled IgG-latex beads into Kupffer cells by flow cytometry after a 24 hour incubation.

5.2.10 Opsonization of Targeted G5-(FI)$_6$-(Ac)-(cPEG) Conjugates and Phagocytosis by Kupffer cells

To determine the effect of PEGylation on particle opsonization a bovine serum albumin (BSA) binding assay was performed as a function of particle composition and incubation time. Specifically, G5-(Fl)$_6$-(NH$_2$)$_{122}$ dendrimers, G5-(Fl)$_6$-(Ac)$_{107}$-(cPEG)$_{15}$, G5-(Fl)$_6$-(Ac)$_{108}$-(NAcGal)$_{14}$, G5-(Fl)$_6$-(Ac)$_{108}$-(cPEG[NAcGal$_\beta$])$_{14}$ or G5-(Fl)$_6$-(Ac)$_{108}$-(cPEG[SP94])$_{14}$ conjugates were diluted in PBS (pH 7.4) at a 10 nM particle concentration in a quartz cuvette, and opsonization initiated by addition of 0.2 mg/mL BSA. Quenching of the intrinsic BSA tryptophan fluorescence upon binding to the conjugate surface was recorded using a QM4 fluorescence spectrophotometer (Perkin-Elmer, Waltham, MA) maintained at 37 °C. Analysis was performed at an excitation wavelength of 280nm and emission scanned from 300-400nm over a 60 minute incubation period. The fluorescence quenching efficiency was calculated as I^o/I, where I^o and I are the peak fluorescence intensity at initiation of opsonization and at selected time points, respectively. All experiments were performed in triplicate and results expressed as the average quenching efficiency ± SEM as a function of time.

Uptake of opsonized G5 carriers into mouse Kupffer cells was assessed as a function of surface composition and targeting ligand. Briefly, G5-(Fl)$_6$-(NH$_2$)$_{122}$ dendrimers, G5-(Fl)$_6$-(Ac)$_{107}$-(cPEG)$_{15}$, G5-(Fl)$_6$-(Ac)$_{108}$-(NAcGal)$_{14}$, G5-(Fl)$_6$-(Ac)$_{108}$-(cPEG[NAcGal$_\beta$])$_{14}$ or G5-(Fl)$_6$-(Ac)$_{108}$-(cPEG[SP94])$_{14}$ conjugates were dissolved in mouse serum to a total volume of 0.5 mL and incubated at 37 °C for 1 hour to allow for particle opsonization. Conjugate solutions were then diluted in 1mL total volume with RPMI medium containing 5% FBS at a 4000 nM equivalent ligand concentration and incubated with isolated Kupffer cells plated at 5x10^5 cells/well in a 24-well plate for 2 hours at normal culture conditions before analysis by flow cytometry as previously
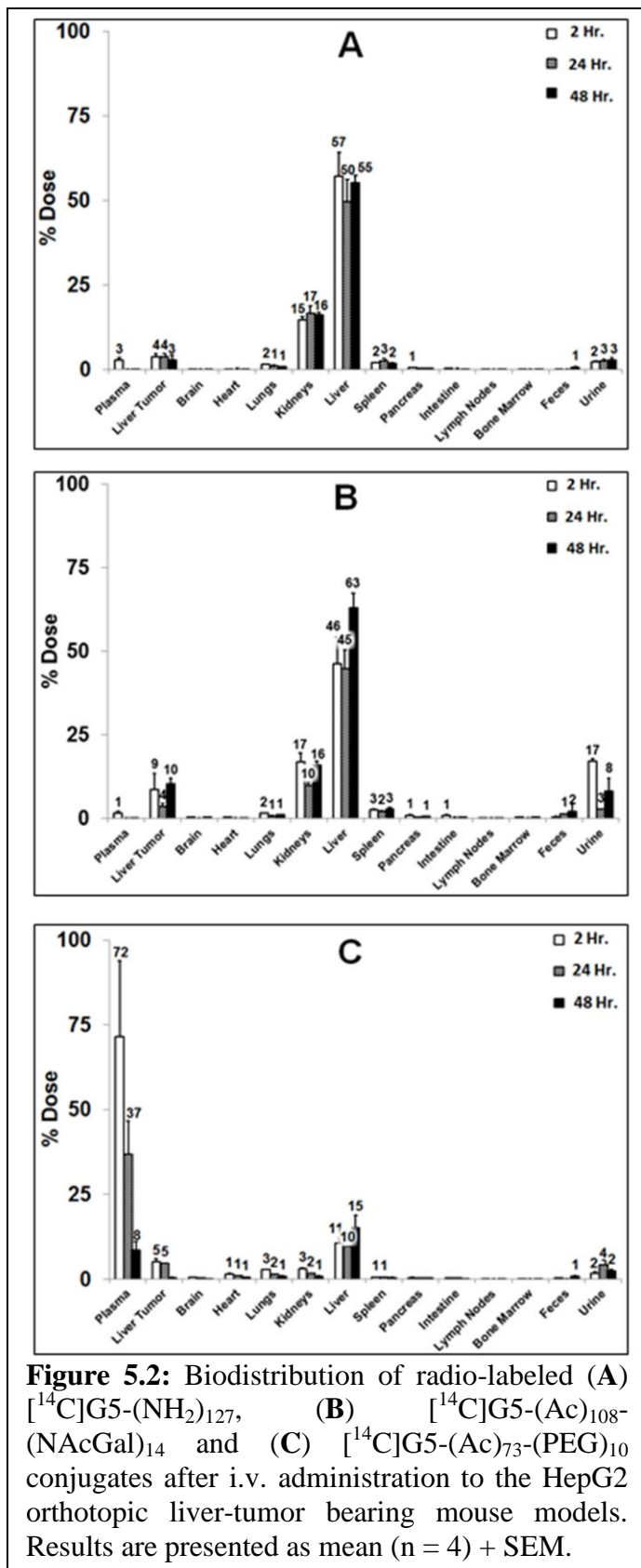
242

described. Uptake of each conjugate was compared to untreated controls in triplicate for each experimental condition, and results expressed as the % of treated cells which displayed fluorescence due to particle phagocytosis $\pm$ SEM

5.3   Results

5.3.1 Synthesis and Biodistribution of $[^{14}C]G5\text{-}(NH_2)_{127}$, $[^{14}C]G5\text{-}(Ac)_{108}\text{-}(NAcGal)_{14}$, and $[^{14}C]G5\text{-}(Ac)_{73}\text{-}(PEG)_{10}$ Conjugates in Tumor-Bearing Mice

$[^{14}C]G5\text{-}(NH_2)_{127}$ dendrimers possessed an average of 1.02 $[^{14}C]$-labels as determined by liquid scintillation counting, and utilized to prepare $[^{14}C]G5\text{-}(Ac)_{108}\text{-}(NAcGal)_{14}$ conjugates which contained 11 mole% NAcGal content. $[^{14}C]G5\text{-}(Ac)_{73}\text{-}(PEG)_{10}$ conjugates were synthesized and possessed an average of 10 PEG chains per dendrimer as determined by MALDI-TOF analysis. Administration of $[^{14}C]G5\text{-}(NH_2)_{127}$ to the orthotopic liver tumor-bearing mouse model via tail vein injection resulted in rapid clearance of particles from the systemic circulation 2 hours after administration, with 3% of the injected dose assayed in the plasma resulting in a plasma half-life ($t_{1/2}$) of 1.03 hours (**Figure 5.2**; Panel **A**). 4% of the injected dose of $[^{14}C]G5\text{-}(NH_2)_{127}$ distributed to liver tumor tissue 2 hours after administration and was retained there up to 48 hours. Intravenous injection of $[^{14}C]G5\text{-}(NH_2)_{127}$ dendrimers to the mouse model also resulted in 50%-57% of the injected particle dose distributing to normal liver tissue between 2 and 48 hours after administration, with 16% in kidney tissue 48 hours after i.v. injection. Results also showed <1% of the injected dose of $[^{14}C]G5\text{-}(NH_2)_{127}$ dendrimers distributed to both heart and bone marrow tissue 48 hours after i.v. administration.

243

To determine the effect of NAcGal-targeting on G5 dendrimer biodistribution $[^{14}C]G5\text{-}(Ac)_{108}\text{-}(NAcGal)_{14}$ conjugates were administered i.v. to the liver tumor bearing mice. Similar to non-targeted $[^{14}C]G5\text{-}(NH_2)_{127}$ dendrimers $[^{14}C]G5\text{-}(Ac)_{108}\text{-}(NAcGal)_{14}$ conjugates showed rapid clearance from the systemic circulation with 1% of the injected dose remaining in the plasma 2 hours after administration ($t_{1/2}$ = 1.01 hours) (**Figure 5.2**; Panel **B**). 9% of the injected $[^{14}C]G5\text{-}(Ac)_{108}\text{-}(NAcGal)_{14}$ dose distributed to tumor tissue after 2 hours, increasing to 10% after 48 hours. 45%-46% of the injected $[^{14}C]G5\text{-}(Ac)_{108}\text{-}(NAcGal)_{14}$ dose was cleared by the normal liver tissue between 2 and 24 hours

Figure 5.2: Biodistribution of radio-labeled (**A**) $[^{14}C]G5\text{-}(NH_2)_{127}$, (**B**) $[^{14}C]G5\text{-}(Ac)_{108}\text{-}(NAcGal)_{14}$ and (**C**) $[^{14}C]G5\text{-}(Ac)_{73}\text{-}(PEG)_{10}$ conjugates after i.v. administration to the HepG2 orthotopic liver-tumor bearing mouse models. Results are presented as mean (n = 4) + SEM.

after injection, and increased to 63% after 48 hours of distribution. $[^{14}C]G5$-$(Ac)_{108}$-$(NAcGal)_{14}$ conjugates also showed a distribution profile to kidney tissue comparable to non-targeted $[^{14}C]G5$-$(NH_2)_{127}$ dendrimers with 16% retention of the injected dose 48 hours after administration. Similarly, <1% of administered $[^{14}C]G5$-$(Ac)_{108}$-$(NAcGal)_{14}$ conjugates accumulated in heart and bone marrow tissue for all tested time points.

To minimize the non-specific distribution of G5 dendrimers to the normal liver tissue PEGylated carriers were prepared via immobilization of 2kDa PEG chains to the dendrimer surface via stable amide linkages to prepare $[^{14}C]G5$-$(Ac)_{73}$-$(PEG)_{10}$ conjugates. Biodistribution results showed 72% of the injected $[^{14}C]G5$-$(Ac)_{73}$-$(PEG)_{10}$ dose remained in the plasma 2 hours after administration, decreasing to 8% at 48 hours ($t_{1/2}$ = 16.7 hours) (**Figure 5.2**; Panel **C**). 11%-15% of the injected dose of $[^{14}C]G5$-$(Ac)_{73}$-$(PEG)_{10}$ conjugates distributed to normal liver tissue between 2 and 48 hours after administration, while ≤3% accumulated in the kidneys between the same time points. There was no significant improvement in tumor specific delivery of $[^{14}C]G5$-$(Ac)_{73}$-$(PEG)_{10}$ conjugates compared to the previous $[^{14}C]G5$-$(NH_2)_{127}$ dendrimers and $[^{14}C]G5$-$(Ac)_{108}$-$(NAcGal)_{14}$ conjugates, with 5% of the injected dose accumulating in the liver tumor 2 and 24 hours after administration, and <1% remaining at 48 hours.

5.3.2 Synthesis and Characterization of Targeted G5-(Fl)$_6$-(Ac)-(cPEG) Conjugates

Based on these biodistribution results we synthesized targeted G5-(*c*PEG) carriers which display the NAcGal sugar or SP94 peptide active targeting ligands at the terminal end of PEG 'brushes' to combine the stealth properties of PEGylation with the ability of

the targeting ligand to achieve cell-specific internalization into hepatic cancer cells. NAcGal- (**Scheme 5.1**) or SP94-targeted (**Scheme 5.2**) G5-(FI)$_6$-(Ac)-(cPEG) conjugates were synthesized by covalently coupling the targeting ligand to a Boc-protected PEG-NHS ester. The protective Boc group was then reduced to allow attachment of the PEG-ligand chains to the G5 dendrimer surface amine groups via an acid-sensitive *cis*-aconityl linker. By utilizing a single batch of fluorescently-labeled G5-(FI)$_6$-(NH$_2$)$_{122}$ dendrimers, targeted G5-(FI)$_6$-(Ac)-(cPEG) conjugates were synthesized with an identical number of attached FI molecules allowing for the direct comparison of their fluorescent signal intensity during *in vitro* studies to determine relative intracellular particle concentrations as a function of conjugate's composition and cell type. The controlled synthetic chemistries utilized to synthesize the targeted G5-(FI)$_6$-(Ac)-(cPEG) conjugates allowed for the comparable coupling of 14-15 targeting groups attached per G5-(FI)$_6$-(Ac) carrier (**Table 5.1**). This resulted in a corresponding increase in molecular weight for the targeted G5-(cPEG) carriers of 68kDa for the non-targeted G5-(FI)$_6$-(Ac)$_{107}$-(cPEG)$_{15}$ conjugates, 73 kDa and 75 kDa for G5-(Fl)$_6$-(Ac)$_{108}$-(cPEG[NAcGal$_\beta$])$_{14}$ and G5-(Fl)$_6$-(Ac)$_{107}$-(cPEG[NAcGal$_\alpha$])$_{15}$, respectively, and 95 kDa for G5-(Fl)$_6$-(Ac)$_{108}$-(cPEG[SP94])$_{14}$ conjugates. In addition, coupling of PEG to G5 dendrimers with or without the addition of the targeting ligand resulted in an increase in particle size from 7.37 nm for G5-(FI)$_6$-(Ac)$_{107}$-(cPEG)$_{15}$ conjugates to 7.61 nm, 8.30 nm and 9.91 nm for G5-(Fl)$_6$-(Ac)$_{107}$-(cPEG[NAcGal$_\alpha$])$_{15}$, G5-(Fl)$_6$-(Ac)$_{108}$-(cPEG[NAcGal$_\beta$])$_{14}$, and G5-(Fl)$_6$-(Ac)$_{108}$-(cPEG[SP94])$_{14}$ conjugates, respectively (**Table 5.1**). G5-(FI)$_6$-(Ac)$_{107}$-(cPEG)$_{15}$, G5-(Fl)$_6$-(Ac)$_{107}$-(cPEG[NAcGal$_\alpha$])$_{15}$, and G5-(Fl)$_6$-(Ac)$_{108}$-(cPEG[NAcGal$_\beta$])$_{14}$conjugates possessed an approximate neutral charge as determined by

246

Table 5.1: Composition and Characterization of Targeted G5-(*c*PEG) Conjugates.

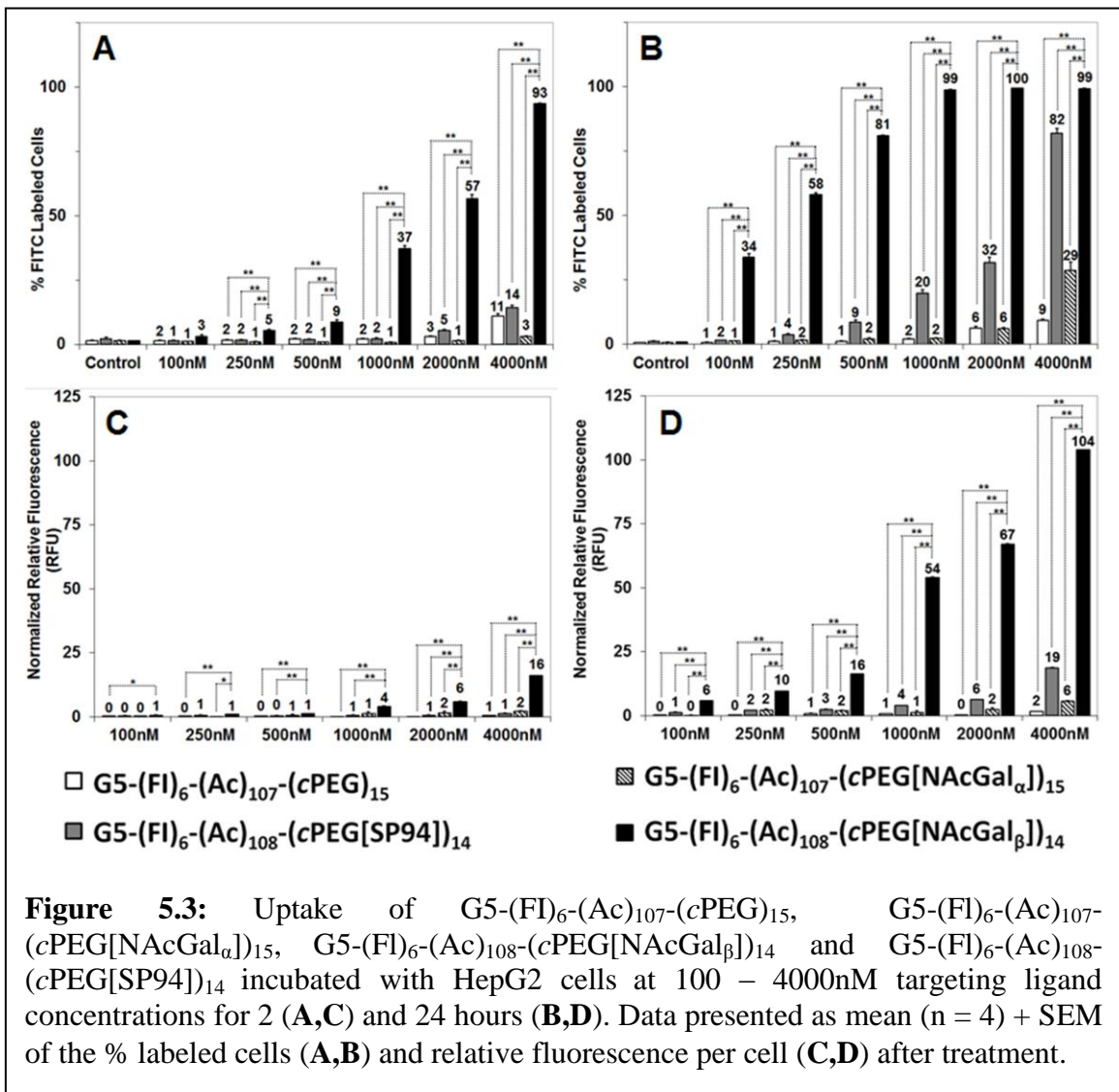| Particle Composition	Molecular Weight [kDa]	Targeting ligands per dendrimer (x)	Size [nm]	Zeta Potential [mV]
G5-(Fl)$_6$-(Ac)$_{107}$-(*c*PEG)$_X$	68.6	15	7.37 ± 0.78	-0.03 ± 0.01
G5-(Fl)$_6$-(Ac)$_{107}$-(*c*PEG[NAcGal$_\alpha$])$_x$	75.7	15	7.61 ± 0.29	-0.01 ± 0.01
G5-(Fl)$_6$-(Ac)$_{108}$-(*c*PEG[NAcGal$_\beta$])$_x$	73.1	14	8.03 ± 1.03	-0.03 ± 0.02
G5-(Fl)$_6$-(Ac)$_{108}$-(*c*PEG[SP94])$_x$	95.2	14	9.91 ± 1.08	-0.38 ± 0.22

zeta potential analysis, while G5-(Fl)$_6$-(Ac)$_{108}$-(cPEG[SP94])$_{14}$ had a slightly negative charge.

The pH-sensitive release of PEG from *cis*-aconityl linked G5-(FI)$_6$-(Ac)$_{107}$-(cPEG)$_{15}$ was evaluated by incubating conjugates in pH 5.0 citrate buffer at 37 °C for 24 hours and analyzing PEG release by GPC at selected time points (**Appendix Figure S26**). Results show 30% of the loaded PEG was released from G5-(FI)$_6$-(Ac)$_{107}$-(cPEG)$_{15}$ conjugates within 0.5 hours of incubation at pH 5.0, followed by a linear increase to achieve 96% total PEG release after 24 hours ($t_{1/2}$ = 5.20 hours). No free PEG was detected by GPC analysis during the 24 hour incubation of G5-(FI)$_6$-(Ac)$_{107}$-(cPEG)$_{15}$ conjugates at pH 7.4.

5.3.3 Uptake of NAcGal- or SP94-Targeted G5-(Fl)$_6$-(Ac)-(cPEG) Conjugates by HepG2 Cancer Cells

The ability of G5-(FI)$_6$-(Ac)-(cPEG) conjugates to be internalized into HepG2 hepatic cancer cells was evaluated as a function of particle composition, ligand concentration and incubation time, with results expressed as the % of treated cells showing fluorescence as determined by flow cytometry (**Figure 5.3**; Panels **A** & **B**). Limited internalization of G5-(FI)$_6$-(Ac)$_{107}$-(cPEG)$_{15}$ conjugates was observed for all concentrations and time points tested, with 11% and 9% fluorescently-labeled cells after a 2 and 24 hour incubation period, respectively. 2 hour uptake of G5-(Fl)$_6$-(Ac)$_{108}$-(cPEG[SP94])$_{14}$ conjugates showed a similar profile with 2%-14% of treated HepG2 cells internalizing the conjugates at the 250 – 4000 nM tested ligand concentrations (**Figure 5.3**; Panel **A**).

However, uptake of G5-(Fl)$_6$-(Ac)$_{108}$-(cPEG[SP94])$_{14}$ conjugates improved after

24 hours of incubation with a linear increase in the % of fluorescently-labeled cells from

4% to 82% between 250 nM and 4000 nM ligand concentrations (**Figure 5.3**; Panel **B**).

Uptake of G5-(Fl)$_6$-(Ac)$_{107}$-(cPEG[NAcGal$_\alpha$])$_{15}$ and G5-(Fl)$_6$-(Ac)$_{108}$-(cPEG[NAcGal$_\beta$])$_{14}$

conjugates into HepG2 cells showed a significant effect of sugar conformation on binding

affinity to the ASGPR and subsequent receptor-mediated endocytosis into HepG2 cells.

Specifically, ≤3% of treated HepG2 cells showed fluorescence after a 2 hour incubation

Figure 5.3: Uptake of G5-(Fl)$_6$-(Ac)$_{107}$-(cPEG)$_{15}$, G5-(Fl)$_6$-(Ac)$_{107}$-(cPEG[NAcGal$_\alpha$])$_{15}$, G5-(Fl)$_6$-(Ac)$_{108}$-(cPEG[NAcGal$_\beta$])$_{14}$ and G5-(Fl)$_6$-(Ac)$_{108}$-(cPEG[SP94])$_{14}$ incubated with HepG2 cells at 100 – 4000nM targeting ligand concentrations for 2 (**A,C**) and 24 hours (**B,D**). Data presented as mean (n = 4) + SEM of the % labeled cells (**A,B**) and relative fluorescence per cell (**C,D**) after treatment.

with the $NAcGal_\alpha$-targeted $G5\text{-}(Fl)_6\text{-}(Ac)_{107}\text{-}(cPEG[NAcGal_\alpha])_{15}$ conjugates across the 100 – 4000 nM tested ligand concentrations (**Figure 5.3**; Panel **A**). A 2 hour incubation of $G5\text{-}(Fl)_6\text{-}(Ac)_{108}\text{-}(cPEG[NAcGal_\beta])_{14}$ conjugates with HepG2 cells however showed a linear increase in the % of labeled cells from 5% to 93% between the 250 nM and 4000 nM tested ligand concentrations. After a 24 hour incubation period 34%-81% of HepG2 cells treated with $G5\text{-}(Fl)_6\text{-}(Ac)_{108}\text{-}(cPEG[NAcGal_\beta])_{14}$ conjugates internalized the particles at the 100 – 500 nM ligand concentrations, which saturated the cell population at ≥ 1000 nM (**Figure 5.3**; Panel **B**).
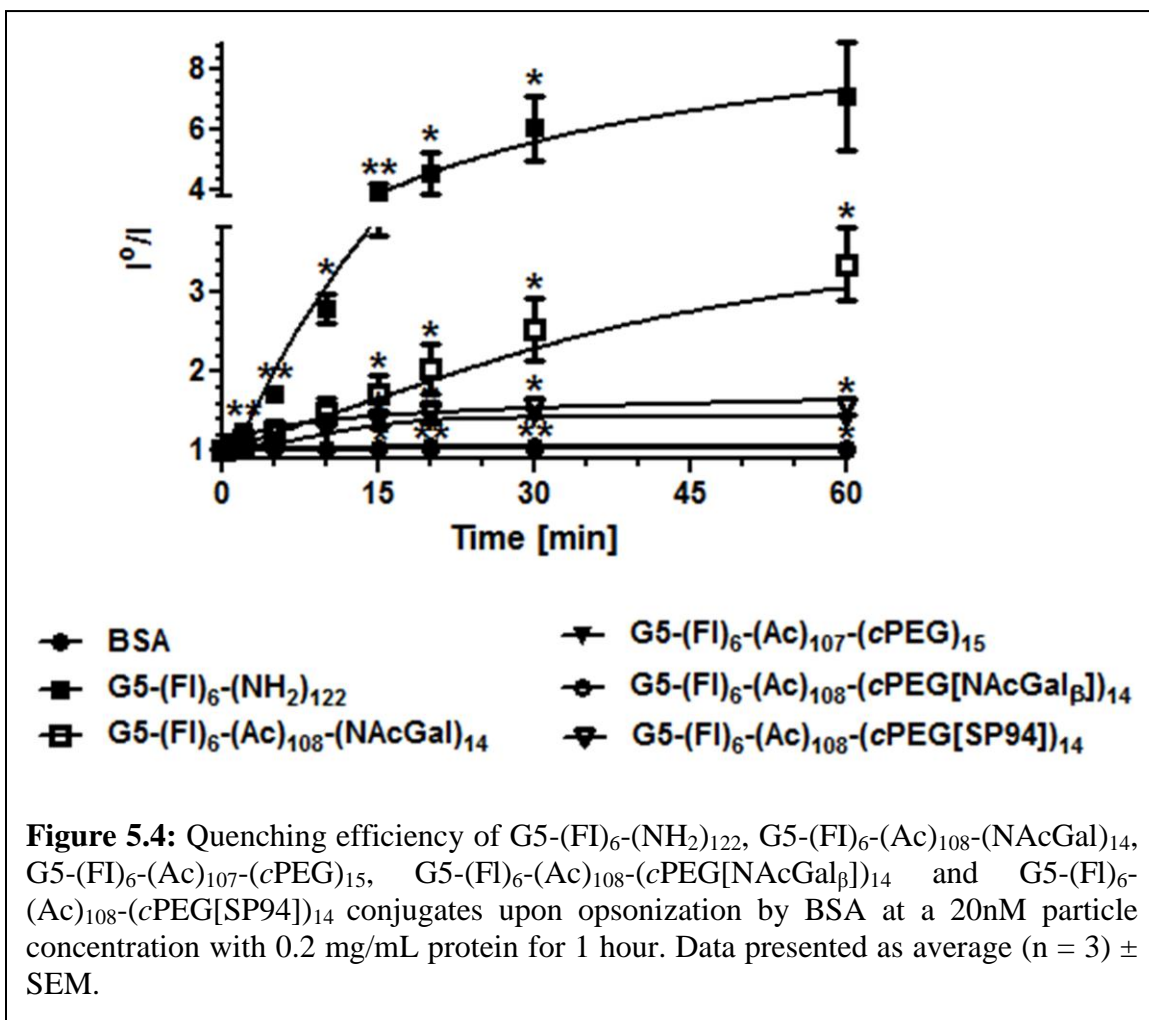
To compare the intracellular particle concentration of targeted G5-(cPEG) conjugates in HepG2 cells as a function of particle composition, ligand concentration and incubation time the relative intracellular fluorescence intensity (normalized to untreated control cells) was reported from the flow cytometry signal (**Figure 3**; Panels **C** & **D**). No significant difference in the relative intracellular particle concentrations of $G5\text{-}(Fl)_6\text{-}(Ac)_{107}\text{-}(cPEG)_{15}$, $G5\text{-}(Fl)_6\text{-}(Ac)_{107}\text{-}(cPEG[NAcGal_\alpha])_{15}$, and $G5\text{-}(Fl)_6\text{-}(Ac)_{108}\text{-}(cPEG[SP94])_{14}$ treated HepG2 cells was observed for all tested ligand concentrations after 2 hours of incubation (**Figure 5.3**; Panel **C**). $G5\text{-}(Fl)_6\text{-}(Ac)_{108}\text{-}(cPEG[NAcGal_\beta])_{14}$ conjugates however showed an increase in the intracellular particle concentration within treated HepG2 cells relative to the other conjugate compositions as a function of ligand concentration, achieving an 8-16 fold enhancement at the highest tested 4000 nM ligand concentration (**Figure 5.3**; Panel **C**). After 24 hours of incubation no significant improvement in the intracellular particle concentration of HepG2 cells treated with $G5\text{-}(Fl)_6\text{-}(Ac)_{107}\text{-}(cPEG)_{15}$ conjugates was observed (**Figure 5.3**; Panel **D**) for all tested ligand concentrations compared to the 2 hour results (**Figure 5.3**; Panel **C**). Similarly,

HepG2 cells treated with G5-(Fl)$_6$-(Ac)$_{107}$-(cPEG[NAcGal$_\alpha$])$_{15}$ conjugates showed a 3-fold increase in relative intracellular particle concentration only at the 4000 nM tested ligand concentration after 24 hours of incubation compared to the 2 hour time point (**Figure 5.3**; Panel **D**). However, a significant increase in the intracellular particle concentration of HepG2 cells incubated with G5-(Fl)$_6$-(Ac)$_{108}$-(cPEG[SP94])$_{14}$ conjugates for 24 hours was observed increasing to 19-folds the 2 hour incubation results at the 4000 nM ligand concentration. Similarly, a substantial increase in the intracellular G5-(Fl)$_6$-(Ac)$_{108}$-(cPEG[NAcGal$_\beta$])$_{14}$ concentration was observed for HepG2 cells treated at 100 – 4000 nM ligand concentration for 24 hours compared to 2 hours of incubation. This resulted in a 5-14 fold higher concentration of G5-(Fl)$_6$-(Ac)$_{108}$-(cPEG[NAcGal$_\beta$])$_{14}$ particles in HepG2 cells after a 24 hour incubation period compared to G5-(Fl)$_6$-(Ac)$_{108}$-(cPEG[SP94])$_{14}$ treated cells at the same incubation time between the 1000 – 4000 nM tested ligand concentrations (**Figure 5.3**; Panel **D**). Furthermore, at the 4000 nM ligand concentration G5-(Fl)$_6$-(Ac)$_{108}$-(cPEG[NAcGal$_\beta$])$_{14}$ treated HepG2 cells showed a >60-fold increase in the intracellular particle concentration compared to G5-(FI)$_6$-(Ac)$_{107}$-(cPEG)$_{15}$ and G5-(Fl)$_6$-(Ac)$_{107}$-(cPEG[NAcGal$_\alpha$])$_{15}$ conjugates over 24 hours of incubation.

5.3.4 Opsonization of Targeted G5-(FI)$_6$-(Ac)-(cPEG) Conjugates and Phagocytosis by Kupffer Cells

Opsonization of G5-(cPEG) conjugates with and without targeting was studied following a previously published BSA binding assay[35] to monitor the quenching of the intrinsic tryptophan fluorescence signal upon binding of albumin proteins to the surface
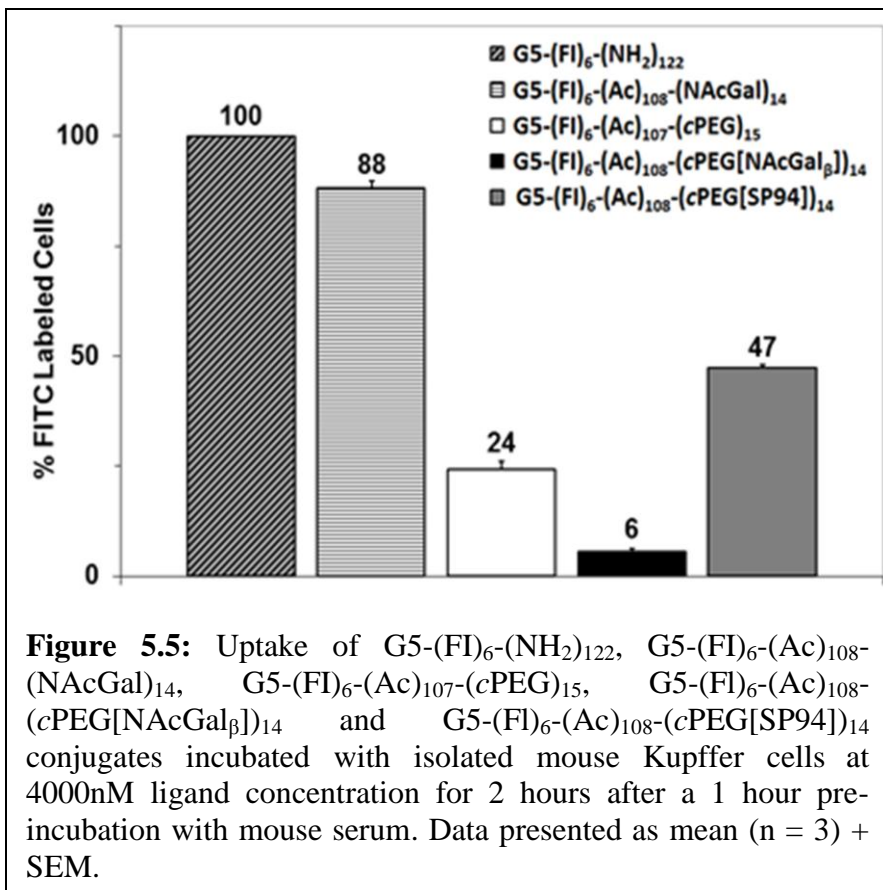
of nanoparticles. Quenching efficiency was determined as a function of particle composition and incubation time by dividing the initial BSA fluorescence signal (I_o) by the change in fluorescence intensity (I) over a 60 minute incubation period (**Figure 5.4**). Results show G5-(Fl)$_6$-(NH$_2$)$_{122}$ dendrimers, tested as the cationic polymer control, strongly quenched the BSA fluorescence indicating rapid binding of the particles to the protein, which increased sharply between 0 - 15 minutes of incubation and reached a maximum at 60 minutes. This quenching efficiency was reduced 2-fold upon incubation of BSA with G5-(Fl)$_6$-(Ac)$_{108}$-(NAcGal)$_{14}$ conjugates compared to the G5-(Fl)$_6$-(NH$_2$)$_{122}$ dendrimers, and showed a steady linear increase over the entire 60 minute incubation

Figure 5.4: Quenching efficiency of G5-(Fl)$_6$-(NH$_2$)$_{122}$, G5-(Fl)$_6$-(Ac)$_{108}$-(NAcGal)$_{14}$, G5-(Fl)$_6$-(Ac)$_{107}$-(cPEG)$_{15}$, G5-(Fl)$_6$-(Ac)$_{108}$-(cPEG[NAcGal$_\beta$])$_{14}$ and G5-(Fl)$_6$-(Ac)$_{108}$-(cPEG[SP94])$_{14}$ conjugates upon opsonization by BSA at a 20nM particle concentration with 0.2 mg/mL protein for 1 hour. Data presented as average (n = 3) ± SEM.

period. PEGylation of G5 dendrimers further inhibited opsonization with G5-$(Fl)_6$-$(Ac)_{107}$-$(cPEG)_{15}$ carriers reducing BSA binding >5-folds compared to the cationic G5-$(Fl)_6$-$(NH_2)_{122}$ dendrimers and >2-folds compared to G5-$(Fl)_6$-$(Ac)_{108}$-$(NAcGal)_{14}$ conjugates. Display of the hydrophilic NAcGal ligand for G5-$(Fl)_6$-$(Ac)_{108}$-$(cPEG[NAcGal_\beta])_{14}$ conjugates resulted in no statistical difference in BSA fluorescence quenching compared to the control solution of protein alone. Conversely, attachment of SP94 peptides ligands to the terminal end of the PEG chains increased the fluorescence quenching efficiency for G5-$(Fl)_6$-$(Ac)_{108}$-$(cPEG[SP94])_{14}$ conjugates by roughly 11% compared to G5-$(Fl)_6$-$(Ac)_{107}$-$(cPEG)_{15}$ conjugates after a 1 hour incubation with BSA proteins.

To determine the effect of particle opsonization on the recognition and phagocytosis of G5-($cPEG$) conjugates by liver macrophages each conjugate was pre-treated in mouse serum at 37 °C followed by incubation with isolated mouse Kupffer cells (**Figure 5.5**). Isolation of mouse Kupffer cells was performed by digestion of pronase perfused liver tissue, followed by a differential Percoll gradient centrifugation procedure. This protocol resulted in isolated cells which were >90% viable, and confirmed to be >80% pure for Kupffer cells via a latex bead phagocytosis assay, with endothelial and stellate cells making up the remainder of the cell population as previously described.[34] Results show the extent of G5 carrier internalization into Kupffer cells correlated to their opsonization profiles, and was a function of carrier surface composition. Specifically, 100% of treated Kupffer cells internalized pre-opsonized G5-$(Fl)_6$-$(NH_2)_{122}$ dendrimers after 2 hours of incubation as determined by flow cytometry, while G5-$(Fl)_6$-$(Ac)_{108}$-$(NAcGal)_{14}$ conjugates were phagocytized by 88% of Kupffer

cells under the same conditions. PEGylation of G5 dendrimers to prepare $G5\text{-}(Fl)_6\text{-}(Ac)_{107}\text{-}(cPEG)_{15}$ resulted in 24% of Kupffer cells internalizing these particles after a 2 hour incubation period. Coupling of hydrophilic
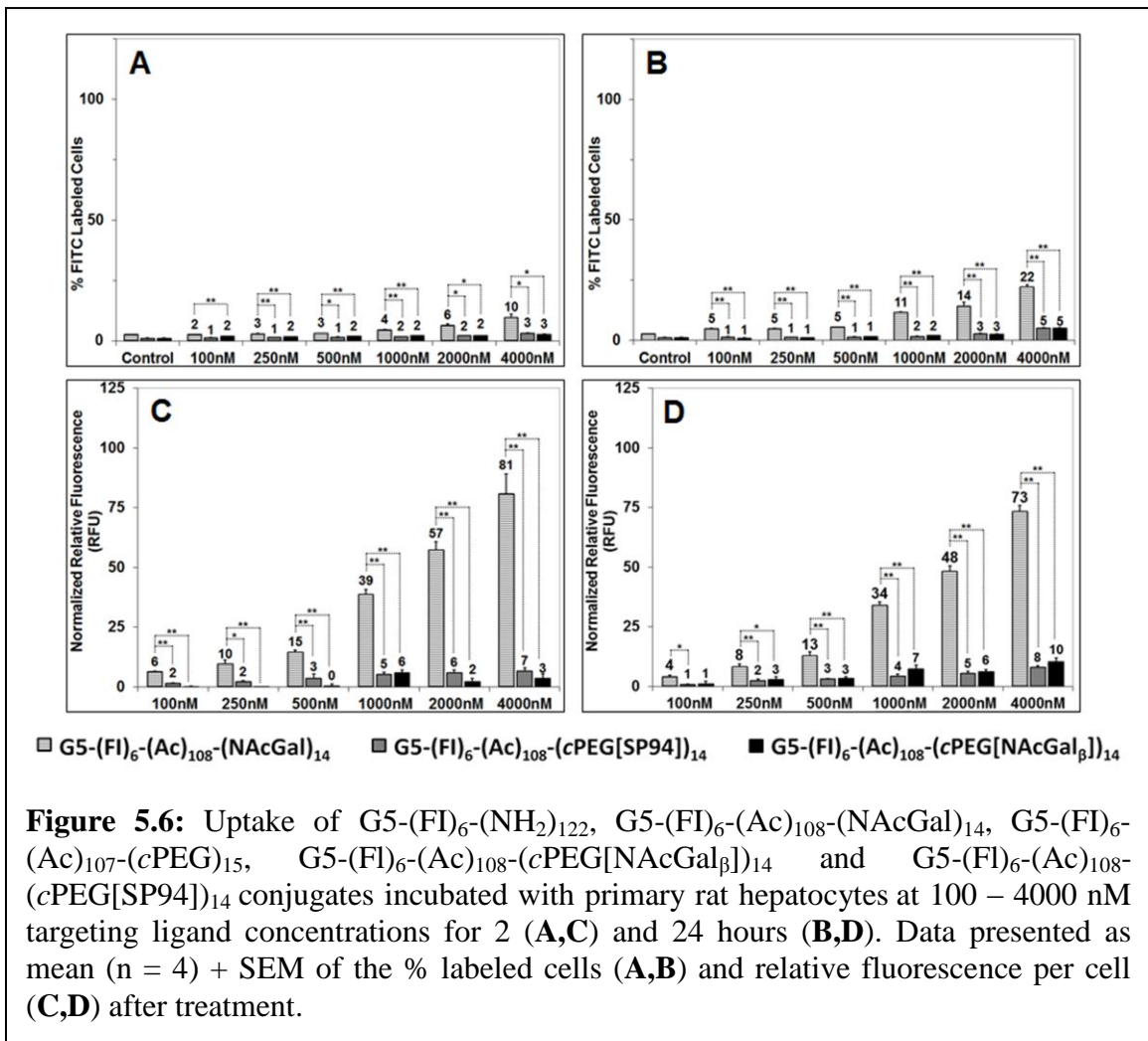

Figure 5.5: Uptake of $G5\text{-}(Fl)_6\text{-}(NH_2)_{122}$, $G5\text{-}(Fl)_6\text{-}(Ac)_{108}\text{-}(NAcGal)_{14}$, $G5\text{-}(Fl)_6\text{-}(Ac)_{107}\text{-}(cPEG)_{15}$, $G5\text{-}(Fl)_6\text{-}(Ac)_{108}\text{-}(cPEG[NAcGal_\beta])_{14}$ and $G5\text{-}(Fl)_6\text{-}(Ac)_{108}\text{-}(cPEG[SP94])_{14}$ conjugates incubated with isolated mouse Kupffer cells at 4000nM ligand concentration for 2 hours after a 1 hour pre-incubation with mouse serum. Data presented as mean (n = 3) + SEM.

NAcGal ligands to G5-(cPEG) carriers further reduced particle phagocytosis resulting in 6% of treated Kupffer cells internalizing $G5\text{-}(Fl)_6\text{-}(Ac)_{108}\text{-}(cPEG[NAcGal_\beta])_{14}$ conjugates after 2 hours of incubation, while $G5\text{-}(Fl)_6\text{-}(Ac)_{108}\text{-}(cPEG[SP94])_{14}$ conjugates were phagocytized by 47% of treated Kupffer cells under the same conditions.

5.3.5 Uptake of NAcGal- and SP94-Targeted $G5\text{-}(Fl)_6\text{-}(Ac)\text{-}(cPEG)$ Conjugates into Primary Rat Hepatocytes

To evaluate the potential for targeted G5-(cPEG) conjugates to be internalized into healthy hepatocytes each conjugate was incubated with plated rat hepatocytes and the % of treated cells showing fluorescence was determined as a function of particle

composition, ligand concentration and incubation time via flow cytometry (**Figure 5.6**; Panels **A** & **B**). For both 2 and 24 hour incubation times ≤5% of treated hepatocytes showed intracellular fluorescence after exposure to G5-(Fl)$_6$-(Ac)$_{108}$-(cPEG[SP94])$_{14}$ or G5-(Fl)$_6$-(Ac)$_{108}$-(cPEG[NAcGal$_\beta$])$_{14}$ conjugates at 100 – 4000 nM ligand concentrations (**Figure 5.6**; Panels **A** & **B**). These results were compared to the uptake of G5-(Fl)$_6$-(Ac)$_{108}$-(NAcGal)$_{14}$ conjugates to determine the effect of PEGylation on carrier internalization into normal hepatocytes. Results showed an increase in the % of labeled hepatocytes after a 2 hour incubation with G5-(Fl)$_6$-(Ac)$_{108}$-(NAcGal)$_{14}$ conjugates from 2% to 10% at the 100 nM and 4000 nM test ligand concentration, respectively (**Figure**

Figure 5.6: Uptake of G5-(Fl)$_6$-(NH$_2$)$_{122}$, G5-(Fl)$_6$-(Ac)$_{108}$-(NAcGal)$_{14}$, G5-(Fl)$_6$-(Ac)$_{107}$-(cPEG)$_{15}$, G5-(Fl)$_6$-(Ac)$_{108}$-(cPEG[NAcGal$_\beta$])$_{14}$ and G5-(Fl)$_6$-(Ac)$_{108}$-(cPEG[SP94])$_{14}$ conjugates incubated with primary rat hepatocytes at 100 – 4000 nM targeting ligand concentrations for 2 (**A,C**) and 24 hours (**B,D**). Data presented as mean (n = 4) + SEM of the % labeled cells (**A,B**) and relative fluorescence per cell (**C,D**) after treatment.

255

5.6; Panel **A**). This is a >3-fold increase in the number of hepatocytes internalizing non-PEGylated G5-(Fl)$_6$-(Ac)$_{108}$-(NAcGal)$_{14}$ conjugates compared to G5-(Fl)$_6$-(Ac)$_{108}$-(cPEG[SP94])$_{14}$ or G5-(Fl)$_6$-(Ac)$_{108}$-(cPEG[NAcGal$_\beta$])$_{14}$ carriers under identical conditions. Similarly, after a 24 hour incubation G5-(Fl)$_6$-(Ac)$_{108}$-(NAcGal)$_{14}$ treated hepatocytes showed 22% fluorescent labeling at the 4000 nM ligand concentration, while only 5% of hepatocytes internalized G5-(Fl)$_6$-(Ac)$_{108}$-(cPEG[SP94])$_{14}$ and G5-(Fl)$_6$-(Ac)$_{108}$-(cPEG[NAcGal$_\beta$])$_{14}$ conjugates at the same concentration and incubation time (**Figure 5.6**; Panel **B**).

Results were also expressed as the relative fluorescence intensity of treated hepatocytes analyzed by flow cytometry to compare the intracellular particle concentrations for each conjugate as a function of surface composition, ligand concentration and incubation time (**Figure 5.6**; Panels **C** & **D**). Results show hepatocytes incubated with G5-(Fl)$_6$-(Ac)$_{108}$-(NAcGal)$_{14}$ conjugates for 2 hours show a significant increase in the intracellular particle concentrations compared to cells treated with G5-(Fl)$_6$-(Ac)$_{108}$-(cPEG[SP94])$_{14}$ and G5-(Fl)$_6$-(Ac)$_{108}$-(cPEG[NAcGal$_\beta$])$_{14}$ conjugates under the same conditions (**Figure 5.6**; Panel **C**). Specifically, at a 500 nM ligand concentration a 5- and 15-fold increase in intracellular G5-(Fl)$_6$-(Ac)$_{108}$-(NAcGal)$_{14}$ concentration was observed in hepatocytes after a 2 hour incubation period compared to cells treated with G5-(Fl)$_6$-(Ac)$_{108}$-(cPEG[SP94])$_{14}$ and G5-(Fl)$_6$-(Ac)$_{108}$-(cPEG[NAcGal$_\beta$])$_{14}$ conjugates, respectively. This difference became greater with an increase in the ligand concentration, resulting in a 16-fold increase in intracellular particle concentration for hepatocytes incubated with G5-(Fl)$_6$-(Ac)$_{108}$-(NAcGal)$_{14}$ conjugates for 2 hours compared to the other tested carrier compositions (**Figure 5.6**; Panel **C**). A similar rank order of intracellular

carrier concentration was observed at 24 hours of incubation as a function of particle composition (**Figure 5.6**; Panel **D**), resulting in an 8-fold increase in intracellular G5-$(Fl)_6$-$(Ac)_{108}$-$(NAcGal)_{14}$ concentration in treated hepatocytes compared to cells incubated with G5-$(Fl)_6$-$(Ac)_{108}$-$(cPEG[SP94])_{14}$ and G5-$(Fl)_6$-$(Ac)_{108}$-$(cPEG[NAcGal_\beta])_{14}$ conjugates at the 2000 nM and 4000 nM ligand concentrations.

5.4   Discussion

5.4.1   Biodistribution of $[^{14}C]G5$-$(NH_2)_{127}$, $[^{14}C]G5$-$(Ac)_{108}$-$(NAcGal)_{14}$, and $[^{14}C]G5$-$(Ac)_{73}$-$(PEG)_{10}$ Conjugates in Tumor-Bearing Mice

To determine the intrinsic tumor-specific accumulation of G5 PAMAM dendrimers in our *in vivo* tumor model we studied the biodistribution of $[^{14}C]G5$-$(NH_2)_{127}$ carriers between 2 and 48 hours after administration to liver tumor-bearing mice. This resulted in a small fraction of the injected $[^{14}C]G5$-$(NH_2)_{127}$ dose distributing to tumor tissue 2 hours after administration due to EPR-mediated passive targeting,[28,36] and were retained there up to 48 hours. However, the majority of these $[^{14}C]G5$-$(NH_2)_{127}$ dendrimers were rapidly cleared by the healthy liver tissue after intravenous administration due to opsonization of the cationic PAMAM dendrimers by serum albumin,[37] which we believe led to their recognition and uptake by liver macrophage Kupffer cells. In addition, a substantial fraction (16%) of the administered $[^{14}C]G5$-$(NH_2)_{127}$ dendrimers accumulated in kidney tissue up to 48 hours after injection, which matches results from other published studies on the *in vivo* biodistribution of cationic dendrimers.[38-40] This is in contrast to linear polymers which do not readily accumulate in

renal tissue indicating the hyperbranched conformation of dendrimer carriers affects renal reabsorption and retention.[39] Previous studies have reported that G4 PAMAM-Gd complexes accumulate in the proximal straight tubules in the outer medulla stripe of the kidneys, and are localized to the lysosomes of proximal tubule cells which is only possible upon dendrimer filtration.[41] Finally, administration of $[^{14}C]G5\text{-}(NH_2)_{127}$ dendrimers to the mouse model resulted in negligible carrier distribution to the heart and bone marrow tissue for up to 48 hours after injection, which is advantageous as these are common sites of non-specific toxicity during clinical therapy using chemotherapeutic agents (e.g. Doxorubicin).[42]

We evaluated the potential of NAcGal-targeted G5 carriers to show enhanced distribution and retention in liver tumor tissue by preparing $[^{14}C]G5\text{-}(Ac)_{108}\text{-}(NAcGal)_{14}$ conjugates which contained 11 mole% NAcGal content, a loading ratio previously shown to result in selective uptake of G5-NAcGal targeted carriers into hepatic cancer cells.[24] Administration of $[^{14}C]G5\text{-}(Ac)_{108}\text{-}(NAcGal)_{14}$ conjugates to the tumor-bearing mouse model showed rapid systemic clearance of particles similar to the $[^{14}C]G5\text{-}(NH_2)_{127}$ dendrimer control. In addition, cardiac, bone marrow and kidney distribution was similar between $[^{14}C]G5\text{-}(Ac)_{108}\text{-}(NAcGal)_{14}$ conjugates and the non-targeted $[^{14}C]G5\text{-}(NH_2)_{127}$ dendrimer control. However, there was a 2-3 fold increase in the accumulation of $[^{14}C]G5\text{-}(Ac)_{108}\text{-}(NAcGal)_{14}$ conjugates in tumor tissue compared to $[^{14}C]G5\text{-}(NH_2)_{127}$ dendrimers between 2 and 48 hours after administration to liver tumor bearing mice. This is due to recognition of the displayed NAcGal ligands of the $[^{14}C]G5\text{-}(Ac)_{108}\text{-}(NAcGal)_{14}$ conjugates in the systemic circulation by the ASGPR present on the sinusoidal surface of hepatic cells,[43] resulting in rapid receptor-mediated endocytosis of the conjugates into

258

hepatic cancer cells. However, NAcGal-targeting also increased distribution of [^{14}C]G5-(Ac)$_{108}$-(NAcGal)$_{14}$ conjugates to normal liver tissue 48 hours after administration by nearly 10% of the injected dose compared to the [^{14}C]G5-(NH$_2$)$_{127}$ controls. This is due to recognition of the displayed NAcGal ligands by the ASGPR present on the surface of normal hepatocytes,[43] as well as the related galactose-receptor of liver macrophage Kupffer cells.[27] These results are similar to the behavior of galactosamine (Gal) targeted polymer nanoparticles after i.v. administration to *in vivo* tumor models.[44,45] Specifically, Gal-targeted poly(γ-glutamic acid) and poly(lactide) co-polymer conjugates displayed a >3-fold increase in particle concentration in normal liver tissue compared to the tumor between 1-24 hours after i.v. administration to a hepatoma-bearing nude mouse model.[44] Similarly, i.v. injection of ^{123}I-labeled Gal-functionalized HPMA-DOX conjugates to a liver-tumor bearing mouse metastatic model resulted in a roughly 8-fold increase in the % of the injected dose of the particle accumulating per gram of normal liver tissue versus the tumor 1 hour after injection.[45] This led to Gal-targeted HPMA-DOX conjugates displaying a 5-fold increase in distribution to the healthy liver compared to tumor tissue in three hepatoma patients during phase I clinical trials.[46]

The recognition of nanoparticles by the RES system and their non-specific clearance to healthy liver tissue can be minimized via attachment of PEG chains ≥2 kDa in size to the carrier surface, resulting in reduced opsonization of the particles in the systemic circulation and subsequently limiting clearance by hepatic macrophages.[22,47-49] As a result we synthesized [^{14}C]G5-(Ac)$_{73}$-(PEG)$_{10}$ conjugates possessing an average of 10 PEG chains per dendrimer, which after i.v. administration to liver tumor-bearing mice resulted in a >4-fold reduction in hepatic clearance of the conjugates between 2 and 48

hours compared to $[^{14}C]G5$-$(NH_2)_{127}$ and $[^{14}C]G5$-$(Ac)_{108}$-$(NAcGal)_{14}$ carriers. This reduced distribution to normal liver tissue, and a >5-fold reduction in kidney distribution of the particle between 2 and 48 hours relative to $[^{14}C]G5$-$(NH_2)_{127}$ and $[^{14}C]G5$-$(Ac)_{108}$-$(NAcGal)_{14}$ conjugates, resulted in a 16-fold increase in plasma circulation time of $[^{14}C]G5$-$(Ac)_{73}$-$(PEG)_{10}$ conjugates compared to the other tested carriers. This biodistribution profile is a result of increased MW weight and particle hydrodynamic radius of the PEGylated dendrimer carrier due to attachment of the PEG moieties which leads to decreased renal filtration and as a result longer residence in the systemic circulation.[50] This supports previous studies which found that attachment of 2kDa PEG to G4 PAMAM-NH_2 dendrimers resulted in a >8-fold reduction of the % of the injected dose distributing to kidney per gram of tissue weight compared to the non-PEGylated carrier 24 hours after administration.[51] Interestingly, this increase in plasma circulation time and limited distribution to non-specific RES organs for $[^{14}C]G5$-$(Ac)_{73}$-$(PEG)_{10}$ conjugates did not significantly improve tumor specific delivery compared to $[^{14}C]G5$-$(Ac)_{108}$-$(NAcGal)_{14}$ and $[^{14}C]G5$-$(NH_2)_{127}$ carriers between 2 and 24 hours after administration. Okuda et al. previously showed that G6 lysine dendrimers (with a similar size and number of surface NH_2 groups to G5 PAMAM dendrimers utilized in this study) functionalized with 76 PEG groups (5 kDa MW) showed a 2-6 fold increase in tumor distribution compared to the non-PEGylated parent dendrimers between 3 and 24 hours after intravenous administration to a colon carcinoma xenograft mouse model.[52] This was due to the large increase in MW as a result of coupling 76 PEG groups to the carrier surface increasing its MW by 380 kDa. The $[^{14}C]G5$-$(Ac)_{73}$-$(PEG)_{10}$ conjugates utilized in this study were prepared with 10 PEG groups, resulting in a gain of 20 kDa which may

not have been sufficient to enhance tumor-specific accumulation. However, this PEGylation density was designed to ensure the conjugates were below the renal excretion limit (~50 kDa) in order to prevent long term residence of the carrier in the body leading to systemic toxicity.[50,53] In addition, it is advantageous to limit the number of PEG groups attached to the surface of dendrimer carriers for the delivery of chemotherapeutic agents to limit steric crowding and maximize the payload of conjugated anticancer drugs.[54] Finally, at 48 hours <1% of the injected dose was detected in the tumor indicating that $[^{14}C]G5$-$(Ac)_{73}$-$(PEG)_{10}$ conjugates are washed out of tumor tissue at long biodistribution times.

These results suggest that while PEGylation of G5 dendrimers decreases non-specific liver distribution and increases plasma-residence time of the G5 carrier, display of an active targeting ligand is necessary for long term carrier residence in tumor tissue. This is supported by previous reports which show that coupling of folate-ligands to the terminal end of a PEGylated Gd nanoparticle resulted in improved tumor retention of the targeted imaging agents compared to non-targeted Gd-PEG particles between 8 and 24 hours after administration to a folate-receptor positive tumor xenograft mouse model.[55] As a result we synthesized a second generation G5 carrier incorporating PEG 'brushes' coupled to the dendrimer surface via acid-sensitive *cis*-aconityl linkages, which display an NAcGal sugar or SP94 peptide targeting ligand at the terminal PEG end to achieve selective delivery of these carriers to hepatic cancer cells while avoiding internalization into normal liver Kupffer cells and hepatocytes

5.4.2 Synthesis and Characterization of Targeted G5-(FI)$_6$-(Ac)-(cPEG) Conjugates

To combine the stealth ability of PEGylated G5 with the tumor targeting attained by NAcGal coupling we designed targeted G5-PEG carriers to achieve selective delivery of these nanoparticles to hepatic cancer cells. Targeted G5-PEG conjugates were synthesized via attachment of NAcGal ligands, or the recently reported SP94 hepatic cancer-cell specific peptide,[26] to 2kDa PEG chains which were subsequently covalently linked to the surface amine groups of G5 dendrimers via acid-sensitive *cis*-aconityl linkages. This pH-sensitive coupling strategy has been employed previously for the covalent attachment of chemotherapeutic agents to a polymer backbone, resulting in selective drug release to the acidic tumor microenvironment or within the endosomes and lysosomes of cancer cells.[4] We incorporated these acid-sensitive linkers into targeted G5-(cPEG) conjugates to achieve 'shedding' of the PEG corona after endocytosis which has been shown to reduce the sterically crowded surface of PEGylated carriers and allow for effective drug release.[32] Furthermore, liberation of the coupled PEG chains will reduce the molecular weight of the carrier below the renal excretion limit (~50 kDa) and allow for its secretion in the urine.[50,53] To test the PEG release rate from G5-(cPEG) carriers in acidic conditions we incubated G5-(FI)$_6$-(Ac)$_{107}$-(cPEG)$_{15}$ conjugates in pH 5.0 buffer at 37 °C, resulting in a near complete release of the loaded PEG from the G5 carrier surface within 24 hours (**Appendix Figure S26**). The PEG release half-life was calculated as $t_{1/2}$ = 5.20 hours, which is similar to release kinetics from DOX-poly(L-lactic acid)-PEG micelles in which DOX molecules were conjugated to the polymer backbone via *cis*-aconityl linkages resulting in a drug release half-life of 5 hours in pH 5.0 PBS.[56] No free

PEG was detected by GPC analysis during the 24 hour incubation period of G5-(Fl)$_6$-(Ac)$_{107}$-(cPEG)$_{15}$ at pH 7.4, demonstrating the stability of these conjugates in normal physiologic conditions while achieving pH-sensitive PEG release after delivery to the endosome.

All targeted G5-(cPEG) conjugates were characterized for particle size, surface charge and molecular weight by dynamic light scattering, zeta potential measurements, and MALDI-TOF analysis, respectively. Coupling of 2kDa PEG increased the particle size of G5-(Fl)-(Ac) dendrimers previously reported at 5.00 nm[24] to 7.37 nm for G5-(Fl)$_6$-(Ac)$_{107}$-(cPEG)$_{15}$ conjugates (**Table 5.1**). An increase of $0.36 - 0.66$ nm was observed for G5-(Fl)$_6$-(Ac)$_{107}$-(cPEG[NAcGal$_\alpha$])$_{15}$ and G5-(Fl)$_6$-(Ac)$_{108}$-(cPEG[NAcGal$_\beta$])$_{14}$ conjugates compared to the non-targeted G5-(Fl)$_6$-(Ac)$_{107}$-(cPEG)$_{15}$ carriers due to the addition of the NAcGal targeting ligand. Similarly, G5-(Fl)$_6$-(Ac)$_{108}$-(cPEG[SP94])$_{14}$ particles had a 2.54 nm increase in particle size compared to the G5-(Fl)$_6$-(Ac)$_{107}$-(cPEG)$_{15}$ control due to the addition of the large 12-amino acid SP94-peptide. PEGylation of the G5 carriers also led to a corresponding increase in carrier molecular weight, which was further increased due to the addition of NAcGal sugars or SP94 peptides. As a result G5-(Fl)$_6$-(Ac)$_{107}$-(cPEG)$_{15,}$ G5-(Fl)$_6$-(Ac)$_{107}$-(cPEG[NAcGal$_\alpha$])$_{15}$ and G5-(Fl)$_6$-(Ac)$_{108}$-(cPEG[NAcGal$_\beta$])$_{14}$ conjugates had neutral surface charge due to the complete functionalization of the dendrimer surface amine with neutral PEG and acetyl groups, while G5-(Fl)$_6$-(Ac)$_{108}$-(cPEG[SP94])$_{14}$ conjugates had a slightly negative charge due to the carboxylic acid group present on the SP94 peptide cysteine residue which has a pKa of ~3.5.[57]

5.4.3 Uptake of NAcGal- and SP94-Targeted G5-(Fl)$_6$-(Ac)-(cPEG) Conjugates into Hepatic Cancer Cells

The effect of ligand type on the internalization of targeted G5-(cPEG) carriers into hepatic cancer cells was evaluated as the % of treated HepG2 cells which internalized the conjugates, as well as the relative intracellular particle concentration, as a function of carrier composition, ligand concentration and incubation time. Incubation of HepG2 cells with G5-(Fl)$_6$-(Ac)$_{107}$-(cPEG)$_{15}$ conjugates showed limited internalization and low intracellular concentrations of the particles into tested cells across all ligand concentrations and incubation times. This is due the reported steric inhibition of PEGylated carriers from interacting with the cell membrane and therefore reduces carrier internalization; an effect described as the 'PEG dilemma'.[58] To address this we displayed the NAcGal or SP94 targeting ligand at the terminal end of the PEG chains to achieve receptor-mediated endocytosis of the targeted G5-(cPEG) conjugates into hepatic cancer cells. Interestingly, limited internalization and low intracellular particle concentrations of G5-(Fl)$_6$-(Ac)$_{108}$-(cPEG[SP94])$_{14}$ treated HepG2 cells was observed for all tested ligand concentrations after 2 hours of incubation, and was comparable to the non-targeted G5-(Fl)$_6$-(Ac)$_{107}$-(cPEG)$_{15}$ control. However, internalization of G5-(Fl)$_6$-(Ac)$_{108}$-(cPEG[SP94])$_{14}$ conjugates into HepG2 cells substantially increased after 24 hours of incubation with up to a 19-fold enhancement in the intracellular particle concentration between the two time points studied. These results suggest a significant lag-time between extracellular delivery of G5-(Fl)$_6$-(Ac)$_{108}$-(cPEG[SP94])$_{14}$ conjugates and internalization into hepatic cancer cells, which was not observed during previous studies using hyperspectral confocal fluorescent microscopy analysis to visualize the internalization of

264

fluorescent SP94-targeted nanoporous particles into Hep3B human hepatic cancer cells.[59] This study found binding, internalization and trafficking of the SP94-targeted nanoparticles to the endosome occurred within 15 minutes after incubation with Hep3B cells at 37 °C. The difference of these results to our uptake data may be due to reduced expression or lower affinity of the target receptor (which currently has not been identified) to the SP94 peptide for HepG2 cells utilized in this study as compared to the Hep3B cell line. This is supported by a published report by Lo et al. who showed a 25% reduction in labeling of HepG2 cells versus the Hep3B cell line after incubation with SP94 peptides for 1 hour, followed by staining with fluorescent anti-mouse IgG and analysis by flow cytometry.[26]

Incubation of HepG2 cells with $G5-(Fl)_6-(Ac)_{107}-(cPEG[NAcGal_\alpha])_{15}$ and $G5-(Fl)_6-(Ac)_{108}-(cPEG[NAcGal_\beta])_{14}$ conjugates showed a significant difference in internalization as a function of NAcGal sugar conformation as expected. Specifically, attachment of $NAcGal_\beta$-sugar molecules to prepare $G5-(Fl)_6-(Ac)_{108}-(cPEG[NAcGal_\beta])_{14}$ conjugates resulted in a substantial increase in HepG2 particle internalization compared to $NAcGal_\alpha$-targeted carriers after 2 and 24 hours of incubation. This led to a corresponding increase in relative intracellular $G5-(Fl)_6-(Ac)_{108}-(cPEG[NAcGal_\beta])_{14}$ concentration compared to $G5-(Fl)_6-(Ac)_{107}-(cPEG[NAcGal_\alpha])_{15}$ conjugates, resulting in a >5-fold difference after 24 hours of incubation. This is due to the specific recognition of sugars in the β-conformation by the ASGPR expressed on hepatic cells as reported in the literature.[27] Furthermore, the limited internalization of $G5-(Fl)_6-(Ac)_{107}-(cPEG[NAcGal_\alpha])_{15}$ conjugates into HepG2 cells confirms that uptake of $G5-(Fl)_6-(Ac)_{108}-(cPEG[NAcGal_\beta])_{14}$ into hepatic cancer cells is mediated by binding of the

displayed NAcGal by the ASGPR leading to receptor-mediated endocytosis. Finally, the substantial increase in fluorescent labeling and intracellular particle concentrations of HepG2 cells treated with G5-(Fl)$_6$-(Ac)$_{108}$-(cPEG[NAcGal$_\beta$])$_{14}$ conjugates as compared to G5-(Fl)$_6$-(Ac)$_{108}$-(cPEG[SP94])$_{14}$ for all tested ligand concentrations and incubation times suggests that receptor-mediated endocytosis of the particles into hepatic cancer cells via the ASGPR is more rapid than SP94-receptor mediated internalization. Based on these results G5-(Fl)$_6$-(Ac)$_{108}$-(cPEG[NAcGal$_\beta$])$_{14}$ was identified as the optimal carrier composition to achieve rapid and cell-specific internalization of G5 dendrimers into hepatic cancer cells.

5.4.4 Opsonization of Targeted G5-(cPEG) Conjugates and Phagocytosis by Kupffer Cells

The potential of targeted G5-(cPEG) conjugates to be opsonized within the systemic circulation was evaluated using a bovine serum albumin (BSA) fluorescence quenching assay. Serum albumins were selected as a model protein for opsonization studies as they are the major component of soluble protein blood fractions,[8] and has been widely utilized to monitor protein binding to nanoparticles.[7,35] The BSA fluorescence quenching assay relies on the instrinsic fluorescence of two tryptophan residues located within hydrophobic biding pocket of bovine serum albumin which show a decrease in the quantum yield of fluorescence due to a variety of molecular interaction with PAMAM dendrimer quenchers including particle complexation and change in local hydrophobicity.[60] Co-incubation of BSA proteins with cationic G5-(Fl)$_6$-(NH$_2$)$_{122}$ dendrimers resulted in a strong quenching of the BSA tryptophan residues within 15

minutes indicating rapid binding of the protein to the dendrimer surface. The binding affinity of BSA to PAMAM dendrimers has been previously reported to be a result of hydrophilic complexation of the protein with the polycationic dendrimer surface, as well as interaction of the dendrimers aliphatic chains with the protein hydrophobic binding pocket.[60] This quenching efficiency is reduced by neutralizing the dendrimer surface with hydrophilic acetyl groups and NAcGal-sugar moieties, indicated by a 2-fold reduction in BSA binding to $G5\text{-}(Fl)_6\text{-}(Ac)_{108}\text{-}(NAcGal)_{14}$ conjugates compared to $G5\text{-}(Fl)_6\text{-}(NH_2)_{122}$ dendrimers. Attachment of PEG groups to the dendrimer surface showed the most significant reduction in BSA binding affinity resulting in >5-fold reduction in protein fluorescence quenching in the presence of $G5\text{-}(Fl)_6\text{-}(Ac)_{107}\text{-}(cPEG)_{15}$ particles compared to the $G5\text{-}(Fl)_6\text{-}(NH_2)_{122}$ dendrimer control. This ability of PEG to reduce opsonization of polymeric nanoparticles is well established, resulting from a steric repulsion of proteins from the polymer surface by the hydrophilic PEG corona.[47] Moreover, display of hydrophilic NAcGal sugar residues on the terminus of PEG chains for $G5\text{-}(Fl)_6\text{-}(Ac)_{108}\text{-}(cPEG[NAcGal_\beta])_{14}$ conjugates virtually eliminated protein binding by further reducing any remaining hydrophobic interaction of carrier with BSA proteins. Conversely, attachment of hydrophobic SP94 peptides increased $G5\text{-}(Fl)_6\text{-}(Ac)_{108}\text{-}(cPEG[SP94])_{14}$ opsonization by BSA proteins compared to the $G5\text{-}(Fl)_6\text{-}(Ac)_{107}\text{-}(cPEG)_{15}$ control due to the hydrophobic nature of the leucine- and isoleucine-rich peptide.

To correlate these opsonization profiles of targeted G5-(cPEG) carriers with their potential recognition and clearance by hepatic macrophages, conjugates were incubated with isolated mouse Kupffer cells for 2 hours after a pre-treatment in mouse serum for 1 hour, and uptake quantified by flow cytometry (**Figure 5.5**). As expected the cationic G5-

(Fl)$_6$-(NH$_2$)$_{122}$ dendrimers were readily phagocytosed by Kupffer cells due to their extensive opsonization (**Figure 5.4**), resulting in saturation of 100% of the treated cells after 2 hours of incubation. G5-(Fl)$_6$-(Ac)$_{108}$-(NAcGal)$_{14}$ conjugates were also rapidly phagocytized by Kupffer cells which is a result of significant BSA opsonization, as well as recognition of displayed NAcGal-moieties by the galactose receptor present on Kupffer cells.[61] Specifically, published reports have shown that short chemical spacers (≤4Å) separating galactose moieties from its glycoside branching point resulted in their recognition by the related macrophage receptor on liver Kupffer cells.[61,62] However, these same studies demonstrated that long chemical spacers (>20Å) resulted in selective internalization of the extended glycoside by the hepatocyte-specific ASGPR. The distance between NAcGal-ligands and the dendrimer surface for the G5-(Fl)$_6$-(Ac)$_{108}$-(NAcGal)$_{14}$ conjugates utilized in this study was calculated to be roughly 8-9Å via ChemDraw software chemical analysis, suggesting significant contribution of receptor-mediated endocytosis to G5-(Fl)$_6$-(Ac)$_{108}$-(NAcGal)$_{14}$ internalization into Kupffer cells. By coupling 2 kDa PEG groups to the surface of G5 dendrimers G5-(Fl)$_6$-(Ac)$_{107}$-(cPEG)$_{15}$ carriers showed significant reduction in Kupffer cells phagocytosis compared to the non-PEGylated G5-(Fl)$_6$-(NH$_2$)$_{122}$ dendrimers and G5-(Fl)$_6$-(Ac)$_{108}$-(NAcGal)$_{14}$ conjugates. This confirms the ability of PEGylated G5 dendrimers to avoid phagocytosis by liver macrophages due to reduced opsonization in the presence of serum albumins. In addition, the enhanced hydropholicity of NAcGal-targeted G5-(Fl)$_6$-(Ac)$_{108}$-(cPEG[NAcGal$_\beta$])$_{14}$ conjugates further inhibited opsonization and as a result showed reduced carrier phagocytosis by Kupffer cells compared to G5-(Fl)$_6$-(Ac)$_{107}$-(cPEG)$_{15}$ conjugates. Moreover, the extension of the displayed NAcGal-ligands well beyond the

20Å spacer length reported to shift glycoside specificity towards the ASGPR[61,62] further prevented recognition of G5-(Fl)$_6$-(Ac)$_{108}$-(cPEG[NAcGal$_\beta$])$_{14}$ conjugates by the galactose-receptor of liver Kupffer cells. Finally, incubation of Kupffer cells with G5-(Fl)$_6$-(Ac)$_{108}$-(cPEG[SP94])$_{14}$ conjugates showed almost a 2-fold increase in phagocytosis compared to G5-(Fl)$_6$-(Ac)$_{107}$-(cPEG)$_{15}$ conjugates after the 2 hour incubation period. Interestingly, only a 12% increase in protein binding to G5-(Fl)$_6$-(Ac)$_{108}$-(cPEG[SP94])$_{14}$ conjugates compared to the BSA control was observed during opsonization experiments. This suggests internalization of opsonized G5-(Fl)$_6$-(Ac)$_{107}$-(cPEG)$_{15}$ conjugates into Kupffer cells may be enhanced by hydrophobic interactions of the particle with the liver macophages, or potential contribution of a receptor-mediated internalization pathway for SP94-peptides in Kupffer cells that is not yet identified.

5.4.5 Selectivity of NAcGal- and SP94-Targeted G5-(Fl)$_6$-(Ac)-(cPEG) Conjugates

To evaluate the ability of targeted G5-(cPEG) conjugates to be selectively internalized into hepatic cancer cells their uptake into primary rat hepatocytes was studied as a function of particle composition, ligand concentration and incubation time. Results showed limited internalization of G5-(Fl)$_6$-(Ac)$_{108}$-(cPEG[SP94])$_{14}$ and G5-(Fl)$_6$-(Ac)$_{108}$-(cPEG[NAcGal$_\beta$])$_{14}$ conjugates into primary rat hepatocytes with ≤5% of hepatocytes fluorescently labeled after exposure with G5-(Fl)$_6$-(Ac)$_{108}$-(cPEG[SP94])$_{14}$ and G5-(Fl)$_6$-(Ac)$_{108}$-(cPEG[NAcGal$_\beta$])$_{14}$ conjugates for 2 and 24 hours at the 100 – 4,000 nM tested ligand concentrations. For G5-(Fl)$_6$-(Ac)$_{108}$-(cPEG[NAcGal$_\beta$])$_{14}$ conjugates this represents a >30-fold increase in affinity for particle internalization into HepG2 hepatic cancer cell (**Figure 5.3**; Panel **A**) over hepatocytes (**Figure 5.6**; Panel **A**)

269

after 2 hours of incubation. Moreover, at 24 hours there was almost a 50-fold enhancement in the % of labeled HepG2 cells (**Figure 5.3**; Panel **B**) and 7-fold increase in intracellular particle concentrations (**Figure 5.3**; Panel **D**) after incubation with G5-$(Fl)_6$-$(Ac)_{108}$-$(cPEG[NAcGal_\beta])_{14}$ conjugates at a 1000 nM ligand concentration compared to hepatocytes treated under the same conditions (**Figure 5.6**; Panel **B** & **D**). These results are in spite of reports indicating that cell surface expression of ASGPR and its sugar binding kinetics are similar between HepG2 hepatic cancer cells and isolated rat hepatocytes.[25] However, the recycle time of extracellularly displayed ASGPR on HepG2 cells is reported to occur every 15.9 minutes after ligand binding,[63] while the receptor turnover rate for rat hepatocytes is approximately 20 hours.[64] As a result the ASGPR expressed on the surface of HepG2 cells are able to recycle a bound receptor approximately 75-times faster than hepatocytes, which explains the enhanced uptake of G5-$(Fl)_6$-$(Ac)_{108}$-$(cPEG[NAcGal_\beta])_{14}$ conjugates into hepatic cancer cells versus normal hepatocytes as a function of time.

The increased % of labeled hepatocytes and intracellular particle concentration for cells treated with G5-$(Fl)_6$-$(Ac)_{108}$-$(NAcGal)_{14}$ conjugates compared to G5-$(Fl)_6$-$(Ac)_{108}$-$(cPEG[NAcGal_\beta])_{14}$ at both 2 and 24 hour incubation times is likely due to the smaller size and molecular weight of G5-$(Fl)_6$-$(Ac)_{108}$-$(NAcGal)_{14}$ versus the PEGylated G5-$(Fl)_6$-$(Ac)_{108}$-$(cPEG[NAcGal_\beta])_{14}$ conjugates. Specifically, we have previously shown G5-$(Fl)_6$-$(Ac)_{108}$-$(NAcGal)_{14}$ conjugates have an average particle size of 6.02 nm and molecular weight of 39.5 kDa,[24] while in this report we have characterized G5-$(Fl)_6$-$(Ac)_{108}$-$(cPEG[NAcGal_\beta])_{14}$ conjugate particle size and molecular weight as 8.03 nm and 73.1kDa, respectively. The reduction in endocytosis of polymeric nanoparticles as a

function of increasing particle size and molecular weight is well established in the literature for a variety of cell types,[65,66] and is due to an increase in the entropic penalty of endosome formation as a result of increased particle size and mass.[66]

Interestingly, there was a slight decline in the intracellular G5-(Fl)$_6$-(Ac)$_{108}$-(NAcGal)$_{14}$ concentration observed in hepatocytes incubated for 2 (**Figure 5.6**; Panel **C**) and 24 (**Figure 5.6**; Panel **D**) hours despite a >2-fold increase in the % of labeled hepatocytes under the same conditions (**Figure 5.6**; Panel **A** & **B**). G5-(Fl)$_6$-(Ac)$_{108}$-(cPEG[NAcGal$_\beta$])$_{14}$ conjugates, however, showed a doubling of the intracellular particle concentration in hepatocytes between the 2 and 24 hour incubation periods. This suggests that at long incubation times internalized G5-(Fl)$_6$-(Ac)$_{108}$-(NAcGal)$_{14}$ conjugates may be exocytosed out of the hepatocytes, while the large molecular weight of G5-(Fl)$_6$-(Ac)$_{108}$-(cPEG[NAcGal$_\beta$])$_{14}$ conjugates inhibited their exocytosis after internalization. Intracellular concentrations of G5-(Fl)$_6$-(Ac)$_{108}$-(cPEG[SP94])$_{14}$ conjugates in hepatocytes showed similar values across all tested ligand concentration and incubation times, indicating no affinity of these conjugates for receptor-mediated endocytosis into hepatocytes.

5.5   Conclusion

Utilizing an orthotopic liver tumor mouse model we have shown that coupling of NAcGal ligands to the surface of G5 dendrimers enhances their delivery and retention in liver tumor tissue, while confirming the stealth properties of surface PEGylation results in their escape from hepatic clearance. Based on these results we synthesized targeted G5-(cPEG) carriers to achieve cell-specific drug delivery to the cytoplasm of hepatic

cancer cells while avoiding non-specific internalization into normal liver macrophages and hepatocytes. To accomplish this we coupled NAcGal sugar or SP94 peptide targeting ligands to PEG chains attached to the surface of G5 carriers through acid-sensitive *cis*-aconityl linkages. G5-(*c*PEG) conjugates were found to be stable in physiologic conditions, while efficiently releasing the attached PEG chains in the acidic endosomal environment after receptor-mediated endocytosis. Display of an NAcGal sugar ligand at the terminal end of PEG chains incorporated into G5-(FI)-(Ac)-(cPEG[NAcGal]) conjugates resulted in rapid binding of the carrier to the ASGPR and subsequent receptor-mediated endocytosis into hepatic cancer cells, confirmed to be highly selective for displayed NAcGal sugars in the β-conformation. G5-(FI)-(Ac)-(cPEG[NAcGal$_\beta$]) conjugates were also found to be more rapidly internalized into hepatic cancer cells compared to G5-(FI)$_6$-(Ac)-(*c*PEG[SP94]) conjugates which displayed the hepatic cancer cell-specific SP94 peptide. Furthermore, G5-(FI)-(Ac)-(*c*PEG[NAcGal$_\beta$]) conjugates showed up to a 50-fold enhancement in affinity for HepG2 hepatic cancer cells over normal liver hepatocytes. The coupling of PEG chains to the surface of G5 dendrimers was shown to reduce particle opsonization during a serum albumin binding assay, resulting in their limit phagocytosis by liver macrophage Kupffer cells compared to non-PEGylated dendrimer controls. These results clearly show that G5-(FI)-(Ac)-(*c*PEG[NAcGal$_\beta$]) conjugates are a highly efficient carrier for selective delivery of therapeutic molecules to the cytoplasm of hepatic cancer cells to achieve high anticancer activity while avoiding opsonization in the systemic circulation, escaping clearance by macrophages and limiting non-specific toxicity.

Acknowledgements

References

1   Gillies, E. R. & Fréchet, J. M. J. Dendrimers and dendritic polymers in drug delivery. *Drug Discov. Today* **10**, 35-43 (2005).

2   Tomalia, D. A., Reyna, L. A. & Svenson, S. Dendrimers as multi-purpose nanodevices for oncology drug delivery and diagnostic imaging. *Biochem. Soc. Trans.* **035**, 61-67 (2007).

3   Medina, S. H. & El-Sayed, M. E. H. Dendrimers as carriers for delivery of chemotherapeutic agents. *Chem. Rev.* **109**, 3141-3157 (2009).

4   Ulbrich, K. & Šubr, V. r. Polymeric anticancer drugs with pH-controlled activation. *Adv. Drug Deliver. Rev.* **56**, 1023-1050 (2004).

5   Kono, K. *et al.* Preparation and cytotoxic activity of poly(ethylene glycol)-modified poly(amidoamine) dendrimers bearing adriamycin. *Polymer* **29**, 1664 (2008).

6   Majoros, I. J., Myc, A., Thomas, T., Mehta, C. B. & Baker, J. R. PAMAM dendrimer-based multifunctional conjugate for cancer therapy: synthesis, characterization, and functionality. *Biomacromolecules* **7**, 572-579 (2006).

7   Klajnert, B. & Bryszewska, M. Fluorescence studies on PAMAM dendrimers interactions with bovine serum albumin. *Bioelectrochemistry* **55**, 33-35 (2002).

8   Kragh-Hansen, U. Structure and ligand binding properties of human serum albumin. *Dan. Med. Bull.* **37**, 57-84 (1990).

9   Choi, S. K. *et al.* Photochemical release of methotrexate from folate receptor-targeting PAMAM dendrimer nanoconjugate. *Photoch. Photobio. Sci.* (2012).

10   Quintana, A. *et al.* Design and function of a dendrimer-based therapeutic nanodevice targeted to tumor cells through the folate receptor. *Pharm. Res.* **19**, 1310-1316 (2002).

11   Wang, Y. *et al.* Targeted delivery of doxorubicin into cancer cells using a folic acid-dendrimer conjugate. *Polym. Chem.* **2** (2011).

12   Patri, A. K. *et al.* Synthesis and in vitro testing of J591 antibody−dendrimer conjugates for targeted prostate cancer therapy. *Bioconjugate Chem.* **15**, 1174-1181 (2004).

13   Shukla, R. *et al.* HER2 specific tumor targeting with dendrimer conjugated anti-HER2 mAb. *Bioconjugate Chem.* **17**, 1109-1115 (2006).

14   Thomas, T. P. *et al.* In vitro targeting of synthesized antibody-conjugated dendrimer nanoparticles. *Biomacromolecules* **5**, 2269-2274 (2004).

15   Boswell, C. A. *et al.* Synthesis, characterization, and biological evaluation of integrin αvβ3-targeted PAMAM dendrimers. *Mol. Pharm.* **5**, 527-539 (2008).

16   Lesniak, W. G. *et al.* Synthesis and characterization of PAMAM dendrimer-based multifunctional nanodevices for targeting αvβ3 integrins. *Bioconjugate Chem.* **18**, 1148-1154 (2007).

17   Shukla, R. *et al.* Tumor angiogenic vasculature targeting with PAMAM dendrimer-RGD conjugates. *Chem. Commun.*, 5739-5741 (2005).

18   Shukla, S. *et al.* Synthesis and biological evaluation of folate receptor-targeted boronated PAMAM dendrimers as potential agents for neutron capture therapy. *Bioconjugate Chem.* **14**, 158-167 (2002).

19   Aillon, K. L., Xie, Y., El-Gendy, N., Berkland, C. J. & Forrest, M. L. Effects of nanomaterial physicochemical properties on in vivo toxicity. *Adv. Drug Deliver. Rev.* **61**, 457-466 (2009).

20   Chauhan, A. S., Jain, N. K. & Diwan, P. V. Pre-clinical and behavioural toxicity profile of PAMAM dendrimers in mice. *P. Roy. Soc. A-Math. Phy.* (2009).

21   Greish, K. *et al.* Size and surface charge significantly influence the toxicity of silica and dendritic nanoparticles. *Nanotoxicology* **28**, 1-11 (2011).

22   Kaminskas, L. M. & Boyd, B. J. in *Intracellular Delivery* Vol. 5 *Fundamental Biomedical Technologies* (ed Aleš Prokop) 155-178 (Springer Netherlands, 2011).

23   Jain, K., Kesharwani, P., Gupta, U. & Jain, N. K. Dendrimer toxicity: Let's meet the challenge. *Int. J. Pharm.* **394**, 122-142 (2010).

24   Medina, S. H. *et al.* N-acetylgalactosamine-functionalized dendrimers as hepatic cancer cell-targeted carriers. *Biomaterials* **32**, 4118-4129 (2011).

25   Schwartz, A., Fridovich, S., Knowles, B. & Lodish, H. Characterization of the asialoglycoprotein receptor in a continuous hepatoma line. *J. Biol. Chem.* **256**, 8878-8881 (1981).

26   Lo, A., Lin, C.-T. & Wu, H.-C. Hepatocellular carcinoma cell-specific peptide ligand for targeted drug delivery. *Mol. Cancer Ther.* **7**, 579-589 (2008).

27   Khorev, O., Stokmaier, D., Schwardt, O., Cutting, B. & Ernst, B. Trivalent, Gal/GalNAc-containing ligands designed for the asialoglycoprotein receptor. *Bioorgan. Med. Chem* **16**, 5216-5231 (2008).

28   Maeda, H., Bharate, G. Y. & Daruwalla, J. Polymeric drugs for efficient tumor-targeted drug delivery based on EPR-effect. *Eur. J. Pharm. Biopharm.* **71**, 409-419 (2009).

29   Torchilin, V. P. Recent advances with liposomes as pharmaceutical carriers. *Nat. Rev. Drug Discov.* **4**, 145-160 (2005).

30   Cerritelli, S., Velluto, D. & Hubbell, J. A. PEG-SS-PPS: reduction-sensitive disulfide block copolymer vesicles for intracellular drug delivery. *Biomacromolecules* **8**, 1966-1972 (2007).

31   Takae, S. *et al.* PEG-detachable polyplex micelles based on disulfide-linked block catiomers as bioresponsive nonviral gene vectors. *J. Am. Chem. Soc.* **130**, 6001-6009 (2008).

32   Romberg, B., Hennink, W. & Storm, G. Sheddable coatings for long-circulating nanoparticles. *Pharm. Res.* **25**, 55-71 (2008).

33   Tomayko, M. M. & Reynolds, C. P. Determination of subcutaneous tumor size in athymic (nude) mice. *Cancer Chemother. Pharmacol.* **24**, 148-154 (1989).

34   Su, G. L. *et al.* Activation of human and mouse Kupffer cells by lipopolysaccharide is mediated by CD14. *Am. J. Physiol.-Gastr. L.* **283**, G640-G645 (2002).

35   Arnida, Janát-Amsbury, M. M., Ray, A., Peterson, C. M. & Ghandehari, H. Geometry and surface characteristics of gold nanoparticles influence their biodistribution and uptake by macrophages. *Eur. J. Pharm. Biopharm.* **77**, 417-423 (2011).

36   Maeda, H., Wu, J., Sawa, T., Matsumura, Y. & Hori, K. Tumor vascular permeability and the EPR effect in macromolecular therapeutics: a review. *J. Control. Release* **65**, 271-284 (2000).

37   Pan, G., Lemmouchi, Y., Akala, E. O. & Bakare, O. Studies on PEGylated and drug-loaded PAMAM dendrimers. *J. Bioact. Compat. Pol.* **20**, 113-128 (2005).

38   Malik, N. *et al.* Dendrimers: Relationship between structure and biocompatibility in vitro, and preliminary studies on the biodistribution of 125I-labelled polyamidoamine dendrimers in vivo. *J. Control. Release* **65**, 133-148 (2000).

39   Sadekar, S., Ray, A., Janàt-Amsbury, M., Peterson, C. M. & Ghandehari, H. Comparative biodistribution of PAMAM dendrimers and HPMA copolymers in ovarian-tumor-bearing mice. *Biomacromolecules* **12**, 88-96 (2010).

40   Kobayashi, H. & Brechbiel, M. W. Nano-sized MRI contrast agents with dendrimer cores. *Adv. Drug Deliver. Rev.* **57**, 2271 (2005).

41   Kobayashi, H. *et al.* Renal tubular damage detected by dynamic micro-MRI with a dendrimer-based magnetic resonance contrast agent. *Kidney Int.* **61**, 1980-1985 (2002).

42   Blum, R. H. & Carter, S. K. Adriamcyin: a new anticancer drug with significant clinical activity. *Ann. Intern. Med.* **80**, 249-259 (1974).

43   Stockert, R. J. The asialoglycoprotein receptor: relationships between structure, function, and expression. *Physiol. Rev.* **75**, 591-609 (1995).

44   Liang, H.-F. *et al.* Paclitaxel-loaded poly(γ-glutamic acid)-poly(lactide) nanoparticles as a targeted drug delivery system against cultured HepG2 cells. *Bioconjugate Chem.* **17**, 291-299 (2006).

45   Pimm, M. V., Perkins, A. C., Strohalm, J., Ulbrich, K. & Duncan, R. Gamma scintigraphy of a 123I-labelled N-(2-hydroxypropyl)methacrylamide copolymer-doxorubicin conjugate containing galactosamine following intravenous administration to nude mice bearing hepatic human colon carcinoma. *J. Drug Target.* **3**, 385-390 (1996).

46   Seymour, L. W. *et al.* Hepatic drug targeting: phase I evaluation of polymer-bound doxorubicin. *J. Clin. Oncol.* **20**, 1668-1676 (2002).

47   Owens III, D. E. & Peppas, N. A. Opsonization, biodistribution, and pharmacokinetics of polymeric nanoparticles. *Int. J. Pharm.* **307**, 93-102 (2006).

48   Wijagkanalan, W., Kawakami, S. & Hashida, M. Designing dendrimers for drug delivery and imaging: pharmacokinetic considerations. *Pharm. Res.* **28**, 1500-1519 (2011).

49   van Vlerken, L., Vyas, T. & Amiji, M. Poly(ethylene glycol)-modified nanocarriers for tumor-targeted and intracellular delivery. *Pharm. Res.* **24**, 1405-1414 (2007).

50   Fox, M. E., Szoka, F. C. & Fréchet, J. M. J. Soluble polymer carriers for the treatment of cancer: the importance of molecular architecture. *Accounts Chem. Res.* **42**, 1141-1151 (2009).

51   Kojima, C., Regino, C., Umeda, Y., Kobayashi, H. & Kono, K. Influence of dendrimer generation and polyethylene glycol length on the biodistribution of PEGylated dendrimers. *Int. J. Pharm.* **383**, 293-296 (2010).

52   Okuda, T. *et al.* PEGylated lysine dendrimers for tumor-selective targeting after intravenous injection in tumor-bearing mice. *J. Control. Release* **116**, 330 (2006).

53   Duncan, R. The dawning era of polymer therapeutics. *Nat. Rev. Drug. Discov.* **2**, 347-360 (2003).

54   Yang, H., Lopina, S., DiPersio, L. & Schmidt, S. Stealth dendrimers for drug delivery: correlation between PEGylation, cytocompatibility, and drug payload. *J. Mater. Sci-Mater. M.* **19**, 1991-1997 (2008).

55   Oyewumi, M. O., Yokel, R. A., Jay, M., Coakley, T. & Mumper, R. J. Comparison of cell uptake, biodistribution and tumor retention of folate-coated and PEG-coated gadolinium nanoparticles in tumor-bearing mice. *J. Control. Release* **95**, 613-626 (2004).

56   Yoo, H. S., Lee, E. A. & Park, T. G. Doxorubicin-conjugated biodegradable polymeric micelles having acid-cleavable linkages. *J. Control. Release* **82**, 17-27 (2002).

57   Thurlkill, R. L., Grimsley, G. R., Scholtz, J. M. & Pace, C. N. pK values of the ionizable groups of proteins. *Protein Sci.* **15**, 1214-1218 (2006).

58   Dufort, S., Sancey, L. & Coll, J.-L. Physico-chemical parameters that govern nanoparticles fate also dictate rules for their molecular evolution. *Adv. Drug Deliver. Rev.* **64**, 179-189 (2012).

59   Ashley, C. E. *et al.* The targeted delivery of multicomponent cargos to cancer cells by nanoporous particle-supported lipid bilayers. *Nat. Mater.* **10**, 389-397 (2011).

60   Mandeville, J. S. & Tajmir-Riahi, H. A. Complexes of dendrimers with bovine serum albumin. *Biomacromolecules* **11**, 465-472 (2010).

61   van Berkel, T. J. *et al.* The effect of a water-soluble tris-galactoside-terminated cholesterol derivative on the fate of low density lipoproteins and liposomes. *J. Biol. Chem.* **260**, 2694-2699 (1985).

62   Westerlind, U. *et al.* Ligands of the asialoglycoprotein receptor for targeted gene delivery, part 1: synthesis of and binding studies with biotinylated cluster glycosides containing N-acetylgalactosamine. *Glycoconjugate J.* **21**, 227-241 (2004).

63   Schwartz, A. L., Fridovich, S. E. & Lodish, H. F. Kinetics of internalization and recycling of the asialoglycoprotein receptor in a hepatoma cell line. *J. Biol. Chem.* **257**, 4230-4237 (1982).

64   Warren, R. & Doyle, D. Turnover of the surface proteins and the receptor for serum asialoglycoproteins in primary cultures of rat hepatocytes. *J. Biol. Chem.* **256**, 1346-1355 (1981).

65   Zauner, W., Farrow, N. A. & Haines, A. M. R. In vitro uptake of polystyrene microspheres: effect of particle size, cell line and cell density. *J. Control. Release* **71**, 39-51 (2001).

66 Jiang, W., KimBetty, Y. S., Rutka, J. T. & ChanWarren, C. W. Nanoparticle-mediated cellular response is size-dependent. *Nat. Nano.* **3**, 145-150 (2008).

Synthesis of Fluorescently-labeled G5-(cPEG[NAcGal$_{\alpha/\beta}$]) Conjugates
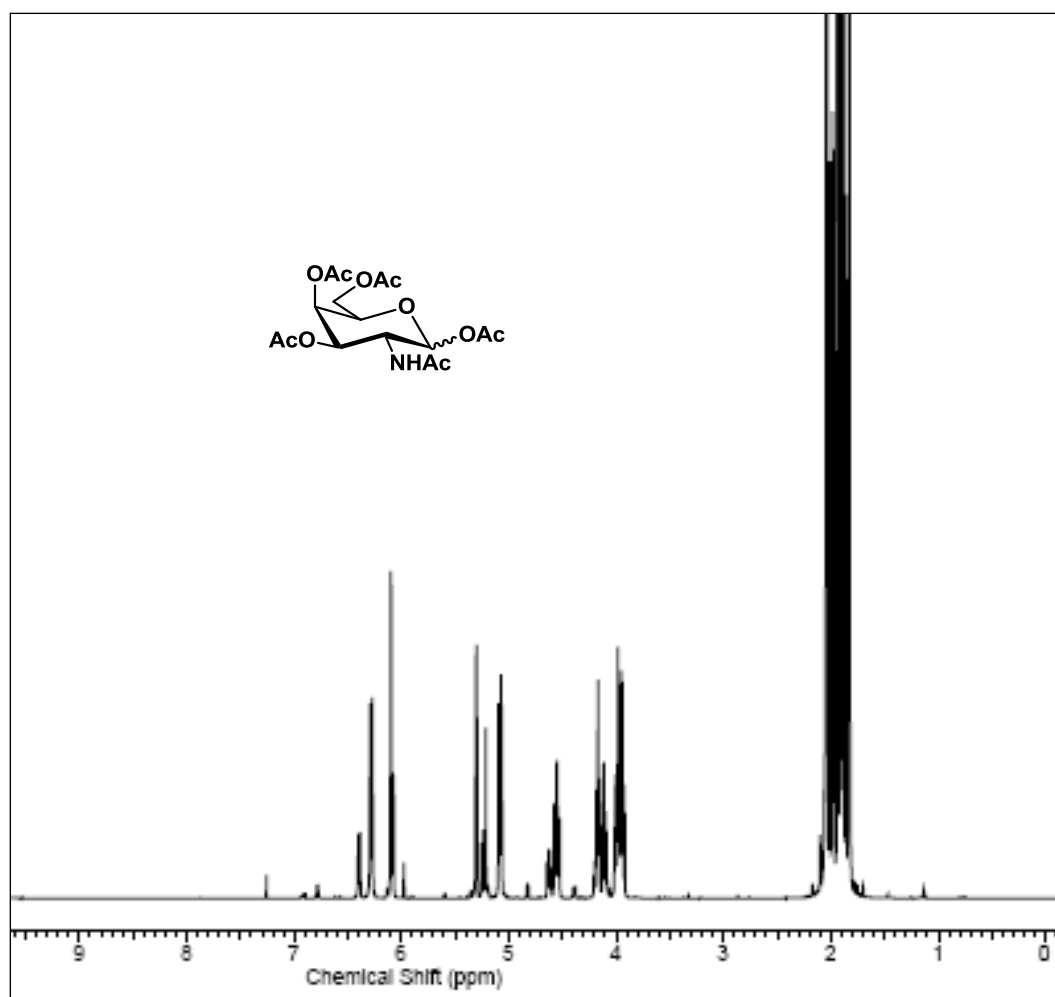
Figure S1: ^{1}H NMR of **(3R,4R,5R,6R)-3-acetamido-6-(acetoxymethyl)tetrahydro-2H-pyran-2,4,5-triyl triacetate** (**1**) dissolved in CDCl$_3$ on a Varian 500 MHz system (Palo Alto, CA).
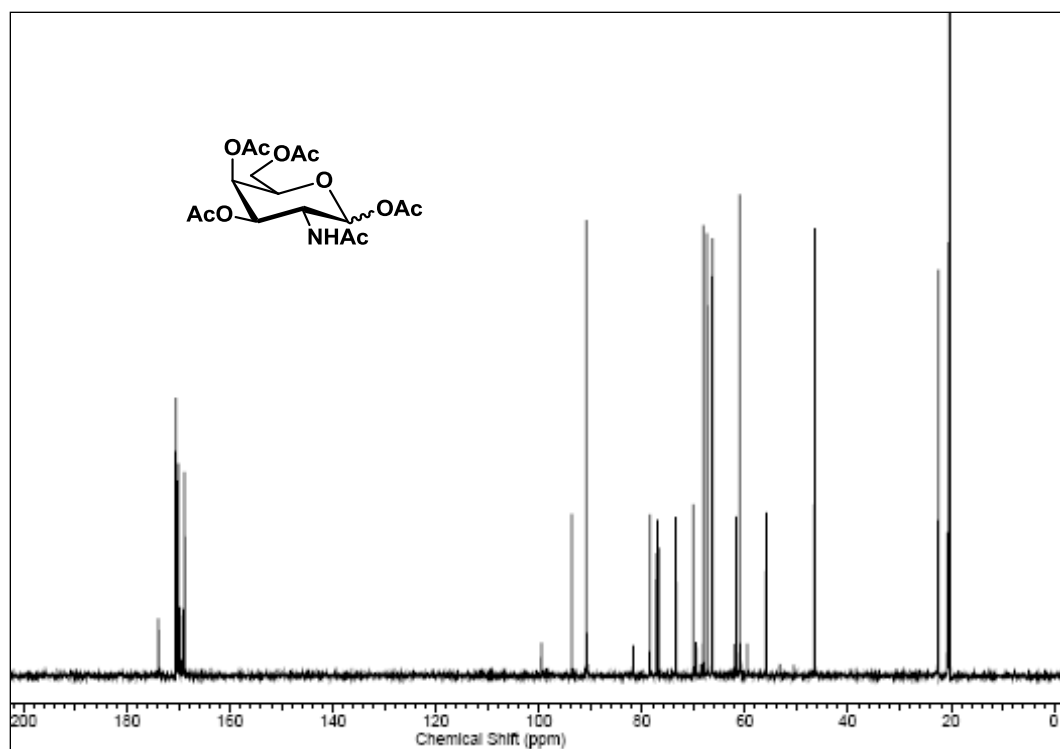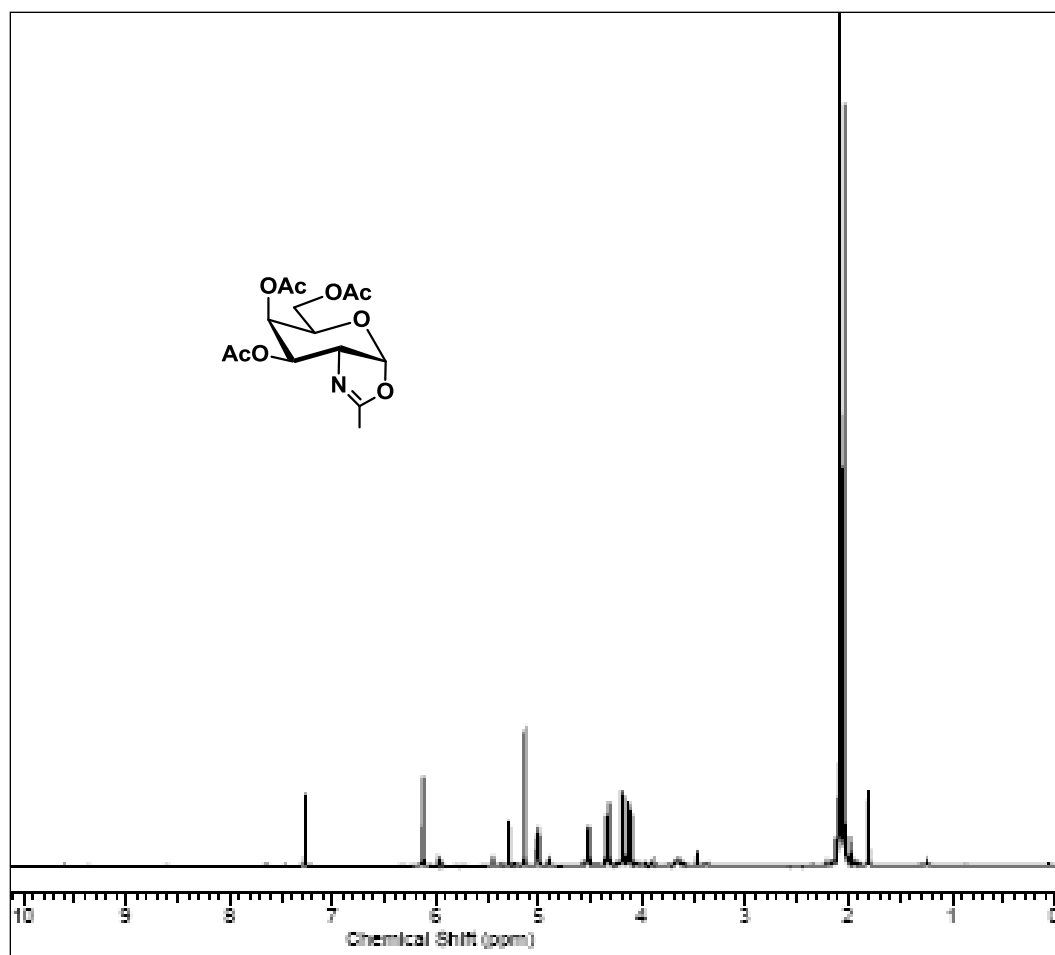
Figure S2: ^{13}C NMR of **(3R,4R,5R,6R)-3-acetamido-6-(acetoxymethyl)tetrahydro-2H-pyran-2,4,5-triyl triacetate** (**1**) dissolved in CDCl$_3$ on a Varian 125 MHz system (Palo Alto, CA).

Figure S3: ^{1}H NMR of **(3aR,5R,6R,7R,7aR)-5-(acetoxymethyl)-2-methyl-5,6,7,7a-tetrahydro-3aH-pyrano[3,2-d]oxazole-6,7-diyl diacetate** (**2**) dissolved in CDCl$_3$ on a Varian 500 MHz system (Palo Alto, CA).
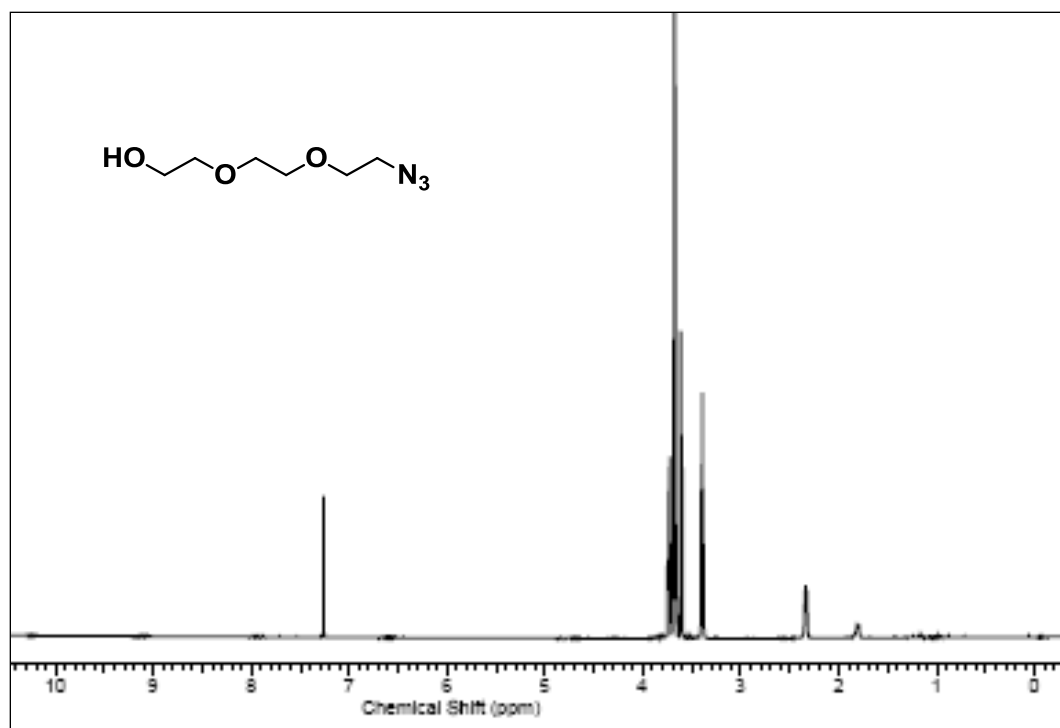
Figure S4: ^{1}H NMR of **2-(2-(2-azidoethoxy)ethoxy)ethanol** (**4**) dissolved in CDCl$_3$ on a Varian 500 MHz system (Palo Alto, CA).
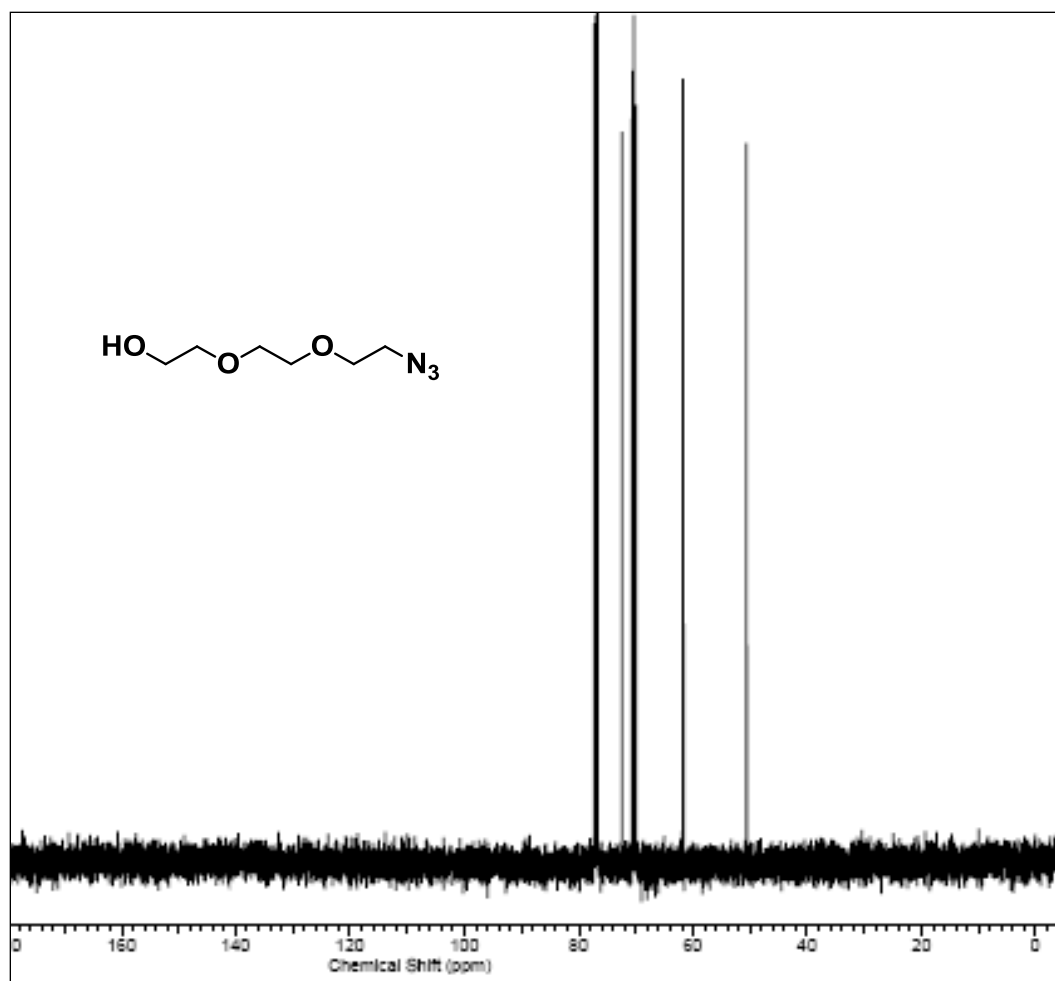
Figure S5: ^{13}C NMR of **2-(2-(2-azidoethoxy)ethoxy)ethanol** (**4**) dissolved in CDCl$_3$ on a Varian 125 MHz system (Palo Alto, CA).
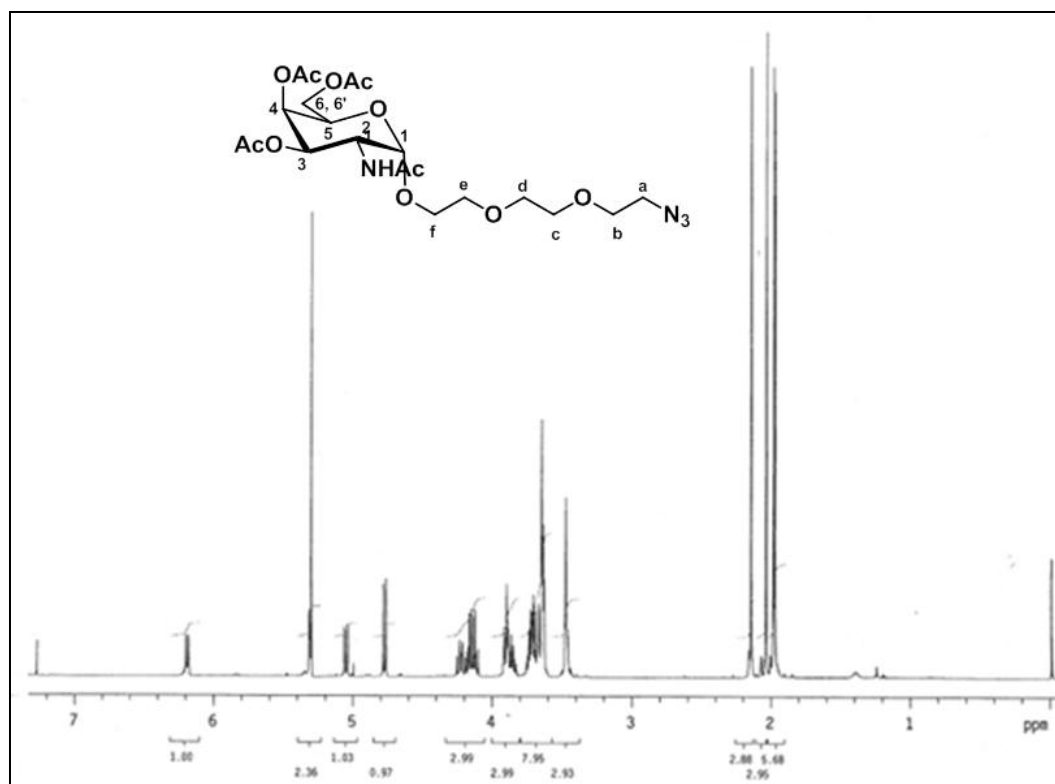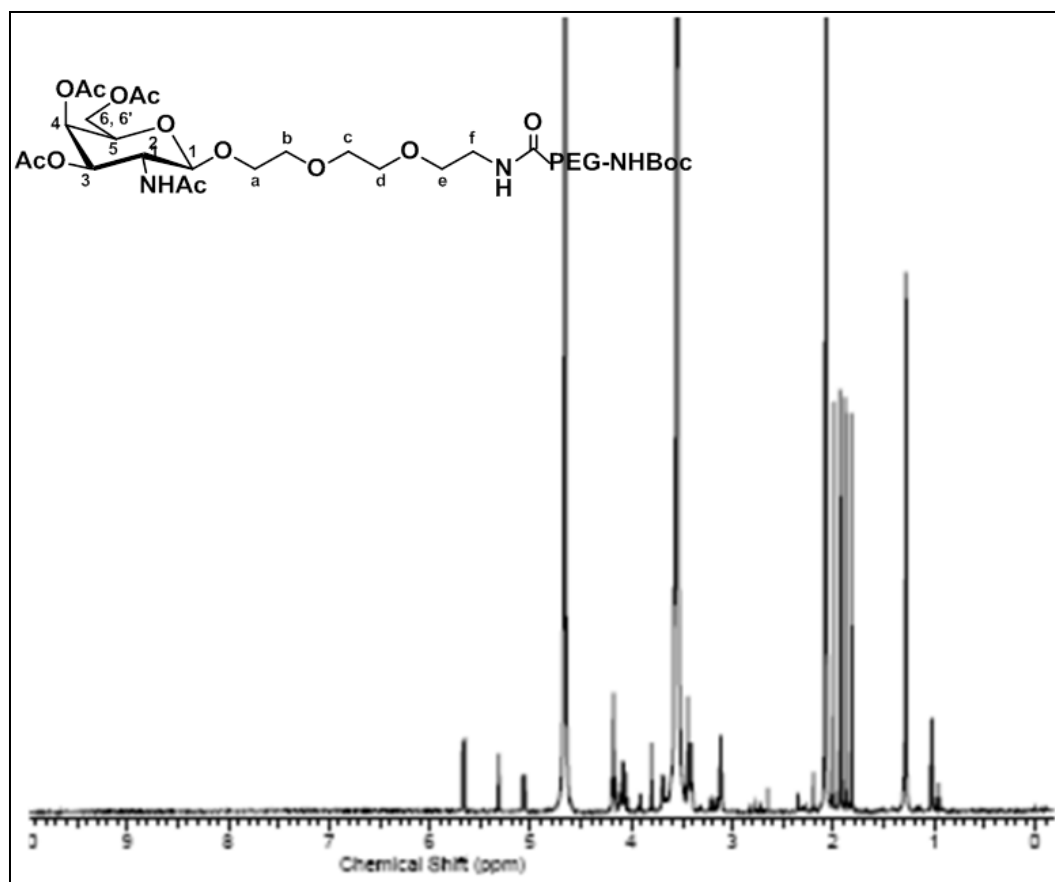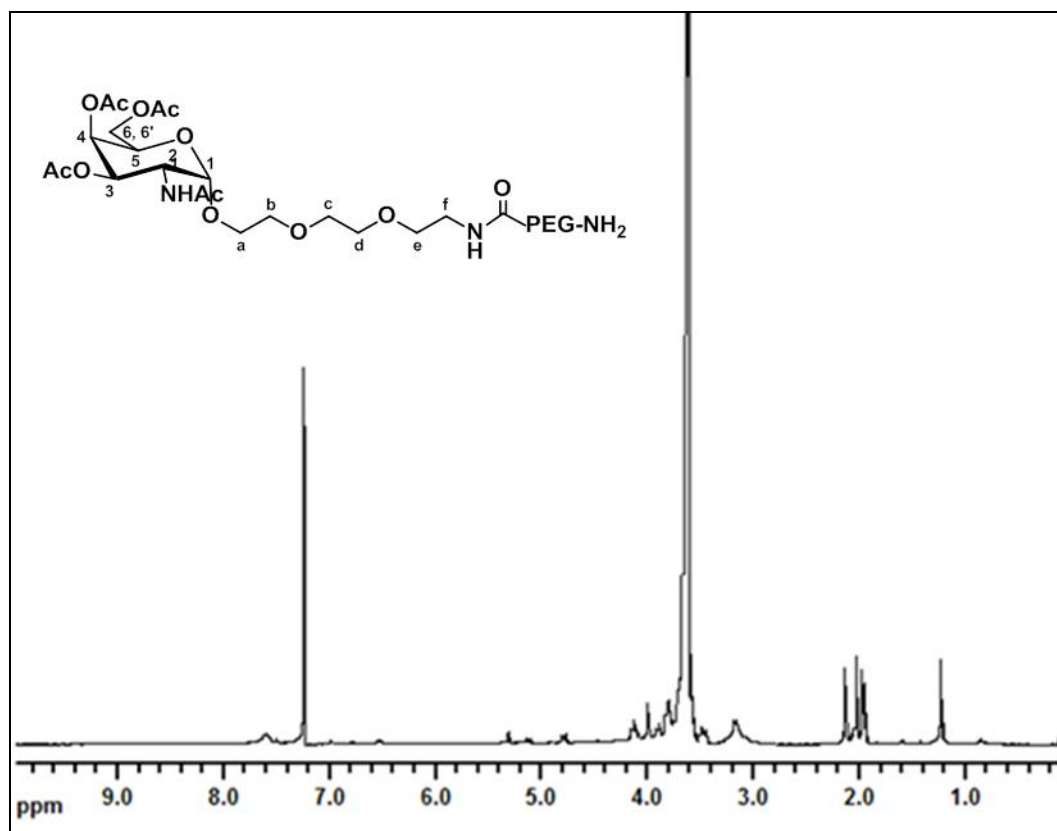
Figure S6: ^{1}H NMR of **(2R,3R,4R,5R,6R)-5-acetamido-2-(acetoxymethyl)-6-(2-(2-(2-azidoethoxy)ethoxy)ethoxy)tetrahydro-2H-pyran-3,4-diyl diacetate** (**5α**) dissolved in CDCl$_3$ on a Varian 500 MHz system (Palo Alto, CA).
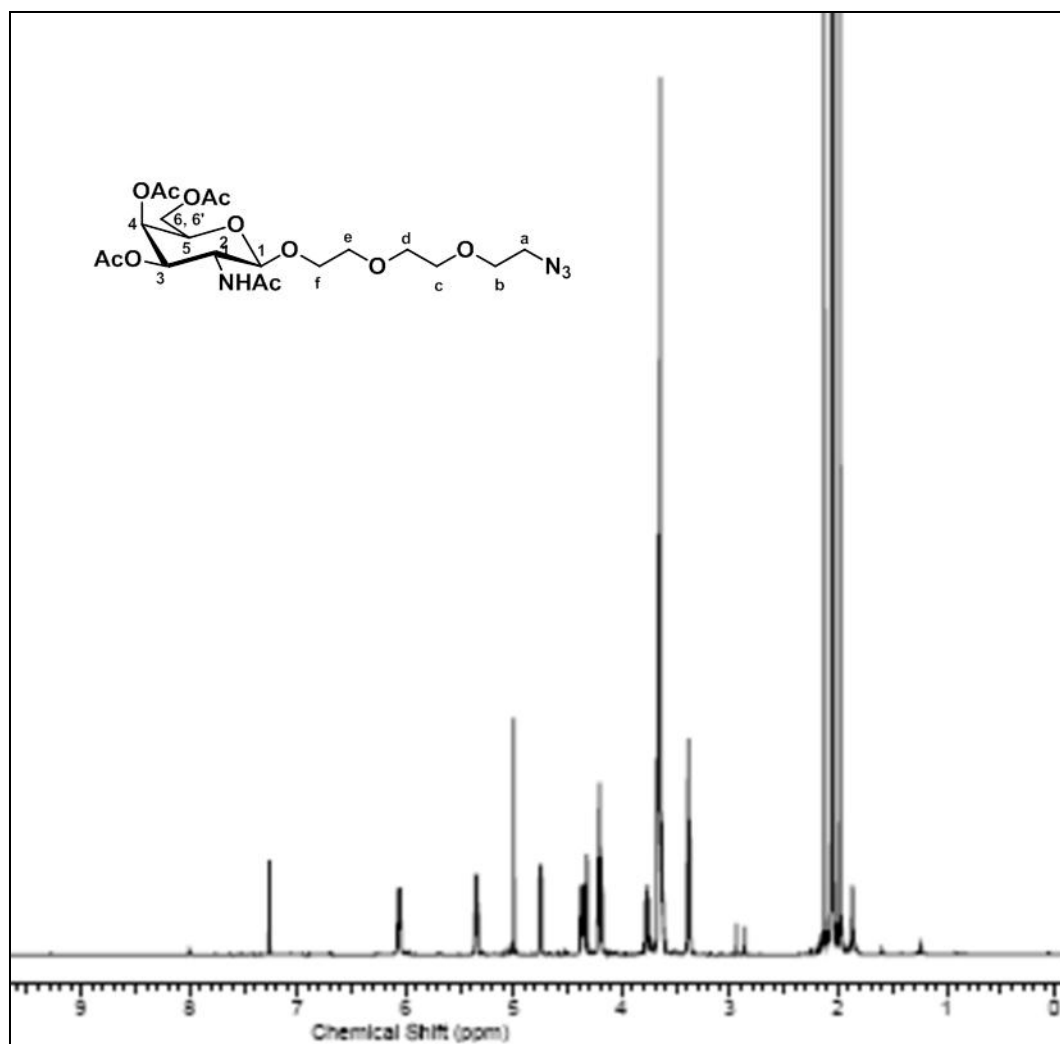
Figure S7: ^{1}H NMR of **(2R,3R,4R,5R,6R)-5-acetamido-2-(acetoxymethyl)-6-(2-(2-(2-azidoethoxy)ethoxy)ethoxy)tetrahydro-2H-pyran-3,4-diyl diacetate** (**5β**) dissolved in CDCl$_3$ on a Varian 500 MHz system (Palo Alto, CA).
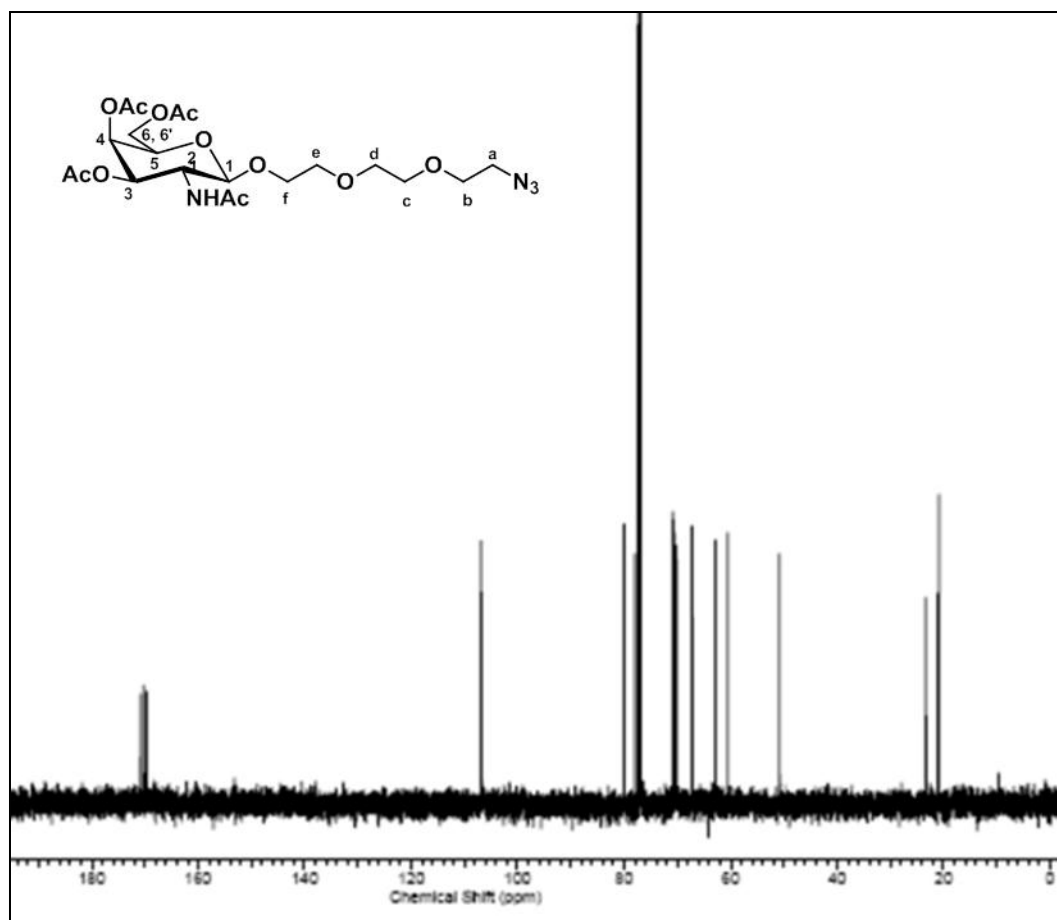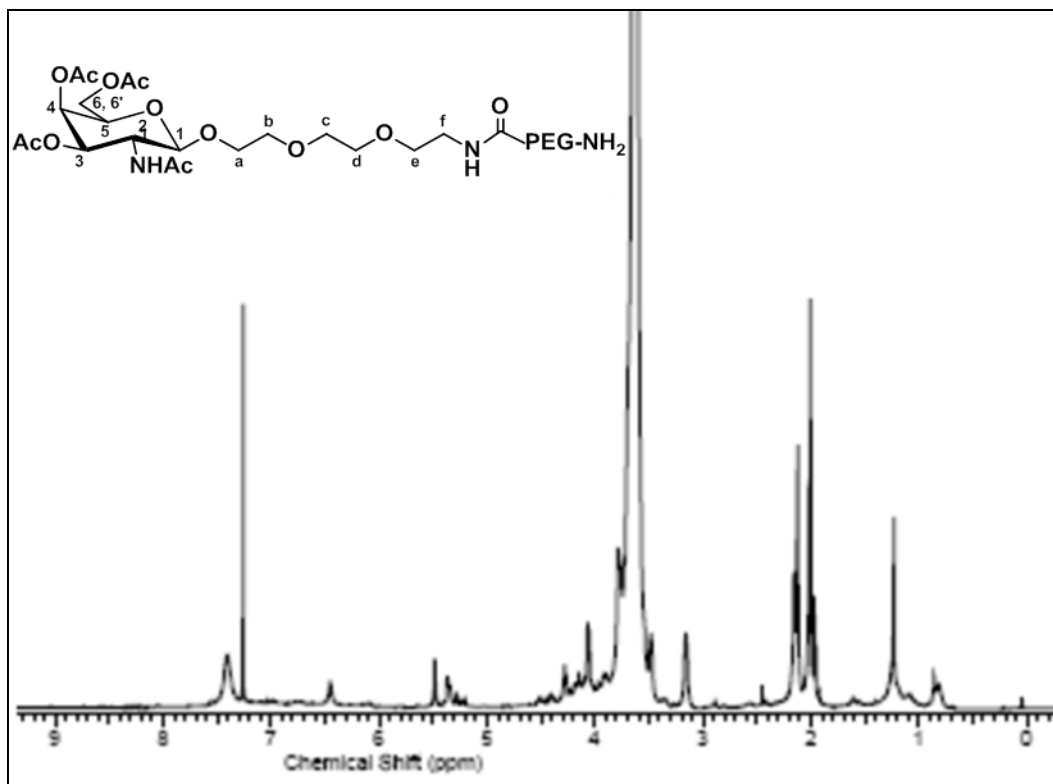
Figure S8: ^{13}C NMR of **(2R,3R,4R,5R,6R)-5-acetamido-2-(acetoxymethyl)-6-(2-(2-(2-azidoethoxy)ethoxy)ethoxy)tetrahydro-2H-pyran-3,4-diyl diacetate** (**5β**) dissolved in CDCl$_3$ on a Varian 125 MHz system (Palo Alto, CA).
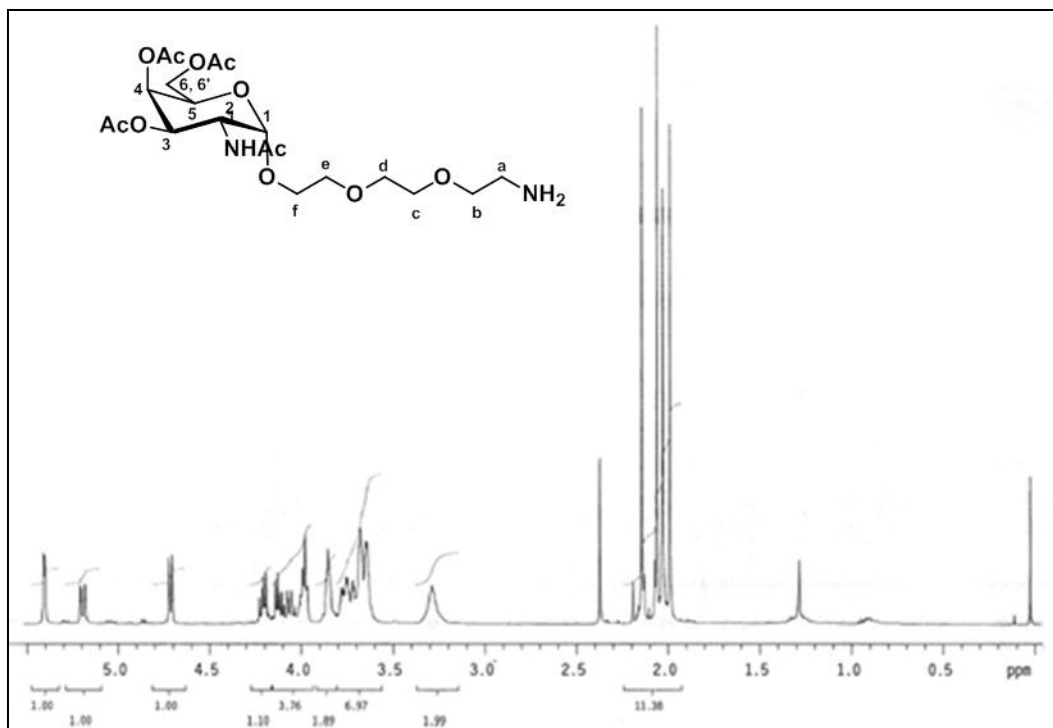
Figure S9: ^{1}H NMR of **(2R,3R,4R,5R,6R)-5-acetamido-2-(acetoxymethyl)-6-(2-(2-(2-aminoethoxy)ethoxy)ethoxy)tetrahydro-2H-pyran-3,4-diyl diacetate** (**6α**) dissolved in CDCl$_3$ on a Varian 500 MHz system (Palo Alto, CA).

286
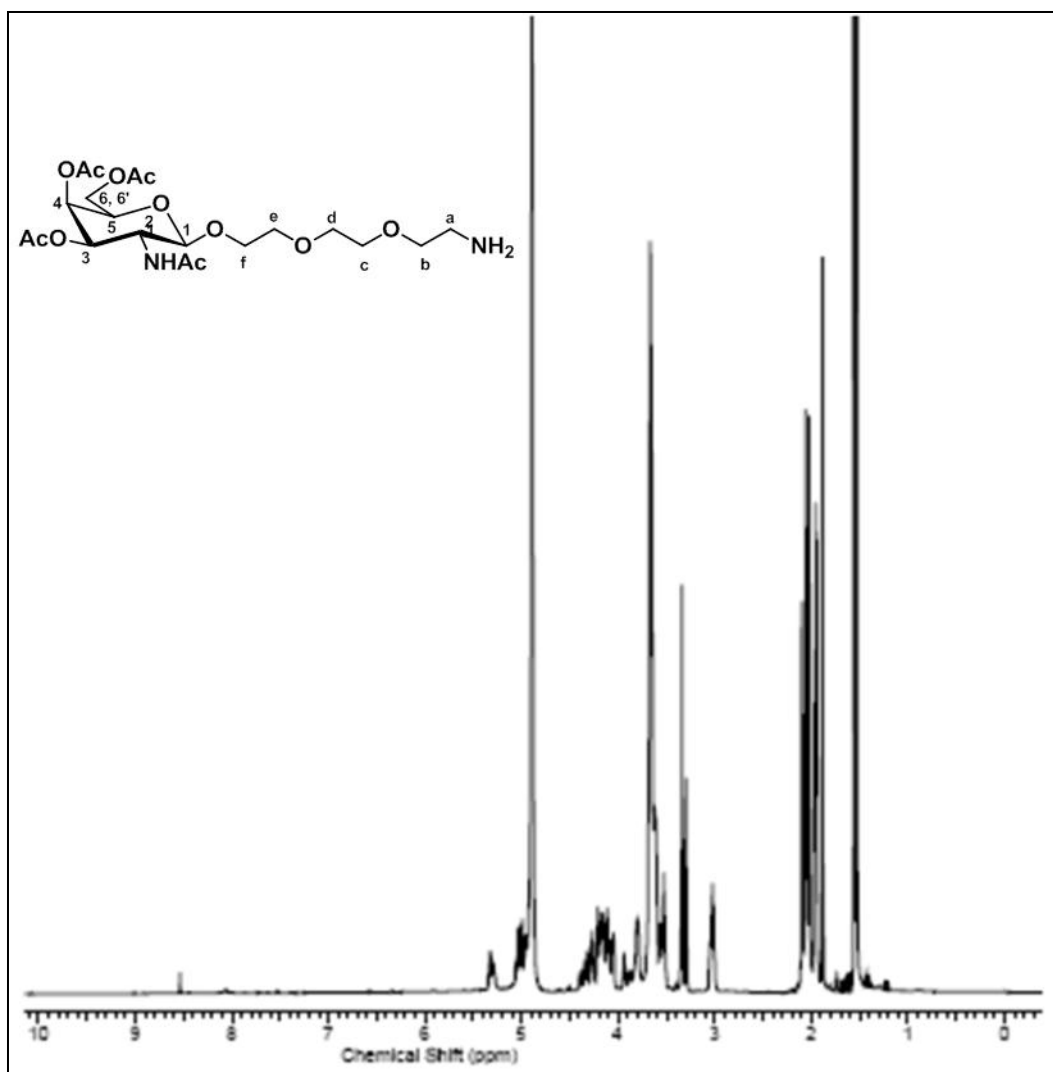
Figure S10: ^{1}H NMR of **(2R,3R,4R,5R,6R)-5-acetamido-2-(acetoxymethyl)-6-(2-(2-(2-aminoethoxy)ethoxy)ethoxy)tetrahydro-2H-pyran-3,4-diyl diacetate (6β)** dissolved in CD_3OD on a Varian 500 MHz system (Palo Alto, CA).
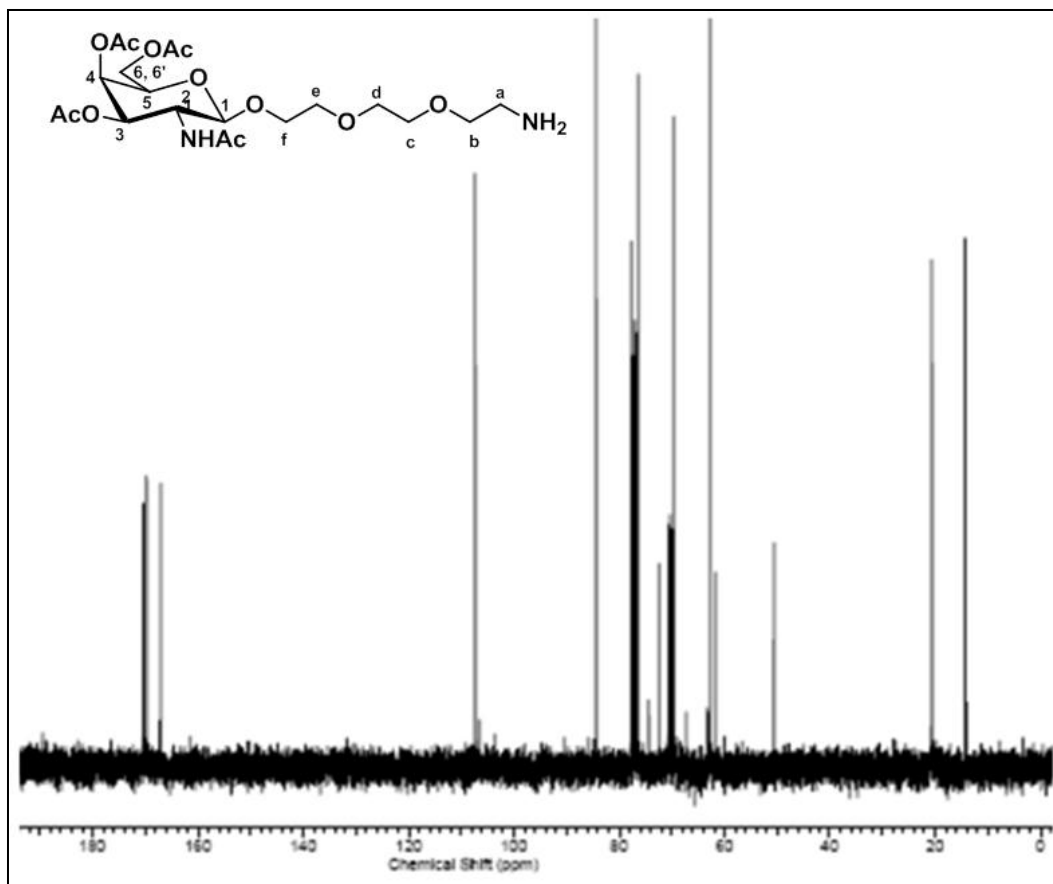
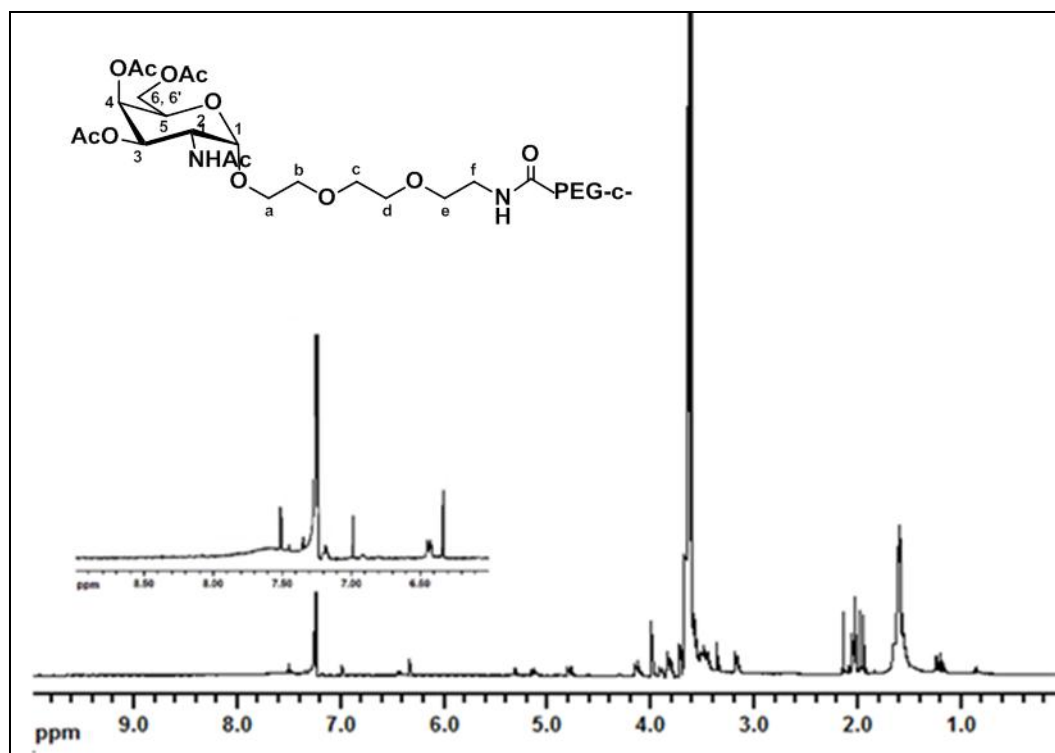**Figure S11**: ^{13}C NMR of **(2R,3R,4R,5R,6R)-5-acetamido-2-(acetoxymethyl)-6-(2-(2-(2-aminoethoxy)ethoxy)ethoxy)tetrahydro-2H-pyran-3,4-diyl diacetate (6β)** dissolved in CD_3OD on a Varian 125 MHz system (Palo Alto, CA).
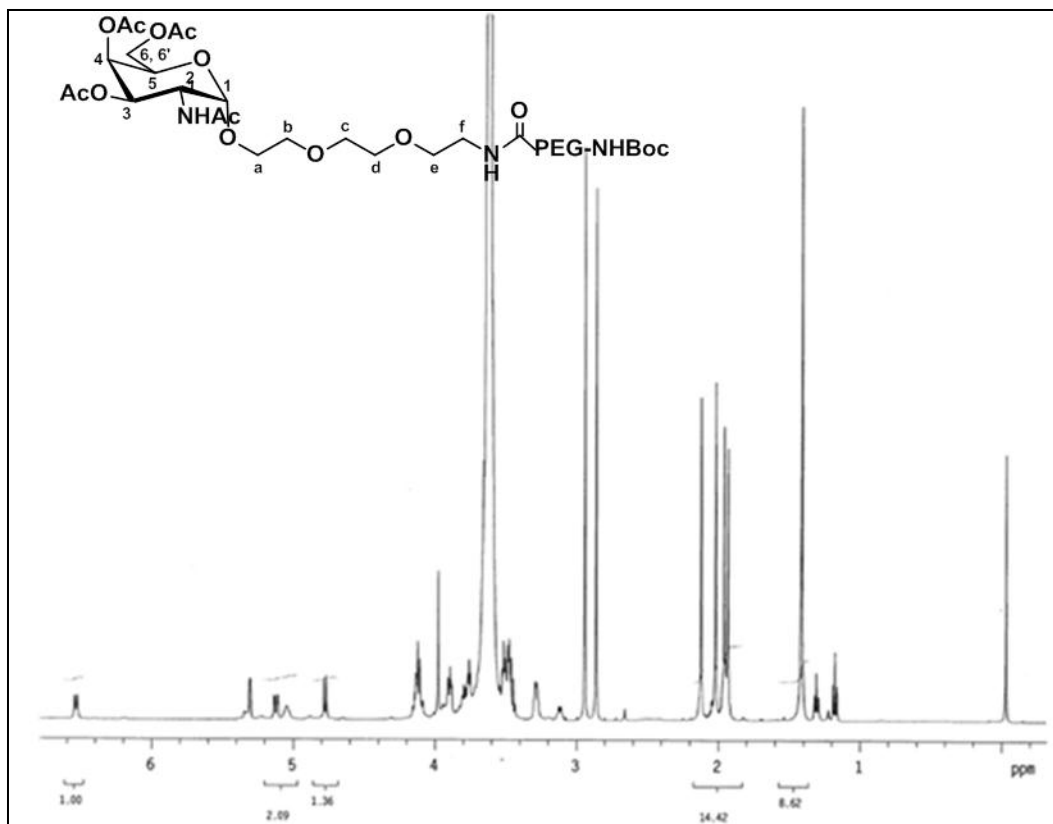
Figure S12: ^{1}H NMR of **(2R,3R,4R,5R,6R)-5-acetamido-2-(acetoxymethyl)-6-(2-(2-(2-amino(Boc amino PEG-)ethoxy)ethoxy)ethoxy)tetrahydro-2H-pyran-3,4-diyl diacetate** (**7α**) dissolved in CDCl$_3$ on a Varian 500 MHz system (Palo Alto, CA).
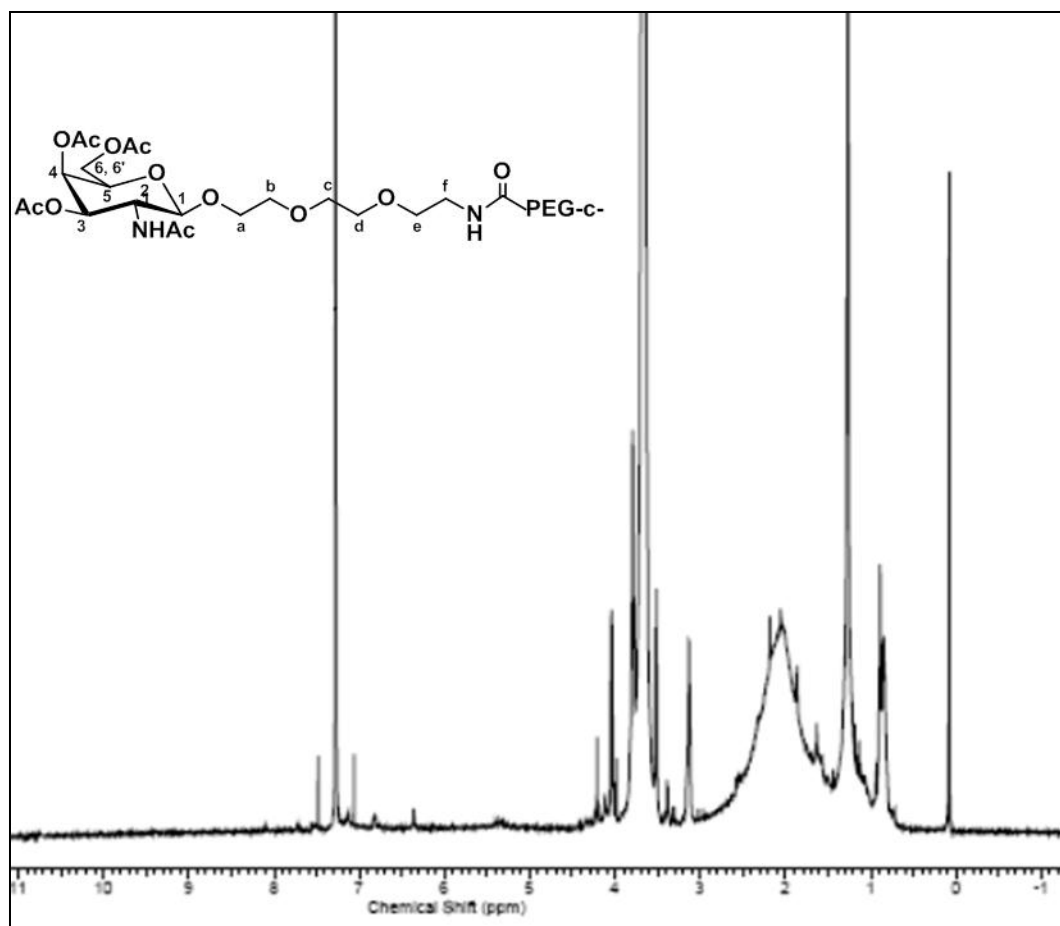
Figure S13: ^{1}H NMR of **(2R,3R,4R,5R,6R)-5-acetamido-2-(acetoxymethyl)-6-(2-(2-(2-amino(Boc   amino   PEG-)ethoxy)ethoxy)ethoxy)tetrahydro-2H-pyran-3,4-diyl diacetate** (**7β**) dissolved in D$_2$O on a Varian 500 MHz system (Palo Alto, CA).
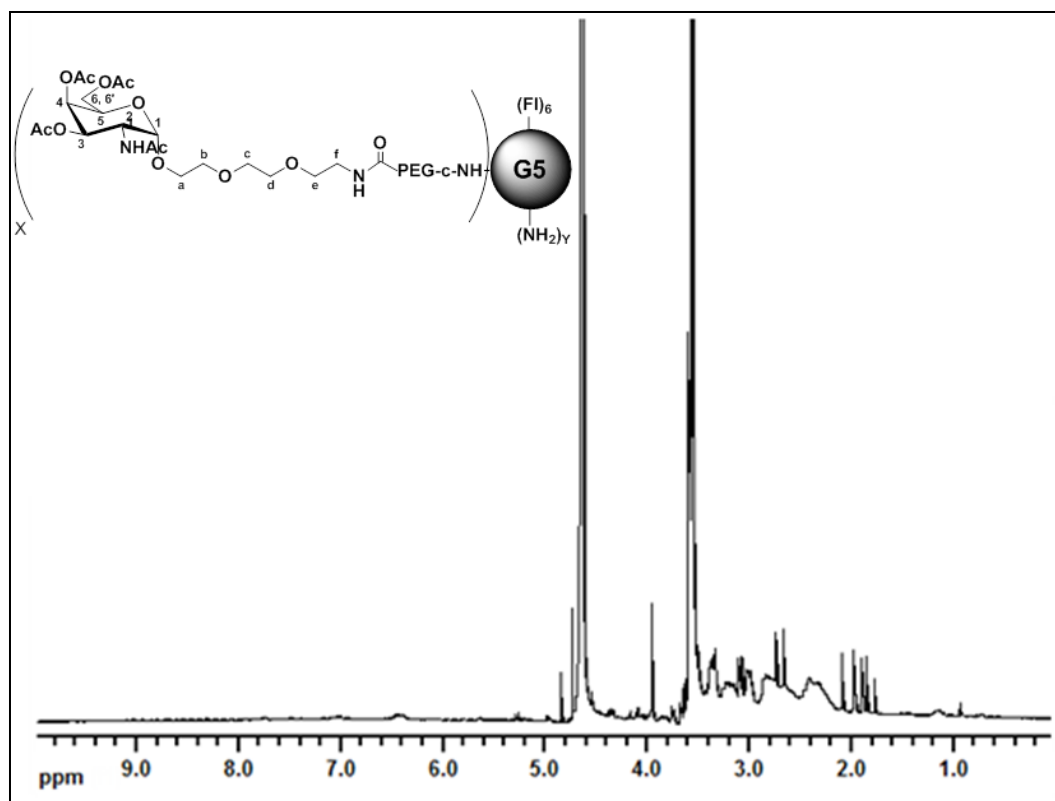
Figure S14: ^{1}H NMR of **(2R,3R,4R,5R,6R)-5-acetamido-2-(acetoxymethyl)-6-(2-(2-(2-amino(amino PEG-)ethoxy)ethoxy)ethoxy)tetrahydro-2H-pyran-3,4-diyl diacetate** (**8α**) dissolved in D$_2$O on a Varian 400 MHz system (Palo Alto, CA).

Figure S15: ^{1}H NMR of **(2R,3R,4R,5R,6R)-5-acetamido-2-(acetoxymethyl)-6-(2-(2-(2-amino(amino PEG-)ethoxy)ethoxy)ethoxy)tetrahydro-2H-pyran-3,4-diyl diacetate** (**8β**) dissolved in CDCl$_3$ on a Varian 500 MHz system (Palo Alto, CA).
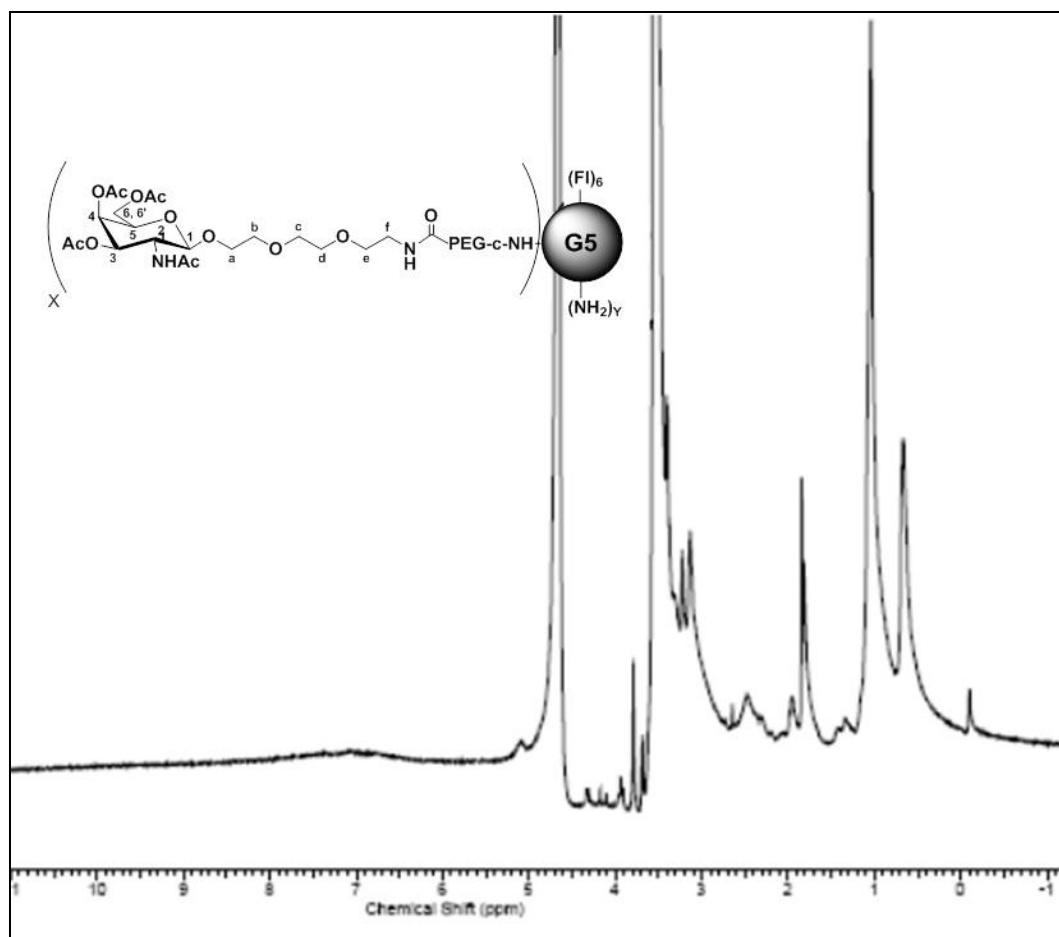
292

Figure S16: ^{1}H NMR of **(2R,3R,4R,5R,6R)-5-acetamido-2-(acetoxymethyl)-6-(2-(2-(2-amino(cis-aconityl-amino PEG-)ethoxy)ethoxy)ethoxy)tetrahydro-2H-pyran-3,4-diyl diacetate (9α)** dissolved in CDCl$_3$ on a Varian 400 MHz system (Palo Alto, CA).

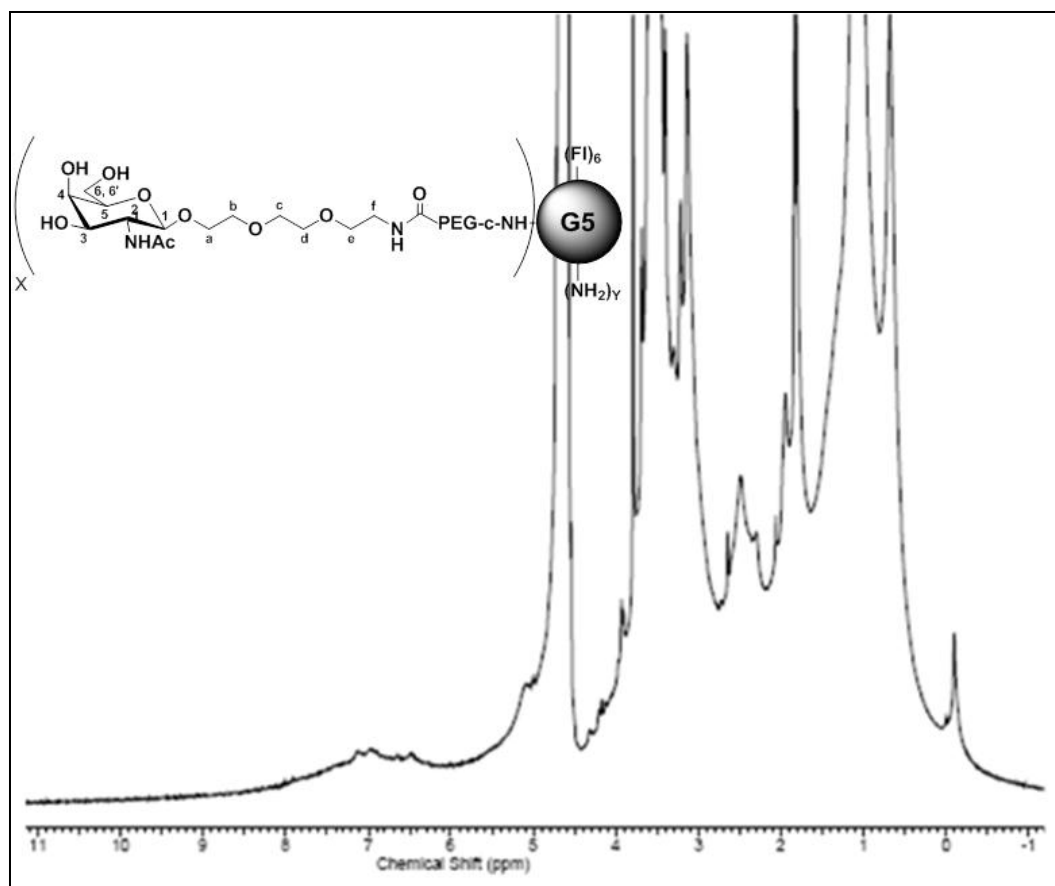**Figure S17**: ¹H NMR of **(2R,3R,4R,5R,6R)-5-acetamido-2-(acetoxymethyl)-6-(2-(2-(2-amino(cis-aconityl-amino   PEG-)ethoxy)ethoxy)ethoxy)tetrahydro-2H-pyran-3,4-diyl diacetate** (**9β**) dissolved in CDCl₃ on a Varian 500 MHz system (Palo Alto, CA).

Figure S18: ^{1}H NMR of **(2R,3R,4R,5R,6R)-5-acetamido-2-(acetoxymethyl)-6-(2-(2-(2-amino(Fl-G5-cis-aconityl-amino PEG-)ethoxy)ethoxy)ethoxy)tetrahydro-2H-pyran-3,4-diyl diacetate** (**10α**) dissolved in D$_2$O on a Varian 400 MHz system (Palo Alto, CA).

Figure S19: ^{1}H NMR of **(2R,3R,4R,5R,6R)-5-acetamido-2-(acetoxymethyl)-6-(2-(2-(2-amino(Fl-G5-cis-aconityl-amino PEG-)ethoxy)ethoxy)ethoxy)tetrahydro-2H-pyran-3,4-diyl diacetate** (**10β**) dissolved in D_2O on a Varian 500 MHz system (Palo Alto, CA).

296

Figure S20: ^{1}H NMR of **(2R,3R,4R,5R,6R)-5-acetamido-2-(acetoxymethyl)-6-(2-(2-(2-amino(FT-G5-(Ac)-cis-aconityl-amino   PEG-)ethoxy)ethoxy)ethoxy)tetrahydro-2H-pyran-3,4-diyl diacetate** (**11β**) dissolved in D_2O on a Varian 500 MHz system (Palo Alto, CA).

297

Synthesis of Fluorescently-labeled G5-(*c*PEG[SP94]) Conjugates
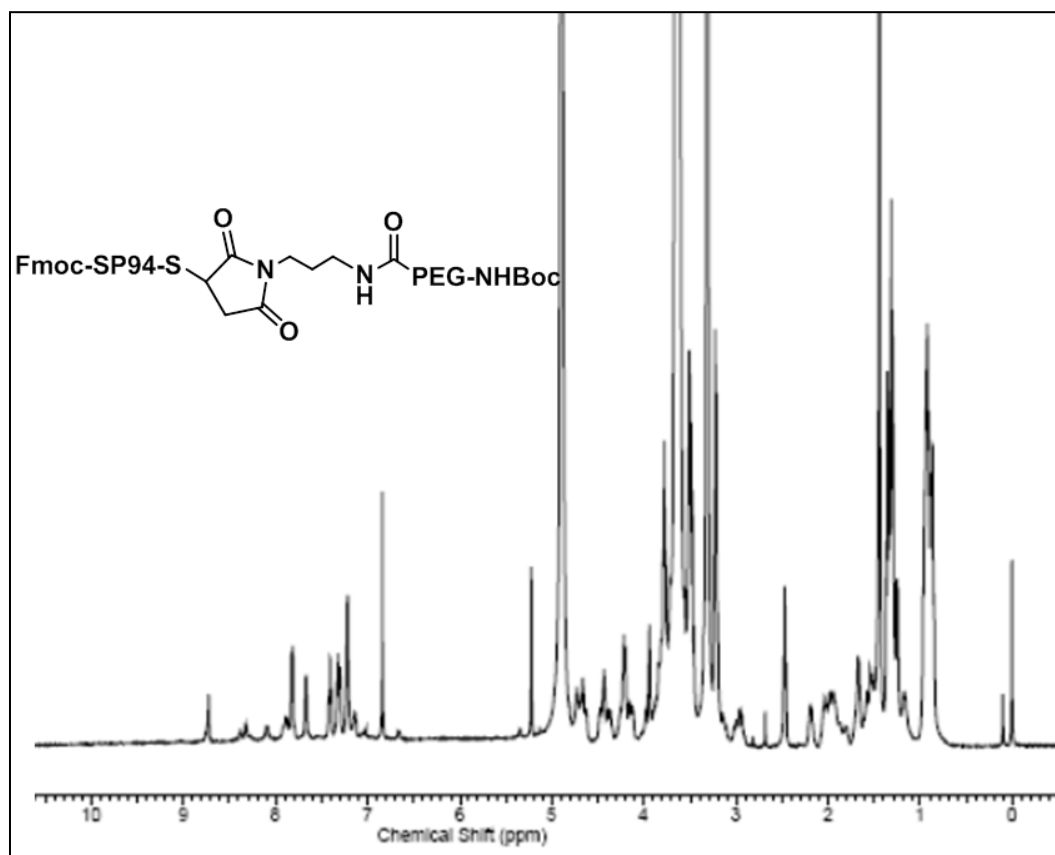
Figure S21: ^{1}H NMR of **Fmoc-SP94-Mal-tert-butyl-(2-(3-(2,5-dioxo-2,5-dihydro-1H-pyrrol-1-yl)propanamido) (polyethylene glycol)ethyl)carbamate** (**13**) dissolved in CD$_3$OD on a Varian 500 MHz system (Palo Alto, CA).
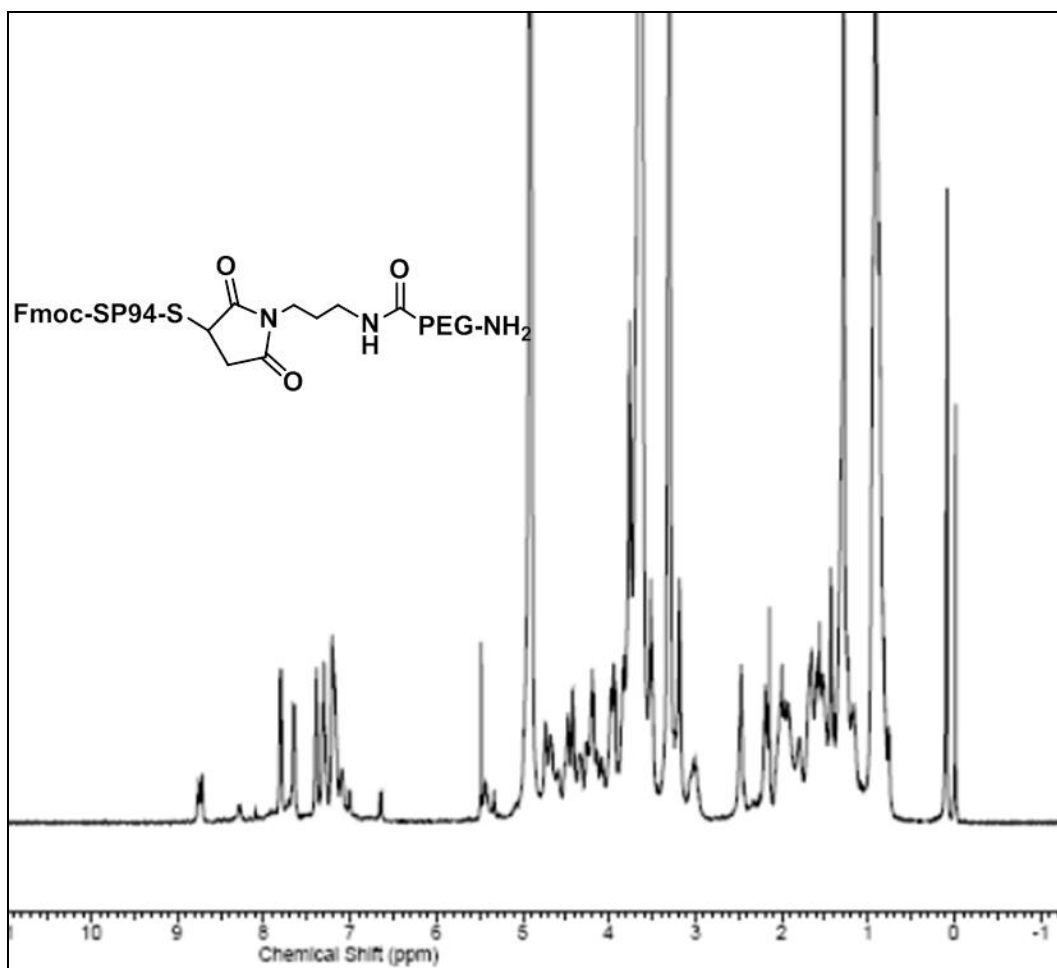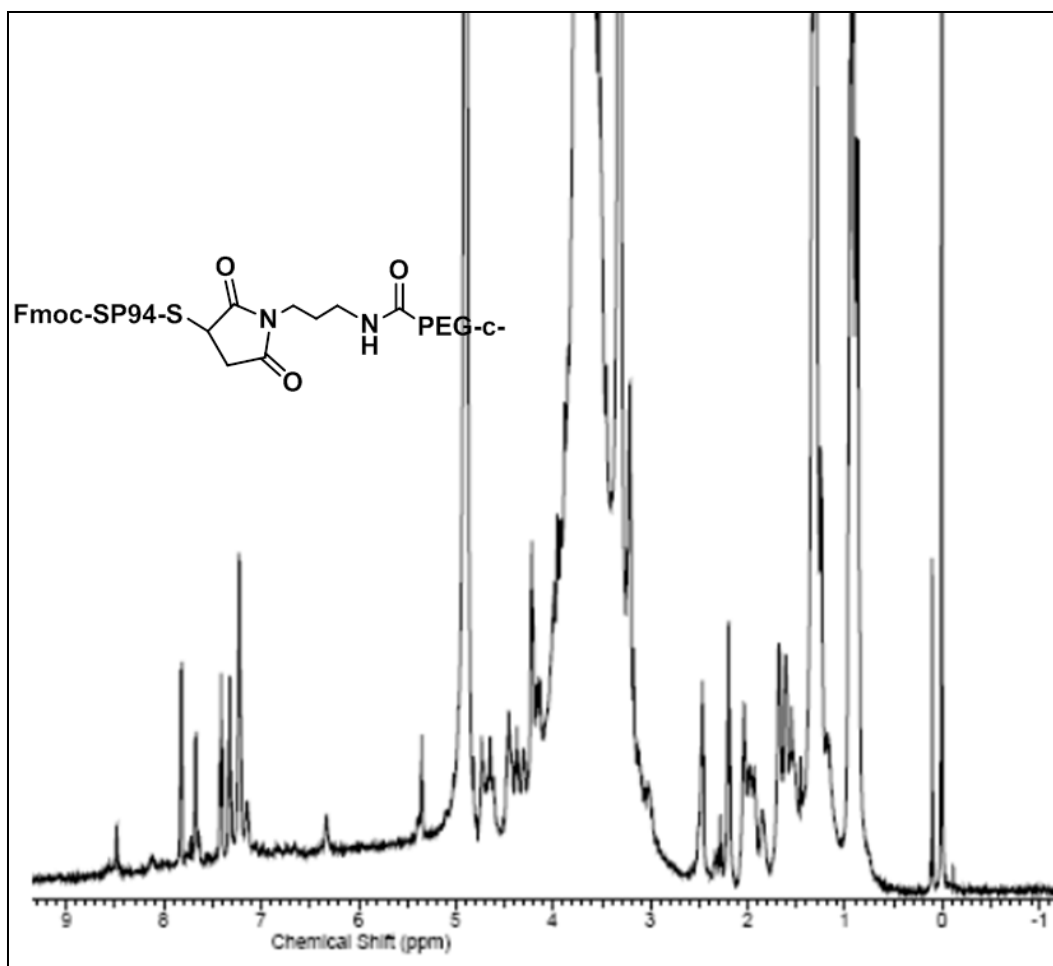
Figure S22: ^{1}H NMR of **Fmoc-SP94-Mal-(2-(3-(2,5-dioxo-2,5-dihydro-1H-pyrrol-1-yl)propanamido) (polyethylene glycol)ethyl)carbamate** (**14**) dissolved in CD$_3$OD on a Varian 500 MHz system (Palo Alto, CA).

Figure S23: ^{1}H NMR of **Fmoc-CGG-peptide-Mal- (2-(3-(2,5-dioxo-2,5-dihydro-1H-pyrrol-1-yl)propanamido)-2-amino(cis-aconityl-amino   PEG-)   (polyethylene glycol)ethyl)carbamate** (**15**) dissolved in CD$_3$OD on a Varian 500 MHz system (Palo Alto, CA).
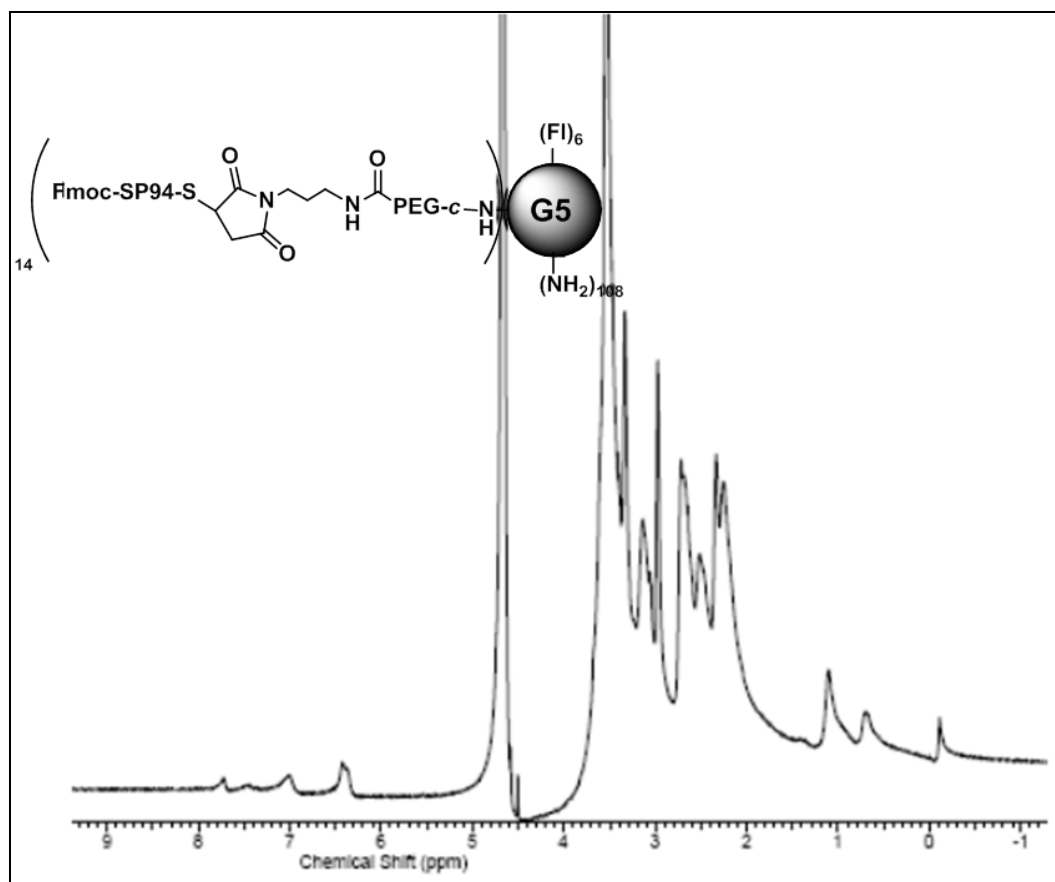
300

Figure S24: ^{1}H NMR of **Fmoc-SP94-Mal- (2-(3-(2,5-dioxo-2,5-dihydro-1H-pyrrol-1-yl)propanamido)-2-amino(Fl-G5-cis-aconityl-amino PEG-) (polyethylene glycol)ethyl)carbamate** (**16**) dissolved in D$_2$O on a Varian 500 MHz system (Palo Alto, CA).
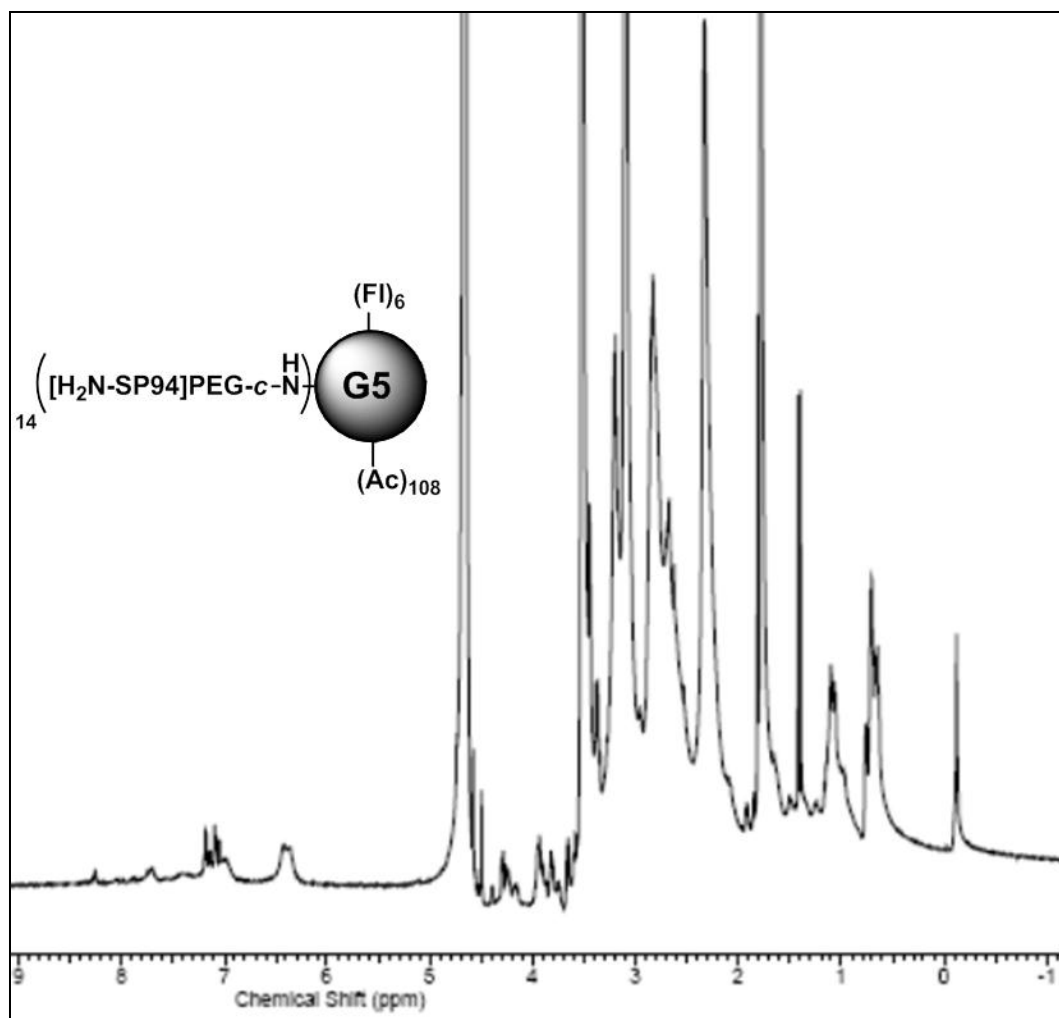
301

Figure S25: ^{1}H NMR of **H$_2$N-SP94-Mal-(2-(3-(2,5-dioxo-2,5-dihydro-1H-pyrrol-1-yl)propanamido)-2-amino(Fl-G5-Ac-cis-aconityl-amino PEG-) (polyethylene glycol)ethyl)carbamate** (**18**) dissolved in D$_2$O on a Varian 500 MHz system (Palo Alto, CA).
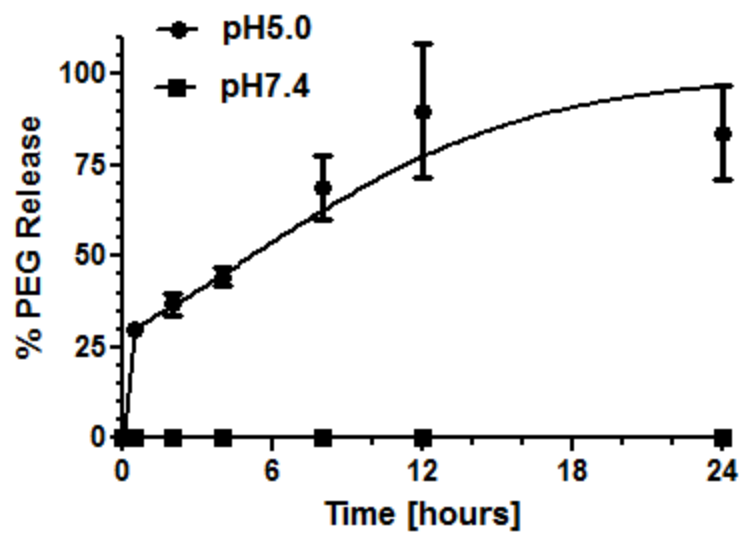
Figure S26: PEG release from G5-(cPEG) conjugates as a function of pH over a 24 hour incubation period at 37°C.

Chapter 6

Conclusion and Future Direction

6.1   Conclusion

6.1.1   Development and Significance of Enzyme-Cleavable Linkers for Hepatic Cancer Cell-Specific Drug Release

We have developed enzyme-activated G5-DOX conjugates which achieved selective release of the loaded DOX molecules to the cytoplasm of hepatic cancer cells for the therapy of primary liver cancer. The results detailed in this dissertation establish the activation and corresponding DOX release from G5-DOX conjugates incorporating enzyme-cleavable azo-linkers reduced specifically in the presence of the azoreductase enzymes present exclusively in hepatic cells. Furthermore, we showed that modulation of the azo-linker electrochemical properties altered its affinity to the enzyme and as a result achieved tunable release of the loaded DOX molecules in the presence of azoreductase. This translated to an increasing rank order of intracellular DOX release and differential cytotoxicity profiles of G5-DOX nano-conjugates towards human hepatic cancer cells. The selectivity of G5-DOX activation by the liver-specific azoreductase enzymes was confirmed by incubation of the nano-conjugates with non-enzymatic control proteins and cytoplasmic enzymes from cardiomyocytes, resulting in minimal DOX release and

limited toxicity of the conjugates to cardiac cells. These results support the translation of enzyme-activated G5-DOX nano-conjugates to pre-clinical *in vivo* therapy and toxicity studies. Specifically, the release of DOX molecules selectively to liver cancer cells after azoreductase activation will result in enhanced therapeutic activity of G5-DOX nano-conjugates *in vivo*, while minimizing DOX delivery to healthy tissues and significantly reducing the non-specific toxicities associated with administration of the free drug.

The design and validation of these enzyme-cleavable chemical linkers represents a significant advancement in the field of drug delivery by providing a release mechanism that achieves selective delivery of chemotherapeutic agents to the diseased tissue, while controlling the rate and extent of drug release via modulation of the linker chemical composition. As a result different linker compositions can be incorporated into a single therapeutic particle to achieve both rapid drug release for immediate anticancer activity, as well as sustained delivery of the chemotherapeutic agents to prevent recurrence and limit extrahepatic spread. This would allow for tailoring of the DOX release profile from these nano-conjugates in the presence of azoreductase enzymes to design a therapeutic regimen customized for patient populations based on their enzyme expression profiles. In addition, the flexibility in the design of G5-DOX conjugates allows for their use in the treatment of a wide variety of liver based malignancies (e.g. hepatitis, cirrhosis, etc.), as well as the treatment of other sarcomas and carcinomas by modifying the linker structure towards activation by target enzymes in the diseased tissue.

6.1.2   Impact of Targeting on Selective Delivery of Dendrimer Carriers to Liver Tumor Tissue

Targeting of the G5 dendrimer carriers to hepatic cancer cells was achieved via coupling of NAcGal sugar ligands to the polymer surface, resulting in ASGPR-mediated endocytosis of these particles into hepatic cancer cells. *In vivo* biodistribution results for G5-NAcGal conjugates in liver-tumor bearing mice showed tumor-specific accumulation, which was also accompanied by extensive distribution to normal liver tissue. This non-specific hepatic clearance of G5 carriers was reduced via PEGylation of the dendrimer surface, prompting the development of targeted G5-PEG carriers bearing a NAcGal moiety at the terminus of the displayed PEG chain. The synthesized G5-(PEG[NAcGal]) conjugates achieved rapid internalization into hepatic cancer cells due to display of the NAcGal-targeting sugar, while minimizing uptake into normal hepatocytes. Furthermore, the PEG corona displayed on surface of G5-(PEG[NAcGal]) carriers reduced particle opsonization in the presence of serum albumins and as a resulted limited carrier phagotcytosis by liver macrophages. These results confirm the ability of targeted G5-PEG carriers to achieve preferential homing and selective drug delivery to liver tumor cells, while avoiding clearance by normal liver tissue and other RES organs to minimize non-specific toxicity.

6.2   Future Direction

To complete the pre-clinical studies and translate targeted G5-DOX conjugates into the clinic we will study the *in vivo* distribution of the NAcGal-functionalized G5-PEG carriers to identify the targeting strategy which results in the greatest preferential accumulation of the conjugates in liver tumor tissue. This is followed by synthesizing G5 nano-conjugates co-loaded with the selected targeting moieties and the azo-linked DOX

molecules to study the anticancer activity and toxicity of targeted G5-DOX conjugates *in vivo*. Finally, we will identify the hepatic enzyme species responsible for azoreductase activity and explore methods to induce its expression *in vitro* and *in vivo* to achieve enhanced activity of targeted G5-DOX nano-conjugates.

6.2.1 *In Vivo* Biodistribution of G5-(cPEG[NAcGal$_\beta$]) Carriers

Studies on the biodistribution of radio-labeled [^{14}C]G5-(cPEG[NAcGal$_\beta$]) carriers will be conducted utilizing the established *in vivo* tumor model, with conjugates prepared at different PEG loading ratios to identify the carrier composition with the greatest tumor-to-liver distribution ratio. Briefly, [^{14}C]G5-(cPEG[NAcGal$_\beta$]) conjugates prepared with 10 - 30 PEG-ligand moieties attached per dendrimer will be administered by i.v. injection to tumor-bearing mice and biodistribution studied at 2 - 48 hour time points following the protocols detailed in Chapter 5 of this thesis. To enhance the binding affinity of NAcGal-targeted G5-PEG carriers towards the ASGPR we will prepare G5-(*c*PEG[NAcGal$_\beta$]) conjugates with multivalent NAcGal-ligands displayed at the PEG terminus. Specifically, previous binding affinity studies have shown trivalent glycosides exponentially increase the binding affinity of sugar molecules to the ASGPR versus an equivalent concentration of monovalent glycoconjugates.[1,2] As a result
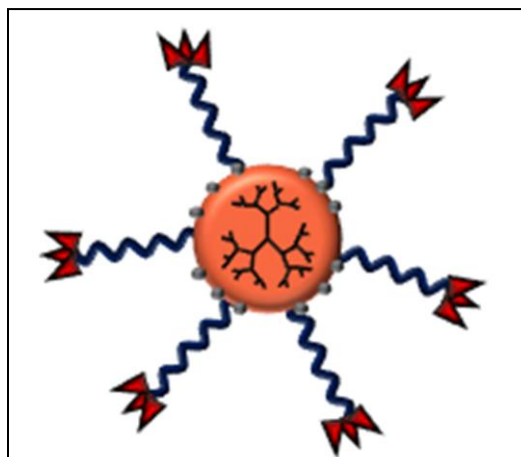

Figure 6.1: Drawing of G5-PEG carriers displaying trivalent [NAcGal$_\beta$]$_3$ glycosides which will enhance the binding affinity of the displayed ligands to the ASGPR and increase particle internalization into hepatic cancer cells

307

trivalent G5-(cPEG[NAcGal$_\beta$]$_3$) carriers (**Figure 6.1**) will be synthesized with intermolecular sugar spacing designed based on the reported spacing of the three ASGPR subunits.[2] These trivalent NAcGal-targeted G5-PEG carriers have the potential to show significant enhancement in particle internalization into hepatic cancer cells *in vitro*, and achieve improved distribution to liver tumor tissue *in vivo*, over the monovalent G5-(cPEG[NAcGal$_\beta$]) carriers described in Chapter 5. These studies will be carried out following the protocols detailed in this dissertation to identify the optimal targeting ligand valency and loading ratio of PEG[NAcGal$_\beta$]-functionalized dendrimer carriers to achieve selective homing to tumor tissue while minimizing accumulation in non-specific organs and healthy liver tissue.

6.2.2 Development and *In Vivo* Activity of Targeted G5-DOX Conjugates

To prepare targeted G5-DOX nano-conjugates the most labile G5-L3-DOX and G5-L4-DOX conjugates will be covalently linked to the PEG[NAcGal$_\beta$]$_x$ moieties through *cis*-aconityl linkages (**Figure 6.2**), with ligand loading ratio selected based on results of the previous targeting studies. Following established protocols described in Chapters 3-4 of this dissertation, the internalization, intracellular drug release, and cytotoxicity of targeted G5-L(x)-DOX
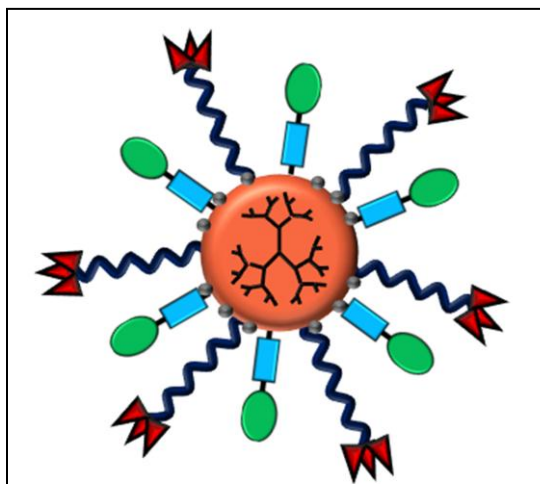

Figure 6.2: Schematic of targeted G5-L(x)-DOX conjugates which will display cell-specific delivery and selective DOX release to the cytoplasm of hepatic cancer cells *in vivo* to achieve high anticancer activity with minimal side effects.

conjugates will be determined upon incubation with hepatic cancer cells to confirm azoreductase-recognition and therapeutic activity of G5-L(x)-DOX conjugates is maintained after PEG-ligand attachment. A decrease in intracellular DOX release and cytotoxicity of targeted G5-L(x)-DOX versus non-targeted conjugates would indicate prevention of the azoreductase enzymes from recognizing the azo-linker due to steric packing of the conjugate surface. In this scenario, decreasing the number of attached PEG[NAcGal$_\beta$] moieties may restore activity, or alternatively azo-DOX molecules could be covalently linked to G5 carriers through a short (e.g. 500 Da) PEG chain to extend the azo-substrate from the polymer carrier, as well as adjacent PEG[NAcGal$_\beta$] chains, to increase enzyme recognition of the azo-linker.

To determine the *in vivo* pharmacokinetics and DOX release from targeted G5-L(x)-DOX conjugates we will synthesize radio-labeled [^{14}C]G5-L3-DOX and [^{14}C]G5-L4-DOX conjugates functionalized with the selected targeting strategy, and administer the conjugates as a single intravenous dose to liver-tumor bearing rat models implanted with a bile duct cannula. At selected time points (2 − 48 hours) after administration the distribution of each conjugates to plasma, vital organs, tumor tissue and waste will be determined following the biodistribution methods detailed in Chapter 5 of this dissertation. To quantify the release of DOX from targeted [^{14}C]G5-L(x)-DOX conjugates after distribution to tumor and liver tissue bile will be collected at specified time intervals based on the established biliary excretion of free DOX after delivery to hepatic tissue.[3] Released DOX is then assayed in the collected bile via liquid-organic extraction and analyzed by HPLC as previously described in Chapter 3. The percentage of DOX released as a function of time is determined by correlating the concentration of

free DOX assayed in the bile to the amount of total DOX delivered to the tumor and liver tissue calculated from the targeted [^{14}C]G5-L(x)-DOX biodistribution results.

This pharmacokinetic study will establish the optimal conjugate composition and dosing frequency of the targeted G5-L(x)-DOX conjugates for *in vivo* therapy and toxicity experiments. To evaluate the anticancer activity of targeted G5-L(x)-DOX conjugates the maximum tolerated dose (MTD) will be determined by administering the conjugate i.v. to non-tumor bearing mice at increasing doses of 8-50 mg/kg (or greater as required) equivalent DOX. The highest dose resulting in ≤15% animal weight loss and no moribund appearance 48 hours after administration will be selected as the MTD. Therapy studies will be performed by administering the MTD of targeted G5-L(x)-DOX or free DOX once per week over 3 weeks to tumor-bearing nude mouse models, with frequency modified based on conjugate biodistribution results and DOX release kinetics as previously determined. Tumor volume reduction for each treatment, as compared to saline receiving controls, at day 0 (initiation of treatment), day 21 (end of treatment period) and day 35 (2 weeks after treatment cessation) is determined via laparotomy to record tumor dimensions by caliper measurement. Animals which show a longest tumor dimension ≥18mm or severe abdominal distention (>10% increase in body weight) are euthanized based on animal care guidelines, with this survival end-point utilized as a metric of treatment activity. Targeted G5-L(x)-DOX conjugates administered at the MTD are considered effective upon both a statistically significant reduction in tumor growth rate and increase in animal survival compared to free DOX and saline control.

Toxicity of each conjugate is determined after a single i.v. injection of targeted G5-L(x)-DOX or free DOX at the MTD to non-tumor bearing mice, with hematologic

function tests and histology results compared to saline-treated controls to evaluate toxicity. Briefly, 24 hours after administration blood is collected from treated animals via intracardiac puncture, followed by separation of the plasma to be assayed for levels of hepatic (ALT, AST, ALP and total Bilirubin), renal (Creatinine and BUN) and cardiac (AST and CPK) function markers. Treatments causing a ≥10% increase in marker expression over the normal ranges (as determined from saline controls) will be considered toxic. In addition, liver, heart, kidney and brain tissue will be isolated after treatment, fixed and embedded in paraffin for analysis by trained pathologists at the University of Michigan Histology Core facility to determine indications of toxicity via histologic examination. Function tests and histology results for animals receiving targeted G5-L(x)-DOX conjugates will be compared to administration of free DOX and saline controls to determine site and severity of toxicity as a function of treatment condition.

Results of these *in vivo* efficacy and toxicity studies will confirm the ability of targeted G5-DOX nano-conjugates to selectively deliver a high dose of DOX molecules to the cytoplasm of hepatic cancer cells and achieve the desired therapeutic activity, while minimizing non-specific toxicity to dose-limiting organs. Furthermore, completion of these studies will provide the preclinical efficacy and toxicity data necessary to translate these nano-conjugates towards human clinical trials.

6.2.3 Identification and Modulation of Azoreductase Enzymes for Enhanced Activity of G5-DOX Conjugates

Previous studies,[4,5] and results of experiments currently underway in our laboratory, suggest cleavage of azo-compounds is mediated by the microsomal CYP450

liver-specific enzymes. To determine the relative contribution of each CYP450 isoenzyme towards the activation of G5-L(x)-DOX, each conjugate will be incubated with commercially available CYP isoenzymes (e.g. CYP1A2, CYP3A4, CYP2D6, CYP2C9, CYP2C19, CYP2E1, CYP2B6 and CYP1A1) following experimental protocols specified in Chapter 3 of this thesis. The concentration of each isoenzyme solution will be prepared based on their relative expression in HepG2 cells from the literature,[6] and percentage DOX released as a function of enzyme identity quantified by HPLC after a 4 hour incubation period. This will be followed by quantification of isoenzyme expression levels in HepG2 and Hep3B human hepatic cancer cells via western blot analysis, and the target active enzyme(s) species determined by comparing the relative contribution of each isoenzyme towards G5-DOX activation to their basal expression levels *in vitro*. This will allow for the upregulation of the identified isoenzyme(s) in HepG2 and Hep3B cells via chemical inducers identified from the literature, with the increase in enzyme expression quantified via western blot analysis before and after chemical pre-incubation. The *in vitro* activity of targeted G5-L(x)-DOX conjugates towards hepatic cancer cells after chemical induction will be determined via intracellular DOX release and clonogenic survival studies, respectively, following the procedures outlined in Chapter 3 to determine the effect of enzyme(s) expression on G5-L(x)-DOX activity.

Successful enhancement in G5-L(x)-DOX activity *in vitr*o after chemical induction of the active CYP450 isoenzyme species will be followed by *in vivo* therapy and toxicity studies of G5-L(x)-DOX conjugates after chemical pre-treatment in tumor models following established protocols from the literature. Specifically, *in situ* enzyme expression of the mouse model tumor tissue will be determined by isolating the tumor,

homogenizing the tissue and performing total RNA and western blot analysis. The basal expression levels for each isoenzyme in tumor tissue will then be correlated to their relative contribution to G5-L(x)-DOX activity to determine the chemical cocktail composition for *in vivo* enzyme induction. This chemical cocktail will then be administered i.p. to tumor-bearing mouse models at a frequency determined from the literature (e.g. once daily for three days), followed by therapy and toxicity studies performed using targeted G5-L(x)-DOX conjugates or free DOX at the MTD, relative to saline receiving controls, as previously described. The results from this study will then be compared to *in vivo* therapy and toxicity of G5-L(x)-DOX conjugates in non-induced mouse models (as described in section 6.2.2) to determine the effect of enzyme expression on the anticancer activity of targeted G5-L(x)-DOX conjugates. These studies will identify the hepatic enzymes responsible for G5-DOX activation, and as a result allow for the personalized design of conjugate compositions and dosing regiments for patients genotyped for CYP450 expression levels in the clinic.

References

1   Lee, R. T. & Lee, Y. C. Preparation of cluster glycosides *N*-acetylgalactosamine that have subnanomolar binding constants towards the mammalian hepatic Gal/GalNAc-specific receptor. *Glycoconjugate J.* **4**, 317-328 (1987).

2   Khorev, O., Stokmaier, D., Schwardt, O., Cutting, B. & Ernst, B. Trivalent, Gal/GalNAc-containing ligands designed for the asialoglycoprotein receptor. *Bioorgan. Med. Chem* **16**, 5216-5231 (2008).

3   Ballet, F., Vrignaud, P., Robert, J., Rey, C. & Poupon, R. Hepatic extraction, metabolism and biliary excretion of doxorubicin in the isolated prefused rat liver. *Cancer Chemoth. Pharm.* **19**, 240-245 (1987).

4   Umeno, M., Yanagita, K., Sagami, I. & Shimizu, T. Azo reduction catalyzed by cytochrome P450 1A2 and NADPH-cytochrome P450 reductase. *J. Inorg. Biochem.* **67**, 379-379 (1997).

5   Zbaida, S. in *Enzyme Systems that Metabolise Drugs and Other Xenobiotics*   555-566 (John Wiley & Sons, Ltd, 2002).

6   Wilkening, S., Stahl, F. & Bader, A. Comparison of primary human hepatocytes and hepatoma cell line HepG2 with regard to their biotransformation properties. *Drug. Metab. Dispos.* **31**, 1035-1042 (2003).